

AD-A061 426

EIC CORP NEWTON MASS
SILVER-HYDROGEN ENERGY STORAGE.(U)
AUG 78 G L HOLLECK, M J TURCHAN, F S SHUKER

F/G 10/3

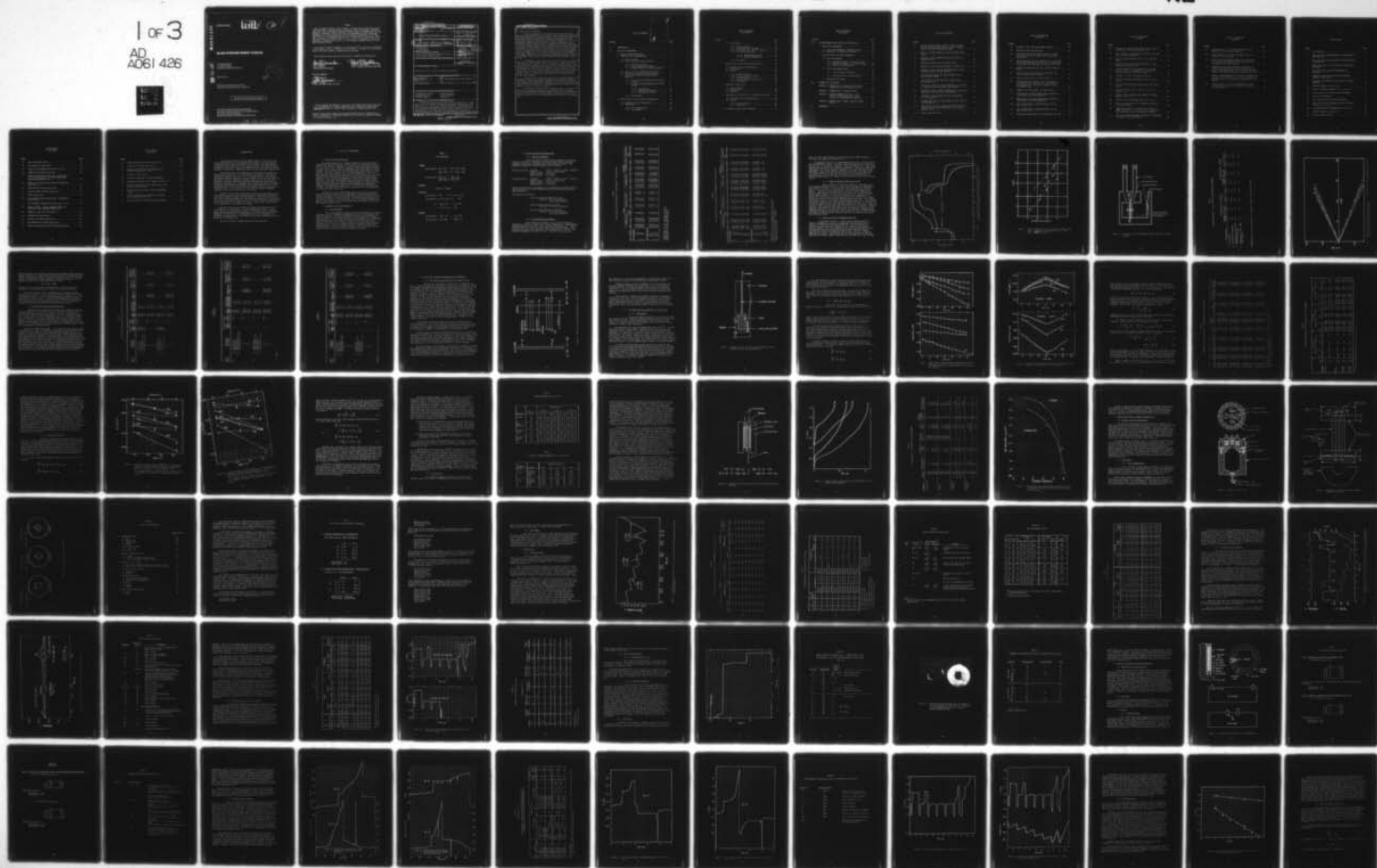
UNCLASSIFIED

AFAPL-TR-78-65

F33615-76-C-2093

NL

1 of 3
AD
A061 426



AD A061426

DDC FILE COPY

AFAPL-TR-78-65

LEVEL II

(2) J

SILVER HYDROGEN ENERGY STORAGE

EIC CORPORATION
55 CHAPEL STREET
NEWTON, MASSACHUSETTS 02158

AUGUST 1978

TECHNICAL REPORT AFAPL-TR-78-65
Final Report for Period June 1976 — June 1978



Approved for public release; distribution unlimited.

AIR FORCE AERO PROPULSION LABORATORY
AIR FORCE WRIGHT AERONAUTICAL LABORATORIES
AIR FORCE SYSTEMS COMMAND
WRIGHT-PATTERSON AIR FORCE BASE, OHIO 45433

78 11 17 042

NOTICE

When Government drawings, specifications, or other data are used for any purpose other than in connection with a definitely related Government procurement operation, the United States Government thereby incurs no responsibility nor any obligation whatsoever; and the fact that the government may have formulated, furnished, or in any way supplied the said drawings, specifications, or other data, is not to be regarded by implication or otherwise as in any manner licensing the holder or any other person or corporation, or conveying any rights or permission to manufacture, use, or sell any patented invention that may in any way be related thereto.

This report has been reviewed by the Information Office (OI) and is releasable to the National Technical Information Service (NTIS). At NTIS, it will be available to the general public, including foreign nations.

This technical report has been reviewed and is approved for publication.

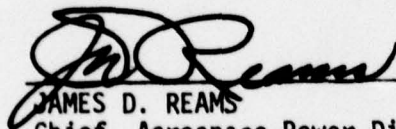


DON R. WARNOCK
Task Scientist
Energy Conversion Branch



ROBERT R. BARTHELEMY
Chief, Energy Conversion Branch

FOR THE COMMANDER



JAMES D. REAMS
Chief, Aerospace Power Division

"If your address has changed, if you wish to be removed from our mailing list, or if the addressee is no longer employed by your organization please notify AFAPL/POE-1 W-PAFB, OH 45433 to help us maintain a current mailing list".

Copies of this report should not be returned unless return is required by security considerations, contractual obligations, or notice on a specific document.

UNCLASSIFIED

SECURITY CLASSIFICATION OF THIS PAGE (When Data Entered)

REPORT DOCUMENTATION PAGE		READ INSTRUCTIONS BEFORE COMPLETING FORM
1. REPORT NUMBER AFAPL TR-78-65	2. GOVT ACCESSION NO.	3. RECIPIENT'S CATALOG NUMBER
4. TITLE (and Subtitle) SILVER-HYDROGEN ENERGY STORAGE		5. TYPE OF REPORT & PERIOD COVERED Final: 15 June 1976 to 15 June 1978
7. AUTHOR(s) G. L. Holleck, M. J. Turchan, F. S. Shuker, D. DeBiccarri, M. J. Turner, P. O. D. Offenhardt		6. PERFORMING ORG. REPORT NUMBER
8. CONTRACT OR GRANT NUMBER(s) F33615-76-C-2093		9. PROGRAM ELEMENT, PROJECT, TASK AREA & WORK UNIT NUMBERS 62203F 3145-21-30
10. PERFORMING ORGANIZATION NAME AND ADDRESS EIC Corporation 55 Chapel Street Newton, MA 02158		11. CONTROLLING OFFICE NAME AND ADDRESS Air Force Aero Propulsion Laboratory (POE-1) Wright-Patterson AFB, OH 45433
12. REPORT DATE August 1978		13. NUMBER OF PAGES 222
14. MONITORING AGENCY NAME & ADDRESS (if different from Controlling Office)		15. SECURITY CLASS. (of this report) UNCLASSIFIED
16. DISTRIBUTION STATEMENT (of this Report) Approved for public release; distribution unlimited.		
17. DISTRIBUTION STATEMENT (of the abstract entered in Block 20, if different from Report) 12 236 p. 9 Final rept. 15 Jun 76-15 Jun 78,		
18. SUPPLEMENTARY NOTES		
19. KEY WORDS (Continue on reverse side if necessary and identify by block number) Silver-Hydrogen Battery Silver Electrode Rechargeable Battery Metal-Gas Battery Secondary Battery Separator		
20. ABSTRACT (Continue on reverse side if necessary and identify by block number) During this program we have demonstrated the feasibility of Ag/H ₂ cells with 35 to 50 Wh/lb, depending on the desired discharge rate, and with a cycle life in excess of 500 deep discharges. This demonstration and the necessary development involved extensive component level studies and performance evaluation using several sets of laboratory cells of approximately 15 Ah in addition to the development of a comprehensive computerized mathematical model for the design and optimization of Ag/H ₂ cells.		

DD FORM 1 JAN 73 1473

EDITION OF 1 NOV 65 IS OBSOLETE

UNCLASSIFIED

SECURITY CLASSIFICATION OF THIS PAGE (When Data Entered)

408 525

78 11 17 042

UNCLASSIFIED

SECURITY CLASSIFICATION OF THIS PAGE (When Data Entered)

20. Abstract (continued)

of rolled stack configuration.

Electrolyte management was identified as the main problem area. The relatively high solubility of silver oxide in the electrolyte necessitates the use of argentistatic membranes similar to those employed in Ag/Zn cells. These membranes have characteristic electrolyte transport properties described by their transference, diffusion and flow parameters. We determined those parameters and showed that a suitable combination of the individual transport characteristics is required to maintain an adequate electrolyte balance during any one charge-discharge cycle and from cycle to cycle. Of the four membranes tested, Visking, P-2291, P-2193 and the NASA separator, only the latter was found suitable for use in practical Ag/H₂ cells. The principal property differentiating it from the other membranes was a much higher rate of electrolyte equilibration via "back-wicking". Electrolyte capacity as well as the pore size and pore size distribution of the absorber layer, were also identified as important parameters. Asbestos is preferable to the relatively open structure of non-woven nylon such as P-2505.

The solubility of the silver oxide in the electrolyte is an inherent property which will eventually lead to cell failure. Rapid formation of soft short circuits, especially by silver dendrites around the plate edges, can be avoided by appropriate cell stack design. A rolled electrode stack configuration was found especially effective. Slow diffusion of silver oxide through the membrane and its subsequent reduction to Ag at the hydrogen electrode is not specifically harmful. Eventually this process will, however, lead to the formation of an electronic path between anode and cathode. No cell failures due to this process were observed during the course of this program.

A final set of 16 laboratory cells, based on the NASA separator but employing different orientations, components and component arrangements according to a mathematical matrix demonstrated the feasibility and performance capability of Ag/H₂ cells. The amount of electrolyte (absorber layer thickness) and the orientation of the NASA separator were found to have the greatest influence on capacity retention.

Our mathematical modeling effort identified silver electrode utilization as the strongest energy density determining factor. Including practical configurational (radius to length ratio) and thermal restrictions a rolled design with three electrode wraps of approximately 25 mil thick silver electrodes and 15 mil thick absorber layers is close to an optimized cell.

UNCLASSIFIED

SECURITY CLASSIFICATION OF THIS PAGE (When Data Entered)

TABLE OF CONTENTS

APPROVED FOR	
DATE	BY
2000	1.5
BY	
DISSEMINATION/AVAILABILITY	
CLASS	CONTROL
A	

SECTION

PAGE

I.	INTRODUCTION.	1
II.	Ag/H ₂ CELL DEVELOPMENT.	2
1.	General System Description.	2
2.	Component Level Investigations.	2
2.1	General Remarks.	2
2.2	Silver Electrode Characterization.	3
2.2.1	Physical Parameters	3
2.2.2	Electrochemical Performance	3
2.2.3	Oxygen Evolution at Silver Electrodes	7
2.3	Effect of Silver on Hydrogen Electrodes.	7
2.4	Electrolyte Distribution and Retention	13
2.5	Electrolyte Transport through Separator Membranes.	17
2.5.1	Description and Definition of Transport Process	17
2.5.2	Diffusion and Electromigration of KOH and H ₂ O	19
2.5.2.1	Experimental	19
2.5.2.2	KOH and H ₂ O Diffusion.	21
2.5.2.3	KOH and H ₂ O Transfer	27
2.5.3	Back Wicking.	31
3.	Boiler Plate Cells of Stacked Configuration	38
3.1	Hardware and Cell Construction	38
3.2	Test Matrix.	38
3.2.1	Cell Configuration.	38
3.2.2	Test Regime	46

TABLE OF CONTENTS
(continued)

SECTION	PAGE
3.3 Test Results.	46
3.3.1 Pretest Cycling.	46
3.3.2 Accelerated Cycle Testing.	53
3.3.3 Electrolyte Loss from Cell Stacks.	57
3.3.4 Cell Failure Analysis.	61
3.3.4.1 Charge Retention Test	61
3.3.4.2 Physical Examination.	61
3.3.5 Discussion	61
4. Boiler Plate Cells of Rolled Configuration	66
4.1 Hardware and Cell Construction.	66
4.2 Test Matrix	66
4.3 Results	66
4.3.1 Pretest Cycling.	66
4.3.2 Accelerated Cycle Testing.	71
4.3.3 Failure Analysis	80
4.3.4 Self-Discharge of Ag/H ₂ Cells.	82
4.3.5 Discussion	88
5. Laboratory Ag/H ₂ Cells	90
5.1 General Remarks	90
5.2 Experimental.	90
5.3 Results	92
6. Advanced Boiler Plate Cells of Rolled Configuration. .	128
6.1 Test Matrix and Cell Construction	128
6.2 Results	131
6.2.1 Pretest Cycling.	131
6.2.2 Cycle Test	131
7. Preliminary Ag/H ₂ Safety Analysis.	144

TABLE OF CONTENTS
(continued)

SECTION	PAGE
III. SILVER-HYDROGEN CELL DESIGN AND OPTIMIZATION.	147
1. Electrolyte Management.	147
1.1 Electrolyte Management Computer Program.	147
1.2 Simulation of Electrolyte Transport.	147
2. Energy Density and Thermal Management	152
2.1 Model Development.	152
2.1.1 Optimal Resistance of Electrode Leads	152
2.1.2 Optimal Resistance of the H ₂ Electrode.	155
2.1.3 Effect of Electrode Tabs.	157
2.2 Use of the Computer Model.	162
2.2.1 Critical Design Parameters.	162
2.2.2 Interpretation of Program Output.	164
2.3 Optimized Cell Design.	169
IV. SUMMARY AND CONCLUSIONS	177
APPENDIX A PROGRAM EICD1: Program for the Design Simulation of Rolled Ag/H ₂ Batteries.	179
APPENDIX B PROGRAM EICD1: Program Listing	183
APPENDIX C PROGRAM FLOWSHEET FOR EICD1: "Cal- culation and Optimization of Energy Density for Silver-Hydrogen Batteries	201
APPENDIX D PROGRAM EICD1: Sample Computer Program OUTPUT.	206
V. REFERENCES.	222

LIST OF ILLUSTRATIONS

FIGURE		PAGE
1	Typical charge-discharge curves of thick (25 mil) and thin (10 mil) Ag electrodes, C-rate, configuration II, 30% KOH, potentials vs. RHE.	8
2	Effect of current density on silver electrode utilization.	9
3	Plexiglas cell for measuring location and rate of oxygen evolution.	10
4	Hydrogen electrode current voltage curves	12
5	Change of anolyte during discharge in a Ag/H ₂ cell. . . .	18
6	Schematic of half cell for the measurement of water and KOH transport through membranes	20
7	Characteristic volume and density changes due to H ₂ O and KOH diffusion	22
8	Characteristic volume and density changes due to electromigration.	23
9	Diffusion of water in various membranes as a function of temperature and electrolyte concentration.	28
10	Diffusion of KOH in various membranes as a function of temperature and electrolyte concentration	29
11	Schematic of back wicking cell and corresponding electrode reaction.	34
12	Voltage-time traces of back wicking in cells using a Visking membrane.	35
13	Back wicking rates for Visking and Permion 2193 as a function of electrolyte saturation of the asbestos absorber layer.	37
14	Boiler plate test cell.	39

LIST OF ILLUSTRATIONS
(continued)

FIGURE		PAGE
15	Schematic of the cell stack support mandrel.	40
16	Component shapes and dimensions.	41
17	Accelerated test cycle regime i_1 and i_2 = current for cells with thin and thick silver electrodes, respectively	47
18	Typical variation in stack temperature, cell voltage, Ag electrode potential, and pressure in a Ag/H ₂ cell (thick electrodes) during an accelerated test cycle. . .	54
19	Temperature change during cycle testing of Cells 11 and 12	55
20	Ag/H ₂ cell potential during the accelerated test cycle in which failure occurred.	59
21	Charge retention test of series Cell No. 9	62
22	Hydrogen electrode absorber layer and membrane of a cycled Ag/H ₂ cell (Cell No. 5). Dark areas on the absorber layer show silver migration around the membrane edge.	64
23	Schematic of rolled Ag/H ₂ cell construction.	67
24	Characteristic voltage changes during formation of rolled Ag/H ₂ cells (2nd formation)	72
25	Characteristic voltage charges during formation of rolled Ag/H ₂ cells (2nd formation)	73
26	Cell voltage during a charge-discharge cycle of Cell 17 at 2.5 A	75
27	Cell voltage during a charge-discharge cycle of Cell 19 at 2.5 A	76
28	Potential of Ag/H ₂ Cell No. 25 during cycle No. 184. . .	78

LIST OF ILLUSTRATIONS
(continued)

FIGURE		PAGE
29	Voltage trace (upper) and pressure profile (lower) of Cell No. 25 during AF Cycle No. 528.	79
30	Cell voltage as a function of current prior (0) and after (Δ) third impregnation.	81
31	Typical charge-discharge curves of cell 26RA and 26RAT	83
32	Logarithmic plot of Ag/H ₂ cell pressure vs. time during self-discharge, 23°C	85
33	Pressure change with time during self discharge test of Cell No. 25 subsequent to extended cycle testing (lower-semi log plot of data)	86
34	Schematic of small experimental Ag/H ₂ cell.	91
35	Cell XXV configuration showing little rate sensitivity.	126
36	Cell XXXIX configuration showing severe rate sensitivity.	127
37	Cell A-1 formation cycle - charge @ 0.5 A, discharge @ 3.0 A	132
38	Typical voltage, pressure and temperature changes during a test cycle	136
39	Typical cell voltage during Cycle 508, Cell A-7	137
40	Effect on energy density of increasing the number of electrode pairs.	166
41	Temperature changes in a battery with 3 pairs of Ag/H ₂ electrodes ΔV is the difference between the cell potential and the electroneutral potential	167
42	Effect on maximum discharge temperature of increasing the number of electrode pairs	168

LIST OF ILLUSTRATIONS
(continued)

FIGURE		PAGE
43	Energy density of a rolled 50 Ah Ag/H ₂ cell as a function of Ag electrode utilization.	170
44	Energy density of a rolled 50 Ah Ag/H ₂ cell as a function of discharge rate.	171
45	Energy density and maximum temperature differences of a rolled 50 Ah Ag/H ₂ cell as a function of cell configuration and discharge rate.	172
46	Change in weight energy density as a function of volume energy density of a rolled 50 Ah Ag/H ₂ cell with corresponding changes in cell pressure and ratio between cell length and radius. Discharge rate C/1.5 . . .	173
47	Change in energy density as a function of mandrel and absorber layer thickness for a 50 Ah rolled Ag/H ₂ cell. Discharge rate C/1.5, volumetric energy density 0.07 Wh/cm ³	175
48	Energy density of a rolled 50 Ah Ag/H ₂ cell with a constant amount of Ag as a function of the number of Ag electrodes.	176

LIST OF TABLES

TABLE		PAGE
1	CELL REACTIONS.	3
2	CYCLE DATA FOR SILVER ELECTRODES IN CONFIGURATION I (TWO SIDED USE)	5
3	CYCLE DATA FOR SILVER ELECTRODES IN CONFIGURATION II (ONE SIDED USE)	6
4	OXYGEN EVOLUTION AT 25 MIL POSITIVE PLATES DURING OVERCHARGE.	11
5	TEST ARRAYS FOR ELECTROLYTE ABSORPTION AND RETENTION	14
6	SUMMARY OF DATA AND CALCULATIONS FOR MEMBRANE DIFFUSION COEFFICIENTS.	25
7	DIFFUSION COEFFICIENTS FOR H ₂ O AND KOH IN VARIOUS MEMBRANES	26
8	TRANSPORT NUMBERS FOR H ₂ O AND K ⁺	32
9	AVERAGE OF TRANSPORT NUMBERS AT 10, 25 AND 40°C	32
10	BACK WICKING OF KOH THROUGH VARIOUS MEMBRANES	36
11	LIST OF TEST VARIABLES.	42
12	THE SIXTEEN HIGHEST-PRIORITY EXPERIMENTS.	44
13	CYCLE DATA FOR SILVER HYDROGEN CELL OF CONFIGURA- TION $m_1 n_o e_o k_p r_o t_1$	48
14	CONFIGURATION AND INSTRUMENTATION OF TEST CELLS	49
15	PRETEST HISTORY OF Ag/H ₂ CELLS.	50
16	DATA FOR PRETEST CYCLE 1.	51

LIST OF TABLES
(continued)

TABLE	PAGE
17 DATA FOR PRETEST CYCLE 6.	52
18 TEST HISTORY OF Ag/H ₂ CELLS	56
19 CAPACITY TEST BETWEEN TEST CYCLES 24 and 25	58
20 SUMMARY OF ELECTROLYTE LOSS DATA.	60
21 CHARGE RETENTION OF FAILED CELLS. CHARGE INPUT 0.52 Ahr FOR THIN AND 1.4 Ahr FOR THICK PLATE CELLS (DATA RECORD NO. 47).	63
22 NUMBER OF ACCELERATED TEST CYCLES TO FAILURE FOR Ag/H ₂ CELLS	65
23 TEST MATRIX FOR ROLLED Ag/H ₂ CELLS.	68
24 PRETEST HISTORY OF ROLLED Ag/H ₂ CELLS	70
25 ROLLED Ag/H ₂ CELLS.	74
26 TEST HISTORY OF ROLLED Ag/H ₂ CELLS. ACCELERATED AF TEST CYCLE	77
27 SELF-DISCHARGE PARAMETERS FOR Ag/H ₂ CELLS AT 23°C	87
28 CHARGE CAPACITY - VOLTAGE BEHAVIOR DURING THE FIRST AND SECOND FORMATION CHARGE CYCLE	89
29 SUMMARY OF SMALL TEST CELL RESULTS.	93
30 VARIABLES AND TEST MATRIX	129
31 CAPACITY OF A-SERIES Ag/H ₂ CELLS.	133
32 CELL PRESSURE OF A-SERIES Ag/H ₂ CELLS	134
33 PRETEST ELECTROLYTE DATA FOR A-SERIES Ag/H ₂ CELLS	135

LIST OF TABLES
(continued)

TABLE		PAGE
34	CHARGE-DISCHARGE VOLTAGES OF Ag/H_2 CELLS.	138
35	CAPACITIES OF ROLLED Ag/H_2 CELLS.	139
36	PRESSURE AND ELECTROLYTE DATA DURING CYCLE TESTING OF ROLLED Ag/H_2 CELLS	140
37	HISTORY OF FAILED CELLS	141
38	FACTORIAL EVALUATION OF CAPACITY RETENTION.	142
39	FACTORIAL EVALUATION OF CELL ENERGY AT CYCLE 514.	143
40	CAPACITY AND VOLTAGE DATA OF ROLLED Ag/H_2 CELLS TESTED AT VARIOUS RATES	145
41	INPUT STRUCTURE FOR THE ELECTROLYTE MANAGEMENT PROGRAM	150
42	OPTIMUM THICKNESS FOR RECTANGULAR ELECTRODES FULLY TABBED ALONG ONE EDGE	158
43	OPTIMUM THICKNESS FOR SEMI-CIRCULAR ELECTRODES.	160

I. INTRODUCTION

A metal gas battery based on the Ag/H₂ couple is an attractive power source, particularly in terms of weight energy density. By replacing the Zn electrode in the Ag/Zn system with the H₂ electrode, the main drawback of Ag/Zn batteries, short cycle life, can be overcome. The relatively high solubility of the silver oxide in the alkaline electrolyte requires, however, retention of argentistatic membranes similar to those employed in Ag/Zn cells.

The main objective of the program was to determine the feasibility of and develop design data for a 35 Wh/lb Ag/H₂ cell capable of 500 deep discharge cycles and one year life in satellite applications. The general experimental approach involved the use of standard state-of-the-art components (Ag and H₂ electrodes, membranes, absorber layers, gas screens) and the building of prototype laboratory cells utilizing modified state-of-the-art Ni/H₂ cell configurations. A mathematically designed test matrix was employed to maximize the information obtainable from a limited number of test cells. During the course of the program it became apparent that the Ag/H₂ system is considerably more complex than had been anticipated leading to extended component level tests and specialized cell designs.

Section II of this report describes the Ag/H₂ cell development effort. This includes component level investigations with comprehensive treatment of electrolyte transport through separator membranes, construction and test of two sets of boilerplate Ag/H₂ cells, an extensive characterization and development effort using small laboratory cells and a final performance demonstration of 16 advanced boilerplate Ag/H₂ cells using a rolled stack. System safety is also addressed in a preliminary discussion.

Section III describes our Ag/H₂ cell design and optimization effort. It consists of the development of a detailed mathematical model of Ag/H₂ cell construction and operation including electrolyte transport through membranes and heat generation and dissipation. This model was then applied to determine the sensitivity of various parameters on cell performance, in particular on energy density. The model was also used to develop an optimized design for a 50 Ah Ag/H₂ cell.

Section IV contains a summary discussion and conclusions.

II. Ag/H₂ CELL DEVELOPMENT

1. General System Description

The silver-hydrogen cell combines elements of the related nickel-hydrogen and silver-zinc systems. Replacing the zinc electrode in Ag/Zn cells by the long life hydrogen fuel cell electrode should greatly increase the cycle life (>500). Similarly, exchange of the nickel oxide electrode in Ni/H₂ cells by silver oxide will markedly boost energy density to about 80 Wh/lb. The main difficulties in the development of practical cells are expected from silver migration and electrolyte management. In fact, we have shown that even in Ni/H₂ cells loss of electrolyte from the cell stack, primarily by a displacement mechanism, has been the major failure mode (Holleck, 1976)¹. Electrolyte management in Ag/H₂ cells requires special attention. First water participates directly in the cell reaction (see Table 1) and secondly, the relatively high solubility of silver oxide mandates multilayer separator systems utilizing argentistatic membranes, similar to those employed in Ag/Zn cells. From the cell reactions shown in Table 1 the Ag/H₂ cell is expected to be as tolerant to overcharge and cell reversal as the Ni/H₂ cell.

The objective of our experimental program was, to evaluate major design variables including (i) type and number of argentistatic membrane layers, (ii) amount of electrolyte (number and location of absorber layers), and (iii) thickness of the Ag electrode. The initial approach was to use 16 laboratory cells of 6 and 15 Ah capacity in a factorially designed test matrix. The results of our cell tests will show that Ag/H₂ cells are much more complex than Ni/H₂ cells.

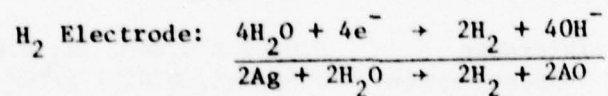
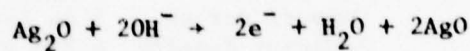
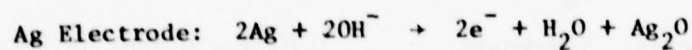
2. Component Level Investigations

2.1 General Remarks

For the development of Ag/H₂ cells we used commercially available components with an established performance record in the environment that they will encounter. Therefore component level tests were restricted to those necessary to obtain additional specific data required for optimum test configuration selection. During such tests and especially during the first phase of boilerplate cell testing, the need for a more detailed understanding of the electrolyte transport processes in argentistatic membranes became apparent. Since only limited data was available we conducted a detailed study of relevant transport processes. This particular task proceeded in parallel with the testing of boiler plate cells.

TABLE 1
CELL REACTIONS

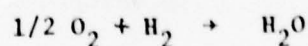
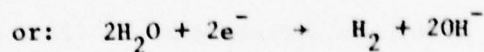
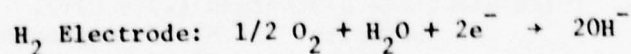
CHARGE



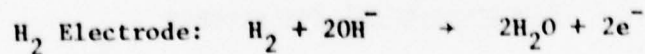
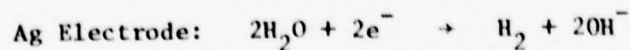
DISCHARGE

Reverse of Charge

OVERCHARGE



REVERSAL



2.2 Silver Electrode Characterization

2.2.1 Physical Parameters

Silver electrodes in sheet form were obtained from Yardney Electric Corporation. They were characterized with respect to physical parameters, electrolyte absorption, and electrochemical behavior. The parameters (average of 6 random samples) were as follows:

Thick Ag Electrode:	Thickness	0.0254 ± 0.0001 in; 0.0645 ± 0.0003 cm
	Support screen	5 Ag 15-1, 0.020 g/cm ²
	Apparent density	4.333 g/cm ³
	Sinter density	4.145 g/cm ³
Thin Ag Electrode:	Thickness	0.0107 ± 0.0001 in; 0.0272 ± 0.003 cm
	Support screen	5 Ag 8-1, 0.0107 g/cm ²
	Apparent density	4.273 g/cm ³
	Sinter density	4.031 g/cm ³

Electrode porosities were determined for the discharged electrodes from the apparent density and by water absorption and for the charged electrode by water absorption.

The values are as follows:

Thick electrode discharged (25.4 mil),
porosity: 58.8% (from density)
57.6% (H₂O absorption)

Thick electrode charged (26.1 mil),
porosity: 38.5% (H₂O absorption)

Thin electrode discharged (10.6 mil),
porosity: 59.4% (from density)
51.8% (H₂O absorption)

2.2.2 Electrochemical Performance

Electrochemical performance of the silver electrodes was evaluated by cycling at various rates in two configurations. Configuration I: counterelectrodes at each side of the electrode; Configuration II: counter-electrode only on one side, the other side covered by Teflon sheet. Both configurations were tested completely flooded (submerged) in 30% KOH. The results are summarized in Tables 2 and 3. A typical current-potential

TABLE 2

CYCLE DATA FOR SILVER ELECTRODES IN CONFIGURATION I (TWO SIDED USE)

Rate 1 2 (mA/cm ²)	Charge			Discharge			Elec- trode Sinter	
	Capacity (Ah)			Potential (V)***				
	Step 1	Step 2	% Over- charge	Step 1	Step 2	Step 3		
Thin Electrode*	Step 1	Step 2	% Over- charge	Step 1	Step 2	Step 3	Total	
	Step 1	Step 2	% Over- charge	Step 1	Step 2	Step 3		
C 15	0.076	0.362	33	1.22	1.51	1.75	0.152	
C 15	0.100	0.270	28	1.22	1.52	1.754	0.137	
2C 30	0.086	0.285	23	1.27	1.55	1.81	0.126	
2C 30	0.072	0.247	100	1.30	1.57	1.84	0.116	
2C 30	0.090	0.258	40	1.27	1.54		0.123	
4C 54	0.078	0.225	25	1.36	1.64	1.90	0.102	
							0.297	
							0.455	
							1.33	
							1.07	
							1.32	
							1.06	
							1.28	
							1.03	
							1.02	
							1.26	
							1.04	
							0.95	
							1.22	
							1.33	
							1.07	
							1.32	
							1.06	
							1.28	
							1.03	
							1.02	
							1.26	
							1.04	
							0.95	
							1.22	
							1.33	
							1.07	
							1.32	
							1.06	
							1.28	
							1.03	
							1.02	
							1.26	
							1.04	
							0.95	
							1.22	
							1.33	
							1.07	
							1.32	
							1.06	
							1.28	
							1.03	
							1.02	
							1.26	
							1.04	
							0.95	
							1.22	
							1.33	
							1.07	
							1.32	
							1.06	
							1.28	
							1.03	
							1.02	
							1.26	
							1.04	
							0.95	
							1.22	
							1.33	
							1.07	
							1.32	
							1.06	
							1.28	
							1.03	
							1.02	
							1.26	
							1.04	
							0.95	
							1.22	
							1.33	
							1.07	
							1.32	
							1.06	
							1.28	
							1.03	
							1.02	
							1.26	
							1.04	
							0.95	
							1.22	
							1.33	
							1.07	
							1.32	
							1.06	
							1.28	
							1.03	
							1.02	
							1.26	
							1.04	
							0.95	
							1.22	
							1.33	
							1.07	
							1.32	
							1.06	
							1.28	
							1.03	
							1.02	
							1.26	
							1.04	
							0.95	
							1.22	
							1.33	
							1.07	
							1.32	
							1.06	
							1.28	
							1.03	
							1.02	
							1.26	
							1.04	
							0.95	
							1.22	
							1.33	
							1.07	
							1.32	
							1.06	
							1.28	
							1.03	
							1.02	
							1.26	
							1.04	
							0.95	
							1.22	
							1.33	
							1.07	
							1.32	
							1.06	
							1.28	
							1.03	
							1.02	
							1.26	
							1.04	
							0.95	
							1.22	
							1.33	
							1.07	
							1.32	
							1.06	
							1.28	
							1.03	
							1.02	
							1.26	
							1.04	
							0.95	
							1.22	
							1.33	
							1.07	
							1.32	
							1.06	
							1.28	
							1.03	
							1.02	
							1.26	
							1.04	
							0.95	
							1.22	
							1.33	
							1.07	
							1.32	
							1.06	
							1.28	
							1.03	
							1.02	
							1.26	
							1.04	
							0.95	
							1.22	
							1.33	
							1.07	
							1.32	
							1.06	
							1.28	
							1.03	
							1.02	
							1.26	
							1.04	
							0.95	
							1.22	
							1.33	
							1.07	
							1.32	
							1.06	
							1.28	
							1.03	
							1.02	
							1.26	
							1.04	
							0.95	
							1.22	
							1.33	
							1.07	
							1.32	
							1.06	
							1.28	
							1.03	
							1.02	
							1.26	
							1.04	
							0.95	
							1.22	
							1.33	
							1.07	
							1.32	
							1.06	
							1.28	
							1.03	
							1.02	
							1.26	
							1.04	
							0.95	
							1.22	
							1.33	
							1.07	
							1.32	
							1.06	
							1.28	
							1.03	
							1.02	
							1.26	
							1.04	
							0.95	
							1.22	
							1.33	
							1.07	
							1.32	
							1.06	
							1.28	
							1.03	
							1.02	
							1.26	
							1.04	
							0.95	
							1.22	
							1.33	
							1.07	
							1.32	
							1.06	
							1.28	
							1.03	
							1.02	
							1.26	
							1.04	
							0.95	
							1.22	
							1.33	
							1.07	
							1.32	
							1.06	
							1.28	
							1.03	
							1.02	
							1.26	
							1.04	
							0.95	
							1.22	
							1.33	
							1.07	
							1.32	
							1.06	
							1.28	
							1.03	
							1.02	
							1.26	
							1.04	

TABLE 3

CYCLE DATA FOR SILVER ELECTRODES IN CONFIGURATION II (ONE SIDED USE)

		Charge				Discharge					
		Capacity (Ah)		Potential (V)++		Capacity (Ah)		Potential (V)++		Utilization %	
Rate+ (mA/cm ²)		Step 1	Step 2	Step 1	Step 2	Step 3	Step 1	Step 2	Step 1	Step 2	Elec- trode Sinter
		% Over-									
		charge	charge								
Thin Electrode*											
		Step 1	Step 2	Step 1	Step 2	Step 3	Step 1	Step 2	Step 1	Step 2	
C/4	8.3	0.121	0.307	1.21	1.53	1.63	0.073	0.354	0.427	1.37	62
C/2	16.6	0.097	0.235	1.23	1.53	1.73	0.115	0.217	0.332	1.38	48
C/2	16.6	0.117	0.242	1.22	1.54	1.69	0.118	0.244	0.362	1.38	53
C	33.2	0.083	0.240	1.24	1.55	1.81	0.112	0.210	0.322	1.35	58
2C	66.4	0.080	0.173	1.27	1.55	1.77	0.084	0.165	0.249	1.22	47
C	30	0.100	0.222	1.42	1.72	1.85	0.106	0.21	0.316	1.27	36
C	30	0.105	0.216	1.23	1.55	1.77	0.099	0.204	0.303	1.29	46
2C	60	0.089	0.223	1.30	1.60	1.86	0.098	0.208	0.306	1.22	44
4C	108	-	-	-	-	>2.0	0.082	0.173	0.26	1.01	45
2C	60	0.106	0.202	1.50	1.79	1.90	0.090	0.215	0.305	1.15	38
2C	60	0.07	0.229	1.28	1.59	1.86	0.095	0.196	0.291	1.22	45
Thick Electrode**											
C/4	21	0.153	0.257	1.22	1.56	1.63	0.102	0.263	0.365	1.37	42
C/2	42	0.131	0.193	1.23	1.56	1.73	0.115	0.220	0.335	1.34	57
C/2	42	0.130	0.228	1.27	1.59	1.72	0.110	0.232	0.342	1.34	49
C	84	0.117	0.217	1.29	1.67	1.90	0.095	0.190	0.285	1.28	50
2C	168	0.080	0.120	1.30	1.71	1.80	0.083	0.195	0.278	1.18	42
C	73.0	0.117	0.225	1.37	1.68	1.95	0.112	0.206	0.318	-	40
C	73.0	0.102	0.210	1.36	1.70	1.91	0.116	0.210	0.326	1.05	46
2C	146.0	0.117	0.190	-	-	-	0.096	0.190	0.286	-	47
4C	270.0	-	-	-	-	>2.0	-	-	0.25	-	42
											37

*Plate size 12.1 cm², thickness 0.0272 cm (10.6 mil).**Plate size 4.8 cm², thickness 0.0645 cm (25.4 mil)++Reported vs. RHE, measured vs. Hg/H₂O.

+Nominal based on 0.4 Ahr.

curve for charge and discharge of silver electrodes is shown in Figure 1. The results are summarized in Tables 2 and 3.

We examined the data for a relationship between rate, electrode thickness and obtainable capacity. The best correlation appears to be given by a plot of $\log i$ vs. Ag sinter utilization. This is shown in Fig. 2 (some points represent the average of more than one measurement). Within the range of our investigation the silver utilization appears to decrease linearly with the logarithms of the current density. Although the location and shape of this line differs somewhat for the various test runs all data (thick and thin electrodes, one or two sided use) fall within a band outlined in Fig. 2 indicating approximately 27% change in utilization for a factor 10 in current density.

2.2.3 Oxygen Evolution at Silver Electrodes

Oxygen evolution at silver electrodes was investigated in a cell schematically shown in Fig. 3. The silver electrode was overcharged at the C/30 and C/70 rates. On a volume basis this corresponds at 30 atmospheres to a C and C/2 rate, respectively. The results are summarized in Table 4. Microscopic observation of the electrode surface showed fairly uniform oxygen evolution over the whole electrode area. Similar to nickel plates bubble emergence is favored at cracks and plate inhomogeneities, however the silver plates are much more uniform than nickel plates. Oxygen evolution at the test electrode was almost equal at both sides. Plate orientation with respect to the counter electrode showed some effect. Gas evolution was favored slightly at the side facing the counterelectrode. The presence of an absorber matrix (Pellon 2505) made gas evolution more difficult at this side leading to higher gas evolution rates at the back of the electrodes. However, contrary to the experience with nickel oxide electrodes gas evolution is not completely diverted to the uncovered side of the electrode. Apparently gas permeation through the smaller pores of the silver electrode is more difficult and cannot be achieved by the relatively small forces exerted by the fairly porous absorber layers.

2.3 Effect of Silver on Hydrogen Electrodes

To determine the effect of silver on the current-potential behavior of hydrogen electrodes, we exposed Teflon-bonded platinum electrodes to 30% KOH which was saturated with AgO. The experiments are conducted on electrodes with 10 mg Pt/cm^2 in a floating configuration. Current potential curves were measured on the fresh electrode and after the electrode has been potentiostatically held at the reversible hydrogen potential for various time intervals (from 30 min to 316 hrs). Figure 4 shows typical results. The polarizations for both hydrogen oxidation and reduction are slightly higher in AgO saturated 30% KOH than in pure 30% KOH.

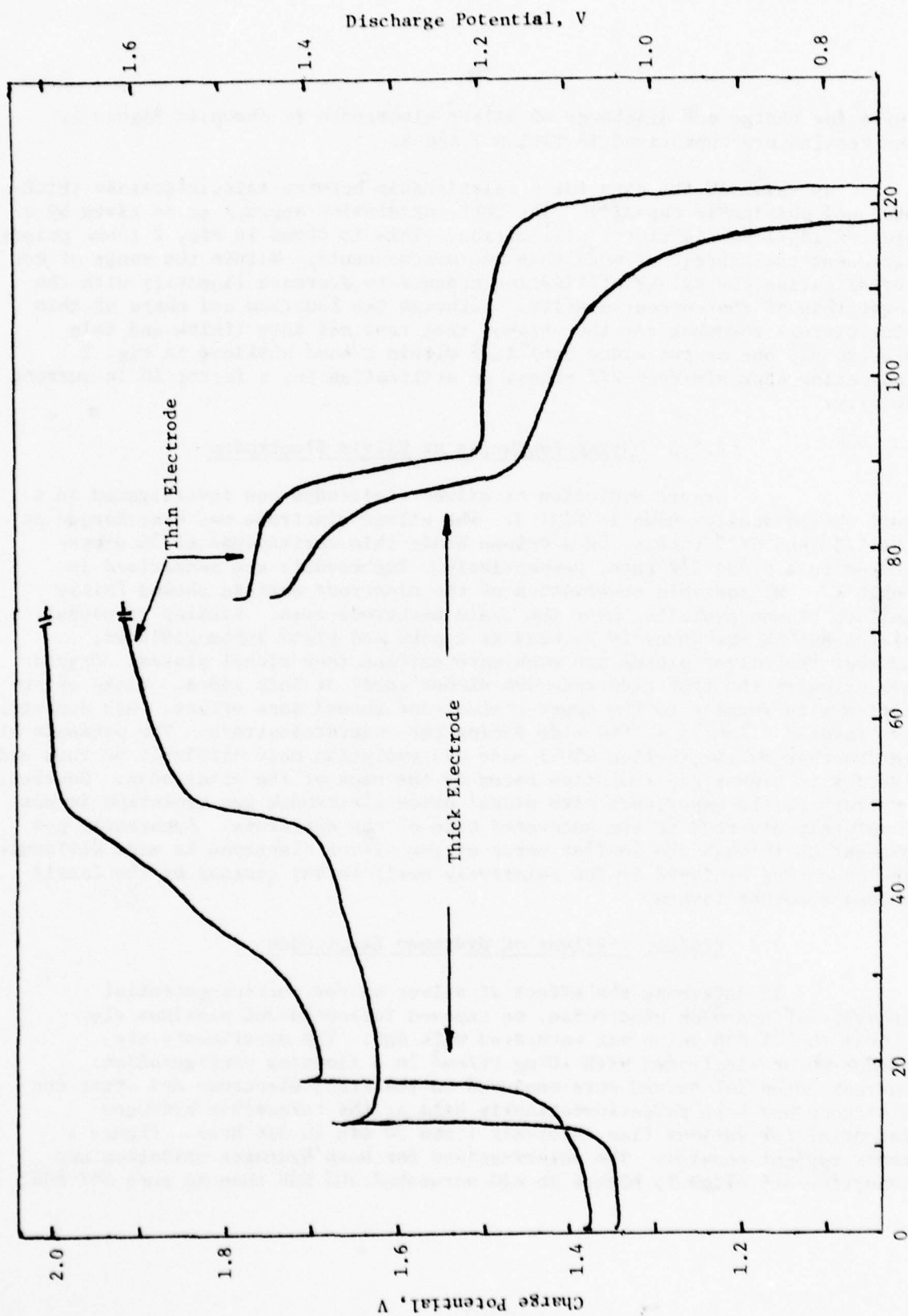


Figure 1. Typical charge-discharge curves of thick (25 mil) and thin (10 mil) Ag electrodes, C-rate, configuration II, 30% KOH, potentials vs. RHE.

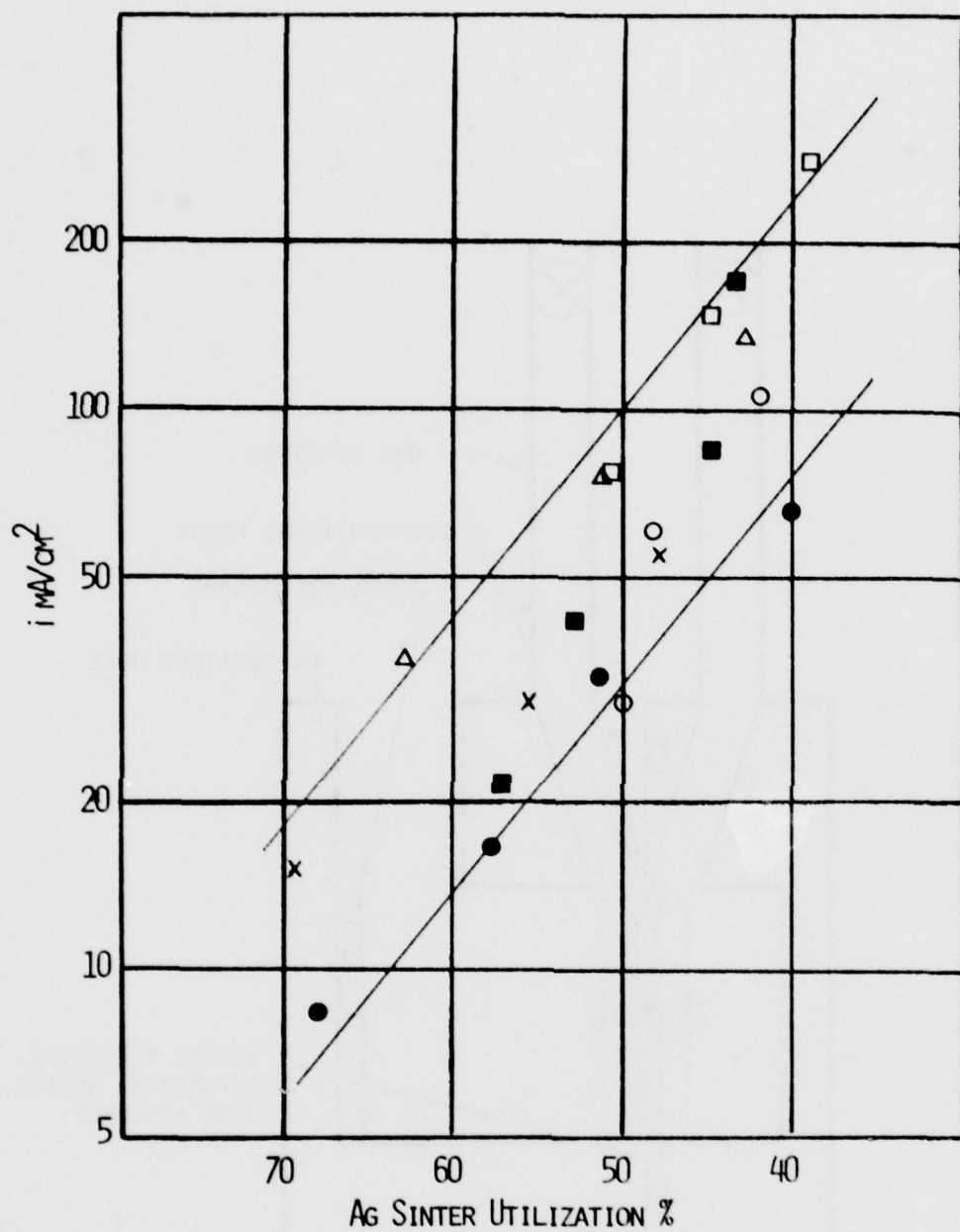


Figure 2. Effect of current density on silver electrode utilization. x thin Conf. I; o, ● thin Conf. II; Δ thick Conf. I, □, ■ thick Conf. II.

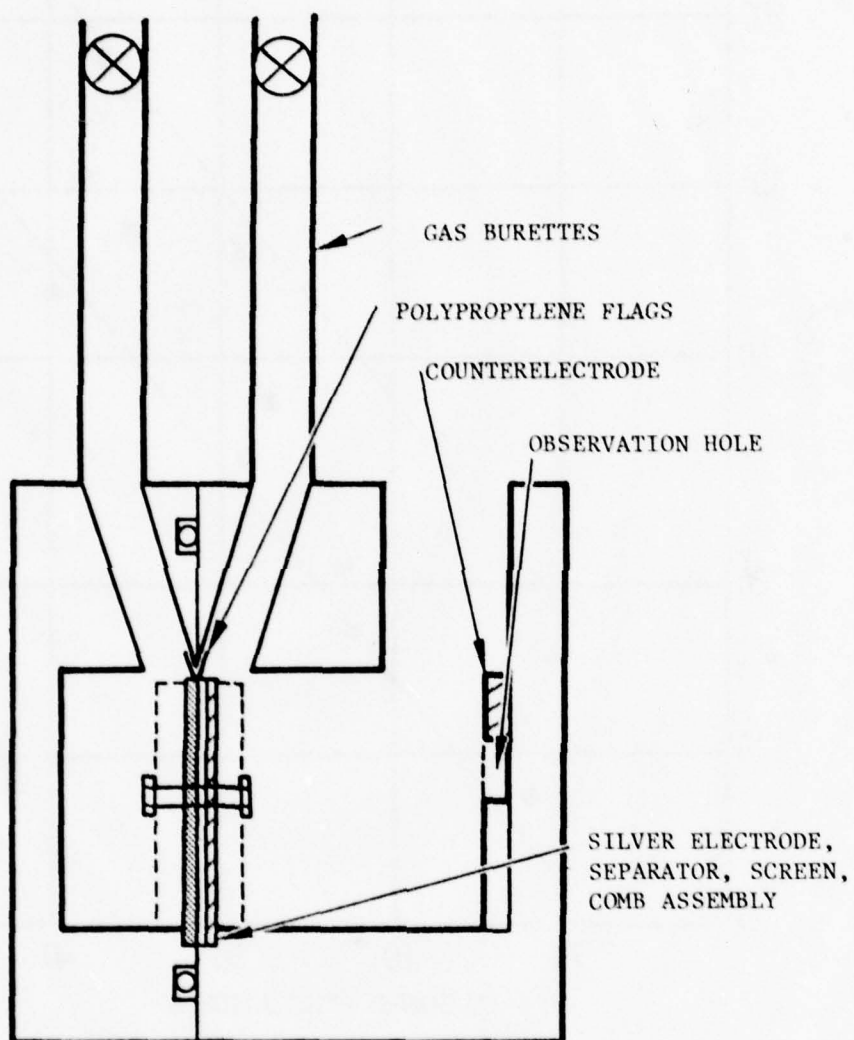


Figure 3. Plexiglas cell for measuring location and rate of oxygen evolution.

TABLE 4
OXYGEN EVOLUTION AT 25 MIL POSITIVE PLATES DURING OVERCHARGE

Configuration	O ₂ Evolution at 2.5 mA/cm ²				O ₂ Evolution at 1.1 mA/cm ²			
	$(\text{cm}^3/\text{sec}, \text{cm}^2) \cdot 10^5$		%		$(\text{cm}^3/\text{sec}, \text{cm}^2) \cdot 10^5$		%	
	Back*	Front*	Back*	Front*	Back*	Front*	Back*	Front*
1. Ag Electrode	5.3	7.3	42.1	57.9	3.0	4.4	40.5	59.5
2. Ag Electrode (reversed)	7.4	7.8	48.7	51.3	3.8	3.1	55.1	44.9
3. Configuration 1 w/2 Pellon 2505 (loose contact)	8.5	7.8	52.1	47.9	3.7	3.4	52.1	47.9
4. Configuration 3 with combs (tight contact)	7.2	5.0	59.0	41.0	3.7	2.0	64.9	35.1

*Location relative to counter electrode. Separators always faced counter electrode.

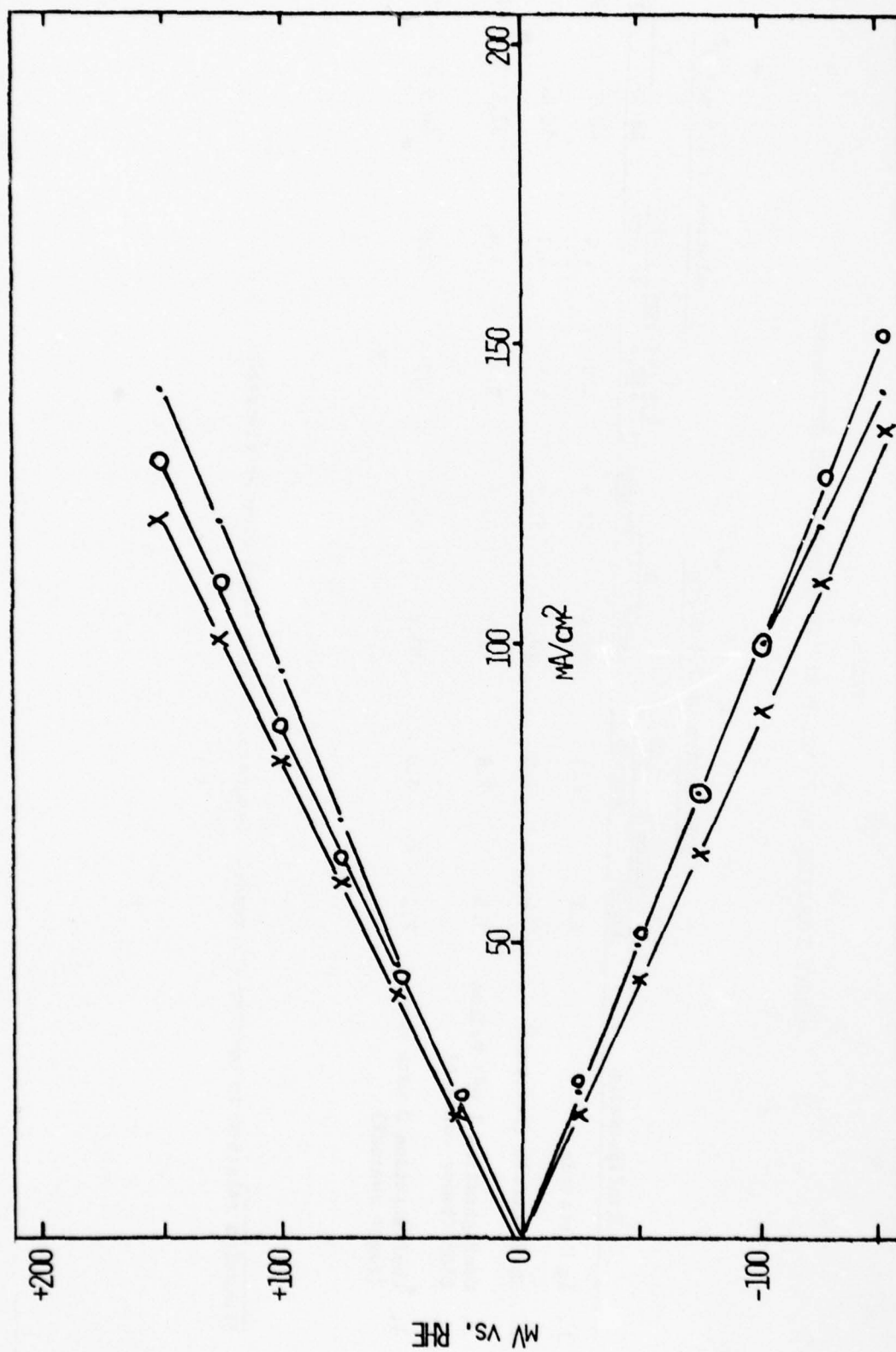
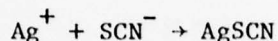


Fig. 4. Hydrogen electrode current voltage curves. (.) in AgO saturated KOH after 47 hrs; (O) in AgO saturated KOH after 68 hrs.

The polarization of the hydrogen electrode did not markedly change with time despite build up of a clearly visible greyish coating of Ag at the electrode surface. Quantitative analysis for Ag was carried out on several electrode samples by dissolution in HNO_3 followed by titration with NH_4SCN . In the presence of silver ions, silver thiocyanate is found:



The end point of the titration is determined by a brownish-red color of $\text{Fe}(\text{SCN})_3$ if a small concentration of ferric ion is used as indicator.

On several samples a large, voluminous mass of spongy silver had deposited on the test electrode. Upon removal from the solution the loosely adhering silver fell off. Chemical analysis showed 1 mg Ag/cm^2 for one and 6 mg Ag/cm^2 for another sample. These findings suggest that the silver plates out in a porous form at the surface of the TFE bonded electrode without penetrating into the interior which remains active for the hydrogen reaction and without significantly blocking electrolyte access.

2.4 Electrolyte Distribution and Retention

Experiments were conducted to determine the electrolyte distribution and retention in saturated and partially saturated component arrays. The experiments were carried out as follows: An array of components (e.g., Ag electrodes, absorber layers, membranes) is mounted at constant pressure (e.g., 0.5 Kg/cm^2) in a spring loaded Teflon jig. It is then vacuum impregnated with 30% KOH. After quick disassembly and component separation the amount of observed electrolyte is determined by the weight change. This is followed by reassembly of the stack under addition of absorbing layers (filter paper). After equilibration for various times (18 to 96 hrs) the new electrolyte distribution is again determined.

Results are summarized in Table 5. The location of electrolyte removal is indicated by an arrow. In addition to the amount and distribution of electrolyte in a fully saturated stack configuration the results show that in a partially saturated array the silver electrode and the NASA separator retain their electrolyte most strongly. After practically all the electrolyte has been removed from the absorber layer (Pellon 2505 or polypropylene 1242-1) the NASA separator and the silver electrode lose electrolyte in approximately equal fractions (see, e.g., Groups V and VI). It is further significant to note that the NASA separator acts as a barrier to rapid electrolyte equilibration. For example Groups II and III show a stable difference in electrolyte between the Pellon layers at both sides of the NASA separator despite an equilibration time of 96 hours. Only prior to electrolyte removal from the NASA separator itself will the more remote absorber layer lose most of its electrolyte.

TABLE 5

TEST ARRAYS FOR ELECTROLYTE ABSORPTION AND RETENTION

Group No.	Components in Stack	(13.4 cm ²) Total		KOH Weight (g)	Electrolyte Distribution (% of Total)	Weight Loss (g)	Distribution of Loss (%)	% Lost of Original KOH in Sample
		Dry Weight (g)	KOH Present					
I	1. H ₂ Electrode	.6382	100.0	.0371	2.8	-	-	-
	2. Pellon 2505	.0893	-	.5080	38.1	-	-	-
	3. NASA Separator	.8351	-	.3857	28.9	-	-	-
	4. Polypropylene, 1242-1	.0947	-	.1384	10.4	-	-	-
	5. Ag Electrode, 10 ml	1.5280	-	.2631	19.7	-	-	-
	1.	-	66.9	.0175	2.0	.0196	4.4	52.8
	2.	-	-	.2676	30.0	.2404	54.6	47.3
	3.	-	-	.3633	40.7	.0224	5.1	5.8
	4.	-	-	.0202	2.3	.1182	26.8	85.4
	5.	-	-	.2233	25.0	.0398	9.0	15.1
II.	1. H ₂ Electrode	.6500	100.0	.0339	1.4	-	-	-
	2. Pellon 2505 (2 pcs)	.1644	-	.9320	37.5	-	-	-
	3. NASA Separator	.8427	-	.3726	15.0	-	-	-
	4. Pellon 2505	.9816	-	.5377	21.6	-	-	-
	5. Ag Electrode, 25 ml	3.8104	-	.6088	24.5	-	-	-
	1.	-	61.6	.0175	1.1	.0164	1.7	48.4
	2.	-	-	.5252	34.3	.4068	42.6	43.6
	3.	-	-	.3554	23.2	.0172	1.8	4.6
	4.	-	-	.0348	2.3	.5029	52.6	93.5
	5.	-	-	.5970	39.0	.0118	1.2	1.9

TABLE 5
(CONTINUED)

Group No.	Components in Stack	(13.4 cm ²)		KOH Present	KOH Weight (g)	Electrolyte Distribution (% of Total)	Weight Loss (g)	Distribution of Loss (%)	% Lost of Original KOH in Sample
		Dry Weight (g)	Total Weight (g)						
III	1. H ₂ Electrode	-	100.0	.0333	2.6	-	-	-	-
	2. Pellon 2505	-	-	.5200	40.1	-	-	-	-
	3. NASA Separator	-	-	.3973	30.6	-	-	-	-
	4. Polypropylene 11242-1	-	-	.1054	8.1	-	-	-	-
	5. Ag Electrode, 10 mil	-	-	.2415	18.6	-	-	-	-
	1.	-	67.0	.0233	2.7	.0100	2.3	30.0	30.0
	2.	-	-	.2266	26.1	.2934	68.6	56.4	56.4
	3.	-	-	.3747	43.1	.0226	5.3	5.7	5.7
	4.	-	-	.0138	1.6	.0916	21.4	86.9	86.9
	5.	-	-	.2312	26.6	.0103	2.4	4.3	4.3
IV	1. H ₂ Electrode	-	100.0	.0335	1.3	-	-	-	-
	2. Pellon 2505 (2 pcs)	-	-	.9436	37.8	-	-	-	-
	3. NASA Separator	-	-	.3818	15.3	-	-	-	-
	4. Pellon 2505	-	-	.5241	21.0	-	-	-	-
	5. Ag Electrode, 25 mil	-	-	.6129	24.6	-	-	-	-
	1.	-	69.3	.0203	1.2	.0132	1.7	39.4	39.4
	2.	-	-	.6728	38.9	.2708	35.4	28.7	28.7
	3.	-	-	.3554	20.5	.0264	3.5	6.9	6.9
	4.	-	-	.0663	3.8	.4578	59.8	87.3	87.3
	5.	-	-	.6159	35.6	(.0030)	(0.4)	(0.5)	(0.5)

() = gain

TABLE 5
(CONTINUED)

Group No.	Components in Stack	(13.4 cm ²) Total		KOH Weight (g)	Electrolyte Distribution (% of Total)	Weight Loss (g)	Distribution of Loss (%)	% Lost of Original KOH in Sample
		Dry Weight (g)	Present					
V	1. H ₂ Electrode	-	100.0	.0269	2.0	-	-	-
	2. Pellon 2505	-	-	.5125	38.8	-	-	-
	3. NASA Separator	-	-	.4005	30.3	-	-	-
	4. Polypropylene, 1242-1	-	-	.1272	9.6	-	-	-
	5. Ag Electrode, 10 mil	-	-	.2544	19.3	-	-	-
	1.	-	41.1	.0178	3.3	.0091	1.2	33.8
	2.	-	-	.0154	2.8	.4971	63.9	97.0
	3.	-	-	.3118	57.4	.0887	11.4	22.1
	4.	-	-	.0045	0.8	.1227	15.8	96.5
	5.	-	-	.1939	35.7	.0605	7.8	23.8
VI	1. H ₂ Electrode	-	100.0	.0269	1.1	-	-	-
	2. Pellon 2505 (2 pcs)	-	-	.9340	37.4	-	-	-
	3. NASA Separator	-	-	.3937	15.8	-	-	-
	4. Pellon 2505	-	-	.5237	21.0	-	-	-
	5. Ag Electrode, 25 mil	-	-	.6202	24.8	-	-	-
	1.	-	39.4	.0181	1.8	.0088	0.6	32.7
	2.	-	-	.0593	6.0	.8747	57.8	93.6
	3.	-	-	.3343	33.9	.0594	3.9	15.1
	4.	-	-	.0241	2.4	.4996	33.0	95.4
	5.	-	-	.5494	55.8	.0708	4.7	11.4

*Arrow marks location of electrolyte removal.

2.5 Electrolyte Transport through Separator Membranes

2.5.1 Description and Definition of Transport Process

The processes occurring in a Ag/H₂ cell are summarized in Fig. 5. During discharge one equivalent of OH⁻ ions per equivalent of charge is consumed at the hydrogen electrode and an equal amount is generated at the silver oxide electrode. At the hydrogen electrode one equivalent of water per equivalent of charge is generated while only half an equivalent is consumed at the cathode. There are three main mechanisms for ion and water transport through the separator membrane: (1) electromigration, (2) diffusion and (3) flow. Electromigration occurs only during current flow. Diffusion of ions and water take place in the presence of concentration gradients (more accurately activity gradients) independent of current flow. Electrolyte flow requires a hydrostatic pressure gradient and is independent of either current or concentration differences. In contrast to the electron flow in metallic conduction, electrical current passes through an electrolyte by movement of ions. Cations (positive ions) move to the cathode (reducing electrode) while anions move in the reverse direction. The fraction of the total electrical current carried by any ionic species is called transference number or transport number of that ionic species. Unless cations and anions happen to have identical mobility the migration of ions will lead to concentration changes in the anode and cathode compartments. In membranes the relative mobility of ions often differs much more than is usually observed in free electrolytes.

By definition transference numbers apply only to charged species and are always equal to or smaller than one. Since ions, however, migrate in a solvated form and cations are generally more strongly solvated than anions, we observe also a transport of solvent which can be formally accounted for by a "transference number" for the solvent. It can have any value.

Solvent transport (in our case water) can also occur by electroosmosis. The term electroosmosis is used for any motion of liquid in an electric field relative to a fixed solid. The basic concept is a solid with an immobile surface charge and a liquid with an equal and opposite space charge of counter ions that move under the influence of an applied electric field tangential to the surface. The electrical force is balanced by a viscous force. Usually the liquid moves to the cathode, motion toward the anode is uncommon.

Strictly speaking, electroosmosis is restricted to convection of liquid by a moving space charge, but this component of the motion is difficult to differentiate from transfer by solvated ions. The effect of electroosmosis is in a first approximation proportional to δ/a where δ is the average thickness of the mobile charged layer and a is a measure for the pore size. For concentrated electrolytes a significant contribution can only be expected in

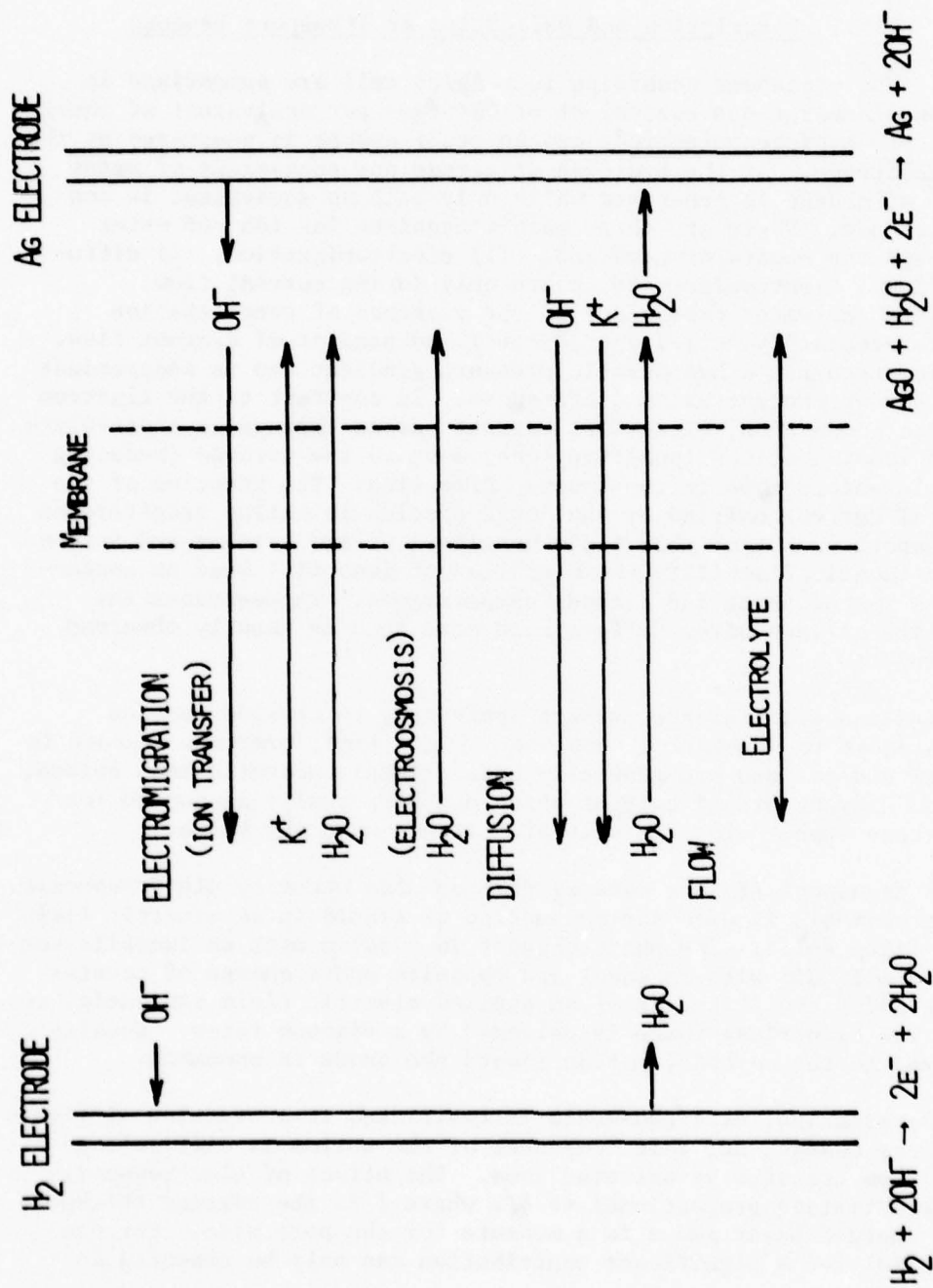


Figure 5. Change of anolyte during discharge in a Ag/H_2 cell.

very small pores. Practical measurements of a "transference number" for water through a membrane would include also electroosmosis effects.

Diffusion processes across the membrane occur in the presence of activity gradients independent of current flow. They can be generally described by Fick's law using appropriate driving forces and diffusion coefficients. The term osmosis describes only a special case where the membrane is impermeable to KOH or one of the ions while permitting water transfer.

In the presence of hydrostatic pressure gradients we can expect further electrolyte flow which is independent of current or concentration differences. In a Ag/H₂ cell electrolyte flow inducing gradients will result from capillary forces if one side of the membrane is in contact with an electrolyte saturated absorber component while the other side is electrolyte starved. We will use the term "back wicking" for this phenomenon.

2.5.2 Diffusion and Electromigration of KOH and H₂O

2.5.2.1 Experimental

The general approach consists of measuring water and ion transport through a membrane in the absence and presence of current flow. More specifically this involves monitoring of concentration and volume changes in a chamber separated by the membrane to be characterized from a solution of constant known composition.

The measurement half cell is schematically shown in Fig. 6. A double wall glass vessel of about 1000 ml capacity, serves as the outer, large volume half of the diffusion cell. Water from a circulating thermostat maintains a set temperature. A magnetic stirrer assures uniform electrolyte concentration. The density change in the small, inner half cell can be measured by the weight change of the sinker, which is suspended from one-arm of a balance on a thin nylon thread. The volume change in the inner half-cell due to osmosis and/or electroosmosis can be observed in the capillary, which consists of part of a two ml graduated pipet of about 3.5 mm inner diameter.

For diffusion measurements the KOH concentration in the two half cells were different and the equilibration process was monitored. The bulk of the transport measurements was taken over the time span of an hour using two layers of separator membrane. This has several implications: Volume and density changes are linear with time since the concentration change is small compared to the concentration difference across the membrane ($\leq 10\%$). Further, the use of two membranes eliminates possible distortion of the results by membrane faults (e.g., holes).

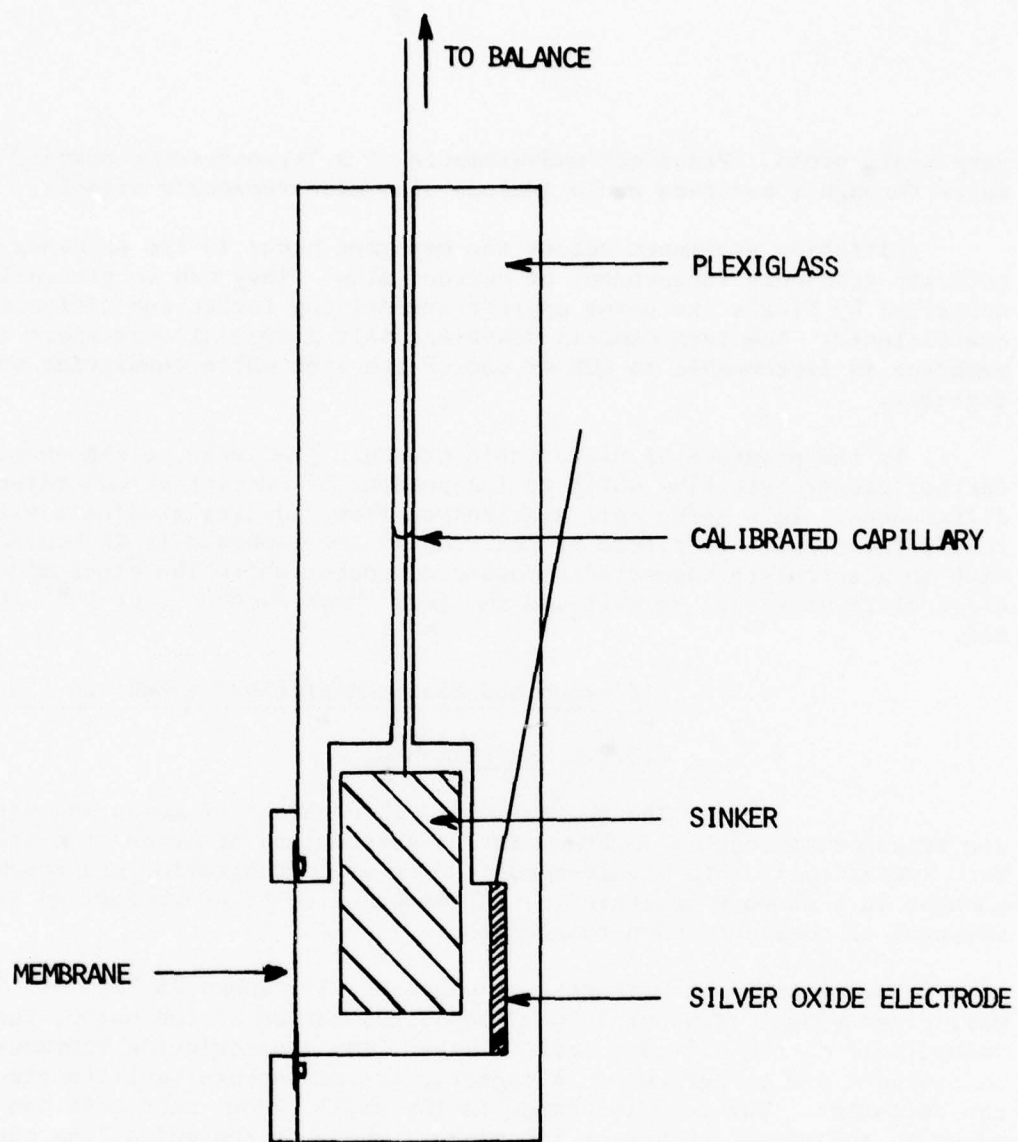


Figure 6. Schematic of half cell for the measurement of water and KOH transport through membranes.

For the measurement of electromigration the initial KOH concentration in the two half cells was identical. A current (charge and discharge) was passed between the Ag electrode in the measurement half cell. Typically, the current density was 64 mA/cm², corresponding approximately to the C rate for a 25 mil Ag electrode.

Four types of separators were evaluated: Permion 2193, Permion 2291 (RAI Corp.), Visking (Union Carbide Corp.) and an inorganic NASA separator. Measurements were carried out at different temperatures and KOH concentration. Typical data obtained during an experimental run are shown in Figs. 7 and 8.

2.5.2.2 KOH and H₂O Diffusion

From Fick's law the amount of material diffusing through a membrane of exposed area, A, under steady-state conditions is given by

$$\frac{1}{A} \frac{d(CV)}{dt} = D \frac{(C' - C)}{\Delta x} \quad (1)$$

where C and V are the concentration and volume respectively of the particular chamber under consideration, D is the diffusion coefficient, and Δx is the membrane thickness. If good mixing of the chamber contents is maintained, the singular concentration gradient $(C' - C)$ appears across the membrane.

It should be specifically pointed out that the driving force for diffusion is the difference in activity rather than in concentration. In more concentrated KOH this difference is quite significant. For example, the activity coefficient for KOH in a 40% electrolyte (molal) is 10. In the following treatment and for the proposed measurements, we used concentrations instead of activities which means that the difference between activation and concentration appears in the diffusion coefficient which will show a concentration dependence.

In order to determine diffusion constants for both KOH and H₂O, two sets of measurements have been made: change in solution volume and change in solution density. The change in volume is readily related to the difference between the diffusion constants:

$$\frac{dn_w}{dt} = D_w'' (C'_w - C_w) \quad (2)$$

$$\frac{dn_k}{dt} = D_k'' (C'_k - C_k) \quad (3)$$

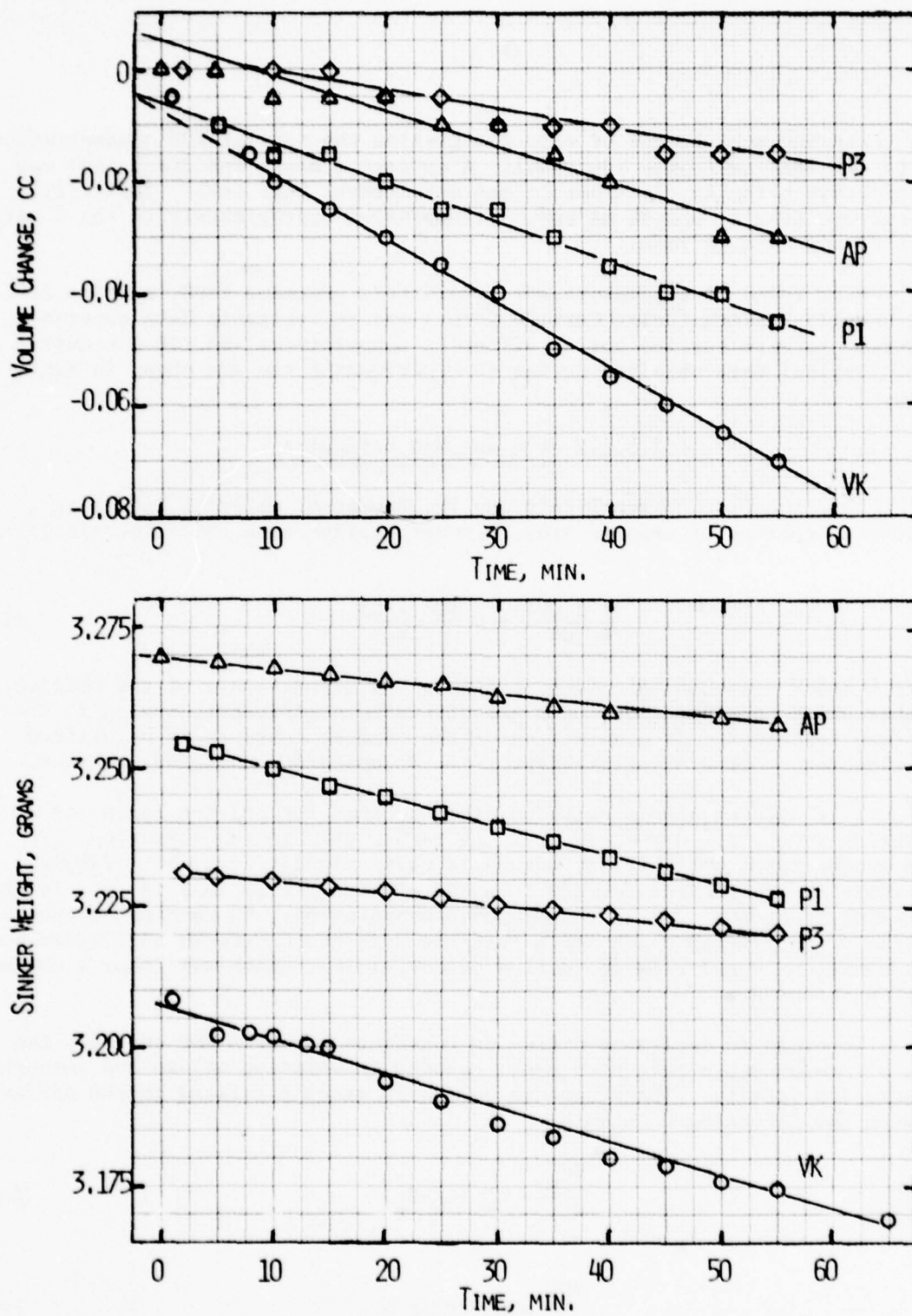


Figure 7. Characteristic volume and density changes due to H_2O and KOH diffusion, 40% KOH inside, 50% KOH outside, $25^\circ C$.
 AP = NASA separator, P1 = Permion 2291, P3 = Permion 2193, VK = Visking.

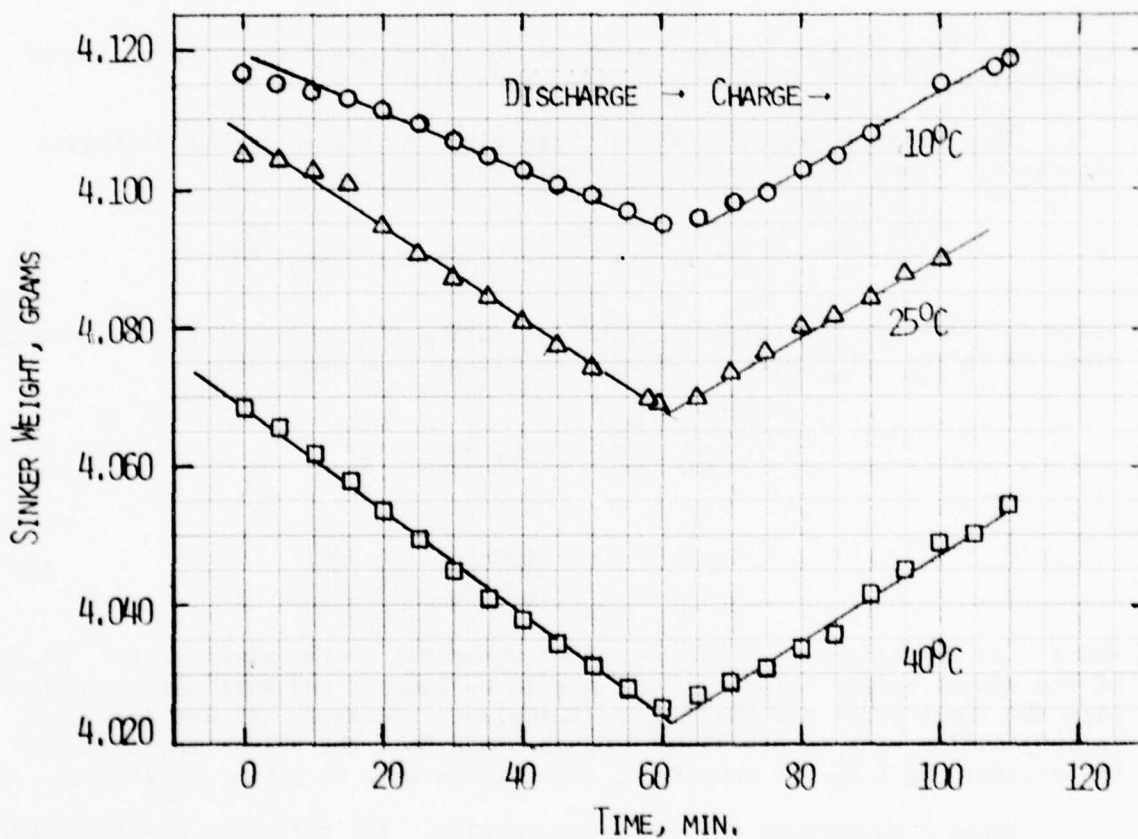
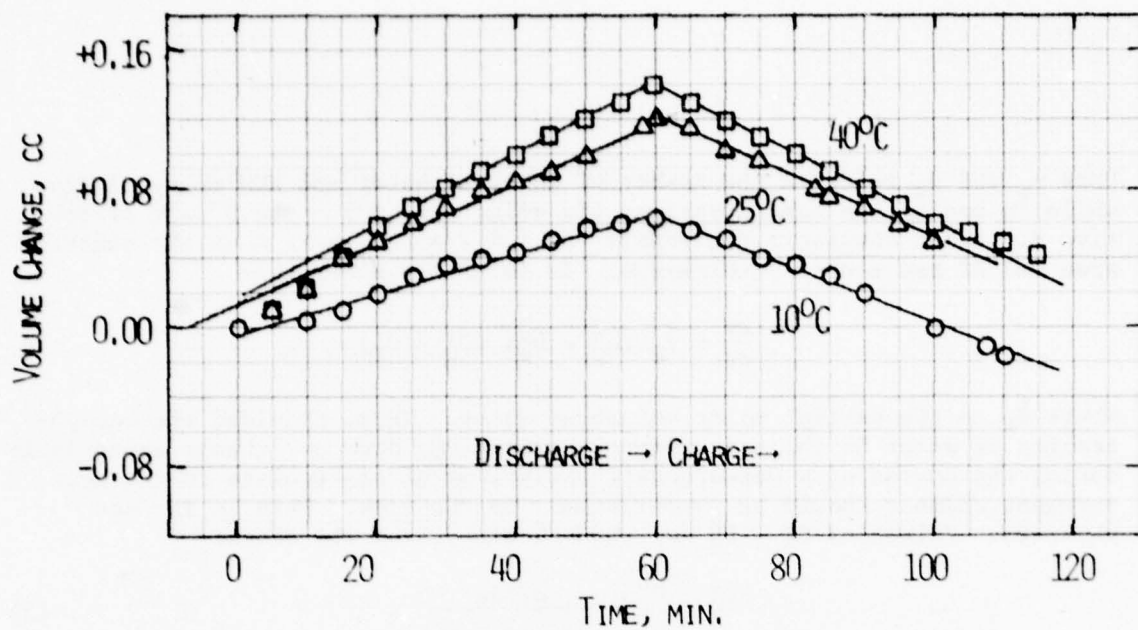


Figure 8. Characteristic volume and density changes due to electro-migration. NASA separator, 20% KOH, 64 mA/cm².

Here n_w and n_k refer to the number of moles of water and KOH respectively, while C_w and C_k are concentrations (in moles per cm^3). The D'' are effective diffusion constants (cm^2/min): $D'' = D \cdot A/\Delta X$, where A is the membrane area and ΔX the membrane thickness. It is easily shown that

$$\frac{dV}{dt} = \bar{V}_w (D''_w - D''_k) (C'_w - C_w) \quad (4)$$

where \bar{V}_w is the partial molar volume of water. Thus, provided the concentration of water in the measurement chamber (C_w) does not change appreciably during the course of a measurement, the volume of electrolyte in the measurement chamber should be proportional to the time. This is in fact observed. Values of $D''_w - D''_k$ are then obtained from the slope:

$$D''_w - D''_k = \frac{dV/dt}{\bar{V}_w (C'_w - C_w)} \quad (5)$$

Typically, $\bar{V}_w \simeq 17.4 \text{ cm}^3/\text{mole}$; values of \bar{V}_w , \bar{V}_k , C_w , and C_k as functions of temperature and KOH concentration were calculated.

The change in solution density can also be related to the diffusion constants. From (2) and (3) it is possible to show that

$$2 \frac{d \ln (C'_w - C_w)}{dt} = - \frac{D''_w + D''_k}{V} + (2C_w \bar{V}_w - 1) \left(\frac{D''_w - D''_k}{V} \right) \quad (6)$$

Since C_w and V are approximately constant during the course of a measurement, plots of $\ln (C'_w - C_w)$ versus t should be linear. In addition,

$$\frac{d \ln (C'_w - C_w)}{dt} = - \frac{1}{C'_w - C_w} \frac{d C_w}{dt} \quad (7)$$

$$= \frac{\text{const}}{C'_w - C_w} \frac{d\rho}{dt} \frac{dw}{dt} \quad (8)$$

where w is the weight of a Teflon sinker submerged in the electrolyte. Plots of the sinker weight versus t are found to be linear, and were used to calculate the slope dw/dt and hence $d \ln (C'_w - C_w)/dt$. Equation (6) was then used, in conjunction with values of $D''_w - D''_k$ obtained from the volume measurements, to calculate $D''_w + D''_k$. A summary of the calculations is given in Table 6.

Table 7 summarizes the diffusion results. The diffusion coefficients are average apparent values for the membranes which, especially for the multi-

TABLE 6

SUMMARY OF DATA AND CALCULATIONS FOR MEMBRANE DIFFUSION COEFFICIENTS

Run No. *	C'_W (moles/l)	C_W (moles/l)	dV/dt (10^{-3} cm ³ /min)	$D''_W K$ (cm ³ /min)	Membrane Thickness (cm)	dw/dt (10^{-4} g/min)	$-d \ln (C'_W - C_W)/dt$ (10^{-3} min ⁻¹)	$D''_W + D''_K$ (cm ³ /min)
P3 102	52.98	50.67	0.55	0.014	0.01522	7.00	1.65	0.033
P3 252	52.56	50.30	1.03	0.026	0.01522	6.84	2.37	0.052
P3 402	52.39	50.22	1.27	0.033	0.01522	6.84	2.98	0.066
P3 104	47.00	50.42	0.00	0.00	0.01522	6.85	0.68	0.009
P3 254	46.70	50.04	0.00	0.00	0.01522	7.01	1.13	0.016
P3 404	46.40	49.69	0.00	0.00	0.01522	7.15	2.41	0.034
P3 255	43.67	47.71	-0.35	0.005	0.0152	7.85	0.43	0.010
P1 102	53.02	50.92	1.43	0.039	0.0051	7.04	0.39	0.035
P1 252	52.73	51.01	1.57	0.052	0.0051	7.13	0.38	0.047
P1 402	52.46	50.51	3.33	0.097	0.0051	7.00	0.78	0.087
P1 104	47.54	50.76	-1.00	0.018	0.0051	6.97	1.02	0.028
P1 254	47.22	50.24	-1.33	0.025	0.0051	6.96	2.52	0.050
P1 404	47.03	49.79	-0.38	0.008	0.0051	6.96	3.81	0.059
P1 255	44.005	47.69	0.70	0.011	0.005	7.67	1.24	0.013
AP 102	52.85	50.64	0.00	0.00	0.0902	7.70	0.85	0.013
AP 252	52.59	50.48	-4.33	-0.117	0.0902	7.60	1.27	?
AP 402	52.26	49.87	0.92	0.022	0.0902	7.74	1.06	0.033
AP 104	47.55	50.58	-1.00	0.019	0.0902	7.66	0.42	0.021
AP 254	47.20	50.17	-0.88	0.017	0.0902	7.66	0.86	0.026
AP 404	46.86	49.92	-0.83	0.016	0.0902	7.68	1.88	0.035
AP 255	44.26	48.06	-0.53	0.008	0.0902	7.77	0.47	0.013
VK 102	52.92	50.78	1.00	0.027	0.0229	7.12	5.91	0.105
VK 252	52.68	50.41	1.60	0.060	0.0229	7.16	4.87	0.116
VK 402	52.32	50.26	2.55	0.070	0.0229	7.20	6.52	0.148
VK 104	47.40	50.32	-2.32	0.046	0.0229	7.63	1.39	0.055
VK 254	46.95	50.00	-2.05	0.038	0.0229	7.02	1.93	0.056
VK 404	46.70	49.29	-2.30	0.050	0.0229	7.01	3.62	0.088
VK 255	44.50	47.55	-1.14	0.021	0.0229	7.76	1.92	0.044

*P3 = Permion 2193; P1 = Permion 2291; AP = NASA Separator; VK = Visking.

Last digit = outer KOH concentration/10; middle digit = temperature.

Inner KOH concentration \approx 30% in all runs.

TABLE 7

DIFFUSION COEFFICIENTS FOR H₂O AND KOH IN VARIOUS MEMBRANES

Component	Temp. (°C)	~ 45% KOH				~ 35% KOH				~ 25% KOH			
		(50% KOH Out 40% KOH In)		(40% KOH Out 30% KOH In)		(20% KOH Out 30% KOH In)		(20% KOH Out 30% KOH In)		(20% KOH Out 30% KOH In)		(20% KOH Out 30% KOH In)	
		D'_H (cm ³ min ⁻¹)	D'_K ($\times 10^{-6}$ cm ² sec ⁻¹)	D_H ($\times 10^{-6}$ cm ² sec ⁻¹)	D_K ($\times 10^{-6}$ cm ² sec ⁻¹)	D'_H (cm ³ min ⁻¹)	D'_K ($\times 10^{-6}$ cm ² sec ⁻¹)	D_H ($\times 10^{-6}$ cm ² sec ⁻¹)	D_K ($\times 10^{-6}$ cm ² sec ⁻¹)	D'_H (cm ³ min ⁻¹)	D'_K ($\times 10^{-6}$ cm ² sec ⁻¹)	D_H ($\times 10^{-6}$ cm ² sec ⁻¹)	D_K ($\times 10^{-6}$ cm ² sec ⁻¹)
Visking	10					0.033	0.003	6.23	0.62	0.043	0.025	8.11	4.78
						0.026	0.003	5.05	0.62				
	25	0.021	0.007	4.02	1.35	0.030	0.006	5.80	1.08	0.057	0.018	10.86	3.42
NASA Separator	40					0.044	0.012	8.50	2.30	0.070	0.025	13.47	4.78
						0.041	0.012	7.83	2.30				
	10					0.013	0.001	9.65	0.39	0.005	0.004	4.09	2.86
Permion No. 2291	25	0.006	0.001	4.85	0.97	0.014	0.003	10.40	2.21	0.013	0.004	9.65	2.86
						0.016	0.006	12.22	4.70	0.017	0.004	13.29	2.86
	40					0.015	0.003	0.63	0.14	0.035	0.016	1.47	0.69
Permion No. 2193	25	0.012	0.005	0.52	0.22	0.024	0.008	1.04	0.35	0.053	0.017	2.26	0.70
						0.021	0.017	0.92	0.70	0.075	0.031	3.21	1.30
	40					0.003	0.003	0.38	0.30	0.015	0.006	1.93	0.80
Permion No. 2193	25	0.005	0.002	0.61	0.20	0.005	0.005	0.64	0.64	0.025	0.008	3.21	1.07
						0.011	0.011	1.39	1.39	0.032	0.010	4.08	1.35
	40												

D' = Apparent diffusion coefficient for one membrane layer.

component membranes, P2193 and the NASA separator are not representative of the actual diffusion behavior within the membrane. We have, therefore, listed also the diffusion parameter D' for one membrane layer which appears more appropriate for practical use. Diffusion transport is similar for all four membranes; on a per membrane basis, it is somewhat greater in Visking and Permion 2291 than in P2193 and the NASA separator. A calculation showed that the diffusion coefficients are sufficiently large to prevent the build up of significant concentration gradients during normal operation of Ag/H₂ cells. Diffusional transport is higher at the lower KOH concentrations. The temperature dependence of the diffusion coefficients is more clearly visible in the Arrhenius plots in Figs. 9 and 10. The activation energy for KOH diffusion is comparable in all membranes and appears to increase significantly with increasing KOH concentration. A similarly strong effect of KOH concentration is not visible for the diffusion of water. In all membranes water diffuses more rapidly than KOH. The diffusion coefficients for water are on average 3 times larger than those of KOH. This causes, during equilibration of a concentration difference across one of the investigated membranes, a net flow of electrolyte from the side of more dilute KOH to the side of more concentrated KOH. As we will discuss in more detail later this has important implications on electrolyte transport and thus Ag/H₂ cell operation.

2.5.2.3 KOH and H₂O Transfer

In order to obtain the electrolyte transference numbers t_+ , t_- , and t_w , measurements were made of both the density and volume of a section of KOH solution separated from the main body of the solution by a membrane. A 0.200 ampere current was passed through the membrane for an hour, following which the direction of the current was reversed, and observations on the density and volume were continued for another hour. To the experimental accuracy, dV/dt and $d\rho/dt$ were constant during each one hour period. However, neither dV/dt nor $d\rho/dt$ was the same on charge and discharge, and there was no clear relationship between their magnitudes and the signs of the current.

The flow of H₂O and KOH through a membrane can be expressed by the equations

$$\frac{dn_w}{dt} = D_w'' (C_w' - C_w) + ki \left(\frac{1}{2} - t_w \right) \quad (9)$$

$$\frac{dn_K}{dt} = D_K'' (C_K' - C_K) - ki t_k \quad (10)$$

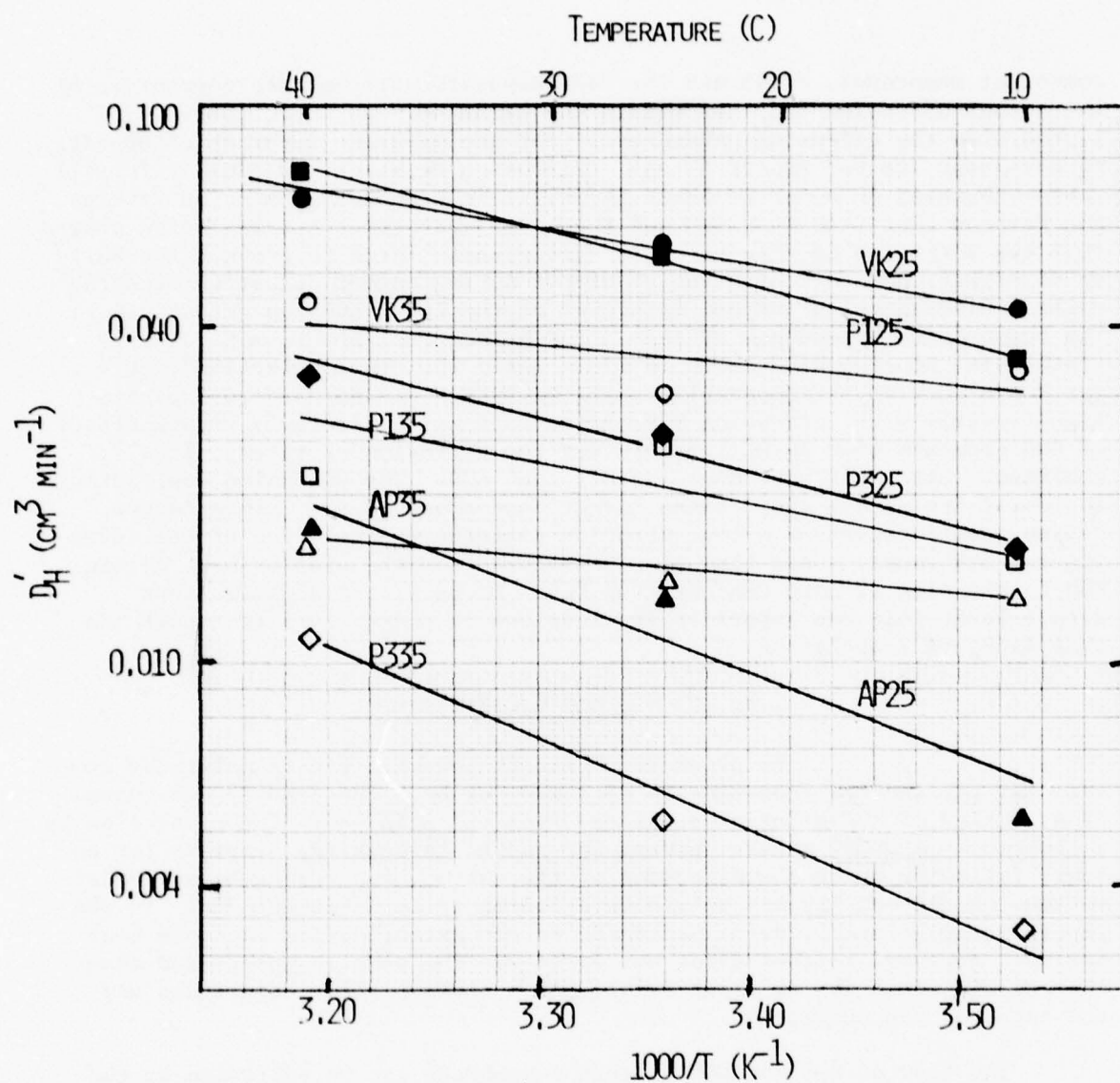


Figure 9. Diffusion of water in various membranes as a function of temperature and electrolyte concentration. (D_H' apparent diffusion coefficient of H_2O per membrane layer).

P3 = Permion 2193; P1 = Permion 2291; AP = NASA Separator; VK = Visking. Last digits = effective KOH concentration.

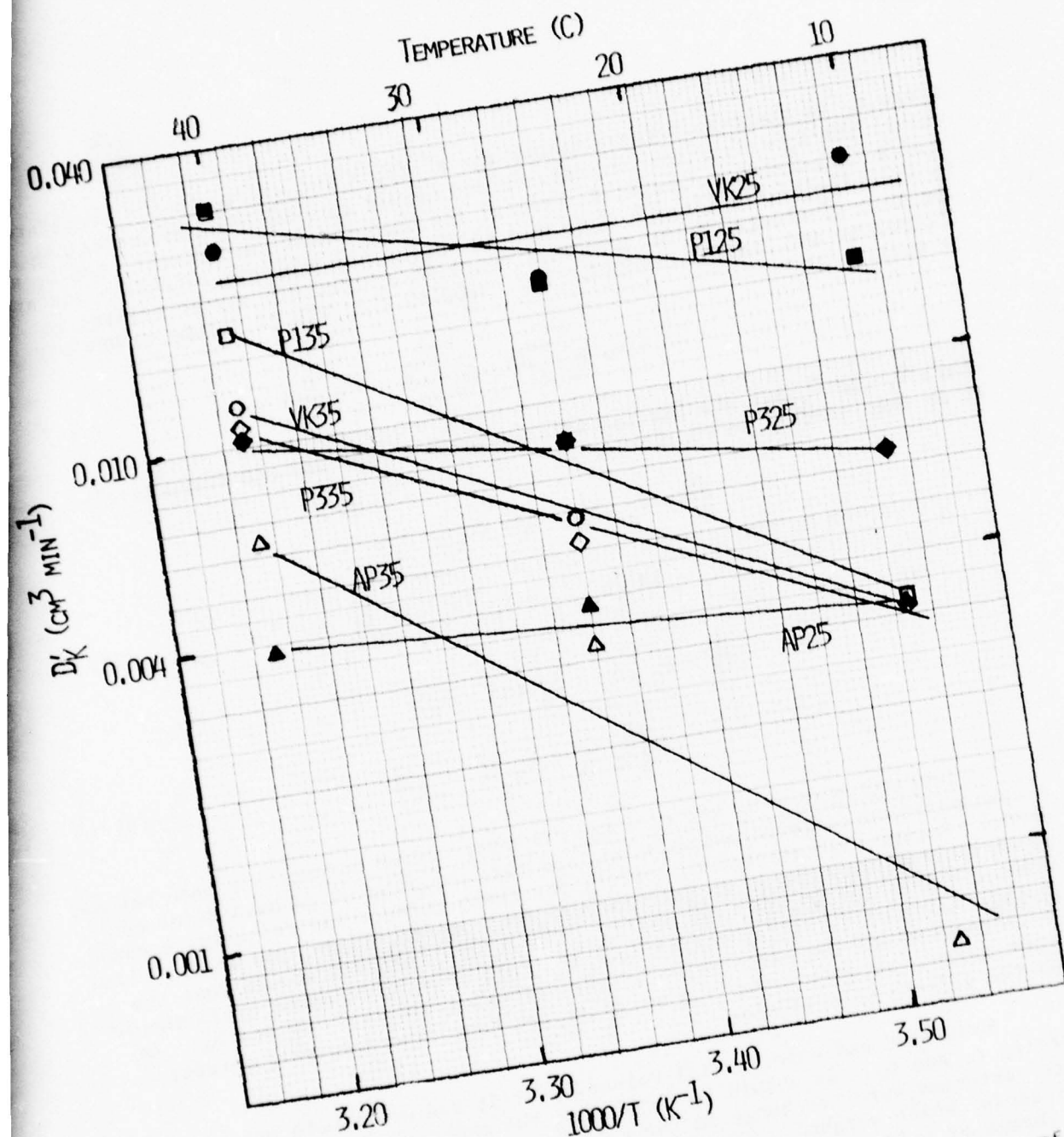


Figure 10. Diffusion of KOH in various membranes as a function of temperature and electrolyte concentration. (D_K^* apparent diffusion coefficient of KOH per membrane layer).
P3 = Permion 2193; P1 = Permion 2291; AP = NASA Separator;
VK = Visking. Last digits = effective KOH concentration.

where t_K is the transference number for K^+ ($t_K = 1 - t_{OH}$), t_W is the transference number for H_2O , i is the current, C_W and C_K are H_2O and KOH concentrations inside (unprimed) and outside (primed) the measurement compartment, and D_K'' and D_W'' are effective diffusion constants corrected for membrane thickness and area. The rate of change of the number of moles of H_2O and KOH may be related to the volume and density changes. For example, the rate of volume change may be written as

$$\frac{dV}{dt} = \bar{V}_K \frac{dn_K}{dt} + \bar{V}_W \frac{dn_W}{dt} \quad (11)$$

where \bar{V}_K and \bar{V}_W are the partial molar volumes of KOH and H_2O respectively. It is then readily shown that

$$\begin{aligned} \frac{dV}{dt} &= \bar{V}_K (D_K'' - D_K') (C_K' - C_K) \\ &\quad - ki \left[\bar{V}_K t_K - \bar{V}_W \left(\frac{1}{2} - t_W \right) \right] \end{aligned} \quad (12)$$

or

$$\begin{aligned} \frac{dV}{dt} &= \bar{V}_W (D_W'' - D_W') (C_W' - C_W) \\ &\quad - ki \left[\bar{V}_K t_K - \bar{V}_W \left(\frac{1}{2} - t_W \right) \right] \end{aligned} \quad (13)$$

Initially, $C_W' = C_W$ and $C_K' = C_K$. However, after current has been passed, a concentration difference builds up, and this contributes to both dV/dt and $d\rho/dt$. Rather than attempt to correct for these effects analytically, a computer program was written to calculate dn_W/dt , dn_K/dt , dV/dt , and $d\rho/dt$, given assumed values for D_W'' , D_K'' , t_K , and t_W . Use of this program showed that the average value of dV/dt (or $d\rho/dt$) over the full charge/discharge cycle should be independent of the exact value of the diffusion constants D_K'' and D_W'' . In other words, reversing the current after one hour experimentally corrects for the effects of diffusion

Predicted and experimental values of dV/dt and $d\rho/dt$ were matched by varying t_K and t_W . It should be noted that the experimental values of dV/dt were corrected for the change in the void volume of the Ag electrode. The electrode, which weighed 0.83g, had a 0.20 cm^3 volume. At 200 ma, the rate of change of void volume is $.00040 \text{ cm}^3/\text{minute}$, which must be added to the absolute value of observed rate of volume change to obtain the rate of volumetric flow across the membrane.

Calculated transport numbers for H_2O and K^+ at 10° , 25° , and $40^\circ C$, and in 20%, 30% and 40% KOH are given in Table 8 for each of the four membranes studied. The estimated average error in the determinations is ± 0.05 for t_{H_2O} and ± 0.03 for t_{K^+} . This error is sufficiently large to obscure the temperature dependence of the transport numbers, which in any case is not expected to be large. On average t_{K^+} and t_{H_2O} increase by approximately 0.003 per degree (i.e., 0.09 between 10° and $40^\circ C$). Table 9 shows the average values of t_{K^+} and t_{H_2O} at each KOH concentration. These data clearly show major differences among the membranes, and the dramatic decreases in t_{H_2O} with increasing KOH concentration. Values of t_{K^+} also decrease rapidly for the Permion membranes, but no effect of KOH concentration is noted for the other two membranes. In qualitative terms, two other major trends may be summarized as follows:

- Values of t_{K^+} are substantially greater in the membranes than in free solution, where $t_{K^+} = 0.22$ from 3N to 12N KOH. The exceptionally large value of t_{K^+} in the Permion membranes are probably related to the cationic exchange properties of these membranes, which enhance K^+ transport. In concentrated KOH solutions (40%), differences among membranes are much smaller.
- Values of t_{H_2O} are also substantially larger for the Permion membranes, although the difference among membranes are again much smaller in 40% KOH.

As we will show later, transport numbers for K^+ and H_2O are important in determining the suitability of a barrier membrane; in general, to minimize electrolyte transport and, hence, the mass of electrolyte needed, t_{K^+} and t_{H_2O} should both be small.

Measurements of t_{K^+} and t_{H_2O} for Visking have previously been carried out by Shaw and Remanick.² Their values of t_{K^+} ranged from 0.31 in 20% KOH to 0.28 in 40% KOH, in reasonable agreement with the results given in Tables 8 and 9. However, their values of t_{H_2O} are consistently larger than those reported here: in 20%, 30% and 40% KOH, the comparative values are 1.7 (1.0), 1.1 (0.8) and 0.7 (0.6) respectively, with values from Table 9 given in parentheses. We have attempted to trace these discrepancies to the observed rates of volume and density change, and have determined that the differences can be explained by assuming that there is a discrepancy in the rate of volume change but no discrepancy in the rate of density change. It appears that in the experiments carried out by Shaw and Remanick, the rates of volume change were ca. 40% larger than what we observed. However, we are unable to explain why this should be so.

2.5.3 Back Wicking

In a component package consisting of relatively "dry" absorber layers on one side of a membrane and relatively "wet" absorber

TABLE 8
TRANSPORT NUMBERS FOR H_2O AND K^+

Membrane	KOH Conc. Wt %	Temperature °C					
		10		25		40	
		t_{H_2O}	t_{K^+}	t_{H_2O}	t_{K^+}	t_{H_2O}	t_{K^+}
Visking	20	0.99	0.33	0.90	0.38	1.04	0.39
	30	0.81	0.26	0.90	0.27	0.71	0.29
	40	0.57	0.25	0.66	0.30	0.52	0.42
NASA Separator	20	1.10	0.24	1.24	0.30	1.29	0.33
	30	0.78	0.28	0.82	0.30	0.87	0.38
	40	0.48	0.21	0.72	0.32	0.78	0.30
Permion 2193	20	1.60	0.42	1.56	0.47	1.84	0.57
	30	1.06	0.33	1.04	0.39	1.13	0.40
	40	0.74	0.26	0.75	0.29	0.82	0.35
Permion 2291	20	1.73	0.61	1.95	0.58	1.94	0.64
	30	1.27	0.43	1.26	0.44	1.22	0.51
	40	0.79	0.32	0.80	0.36	0.76	0.42

TABLE 9
AVERAGE OF TRANSPORT NUMBERS AT 10, 25 AND 40°C

Transport Number	Membrane	KOH Concentration %		
		20	30	40
t_{H_2O}	Visking	0.98	0.81	0.58
	NASA Sep.	1.21	0.82	0.66
	2193	1.67	1.08	0.77
	2291	1.87	1.25	0.78
t_{K^+}	Visking	0.37	0.28	0.32
	NASA Sep.	0.29	0.32	0.27
	2193	0.48	0.38	0.30
	2291	0.61	0.46	0.37

layers on the other side of the membrane electrolyte transport will occur in the hydrostatic pressure gradient caused by capillary action. We conducted measurements to evaluate this effect. Initial experimentation employed component stacks of different relative electrolyte saturation separated by the membrane of interest. Electrolyte transfer was determined by periodic disassembly and monitoring of the weight change in the various components. We were unable to obtain consistent and reliable results by this technique. Therefore, experiments were set up to measure the rate of back wicking in an experimental configuration under Ag/H₂ cell conditions. Specifically, we determined the degree of electrolyte re-equilibration as a function of time across a membrane after drying the absorber layer by unidirectional current flow. The cell arrangement is shown schematically in Fig. 11. The use of a gas electrode instead of the silver plate allows unidirectional operation without restriction of electrode capacity.

The component size is 1-1/2" × 2" except for the membrane which is 1-3/4" × 2-1/2" (19.35 and 28.2 cm², respectively). The stack is compressed with springs to a compression of ~4 psi, vacuum impregnated and drained. The stack was charged in a closed container in air at ~50 mA/cm² to drive electrolyte to the negative side of the cell (i.e., dry out the asbestos). "Dryness" is observed by an increase in the potential of the charge curve. Various times at open circuit are allowed for re-equilibration to occur before the cell is charged again. The charge time necessary to reach the same degree of cell polarization (dryness) can be related to the amount of back wicked electrolyte. After a few initial experiments the test set up was changed to include a wick to the pellaon side from a supply of 40% KOH below the cell. This assured constant electrolyte saturation of the pellaon reservoirs. By disassembling and weighing of the asbestos layer after impregnation, after "drying" due to current flow and after various re-equilibration times we obtained a more quantitative correlation between the back wicking rate and the relative separator saturation with electrolyte.

A typical example of voltage-time traces is shown in Fig. 12. The experimental data are summarized in Table 10. Figure 13 shows the back wicking rate as a function of electrolyte saturation for Visking and Pellaon 2193. The back wicking rate is relatively high at low electrolyte saturation but declines very rapidly as the separator becomes "wetted". Above 80% electrolyte saturation in the asbestos the driving force is so small that the rate of back wicking becomes totally insignificant. For comparison the rate of "drying" at 50 mA/cm² is approximately 200·10⁻⁴g hr⁻¹cm⁻² for Visking and 400·10⁻⁴g hr⁻¹cm⁻² for P2193. Significant hydrogen electrode polarization occurs after "drying" of the asbestos to about 60-70% saturation. The rate of electrolyte back wicking for the NASA separator could not be measured by this technique. It was found to be too high (>5·10⁻²g h⁻¹cm⁻²) so that the large ohmic polarization due to extreme drying did not occur. The use of higher current densities leads to thermal control problems.

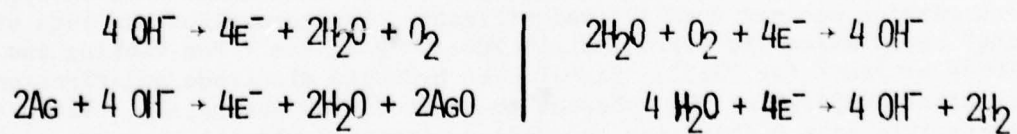
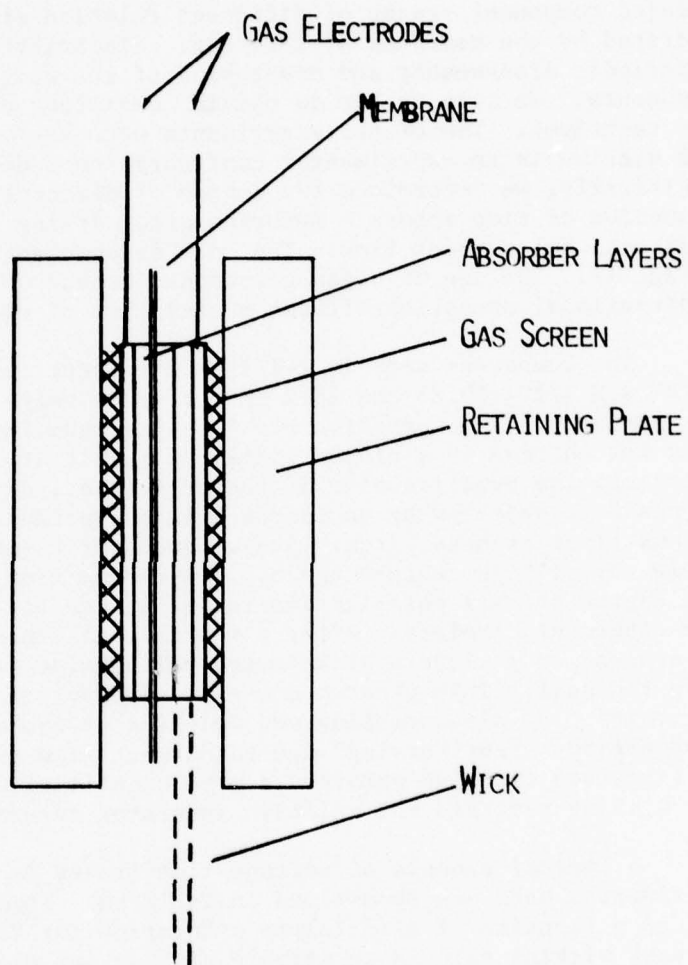


Figure 11. Schematic of back wicking cell and corresponding electrode reactions.

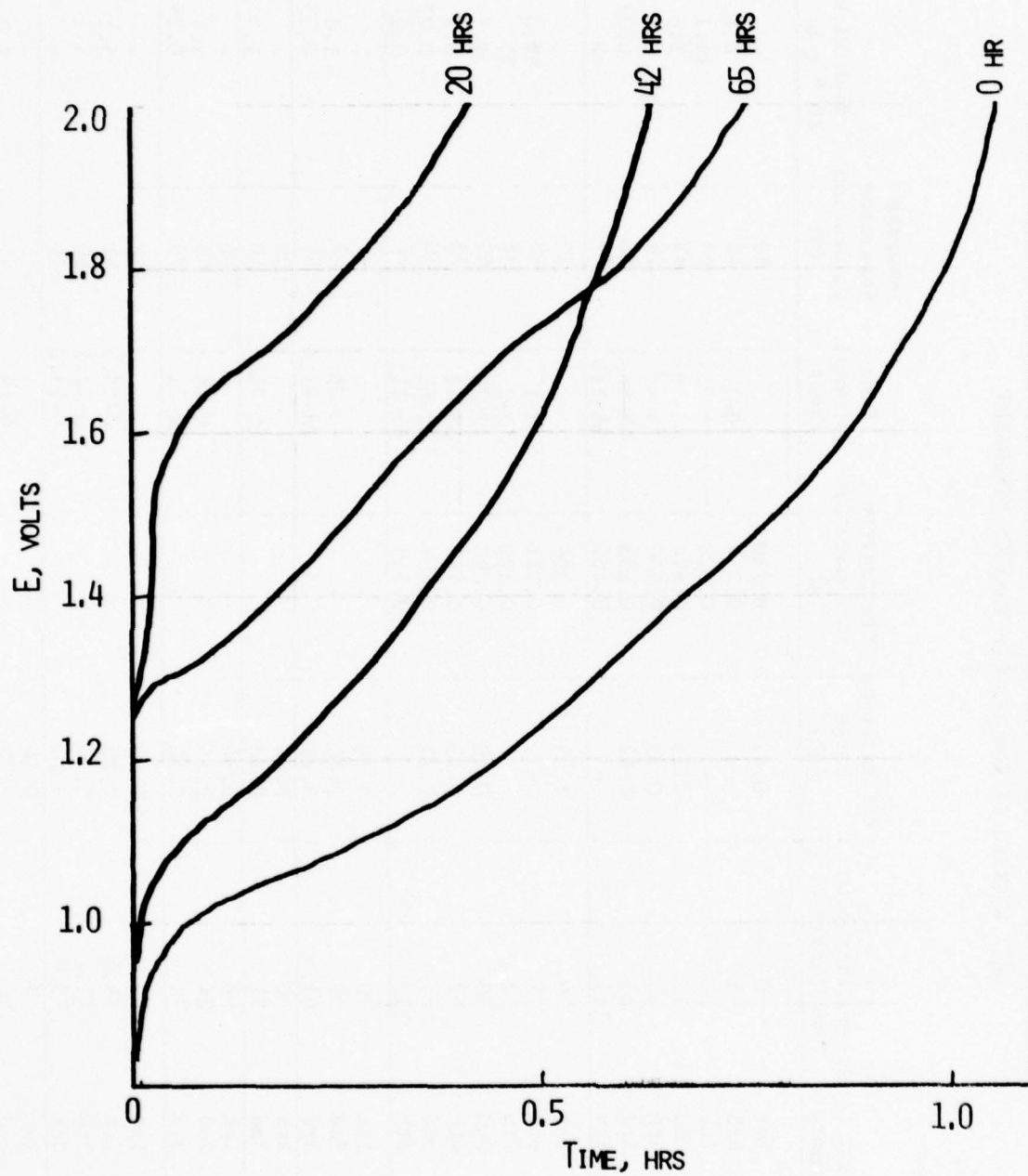


Figure 12. Voltage-time traces of back wicking experiments in cells using a Visking membrane.

TABLE 10

BACK WICKING OF KOH THROUGH VARIOUS MEMBRANES

Membrane	Test Sequence	Re-equilibration Time (hrs)	Polarization Charge (Ah)	Electrolyte in Separator (g)	Time Interval (hrs)	Average Separator Saturation (%)	Back Wicking 10^{-4} g hr $^{-1}$ cm $^{-1}$
Permion 2193	1st	0	0.47	0.250		40	-
	6th	1	-	0.259	0-1	41	4.6
	7th	2	-	0.300	1-2	45	21.1
	2nd	19	0.27	0.470	2-19	62	5.0
	4th	45	0.35	0.500	19-45	78	0.6
	3rd	66	0.42	0.503	45-66	81	0.07
	5th	115	-	0.482	66-115	79	~0
Visking	1st	0	1.03	0.206		33	-
	6th	1	-	0.321	0-1	42	59.0
	7th	2	-	0.392	1-2	58	37
	2nd	20	0.40	0.466	2-20	69	2.1
	4th	42	0.63	0.496	20-42	78	0.7
	3rd	65	0.77	0.499	42-65	78	0.07
	5th	115	-	0.519	65-115	82	0.2
Permion 2291 40/20	I 1st	0	0.70	-	-	-	-
	I 2nd	28	0.10	-	0-28	43	1.0
	I 3rd	91.5	0.18	-	28-91.5	51	0.35
	II 1st	0	0.64	-	-	~38	-
	II 2nd	73	0.40	-	0-73	59	1.7
	III 1st	0	0.64	-	-	~38	-
	III 2nd	24	0.36	-	0-24	56	4.6
	III 3rd	71	0.40	-	24-71	75	0.26
Permion 2291 40/20E	I 1st	0	0.50	-	-	~38	-
	I 2nd	15.5	0.20	-	0-15.5	51	5.1
	I 3rd	52.5	0.30	-	15.5-52.5	69	1.1
	I 4th	93.0	0.14	-	52.5-93.0	66	-
	II 1st	0	0.44	-	-	~38	-
	II 2nd	19	0.22	-	0-19	54	5.2
	II 3rd	47	0.14	-	19-47	64	-

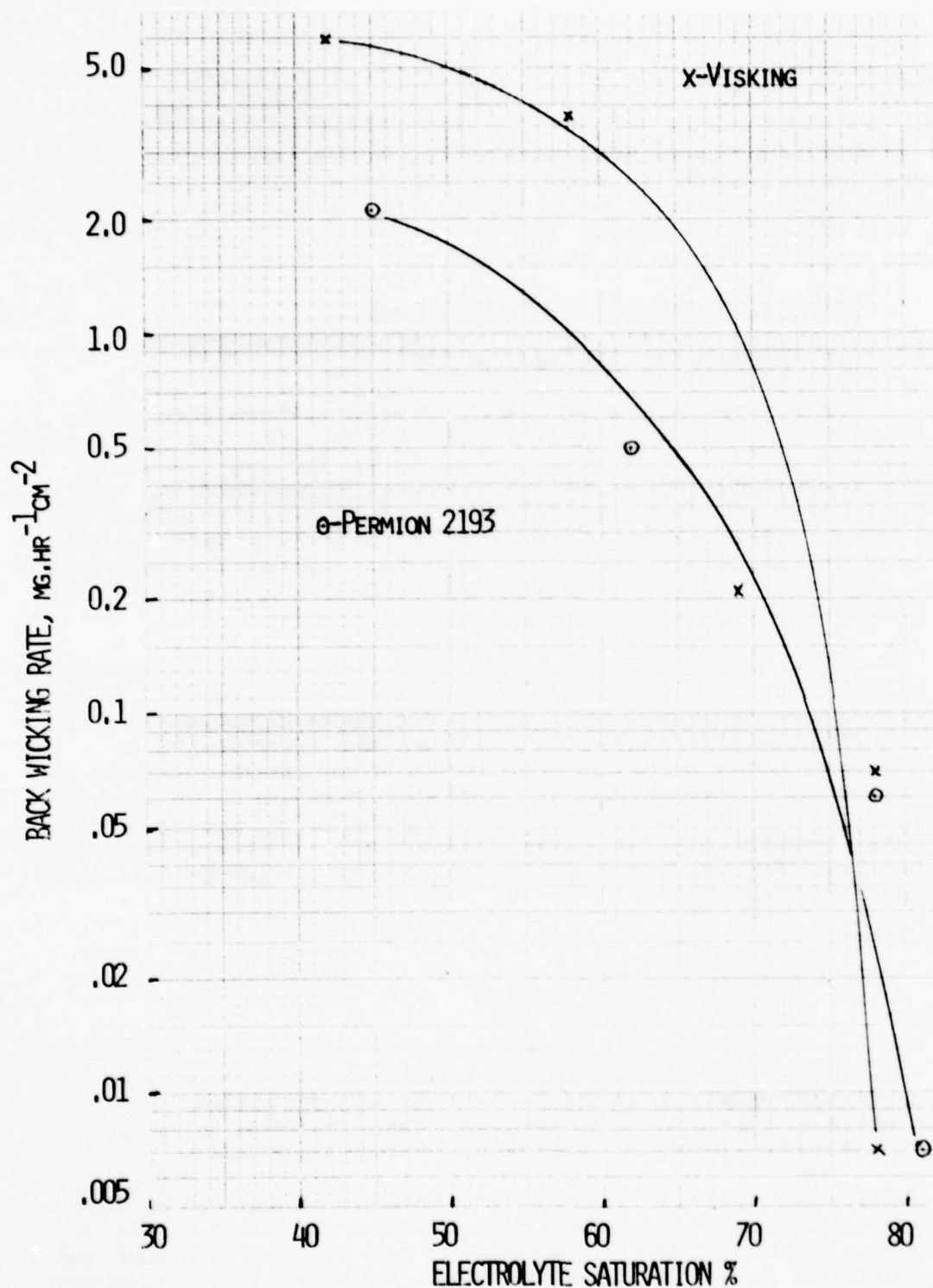


Figure 13. Back wicking rates for Visking and Permion 2193 as a function of electrolyte saturation of the asbestos absorber layer.

As will be discussed later, back wicking or electrolyte flow through the argentistatic membrane is essential to maintain a constant amount of electrolyte in the cell stack during cycling. The rate of back wicking has to be, at a minimum, sufficiently high to compensate for the electrolyte imbalance resulting from excess charge input over the charge delivered.

3. Boiler Plate Cells of Stacked Configuration

3.1 Hardware and Cell Construction

The electrode stacks were housed in heavy wall stainless steel (Type 304) pressure vessels schematically shown in Fig. 14. The inner diameter and height were 8.76 cm and 10.16 cm, respectively. The cover contained glands and feedthroughs (Conax) for the terminals, thermocouples and reference electrode leads as well as a tube connection to the pressure transducer and filling valve. A needle valve in the bottom of the pressure vessel allowed draining of accumulated electrolyte. To facilitate complete electrolyte collection, the vessel bottom was slightly funnel shaped. Polyethylene filler pieces were used to adjust the gas space volume as desired.

The support mandrel is shown in Fig. 15. The Noryl positioning plates are also used to center the electrode stack in the pressure vessel. To provide for ready gas equilibration the positioning plates have flat areas from removal of 80 mil of material every 60 degrees. The center mandrel is machined from Teflon to avoid electrolyte creepage and possible shorting by silver migration. Figure 16 shows the shape and dimensions of the electrodes, absorber layers and membranes. The membranes extend beyond the electrodes and absorber layers to minimize silver migration. To assure a constant stack compression stainless steel wave washers are inserted between the base plate and positioning plate.

3.2 Test Matrix

3.2.1 Cell Configurations

It is clear that a large number of variables can significantly affect the performance of silver-hydrogen batteries. Since the experimental design is limited to between 16 and 32 tests, it is equally clear that only a limited number of variables can be examined. Table 11 lists, by class of priority, the variables we believe to be of greatest significance.

If all eight variables listed were independent of each other, no more than eleven experiments would be needed to determine the effect of each -- one reference experiment, three experiments to test membrane materials, and seven experiments to test the other variables. Additional replications would of course be needed to determine the influence of experimental error.

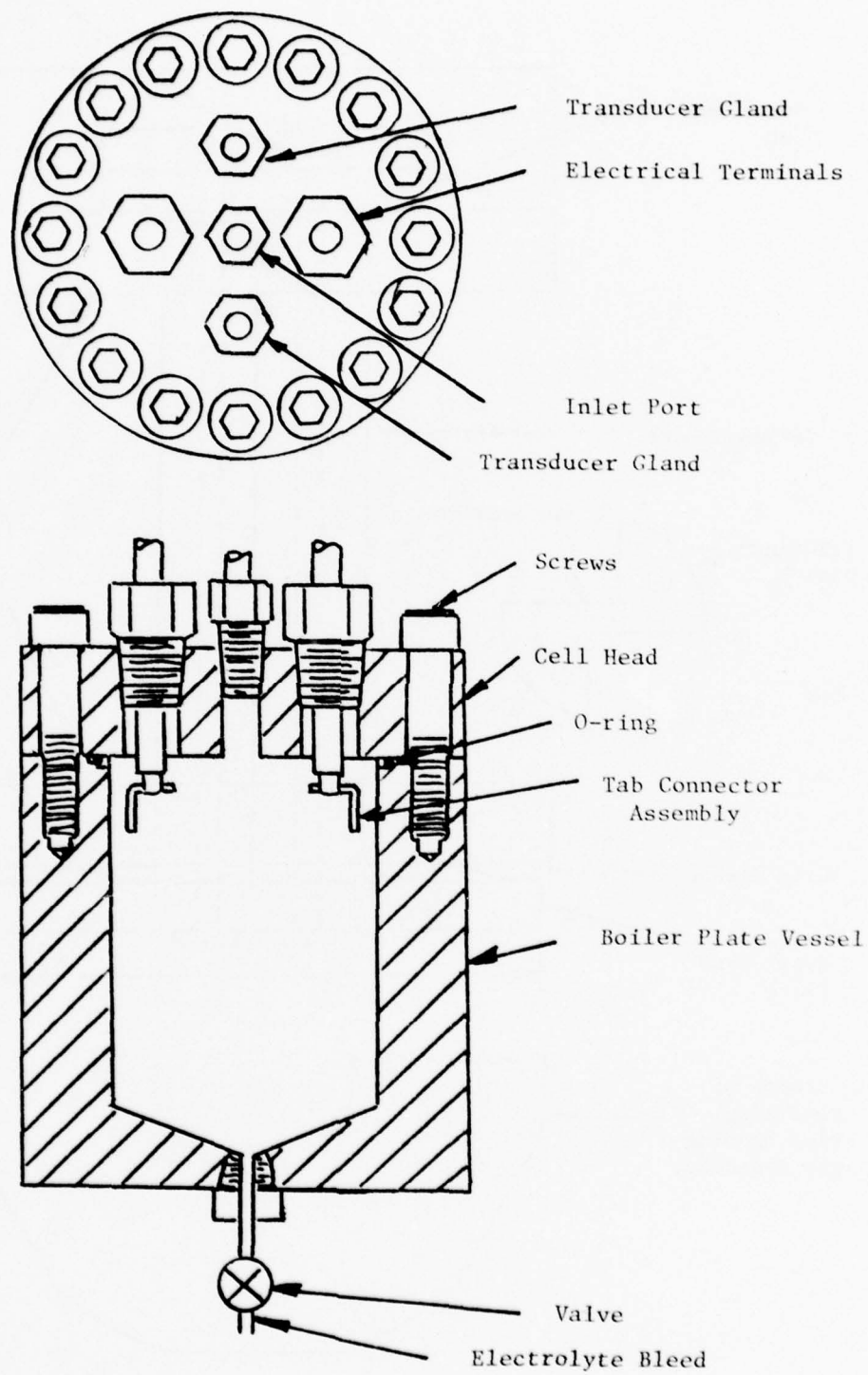


Figure 14. Boiler plate test cell.

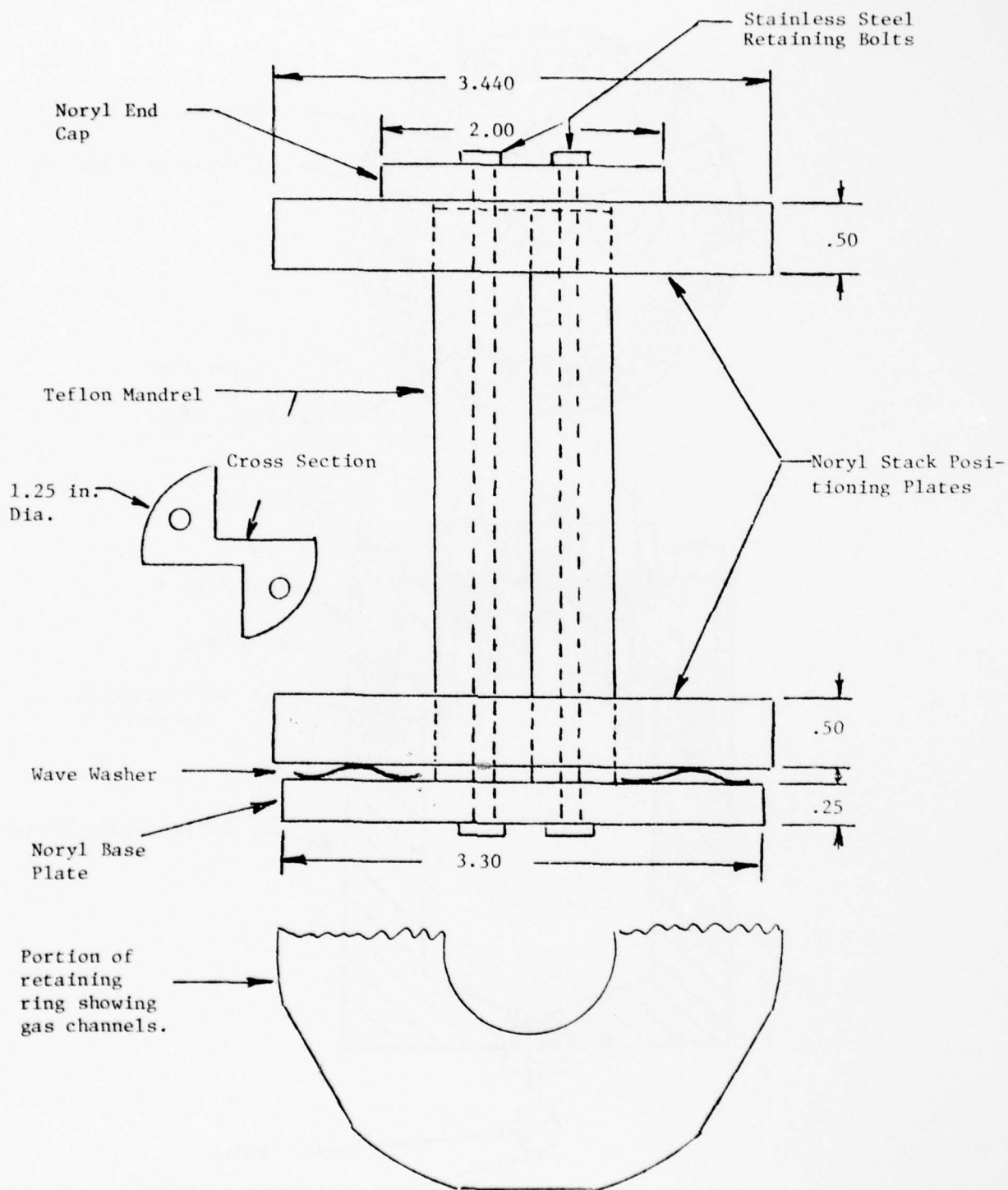


Figure 15. Schematic of the cell stack support mandrel.
(Dimensions in inches).

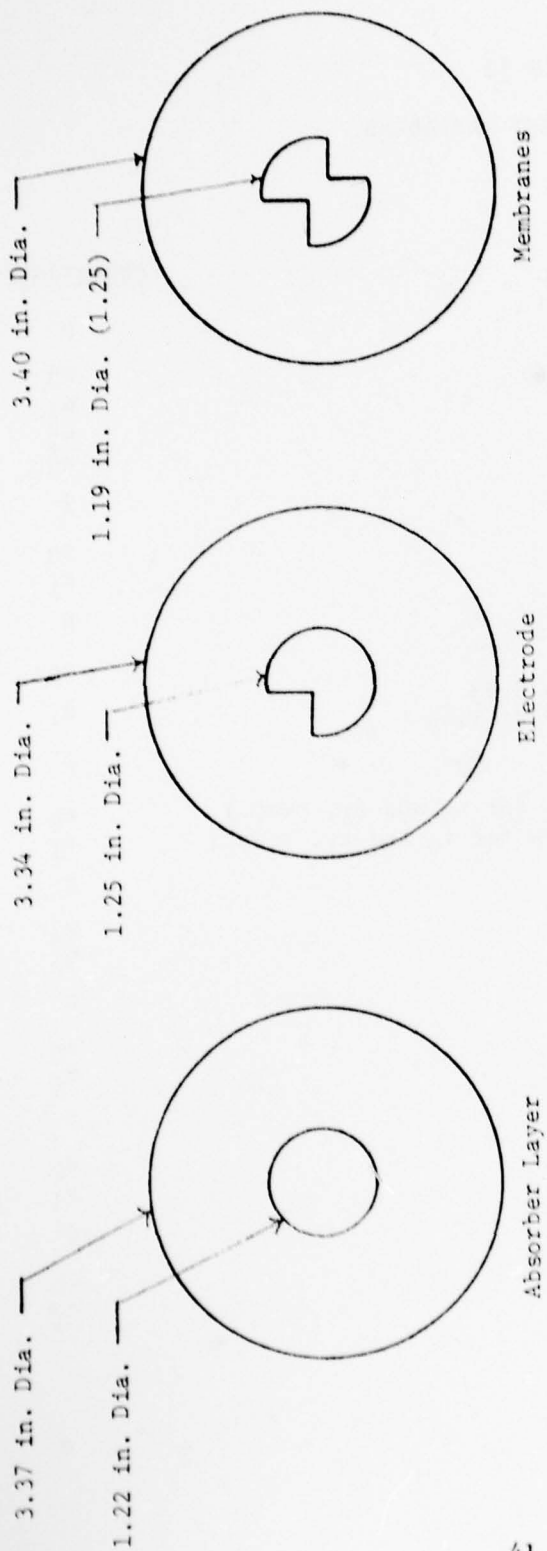


Figure 16. Component shapes and dimensions.

TABLE 11
LIST OF TEST VARIABLES

	<u>Abbreviation</u>
1. Membrane Material	M
a. NASA	m ₀
b. Permion 2193	m ₁
c. Permion 2291	m ₂
d. Visking	m ₃
2. Plate Thickness (Ag)	T
a. T (0.025 cm)	t ₀
b. 2.5 T	t ₁
3. Number of Membrane Layers	N
a. 1 layer	n ₀
b. 2 layers for NASA or Permion 2193	n ₁
3 layers for Permion 2291 or Visking	
4. Amount of Electrolyte	E
a. Low (2 and 3 absorber layers for t ₀ and t ₁ , resp.)	e ₀
b. High (3 and 5 absorber layers for t ₀ and t ₁ , resp.)	e ₁
5. Cells per Pressure Vessel	K
a. Series (2)	k _s
b. Parallel	k _p
6. Stack Configuration	R
a. Back-to-back Ag electrodes	r ₀
b. Recirculation configuration	r ₁
7. Edge Seal	S
a. Absent	s ₀
b. Present	s ₁
8. Electrolyte Concentration	C
a. Low	c ₀
b. High	c ₁

If, on the other hand, all eight variables were mutually dependent, the minimum number of experiments required -- according to the principles of factorial analysis -- is $4 \times 2^7 = 512$. Again, replications are not included. Even a determination of the interdependent effects of the five highest priority variables would require at least $4 \times 2^4 = 64$ experiments.

In experiments involving large numbers of variables, it is often necessary to sacrifice some accuracy by reducing the number of experiments carried out. This reduction can be carried out in a systematic way, so that the main effects of the primary variables (i.e., the "factors" of a factorial analysis) are determined with relatively small error, the effects of pairwise interactions between factors are determined somewhat less precisely, while the effects of higher-order interactions are assumed to be negligible. If the effects of all interactions among three or more factors can be assumed (e.g., ABC, ABCD, ABCDE, etc.), a few additional experiments will provide an estimate of the experimental error.

Considering the number of possible experiments, the relative importance of the various factors and the expected extent of interaction, we designed the following basic experiments: (1) M-T interaction, consisting of eight experiments; (2) T-N-E interaction, also consisting of eight experiments (see Table 12). In the TNE series, all t_0 -level experiments will be carried out in the series arrangement (k_s) and all t_1 -level experiments in the parallel arrangement (k_p). Since the M-T experiments provide a separate estimate of the main effect of T, the total group of 16 will also provide an estimate of the importance of K. A rough estimate of experimental error will be obtained from the three-factor TNE interaction, and from the assumed unimportance of the two-factor TN and NE interactions. However, independent estimates of experimental error are also available from cycling experience of related systems.

The specific stack arrangements are as follows: Two silver electrode thicknesses were selected at 10 and 25 mil. Each electrode stack will contain four silver electrodes. Thus cells with approximately eight and 17 Ah capacity result. For multistack arrangements in a common pressure vessel, we have two stacks with 2,25 mil Ag electrodes (or 4,10 mil Ag electrodes) in series. This results in a capacity of approximately eight Ah and in a pressure range comparable to the 17 Ah cells. This configuration makes it possible to use the same pressure vessels and to cycle test multistack cells together with the other eight Ah cells.

In reference to the test matrix I in Table 12, we note that e_0 needs further specification. This parameter describes a level of electrolyte in a cell unit. Specifically, configuration m_1 , was as follows:

Ag electrode 10 mil
Nylon (Pellon 2505)

TABLE 12

THE SIXTEEN HIGHEST-PRIORITY EXPERIMENTS

I. Parallel Configuration: MT InteractionN,E fixed at n_0, e_0 . Eight experiments.

	t_0	t_1
m_0	(1)	t_1
m_1	m_1	$m_1 t_1$
m_2	m_2	$m_2 t_1$
m_3	m_3	$m_3 t_1$

Main Effects: M,T
Interaction: MT

II. Parallel and Series Configurations: TNE InteractionM fixed at m_1 . Eight experiments.

		k_s, t_0	k_p, t_1
n_0	e_0	(1)	t_1
	e_1	e_1	$e_1 t_1$
n_1	e_0	n_1	$n_1 t_1$
	e_1	$n_1 e_1$	$n_1 e_1 t_1$

Main Effects: T,N,E,(K)
Interactions: NE,TN,TE,TNE

Membrane (P-2193)
Nylon (Pellon 2505)
H₂ electrode

This package absorbs approximately 2.2 cm³ of electrolyte in the discharged state. The overall electrolyte decrease during charge would be approximately 25%.

Configuration m₁t₁ was:

Ag electrode 25 mil
Nylon (Pellon 2505)
Membrane (P2193)
Nylon (Pellon 2505)
Nylon (Pellon 2505)
H₂ electrode

This configuration contains approximately 4.3 cm³ of electrolyte (e₀=4.3 cm³). During charge, the overall change would be about 32%. In arrangements using the NASA separator, this component will replace the membrane and one nylon layer (H₂ side) in the above shown sequences.

The submatrix II in Table XII examines the effects of the number of barrier layers and of the amount of electrolyte with series and parallel arrangements. Specifically, configuration e₁ was a series stack with the following component sequence:

Ag electrode 10 mil
Nylon (Pellon 2505)
Membrane (P2193)
Nylon (Pellon 2505)
Nylon (Pellon 2505)
H₂ electrode

This arrangement contains approximately 3.4 cm³ electrolyte and would show a 16% overall change upon charge. Membrane P2193 was selected because it promised best Ag retention in a single component configuration (it is a laminate). The equivalent high electrolyte configuration e₁t₁ was:

Nylon (Pellon 2505)
Nylon (Pellon 2505)
Ag electrode 25 mil
Nylon (Pellon 2505)
Membrane (P2193)
Nylon (Pellon 2505)
Nylon (Pellon 2505)
H₂ electrode

This cell contained about 5.5 cm^3 of electrolyte in the discharged state and was expected to show changes of about 25% during charge.

3.2.2 Test Regime

The cells were activated by vacuum impregnation with potassium hydroxide (stacked cells 30 wt %), formed at $\sim 60^\circ\text{C}$ and cycled several times at C/2 to determine their capacity. They were then tested in a specialized cycle regime shown in Fig. 17. Each test cycle contains two deep discharges. Testing occurred at constant current with a microprocessor controlled, 16 station battery cycler. Voltage pressure and temperature data were constantly recorded and stored on magnetic tape. Electrolyte expelled from the cell stack was periodically drained from the pressure vessel.

3.3 Test Results

3.3.1 Pretest Cycling

Prior to assembly of all 16 cells specified in the test matrix (Table 12) we assembled one cell (m_1, n_0, k_p, r_0, t_1) and subjected it to straight charge-discharge cycling to establish that the selection of parameters was in a realistically suitable range. The cycle data are summarized in Table 13.

Since the selected parameters appeared to be within a practical range, 16 cells were assembled with the configurations specified in Table 14. Cells No. 10, 11, 12 and 15 were equipped with multiple thermocouples located between two back-to-back silver electrodes. Cells 5, 6, 15 and 16 were equipped with pressure transducers (the other cells had gauges) reference electrodes and oxygen sensors (polarographic O_2 sensor incorporated into the pressure vessel).

Prior to the accelerated test cycling, the cells were formed and subjected to several charge-discharge cycles. The pretest history for the cells is summarized in Table 15. Due to equipment difficulties, data of some intermediate cycles is incomplete and the amount of overcharge was higher than intended (up to 100%). Therefore we re-impregnated all cells with 30% KOH prior to the accelerated cycle testing. Detailed data on Cycles 1 and 6 are summarized in Tables 16 and 17. Cell capacities showed relatively wide variation. Cell voltage within a group (thin Ag electrodes or thick electrodes) showed only small differences. Thick electrodes polarized more strongly than thin electrodes. This effect is much more pronounced on charge. After re-impregnation with electrolyte, the capacities of individual cells showed noticeable changes, however, no general trend could be detected except possibly a decrease in capacity of the cells with thick silver electrodes. Electrode polarization was slightly less after re-impregnation. Again, this effect was more pronounced on charge than on discharge.

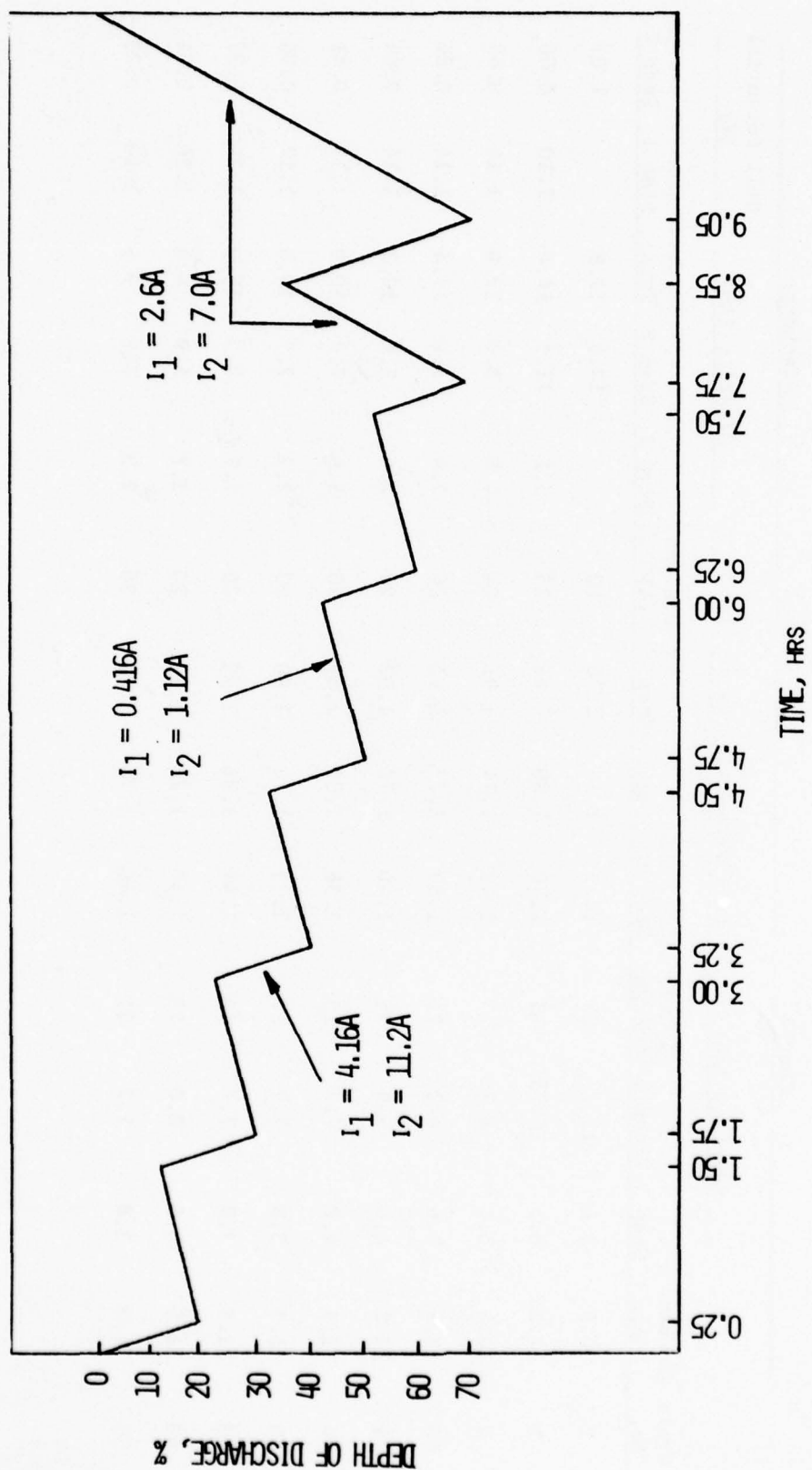


Figure 17. Accelerated test cycle regime i_1 and i_2 = current for cells with thin and thick silver electrodes, respectively.

TABLE 13

CYCLE DATA FOR SILVER HYDROGEN CELL OF CONFIGURATION $m_1 n_o e_k p_o r_o t_1$

Charge										Discharge			
Cycle No.	Current (A)	Capacity (Ah)			% Over-Charge	Cell Potential (V)			Current (A)	Capacity (Ah)			Cell Potential (V)
		Step 1	Step 2	Step 3		Step 1	Step 2	Step 3		Step 1	Step 2	Total	
1	0.3	8.6	13.2	22		1.21	1.56	1.70	10	17.8	17.8		1.03
2	17.25	6.5	10.75	18		1.46	1.80	1.96	25	11.5	14.6	1.10	0.86
4	13.8	5.1	8.7	15		1.40	1.74	1.91	24	8.0	12.0	1.14	0.88
10	13.8	7.6	6.2	21		1.39	1.75	1.91	24	8.0	11.4	1.14	0.86
14	13.8	4.0	9.8	35		1.40	1.76	1.92	24	7.6	10.2	1.14	0.86
16	11.5	4.0	7.5	15		1.38	1.73	1.89	20	7.2	10.0	1.17	0.81
25	11.5	3.8	7.7	15		1.39	1.74	1.90	20	7.7	10.0	1.17	0.90
40	11.5	3.8	7.7	15		1.41	1.76	1.92	20	7.3	10.0	1.20	0.92
60	11.5	3.5	8.0	20		1.40	1.76	1.90	20	6.9	9.6	1.20	0.91
63	11.5	3.8	7.7	21		1.40	1.76	1.92	20	7.2	9.5	1.20	0.93

48

TABLE 14

CONFIGURATION AND INSTRUMENTATION OF TEST CELLS

Cell No.	Station No.	Nominal Capac. Ah	Configuration	Instrumentation	Reference Electrodes	O ₂ Sensor
9	1	7	Series e ₀ n ₀ m ₁ r ₀	Gauge	-	-
11	2	7	Series e ₁ n ₀ m ₁ r ₀	Gauge	2 (3)	-
1	3	7	Parallel e ₀ n ₀ m ₀ r ₀	Gauge	-	-
3	4	7	Parallel e ₀ n ₀ m ₁ r ₀	Gauge	-	-
5	5	7	Parallel e ₀ n ₀ m ₂ r ₀	Transducer	-	+
7	6	7	Parallel e ₀ n ₀ m ₃ r ₀	Gauge	-	-
13	7	7	Series e ₀ n ₁ m ₁ r ₀	Gauge	-	-
18	8	7	Series e ₀ n ₁ m ₁ r ₀	Gauge	-	-
2	9	17	Parallel e ₀ n ₀ m ₀ r ₀	Gauge	-	-
10	10	17	Parallel e ₀ n ₀ m ₁ r ₀	Gauge	3 (4)	-
4	11	17	Parallel e ₀ n ₀ m ₁ r ₀	Gauge	-	-
12	12	17	Parallel e ₁ n ₀ m ₁ r ₀	Gauge	3 (4)	-
6	13	17	Parallel e ₀ n ₀ m ₂ r ₀	Transducer	-	+
14	14	17	Parallel e ₀ n ₁ m ₁ r ₀	Gauge	-	-
8	15	17	Parallel e ₀ n ₀ m ₃ r ₀	Gauge	-	-
16	16	17	Parallel e ₁ n ₁ m ₁ r ₀	Transducer	-	+

e₀ = Low electrolyte volumee₁ = High electrolyte volumen₀ = One membrane layern₁ = Two layers Astropower or Permion 2193

= Three layers Permion 2291 or Visking

r₀ = Back-to-back silver electrodesm₀ = NASA membranem₁ = Permion 2193m₂ = Permion 2291m₃ = Visking cellophane

TABLE 15
PRETEST HISTORY OF Ag/H₂ CELLS

Cycle No.	Data Record No.	Current (A) ⁽¹⁾		Comments
		Charge	Discharge	
1	00, 01, 02, 03	0.17 0.43	3.50 8.50	Formation; cell No. 11 and 18 failed.
2	04, 05	3.50 10.30		Discharge current not constant.
3	06, 07	6.90 19.50	6.0 17.5	Difficulties with voltage limits.
4	08	7.00 19.50	7.00 17.50	Cells 4 and 6 failed - difficulties with voltage limits.
5	09	7.00 19.50	7.00 17.50	
-	0B, 0E, 0F			Charge-discharge tests of Cells 1 and 12
-	0D			Self discharge test.
-				All cells re-impregnated with KOH.
6	10	6.80 17.25	6.90 17.25	Cell 11 reconnected, Cell 15 added; maximum and minimum pressure recorded, displaced electrolyte drained.

(1) Lower and higher current values for cells with thin and thick plates respectively.

TABLE 16
DATA FOR PRETEST CYCLE 1

Cell No.	Station No.	Charge Capacity (Ah)			Discharge Potential ⁽²⁾ (V)	Cap. (Ah)	Pressure ⁽¹⁾ (psig)
		Step 1	Step 2	Step 3			
9	00	2.89	6.10	0.1	1.14	5.56	400
11	01	2.91	6.32	0.87	-	-	360
1	02	3.71	5.28	0.1	1.13	5.56	230
3	03	1.77	7.64	0.79	1.12	5.89	255
5	04	0.39	7.53	1.05	1.13	5.53	-
7	05	0.45	7.76	0.76	1.10	6.67	310
13	06	2.57	9.02	1.0	1.13	5.23	400
18	07	3.09	-	-	-	-	-
2	08	3.8	13.70	1.9	1.07	16.37	455
10	09	4.8	13.33	1.27	1.08	17.09	480
4	0A	6.23	11.56	1.61	1.08	18.7	515
12	0B	5.06	13.49	0.85	1.06	17.98	510
6	0C	6.73	11.27	2.2	1.07	11.5	-
14	0D	6.14	14.06	0	1.05	16.64	430
8	0E	4.97	15.23	0	1.05	17.09	435
16	0F	6.37	13.83	0	1.05	15.66	-

(1) Starting pressures were ~ 105 psig in all cells, high pressure reading after 48 hrs.

(2) Single discharge plateau.

TABLE 17

DATA FOR PRETEST CYCLE 6

Cell No.	Station No.	Charge									Discharge									Pressure (psig)			
		Current			Voltage (V)			Capacity (Ah)			Current			Voltage (V)			Capacity (Ah)						
		A	Step 1	Step 2	Step 3	Step 1	Step 2	Step 3	A	Step 1	Step 2	Step 3	Step 1	Step 2	Step 3	Step 1	Step 2	Step 3	Step 1	Step 2	Step 3	High	Low
9	00	6.9	2.64	3.24	3.5 3.7(2)	0.55	4.15	2.15	6.0	2.8	2.24	1.90	2.20	4.10	380	145							
11	01	6.9	2.62	3.22	3.46	1.65	2.35	2.95	6.0	2.76	2.22	1.58	2.80	4.38	395	165							
1	02	6.9	1.32	1.66	1.88	2.9	3.1	0.9	6.0	1.35	1.11	1.45	4.55	6.00	240	102							
3	03	6.9	1.31	1.61	1.83	0.55	4.7	1.7	6.0	1.36	1.08	1.88	3.15	5.03	240	102							
5	04	6.9	1.32	1.61	1.84	0.62	4.55	1.7	6.0	1.40	1.13	1.90	3.30	5.20	254	99							
7	05	6.9	1.37	1.67	1.93	0.83	3.8	2.2	6.0	1.20	0.95	1.55	3.00	4.55	255	100							
13	06	6.9	2.62	3.24	3.5- 3.7	0.72	4.35	1.8	6.0	2.74	2.2	1.85	3.20	5.05	410	95							
15	07	6.9	2.70	3.34	3.76	1.65	4.0	1.2	6.0	2.82	2.26	1.90	3.60	5.50	395	117							
2	08	17.25	1.45	1.8	2.0	7.2	8.3	1.8	15.0	1.25	0.98	3.80	12.60	16.40	500	105							
10	09	17.25	1.43	1.75	1.95	9.8	10.0	4.5	15.0	1.28	1.02	4.30	9.40	13.70	500	95							
4	0A	17.25	1.45	1.75	1.95	2.8	8.6	5.9	15.0	1.30	1.03	3.90	8.00	11.90	500	105							
12	0B	17.25	1.46	1.8	1.95	3.6	9.1	4.5	15.0	1.20	0.95	3.9	9.5	13.40	505	90							
6	0C	17.25	1.42	1.73	1.92	2.4	10.2	4.0	15.0	1.30	1.03	4.7	9.00	13.70	500	90							
14	0D	17.25	4.48	1.8	2.0	3.05	9.5	4.7	15.0	1.27	0.98	3.94	9.80	13.74	505	95							
8	0E	17.25																					
16	0F	17.25																					

During the pretest cycling we observed relatively high rates of self-discharge in certain cells. We therefore conducted a self-discharge test between cycles 5 and 6. The completely discharged cells (0 V) were charged to approximately 10% state of charge (5 min at 6.9 or 17.25 A) followed by open circuit stand. The cell potential of Cell 3 dropped below 0.1 V after 25 hrs and that of Cell 13 to 1.18V indicating that one of the two cell stacks had failed. Between 40 and 64 hrs the cell potential of Cells 5 and 15 dropped below 0.1V. The remaining cells retained their open circuit voltage of about 1.18V beyond the 64 hour test.

3.3.2 Accelerated Cycle Testing

The cycle regime used for the accelerated testing is shown in Fig. 17. All cells within a group (thin and thick silver electrodes) were cycled with the same current which was based on a nominal capacity of 5.2 Ah for the cells with thin silver electrodes and 14.0 Ah for the cells with thick silver electrodes. Thus the maximum depth of discharge for individual cells is between 60% to 89% to 82% for cells with thin and thick silver electrodes respectively. The final charge of the cycle regime includes 15% overcharge. One complete pass through the regime shown in Fig. 17 is considered as one cycle. It includes two deep discharges.

Cell potentials for a typical cycle are shown in Fig. 18. Charge and discharge potentials for individual cells changed only slightly during cycling. There are clear differences in the time for the transition from the first to the second charge plateau. The cells with thick silver electrodes polarize more than those with thin electrodes. The differences between different cells with thick silver electrodes are very small. Thin silver electrode cells show somewhat larger variations in polarization, however, there appears no immediately recognizable correlation with cell configuration.

Silver electrode potentials versus a hydrogen reference electrode showed that the hydrogen electrode polarizes about 25 to 30 mV during discharge of cells with thin silver electrodes ($\sim 21 \text{ mA/cm}^2$) and 60 to 65 mV during discharge of cells with thick silver electrodes ($\sim 56 \text{ mA/cm}^2$). The silver electrodes polarize during discharge 20 to 30 mV and 120 to 130 mV for thin and thick electrodes respectively (almost C rate). A typical open circuit voltage for a silver hydrogen cell with low state of charge (~ 10 to 20%) is 1.18 to 1.19V.

Temperature excursions in the cells are low but correlate clearly with the cycling regime (Fig. 19). The temperature peak during overcharge is strongly dependent on the amount of overcharge.

The test history is summarized in Table 18. The cycle regime was interrupted during the 24th test cycle by a failure of the cycle control

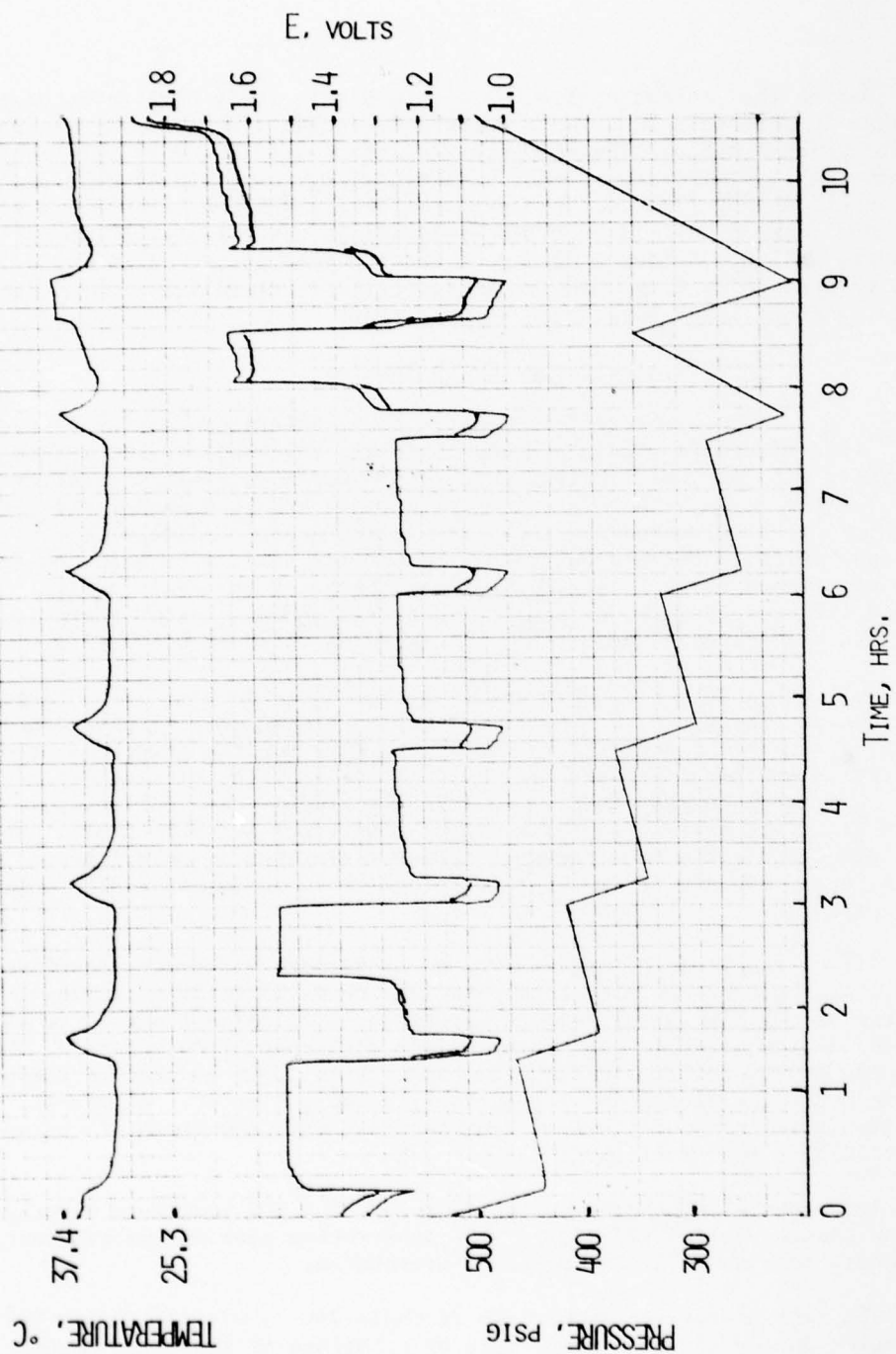


Figure 18. Typical variation in stack temperature, cell voltage, Ag electrode potential, and pressure in a Ag/H₂ cell (thick electrodes) during an accelerated test cycle.

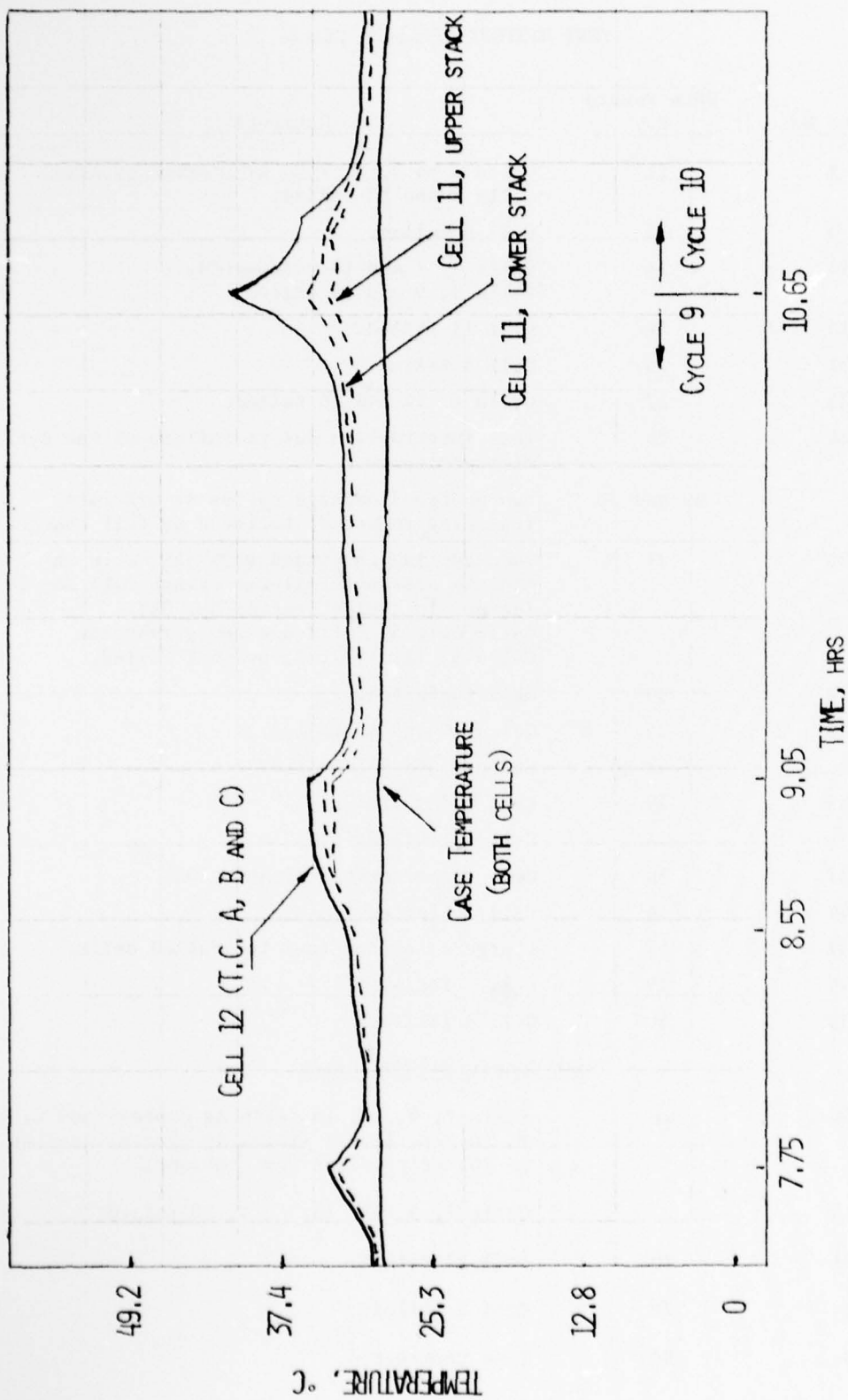


Figure 19. Temperature change during cycle testing of Cells 11 and 12.

TABLE 18
TEST HISTORY OF Ag/H₂ CELLS

Cycle No.	Data Record No.	Comments
1	11	Cells 1 to 3, 5, 7 to 17 started cycling. Cells 7 and 13 failed.
3	13	Cell 5 failed.
11	1A	Cells 5, 7 and 13 reinserted. Cells 5, 9 and 13 failed.
14	1E	Cell 11 failed.
21	25	Cell 3 failed.
23	27	Cells 8, 14 and 16 failed.
24	28	Test interruption due to failure of the cycle microprocessor.
	29 and 30	Two charge-discharge cycles at C/2 rate (capacity recorded) followed by full charge.
25	31	Test cycling continued with all cells including previous failures except Cell No. 2 (defect in cycler Station No. 08). Cells 4II, 5II, 6II are newly rebuilt. Cells 9, 11, 1, 7, 13 and 6II failed.
27	33	Cell 10 failed.
29	35	Cells 14 and 15 failed.
31 or 32	37 or 38	Cells 3 and 5II failed.
33	39	Cell 4II failed.
34	3A	Cell 12 failed.
37	3D	Cell 2 reconnected (Station 0C)
44	44	Cell 16 failed.
47	47	Charge retention test for failed cells.
49	49	Cell 2 failed.
53	4D	Cell 8 failed.
<u>Test Conditions Modified</u>		
54	4E	Cells 7, 9, 11, 15 (thin Ag plates) and 2, 4, 8, 10, 12, 14, 15 (thick Ag plates) started at 70% of previous test currents.
55		Cells 7, 9, 11, 15, 2, 4, 10 failed.
101	7D	Cell 12 failed.
103	7F	Cell 8 failed.
104	80	Test terminated.
		Capacity and overcharge test.

computer. Prior to test continuation, the cells had to be recharged. We used this occasion to carry out a capacity test involving two C/2 charge-discharge cycles. The voltage and capacity data are summarized in Table 19. The capacity, especially of the thin plate cells, was found lower than in the pretest cycle No. 6. All cells, including most of those previously failed, were subjected to this test cycle.

Three new cells 4-II, 5-II and 6-II were assembled and after formation included in subsequent testing. These cells are identical in configuration to the previously failed cells 4, 5 and 6 but contained smaller absorber components (P2505, 3.34 in. OD instead of 3.37 in. OD). The intent was to reduce the tendency for silver migration around the external perimeter by providing a larger overlap of the argentistatic membranes.

During continued cycling cells failed as indicated in Table 18. Generally cells failed during the first or second deep discharge of the cycle regime. An interesting deviation is shown in Fig. 20. Cell 10 almost failed in cycle 26 during the first deep discharge. Subsequently it appeared to recover but then failed early in the following cycle. Cell 5 failed on charge indicating a fairly massive silver bridging.

After test cycle 53 (106 deep discharges) all cells were cut out by the low voltage limit. To obtain additional information all cells were subjected to a charge retention test (see below). Eleven cells retained 10% charge for over four hours. These cells were reconnected to the cycler and cycled at a modified test regime using 70% of the original current values. The test history is also summarized in Table 18. All but four cells failed during the initial two cycles. Cells 8 (n_0 ; m_3 ; t_1 ; e_0) 12 (n_0 ; m_1 ; t_1 ; e_1) 14 (n_1 ; m_1 ; t_1 ; e_0) and 16 (n_1 ; m_1 ; t_1 ; e_1) accumulated 82, 80, 103 and 94 actual cycles respectively corresponding to twice as many deep discharges. Approximately 50 cycles are at the reduced depth of discharge.

3.3.3 Electrolyte Loss from Cell Stacks

To obtain more insight into electrolyte management in Ag/H₂ cells, we measured the amount of electrolyte retained in the stack and in intervals also the electrolyte lost from the cell stack. The data is summarized in Table 20. Accurate measurements especially of the initially retained electrolyte and of the electrolyte retained upon reimpregnation are difficult since they result from the difference of two large values. Also the amount of electrolyte retained in the gas diffusion spaces is not well defined. If one assumes complete expulsion of this electrolyte during the initial cycles, the second draining of electrolyte after impregnation may be a useful indication of electrolyte loss. Here it appears that the loss of electrolyte is less from stacks with high electrolyte level (e_1) than from those with e_0 . In view of the relatively short test time and the

TABLE 19

CAPACITY TEST BETWEEN TEST CYCLES 24 AND 25

Cell No.	Stat. No.	Current A	Charge			Capacity (Ah)	Current A	Discharge			Decrease Capacity %				
			Voltage (V)		Step 3			Voltage (V)		Capacity (Ah)					
			Step 1	Step 2			Step 1	Step 2	Step 1	Step 2	Step 1	Step 2	Total		
9	00	3.0	2.53	2.82 (2) 3.14	3.56	0.60	2.81	2.59	3.0	2.32	2.28	1.20	2.21	3.41	17
11	01		-	-	-	-	-	-	-	-	-	-	-	-	-
1	02	3.0	1.26	1.59	1.78	1.70	1.99	2.31	3.0	1.40	1.13	0.95	2.59	3.54	41
3	03	3.0	1.27	1.57	1.79	0.72	2.84	2.44	3.0	1.40	1.13	1.04	2.37	3.41	32
5-II	04	3.0	1.27	1.58	-	2.24	3.76	-	3.0	1.27	1.15	1.17	4.45	5.62	10
7	05	3.0	1.29	1.61	1.81	1.04	3.22	1.74	3.0	1.39	1.13	1.26	2.84	4.10	10
13	06	3.0	2.52	2.82 (2) 3.16	3.38	1.10	4.07	0.83	3.0	2.64	2.23	1.58	3.25	4.83	4
15	07	3.0	2.56	2.94 (2) 3.22	3.44 (2) 3.62	1.26	3.91	0.82	3.0	2.86	2.32	1.55	3.00	4.55	17
2	08	8.0	-	-	-	-	-	-	7.5	-	-	-	-	-	-
10	09	8.0	1.32	1.63	1.82	2.43	6.64	6.93	7.5	1.36	1.08	3.24	6.16	9.40	33
4-II	0A	4.0	1.27	1.61	1.80	4.40	6.80	5.60	4.0	1.38	1.13	3.60	8.60	12.20	-
12	0B	8.0	1.32	1.65	1.84	3.63	8.00	4.37	7.5	1.37	1.08	3.71	8.37	12.08	-1
6-II	0C	4.0	1.27	1.59	1.78	4.00	10.40	2.40	4.0	1.40	1.13	4.80	9.60	14.40	-
14	0D	8.0	1.34	1.67	1.88	3.95	9.01	3.04	7.5	1.34	1.06	3.79	8.76	12.55	6
8	0E	8.0	1.31	1.63	1.85	4.80	9.84	1.36	7.5	1.36	1.08	4.10	9.95	14.05	-2
16	0F	8.0	1.34	1.66	1.87	2.35	8.93	4.72	7.5	1.35	1.07	3.71	8.05	11.76	14

(1) Capacity change from pretest cycle No. 6.

(2) Variable step in series configurations.

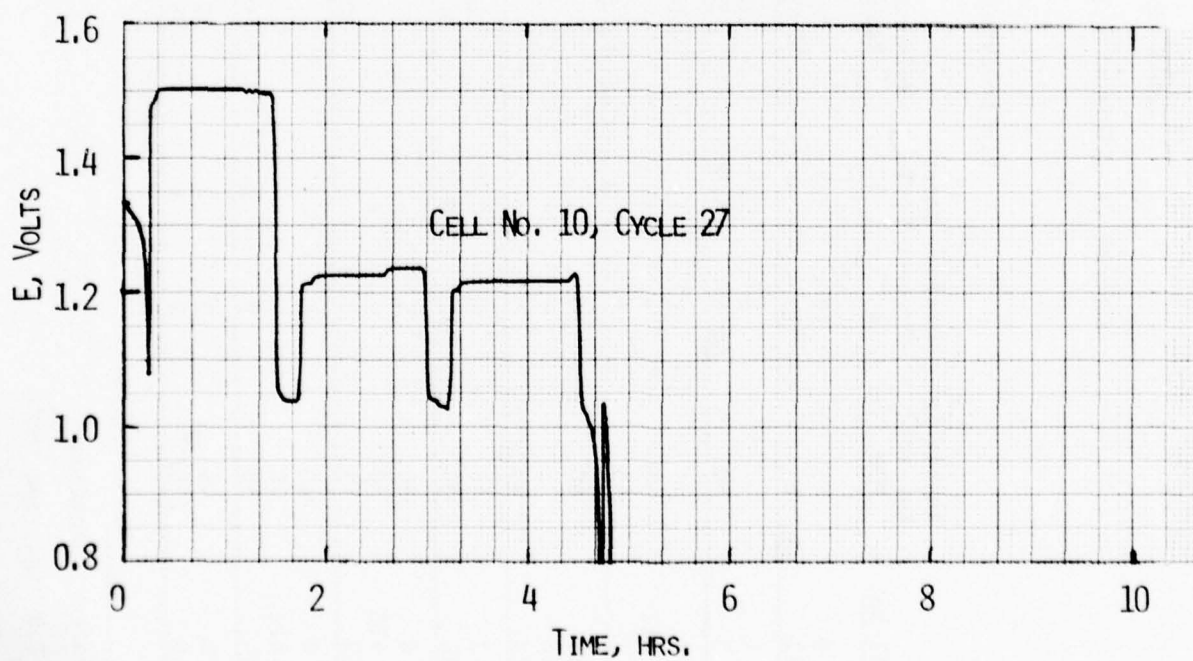
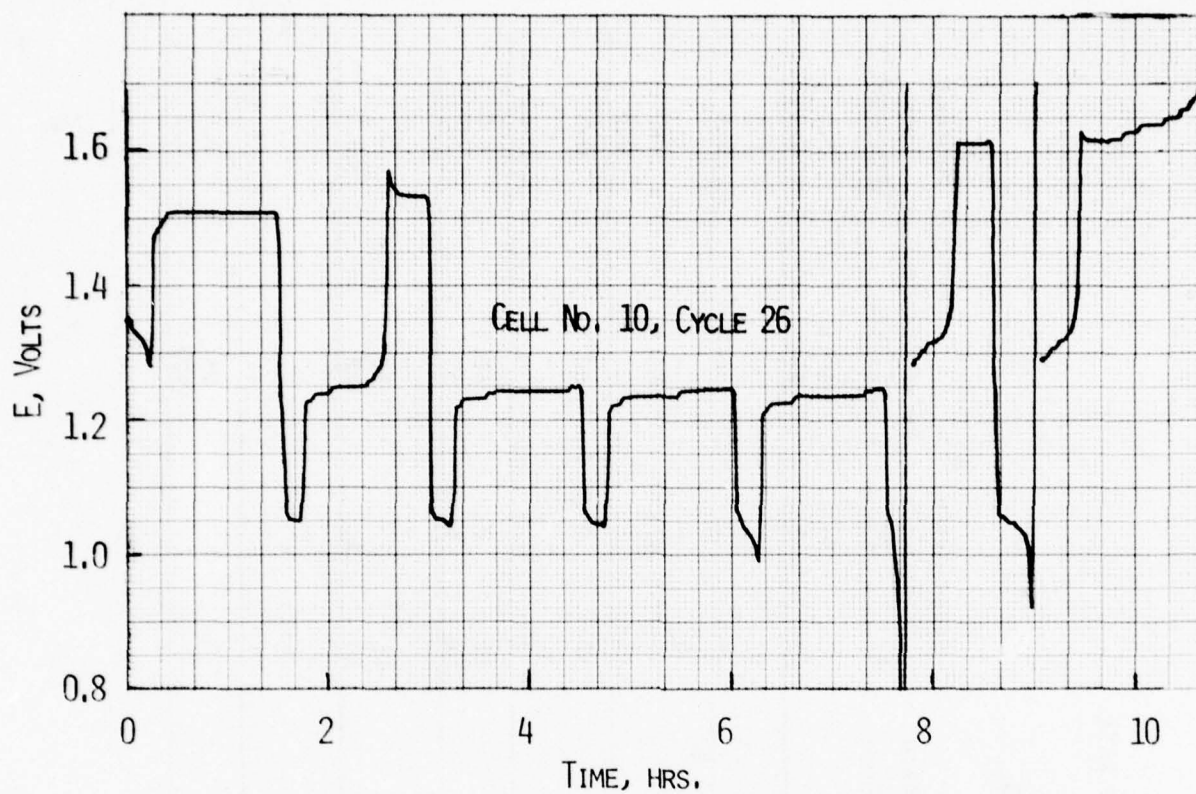


Figure 20. Ag/H₂ cell potential during the accelerated test cycle in which failure occurred.

TABLE 20
SUMMARY OF ELECTROLYTE LOSS DATA

Cell No.	Initially Retained KOH	Electrolyte (cm ³)						Retained after Failure	Drained Upon Disassembly
		Drained after Pretest Cycle 4	Drained after Cycle 5	Reimpregnation Retained	Drained prior to Test Cycle 1	Drained prior to Test Cycle 54			
9	65	12	6.5	35	7	14		60.5	7.4
11	85	15	-	30	3	3		89	4.3
1	-	3	2.5	20	13	1		-	1.2
3	50	5	3.5	25	14	1		51.5	0.4
5	45	1	1	20	6	-		-	-
5II	55	-	-	-	4(1)	0.5		50.5	-
7	45	6	7	25	19	5		33	0.6
13	60	6	1	50	37	6		60	0.5
18	75	-	-	-	-	-		-	-
15	60	-	-	-	3	0.5		56.5	0.4
2	45	4	2.5	20	16	2		40.5	1.0
10	55	11	6	30	12	5		51	-
4	60	2	-	-	-	-		-	-
4II	50	-	-	-	18(1)	3		29	-
12	55	7	2	20	15	3		48	<0.1
6	40	1	-	-	-	-		-	-
6II	40	-	-	-	2(1)	5		33	-
14	50	9	2	25	13	7		44	2.1 + 1.1
8	45	5	2	30	9	6		53	2.9
16	(70)(2)	2	1	25	1	1		(90)	0.2

(1) After formation.

(2) Too high, see text.

greatly varying number of test cycles for each cell, a meaningful interpretation appears not possible.

3.3.4 Cell Failure Analysis

3.3.4.1 Charge Retention Test

The failed cells were subjected to a charge retention test as follows: The completely discharged cells (0 V) were charged to 10% state of charge followed by open circuit stand. Cell voltage was monitored as a function of time.

A typical voltage-time trace for a series cell is shown in Fig. 21. Both stacks show discharge due to silver bridging (the rate of self discharge by reaction of silver oxide with hydrogen is considerably lower) at slightly different rates. The voltage changes after reduction of the silver oxide are quite rapid. Table 21 summarizes the results of the charge retention test.

3.3.4.2 Physical Examination

All failed cells were carefully disassembled and analyzed. The findings were as follows: All cells showed silver migration around the inner and outer edge of the separator membranes indicated by dark areas on the hydrogen side absorber layers, Fig. 22 shows a typical example. Silver deposits can be seen on hydrogen electrodes. Generally, silver migration was heavier at the lower plates of the cell stack and near the tab connection. Localized burned areas were detected apparently caused by heating via silver dendrites. In cell 9 we detected burned Pellon 2505 areas at the top H₂ electrode which appear like oxygen-hydrogen burns. Heavy silver deposits were distributed throughout the silver side absorber layers. This appeared somewhat less severe in the stacks with high electrolyte content. Silver penetrated also through the membranes although not rapidly enough to cause failure in our cells. The NASA separators were quite dark on the hydrogen electrode side indicating silver passage. The hydrogen electrode absorber layer behind Visking was strongly yellow. Silver penetration through Permion 2291 appears more spotty possibly indicating inhomogeneities in the membranes. No Ag penetration was observed with Permion 2193 a multilayer laminate. Most cells appeared quite dry upon disassembly.

3.3.5 Discussion

A summary of the number of accelerated test cycles to failure is shown in Table 22. Each cycle included two deep discharges. In addition, the cells were subjected to several pretest cycles. Time to failure varied

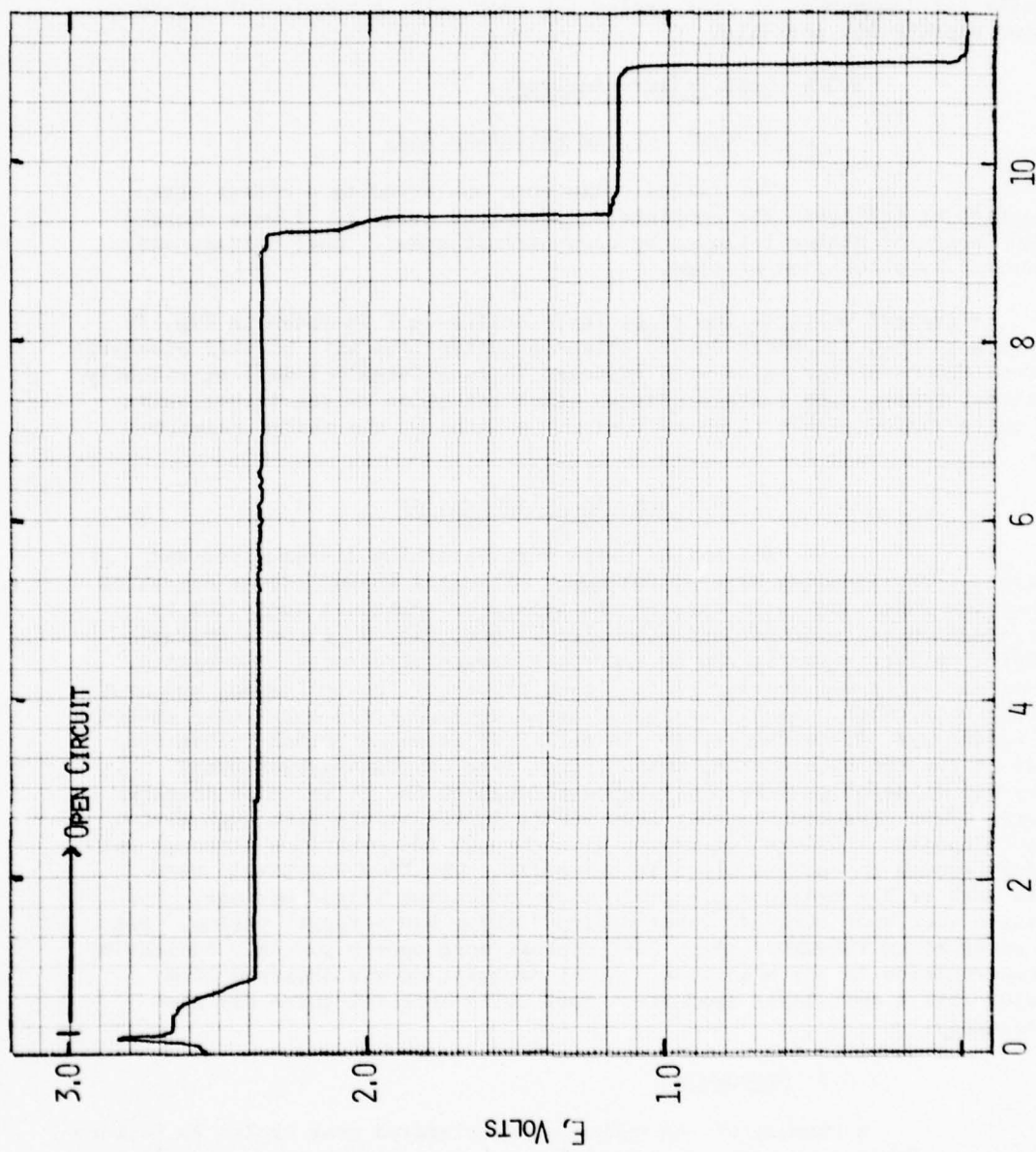


Figure 21. Charge retention test of series Cell No. 9 (see text).

TABLE 21
 CHARGE RETENTION OF FAILED CELLS. CHARGE INPUT 0.52 Ahr
 FOR THIN AND 1.4 Ahr FOR THICK PLATE CELLS (DATA RECORD
 NO. 47)

<u>Cell No.</u>	<u>Station No.</u>	<u>Time to Failure (hrs)</u>	
9	00	9.25, 10.5	Both stacks failed.
11	01	8, > 24	One stack failed.
1	02	4	
3	03	1	
5	04	3.5	
7	05	-	Not tested.
13	06	3, > 24	One stack failed.
15	07	> 24, > 24	Neither stack failed.
-	08	-	Not tested.
10	09	6.5	
4	0A	7	
12	0B	24	
2	0C		Not tested.
14	0D	> 24	
8	0E	-	Not tested.
16	0F	> 24	

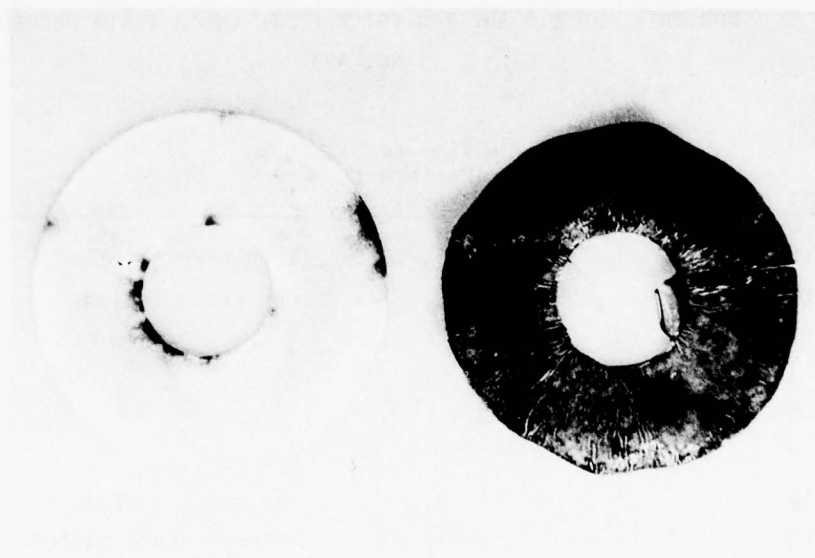


Figure 22. Hydrogen electrode absorber layer and membrane of a cycled Ag/H₂ cell (Cell No. 5). Dark areas on the absorber layer show silver migration around the membrane edge.

TABLE 22
NUMBER OF ACCELERATED TEST CYCLES TO FAILURE FOR Ag/H₂ CELLS

	<u>Cell No.</u>	<u>First Failure</u>	<u>Second Failure</u>	<u>Total</u>
Thin Plates	1	25		25
	3	21	7	28
	5	3		3
	5-II	7		7
	7	1	14	15
	9*	1	1	2
	11*	14	1	15
	13*	1	1	2
	15*	29		29
	18*	-		-
Thick Plates	2	37		37
	4	-		-
	4-II	8		8
	6	-		-
	6-II	1		1
	8	23	28	51
	10	27		27
	12	34		34
	14	23	4	27
	16	23	19	42

*Series configuration.

Cell No.	9	11	13	5	7	13	15	2	10	4	12	6	14	8	16
----------	---	----	----	---	---	----	----	---	----	---	----	---	----	---	----

widely from 1 to 51 - 10.6 hr cycles. Sometimes a failed cell will continue for a substantial number of cycles after a C/2 rate charge-discharge cycle (e.g., cells 3, 7, 8, 16). The general mode of failure was via "soft shorts" caused by silver bridging around the membrane edges. Thus the results are not suitable to evaluate the various parameters of the test matrix. A main effort was to be directed towards finding of an effective solution of the silver bridging problem.

4. Boiler Plate Cells of Rolled Configuration

4.1 Hardware and Cell Construction

Silver migration around the inner and outer edge areas has been identified as the main problem. To eliminate this problem we changed the cell design to a rolled configuration which allows considerably larger membrane overlapping. The cells contain 7.5×25 cm silver and hydrogen electrodes in a single wrap along the inside pressure vessel wall (see Fig. 23). The electrode package is retained by a 30 mil open cylinder of Ni200 and a stainless steel retaining ring (TRUARC). The membranes overlap 1 cm at the top and bottom and 1.5 cm in the gap where the electrodes meet. The NASA separator almost butts in the gap since it was not possible to bend it inwards. Thermocouples are located in the gas screen on the hydrogen electrode side. Reference electrodes consist of a full size component with a small active area on the inside of the wall adjacent to the nickel retaining cylinder. Electrolyte connection is provided via a wick from the hydrogen side.

4.2 Test Matrix

To maximize the information obtainable from the cell tests we decided against exact duplication of the original test matrix. The modified matrix is as shown in Table 23. Forty percent KOH is used for C₁. All other symbols are as described earlier (see Sect. 3.2). The test regime consisted again of the accelerated AF cycle described in paragraph 3.2.2.

4.3 Results

4.3.1 Pretest Cycling

The 16 cells were vacuum impregnated with 40% KOH and filled to 100 psig with H₂. Cells containing the NASA separator cells were soaked over night filled with KOH. Table 24 summarizes the test history of the rolled Ag/H₂ cells. The formation charge was carried out at a C/60 rate (0.333A and 0.133A for thick and thin cells respectively). Despite the low current density some cells exceeded 2.5V and could not be discharged at a reasonable current density (>C/10) without severe polarization. Since the

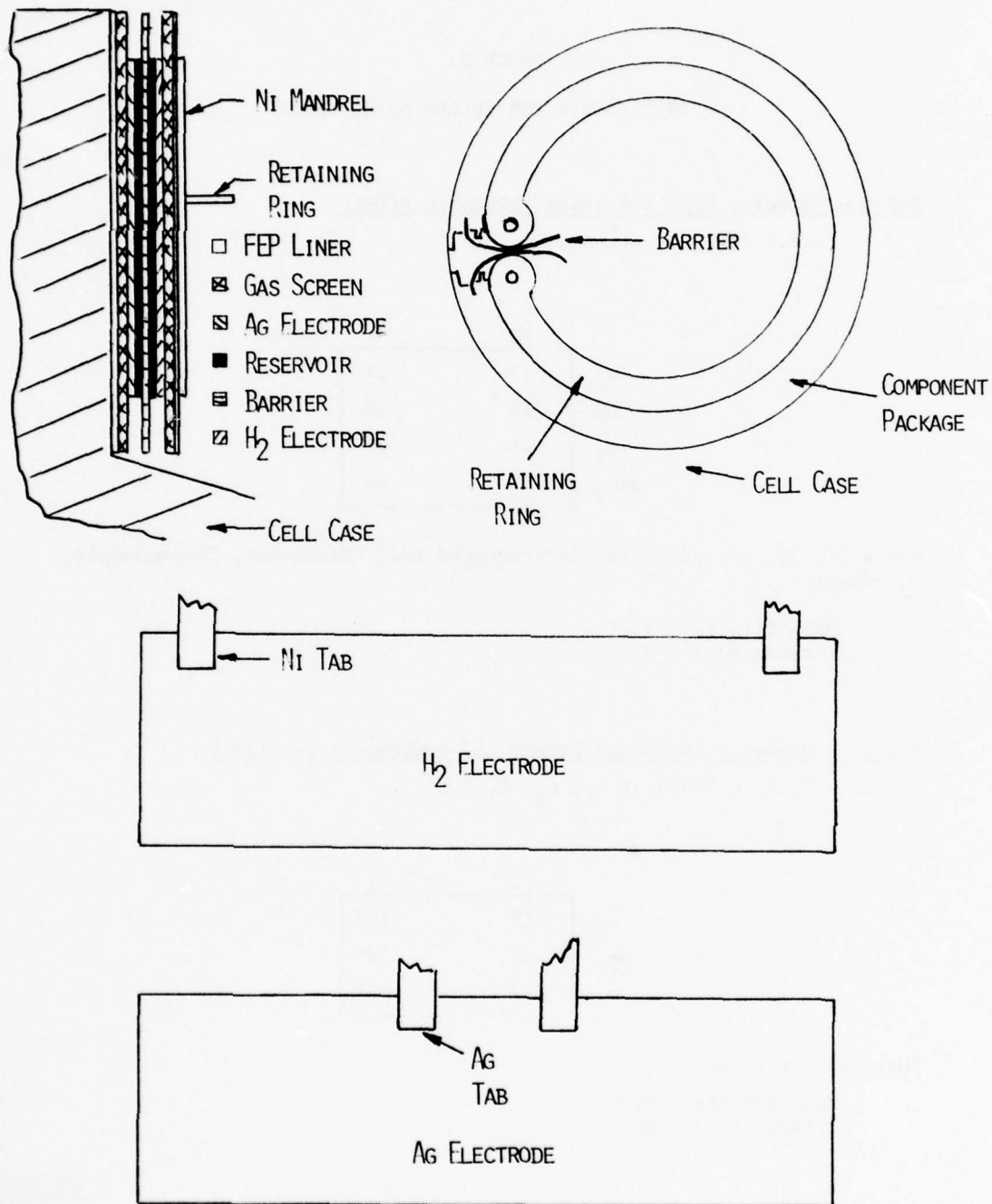


Figure 23. Schematic of rolled Ag/H₂ cell configuration.

TABLE 23
TEST MATRIX FOR ROLLED Ag/H₂ CELLS

Set I - Membrane type and plate thickness effect

N, E, C fixed at m_1 , e_0 , C_1

	t_0	t_1
m_0	17	18
m_1	19	20
m_2	21	22
m_3	23	24

Cells 21, 22, 23 and 24 are instrumented (Ref. Electrode, Thermocouple, O₂ Sensor).

Main Effects: M, T
Interaction: MT

Set II - Number of membrane layers and membrane type effect

T, E, C fixed at t_1 , e_0 , C_1 .

	n_0	n_1
m_0	25	18*
m_2	26	22*
m_3	27	24*

*Carried out in Set I.

Main Effects: M, N
Interaction: MN

TABLE 23
(CONTINUED)

Set III - Effects of electrolyte level, plate thickness and membrane type

A: N, M, C fixed at n_1 , m_1 , C_1

	t_0	t_1
e_0	19*	20*
e_1	28	29

*Carried out in Set I.

Main Effects: E, T
Interaction: ET

B: T, C, N fixed at t_0 , C_1 , n_1

	e_0	e_1
m_0	17*	30
m_2	21*	31
m_3	23*	32

*Carried out in Set I.

Main Effects: E, M
Interaction: EM

TABLE 24

PRETEST HISTORY OF ROLLED Ag/H₂ CELLS

<u>Cycle No.</u>	<u>Data Record No.</u>	
1	81 to 83	<p>Cell formation (16 cells). Cells 22, 24, 26 and 31 exceeded 2.5 V on charge. All cells except 17, 28, 30, 18, 25, 27 polarized below 0.5 V on discharge (1A).</p> <p>All cells reimpregnated. Charged cells discharged.</p>
2	84, 85	<p>Second formation charge. Cells 20, 22, 26 exceeded 2.5 V on charge. Cells 20, 22, 26 and 31 could not be discharged at C/2 rate.</p> <p>Cells 20, 22, 29 and 31 reimpregnated. Cell 26 disassembled and rebuilt as 26R.</p>
3	88	<p>Charge-discharge cycle (C/2 rate). Cells 20, 22, 24, 27, 28 exceeded 2.5 V on charge. Cells 20, 22, 27 polarized below cut out limit. Cells 20 and 22 reimpregnated (4th impreg.)</p>
4	89	<p>Charge-discharge cycle (C/2 rate). All cells including 26R reinserted. Cells 20, 22, 26, 27 exceeded 2.5 V. Cells 20, 22, 26 were cutout by low voltage limit.</p>

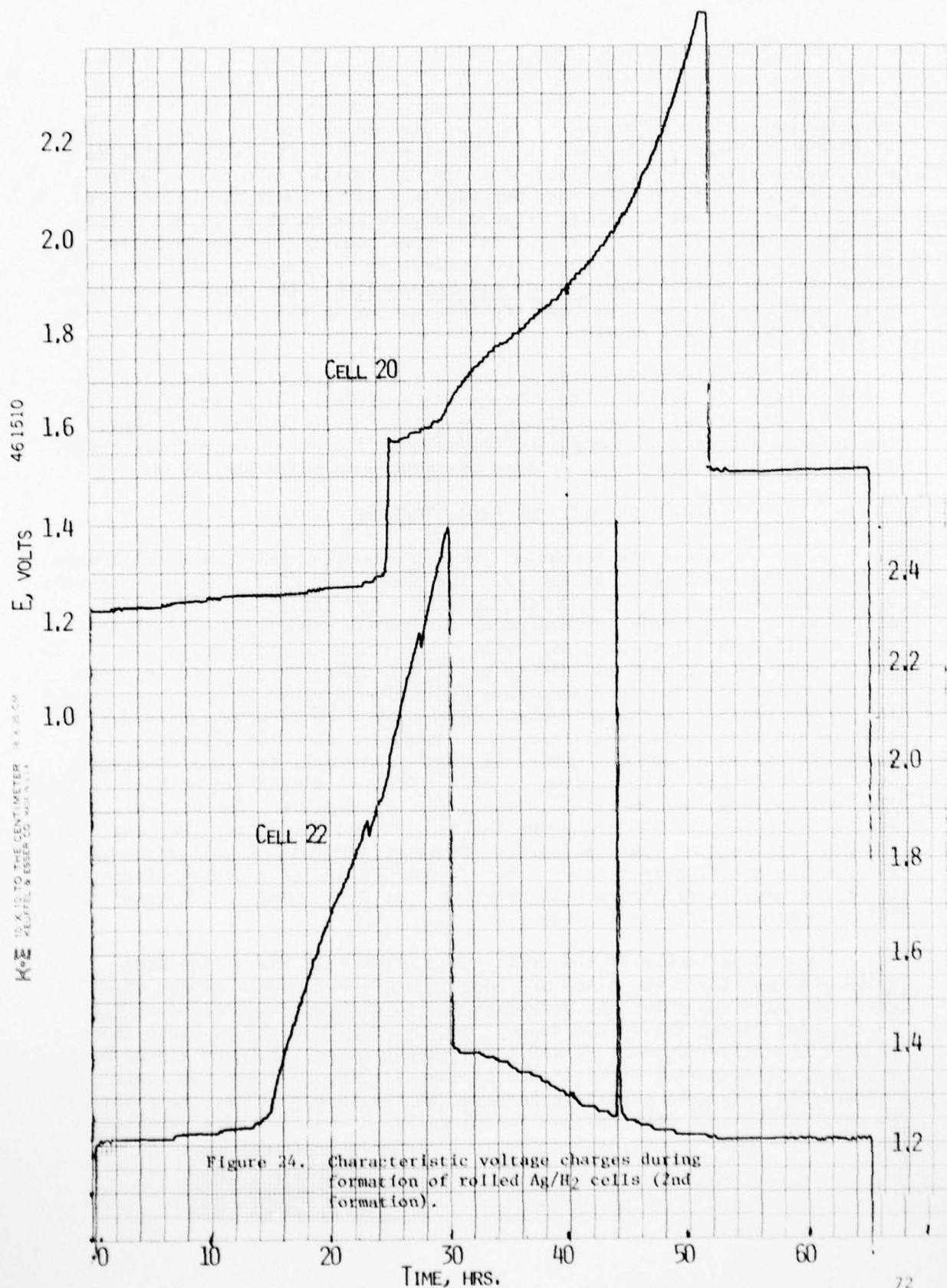
experimental evidence pointed to lack of electrolyte as the cause for the high cell impedance, all cells were reimpregnated. After reimpregnation, cells which previously polarized severely, discharged normally. During a second formation charge the same behavior described above was encountered again. The problems were more pronounced with the thick electrode cells. Figures 24 and 25 show typical potential-time behavior during formation charge. A more detailed comparative evaluation is given in Table 25. It shows that the second impregnation did help moderate the polarization somewhat, however, the basic problem remains, and as we will discuss later, is of a more fundamental nature.

Two characteristic voltage time curves for the C/2 rate cycles are shown in Figs. 26 and 27. The voltage trace of Cell 17 is fairly normal. Cells 21, 23, 31 and 32 show similar behavior. Cell 19 (Fig. 27) shows the voltage increase on charge and the voltage dip on subsequent discharge. This behavior was found more or less pronounced in all other cells.

4.3.2 Accelerated Cycle Testing

After the formation and C/2 capacity cycles, the cells were tested using accelerated AF cycles. The charge and discharge currents were 0.455 A for thin, 1.20 A for thick and 4.55 A for thin 12.0 A for thick plate cells respectively corresponding to nominal capacities of 5.70 Ah for thin and 15.0 Ah for thick plate cells. The thick Ag plate cells 20, 22, 26 and 27 were not included in this test. Of the thick Ag plate cells, only the two cells with the inorganic NASA separator remained in operation beyond the second cycle. Of the thin plate cells, two with Visking failed during the 9th and 21st cycles while the ones containing the NASA separator continued to cycles 48 and 65. Only the thick plate cell (No. 25) completed over 500 AF cycles corresponding to over 1000 deep discharges without failure. The test history is summarized in Table 26. Voltage data for Cell No. 25 during cycle 184 and 528 are shown in Figs. 28 and 29. After the last cycle the cell was left on open circuit to determine its rate of self discharge. The results are discussed later. Subsequently a C/2 rate charge-discharge cycle was used to determine cell capacity. At 7.5A (nominal C/2 rate) the cell capacity to .8V was 12.2 Ah.

Upon disassembly of the cell it was noted that the silver side nylon absorber layer was black and contained a considerable amount of silver. The NASA separator was very dark at the membrane side and dark grey on the side facing the H₂ electrode. The H₂ electrode showed large areas of distinct silver deposition and the adjacent nylon absorber layers were medium grey indicating the presence of some silver. Overall, the cell appeared in very good condition considering the test history. It contained no short circuits. The pressure vessel walls showed oxidative attack.



461510

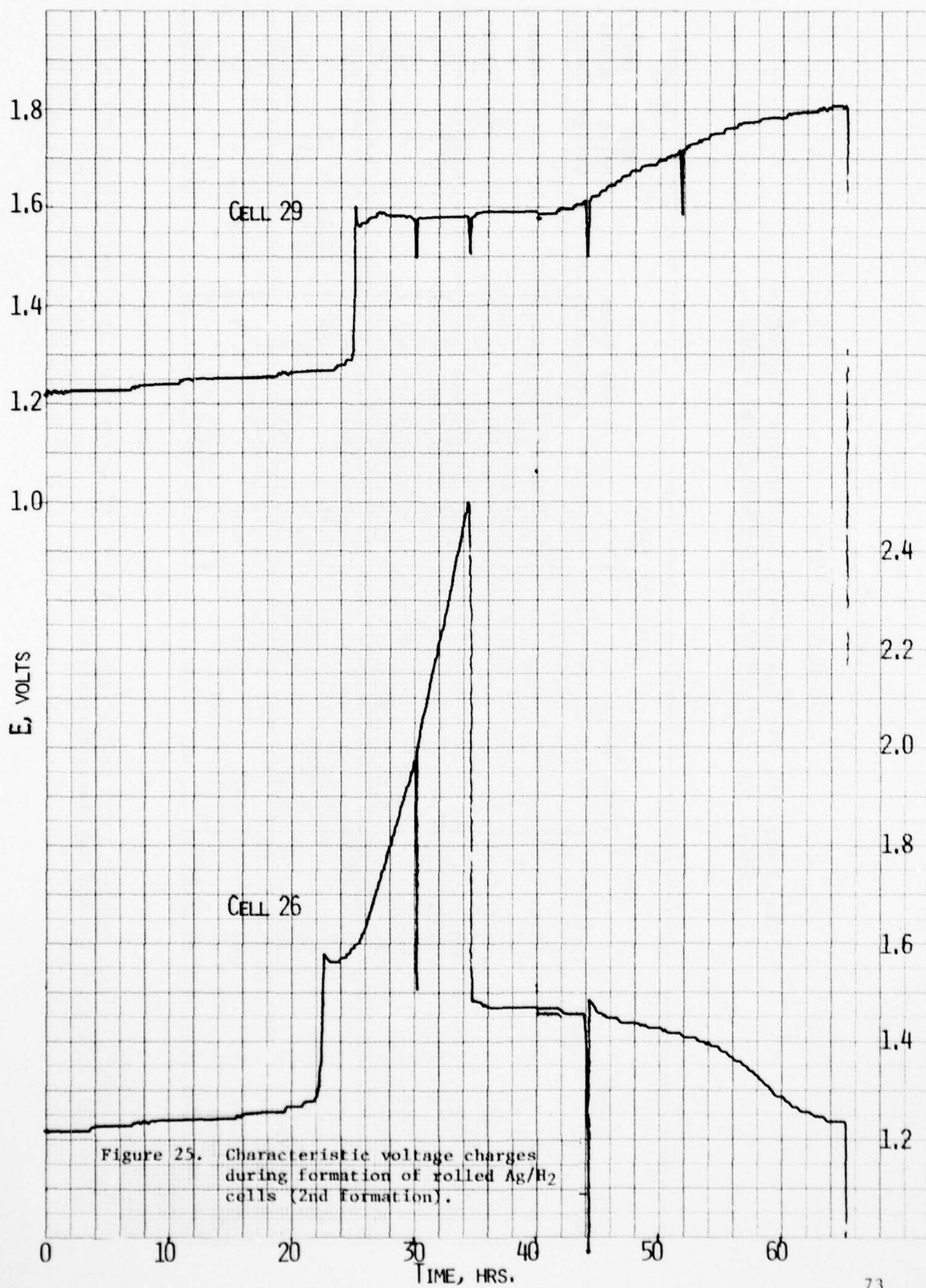


Figure 25. Characteristic voltage charges during formation of rolled Ag/H₂ cells (2nd formation).

TABLE 25

ROLLED Ag/H₂ CELLS

Charge Capacity - Voltage Behavior and Expelled Electrolyte
during the First and Second Formation Charge Cycle

Cell No.	Barrier Type	Layers	First Charge			Capacity (Ahr)			Second Charge		Drained KOH (cm ³)	
			to 1.7 V	to 2.0 V	to 2.5 V	to 1.7 V	to 2.0 V	to 2.5 V	to 1.7 V	to 2.5 V	First Charge	Second Charge
17	NASA	2	7.98 (1.73V)	7.70 (2.3V)	-	6.65 (1.74V)	-	-	-	-	5	1.5
19	RAI 2193	2	3.22	-	-	7.02 (1.77V)	-	-	-	-	6	2
21	RAI 2291	3	1.04 (1.84V)	-	-	6.78 (1.75V)	-	-	-	-	3*	1.5
23	Visking	3	5.18 (1.86V)	-	-	6.41 (1.74V)	-	-	-	-	7	1.5
28	RAI 2193	2	2.80 (1.80V)	-	-	6.97 (1.82V)	-	-	-	-	6	7
30	NASA	2	7.90 (1.73V)	-	-	7.63 (1.72V)	-	-	-	-	4	1.5
31	RAI 2291	3	1.40	6.24	6.61	7.02 (1.92V)	-	-	-	-	9	4.5
32	Visking	3	2.88	8.23 (2.08V)	-	7.05 (1.75V)	-	-	-	-	5	3
18	NASA	2	18.50 (1.73V)	-	-	17.05 (1.77V)	-	-	-	-	3	2
20	RAI 2193	2	11.14	13.39 (2.41V)	-	10.46	14.65	17.18	-	-	9	4
22	RAI 2291	3	8.55	9.25	9.95	6.79	8.33	10.06	-	-	11	6
24	Visking	3	7.85	10.65	14.09	17.85 (1.75V)	-	-	-	-	5	0*
25	NASA	1	19.21 (1.73V)	-	-	15.72 (1.75V)	-	-	-	-	5	1
26	RAI 2291	1	5.82	6.45	7.57	8.86	9.99	11.46	-	-	11	4
27	Visking	1	8.97	17.13 (2.24V)	-	17.58 (1.76V)	-	-	-	-	7	7
29	RAI 2193	2	10.23 (1.88V)	-	-	17.12 (1.80V)	-	-	-	-	9	9.5

*Cell valve leaks.

() Denotes maximum voltage reached; total charge input 8.48 and 8.65 Ah for thin, 19.87 and 21.65 Ah for thick plate cells during the 1st and 2nd charge respectively.

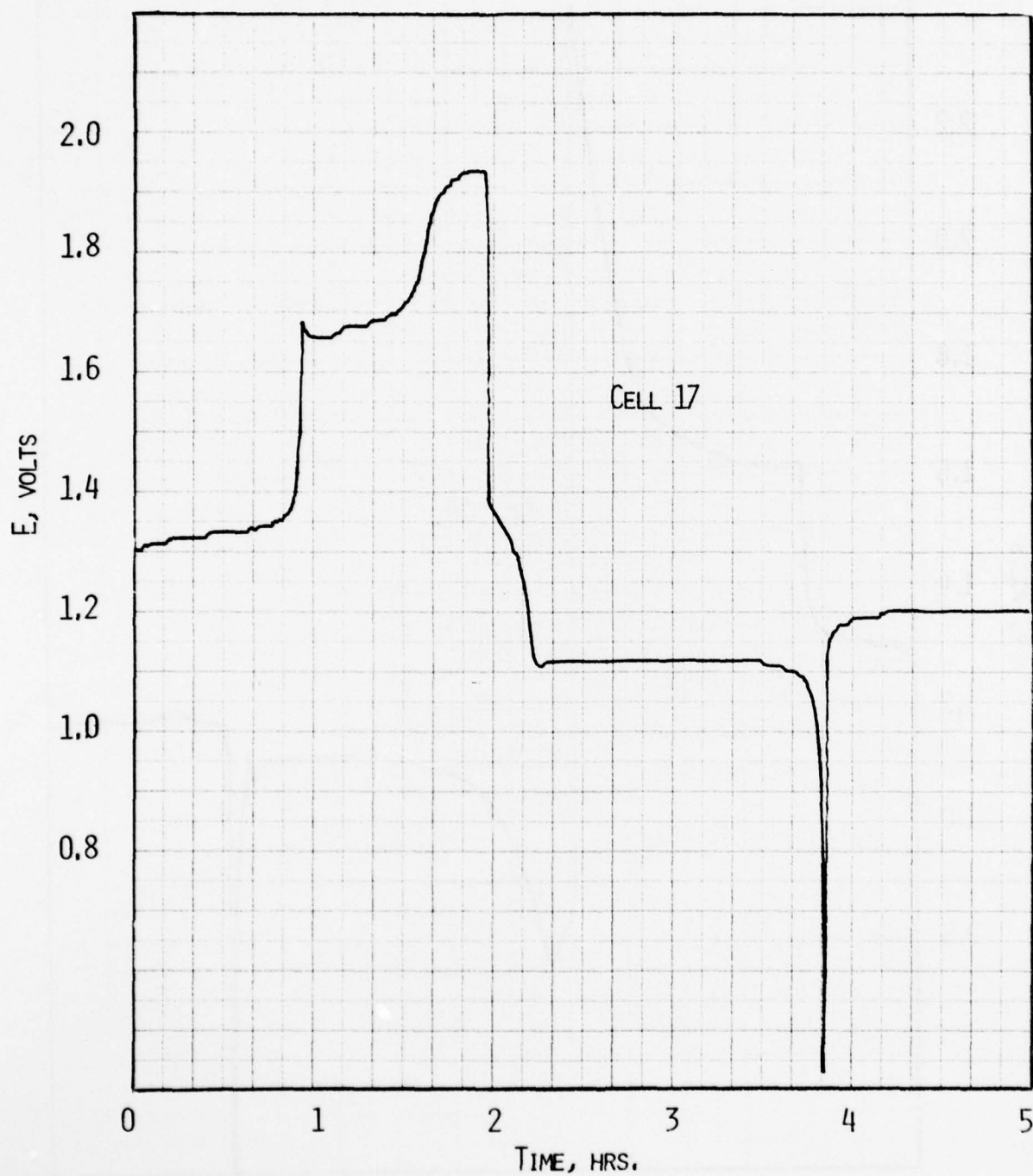


Figure 26. Cell voltage during a charge-discharge cycle of Cell 17 at 2.5 A.

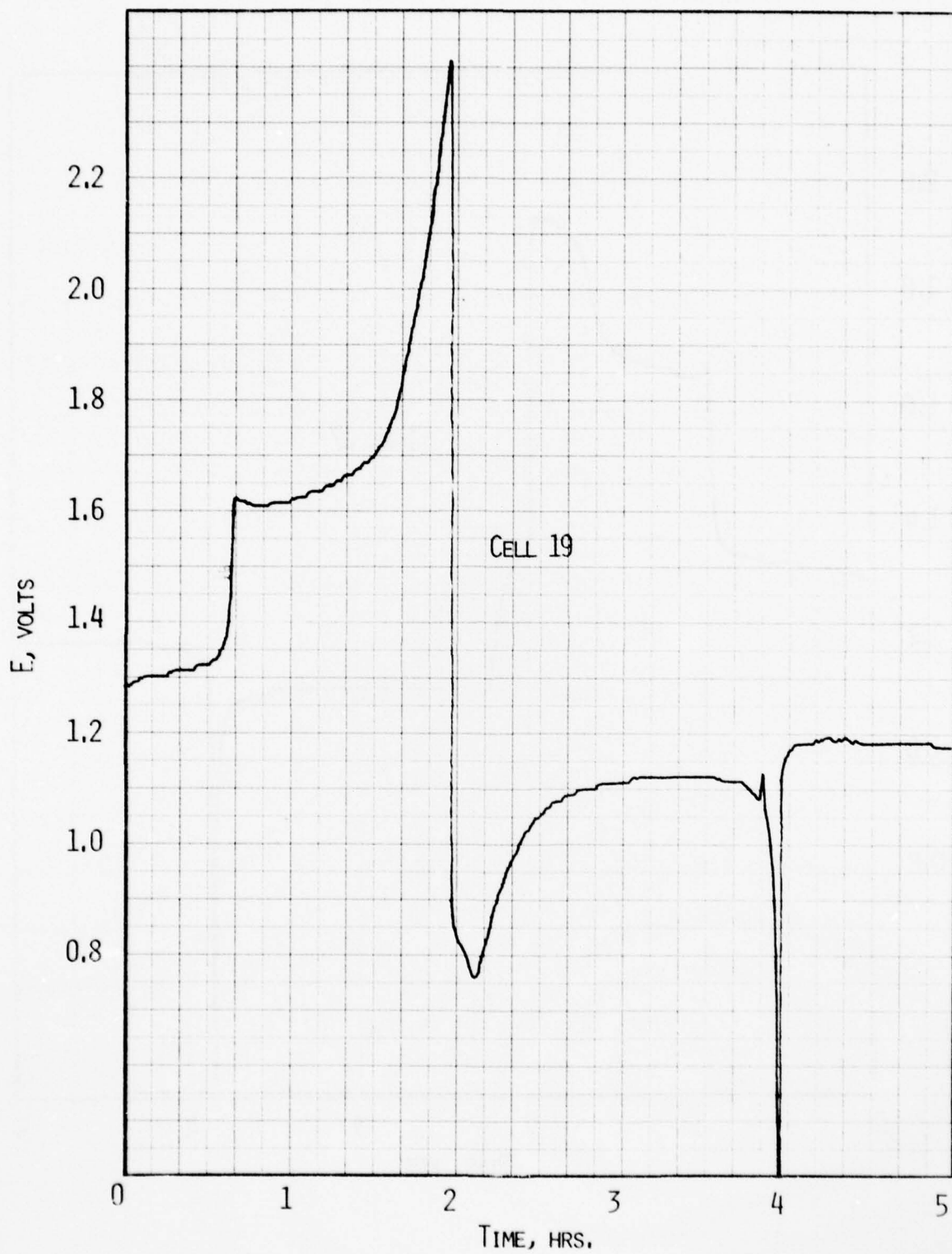


Figure 27. Cell voltage during a charge-discharge cycle of Cell 19 at 2.5 A.

TABLE 26

TEST HISTORY OF ROLLED Ag/H₂ CELLS. ACCELERATED AF TEST CYCLE

<u>Cycle No.</u>	<u>Data Record No.</u>	
1	008A	Cells 17 to 19, 21, 23 to 25, 28 to 32 started cycling.
2	008B	Cells 28, 29 and 31 failed.
6	008F	Cell 21 failed (>2.5 V).
9	0092	Cell 32 failed.
21	009E	Cell 23 failed.
47	00B7	Cell No. 18 failed on discharge.
48	00B8	Cell No. 17 failed on discharge.
65	00C9	Cell No. 30 failed on discharge.
530		Cell No. 25 was removed from test without failure.

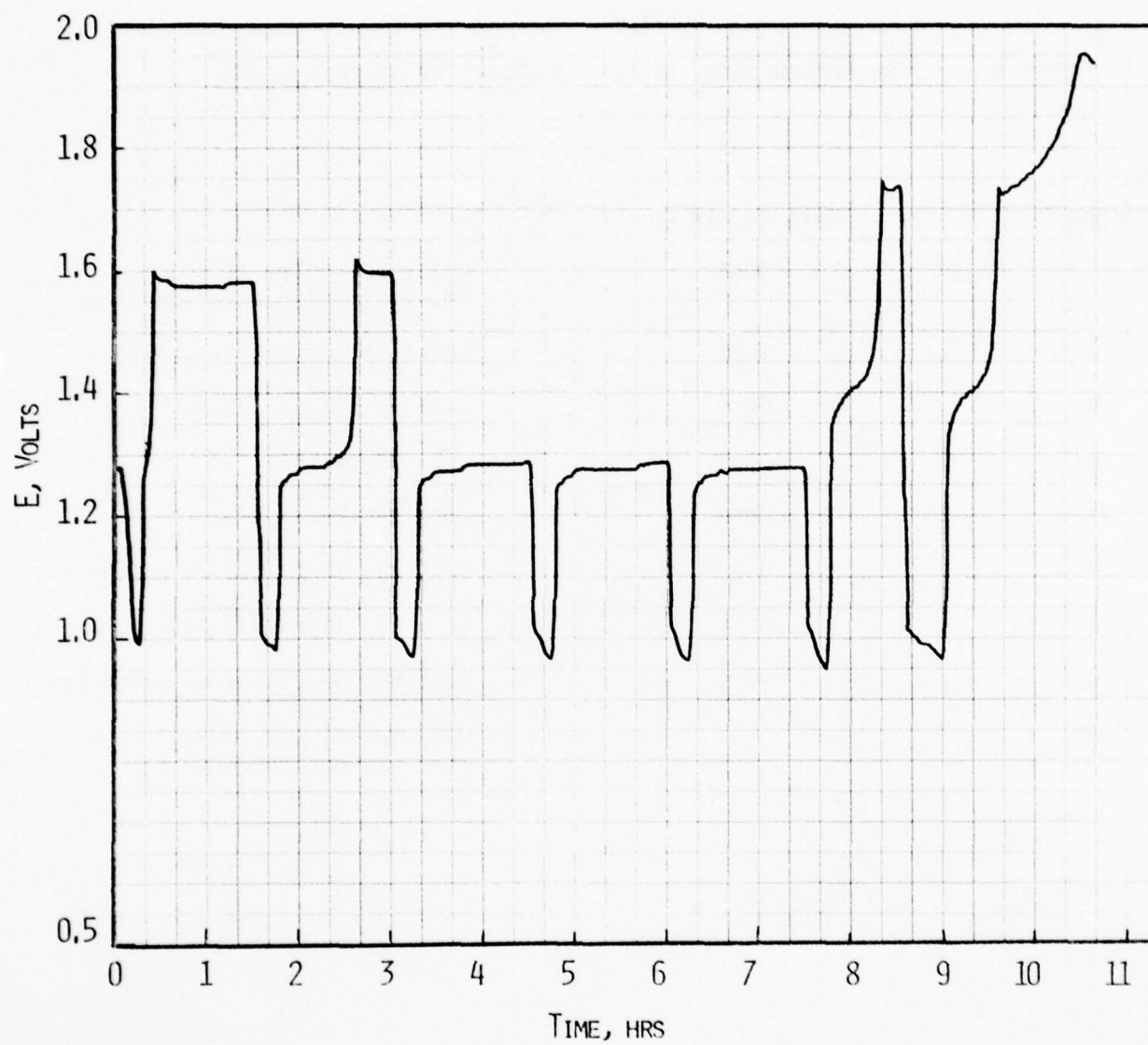


Figure 28. Potential of Ag/H₂ Cell No. 25 during Cycle No. 184.

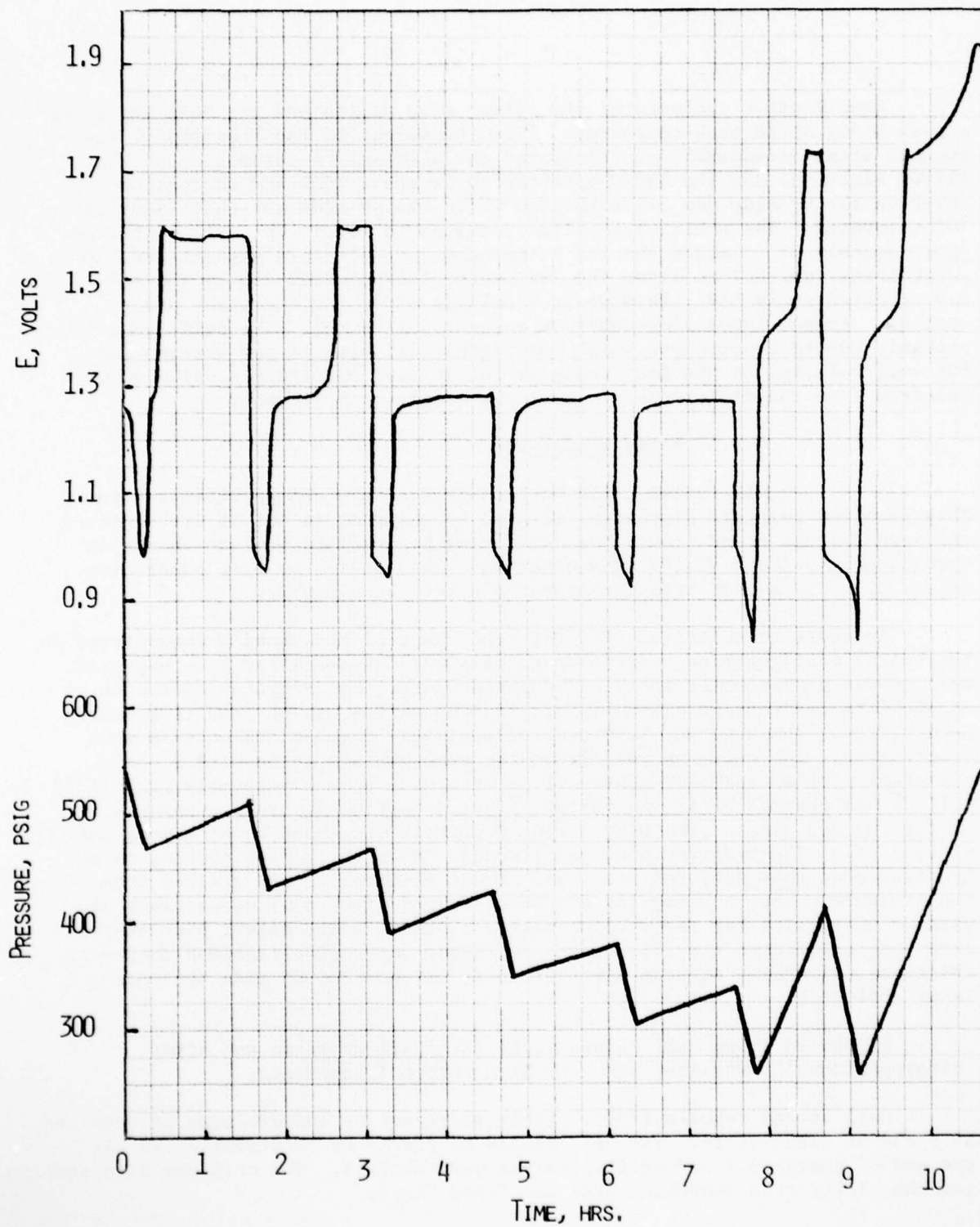


Figure 29. Voltage trace (upper) and pressure profile (lower) of Cell No. 25 during AF Cycle No. 528.

Quantitative analysis of the silver side pella and the NASA separator showed 0.66g Ag in each component. From the weight of the individual components after disassembly we calculated the electrolyte saturation of the silver electrode and the NASA separator to be about 100% and the pella layer on the H₂ side was 74% saturated while the Ag side absorber layer was 70% saturated. The electrolyte history was as follows: The cell contained approximately 37 cc after the 2nd reimpregnation. Drained amounts are 1.0 cc after formation, 0.2 cc after the 2nd cycle, 1.8 cc after 413 cycles and 2.0 cc after cycle 529. This would result in 32 cc for the stack after cycling. From weighed components we account for 24 cm³. The difference is probably due to electrolyte which was visibly clinging to gas screens and the cell wall and to the inaccuracy in the initial electrolyte value which resulted from the difference of two large electrolyte volumes.

4.3.3 Failure Analysis

All failed cells were subjected to a charge retention test. This involved complete discharge followed by charging to ~8% of its capacity and open circuit stand. Over the monitoring period (~24 hrs) no change in open circuit voltage (1.18V) was observed. This indicated that short circuits, e.g., by silver bridging appeared not to be a problem.

In order to positively identify the cause of the problem encountered in the rolled configuration several test cells were disassembled and inspected. Cell 26 was disassembled in the discharged state. No irregularities such as non-uniform compression or spotty utilization of the silver electrode could be detected. The absorber layers were relatively dry but did contain some electrolyte. The cell was rebuilt in the same configuration with a new silver electrode. Similar observations were made upon disassembly of Cell 22. Cell 20 was charged until the voltage started to rise and then disassembled in the charged state. The silver side reservoir was found to be almost completely dry. The hydrogen side was flooded. Even the Teflon backing of the hydrogen electrode appeared wet. 8.3 cm³ of electrolyte was drained from the pressure vessel. Using the component weight after cell disassembly and without correction for the obvious silver deposit in the silver side absorber layer one calculates the following electrolyte saturation (assumed component thickness, 15 mil). Ag side absorber <36%, 1st and 2nd H₂ side absorber layer >68% each.

Figure 30 shows cell polarization (Cell 31) prior to and after reimpregnation illustrating also the high internal impedance.

Cell 26 was rebuilt (26R). After impregnation and draining it retained 35.9 cm³ of electrolyte. The cell failed on charge by exceeding 2.5V. At the end of charge 6.7 cm³ of electrolyte were drained. The cell was disassembled and the silver side absorber layer was found "dry".

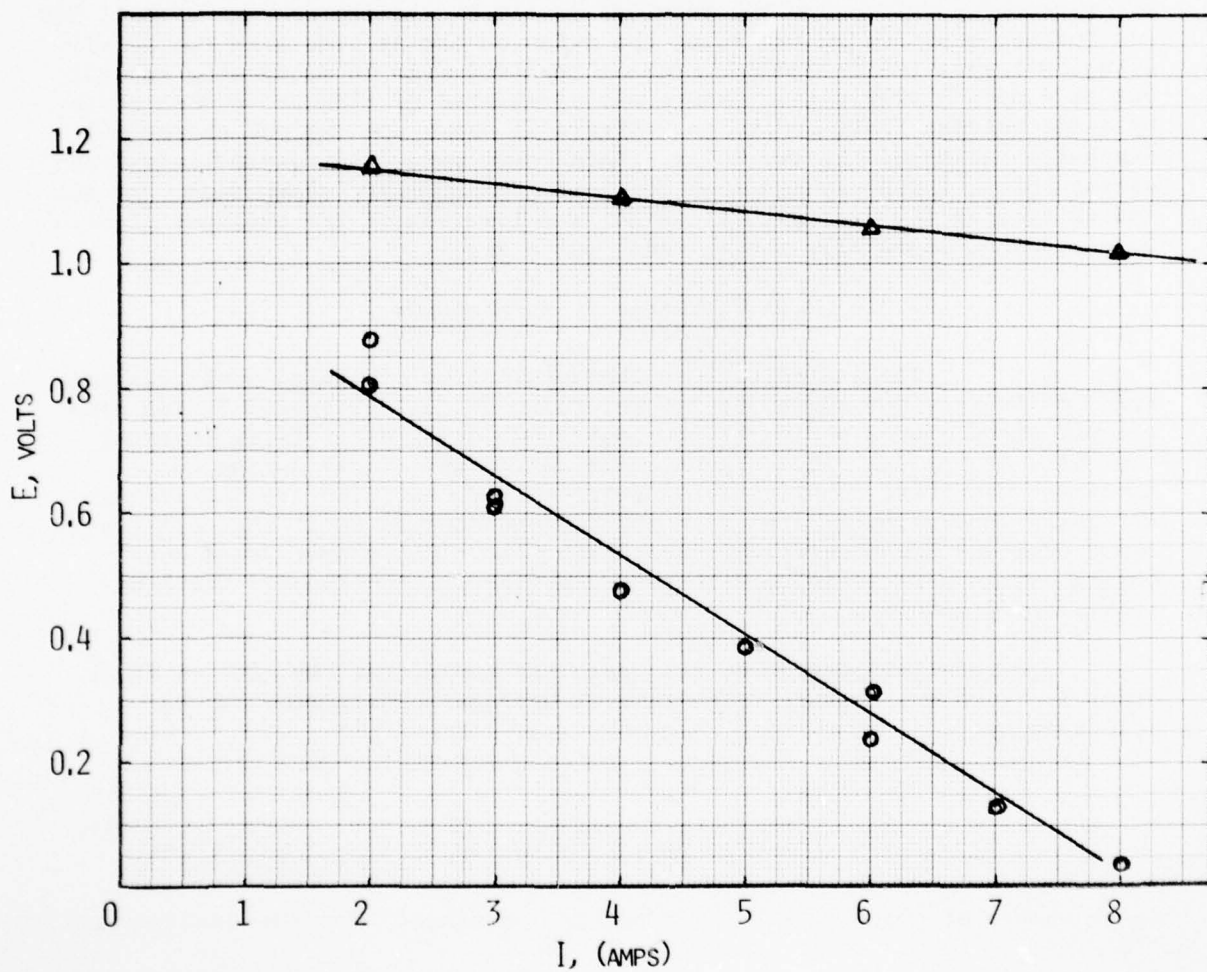


Figure 30. Cell voltage as a function of current prior (O) and after (Δ) third impregnation (Cell 31).

One of our concerns is related to the absorber layer-membrane interface. With a relatively dry non woven nylon, intimate contact which is necessary for back wicking would exist only where nylon fibers touch the membrane and thus exist only over a small surface area. We therefore rebuilt cell 26R in the same configuration but with one layer of 10 mil asbestos on either side of the barrier membrane (Cell 26RA). Charging was terminated after reaching 2.5V. Cycling resulted in rapid capacity decrease. Cell 26R was further modified by replacing the nylon on the Ag side with two 10 mil asbestos layers (Cell 26RAT). Cycling resulted also in decreasing capacity but at a much slower rate. Charge was terminated by time or in most cases by a set voltage limit on charge. Figure 31 shows two typical charge and discharge curves of the two cells. Both cells were electrolyte-limited and excess charge input results in a continuing electrolyte starvation. At the end of cycling (40 cycles), Cell 26RAT had lost 40% of its original electrolyte leaving, especially the Ag side, quite dry.

4.3.4 Self-Discharge of Ag/H₂ Cells

The self-discharge characteristics of rolled configuration Ag/H₂ cells were determined by the recording of cell pressures during open circuit stand over a period of 600 hours (~25 days) after fully charging the cells at the C/2 rate. These cells failed very early during cycle testing. Therefore complications due to silver migration are not present. All cells were reimpregnated with 40% KOH and charged until the capacity input exceeded the theoretical capacity by 15%. Cells that dried out during charge were re-impregnated and charging was continued. The test took place @ 23°C.

A careful evaluation of this data has shown that the rate is first order in hydrogen pressure. The rate of hydrogen consumption can be described by

$$\frac{dn_{H_2}}{dt} = -k p_{H_2} \quad (14)$$

n_{H_2} = number of moles of H₂, t = time, p_{H_2} pressure. From the general gas law,

$$n_{H_2} = \frac{V}{RT} \cdot p \quad (15)$$

V = cell volume, R = gas constant, T = temperature.

AD-A061 426

EIC CORP NEWTON MASS
SILVER-HYDROGEN ENERGY STORAGE.(U)
AUG 78 G L HOLLECK, M J TURCHAN, F S SHUKER

F/G 10/3

F33615-76-C-2093

UNCLASSIFIED

AFAPL-TR-78-65

NL

2 of 3

AD
A061 426



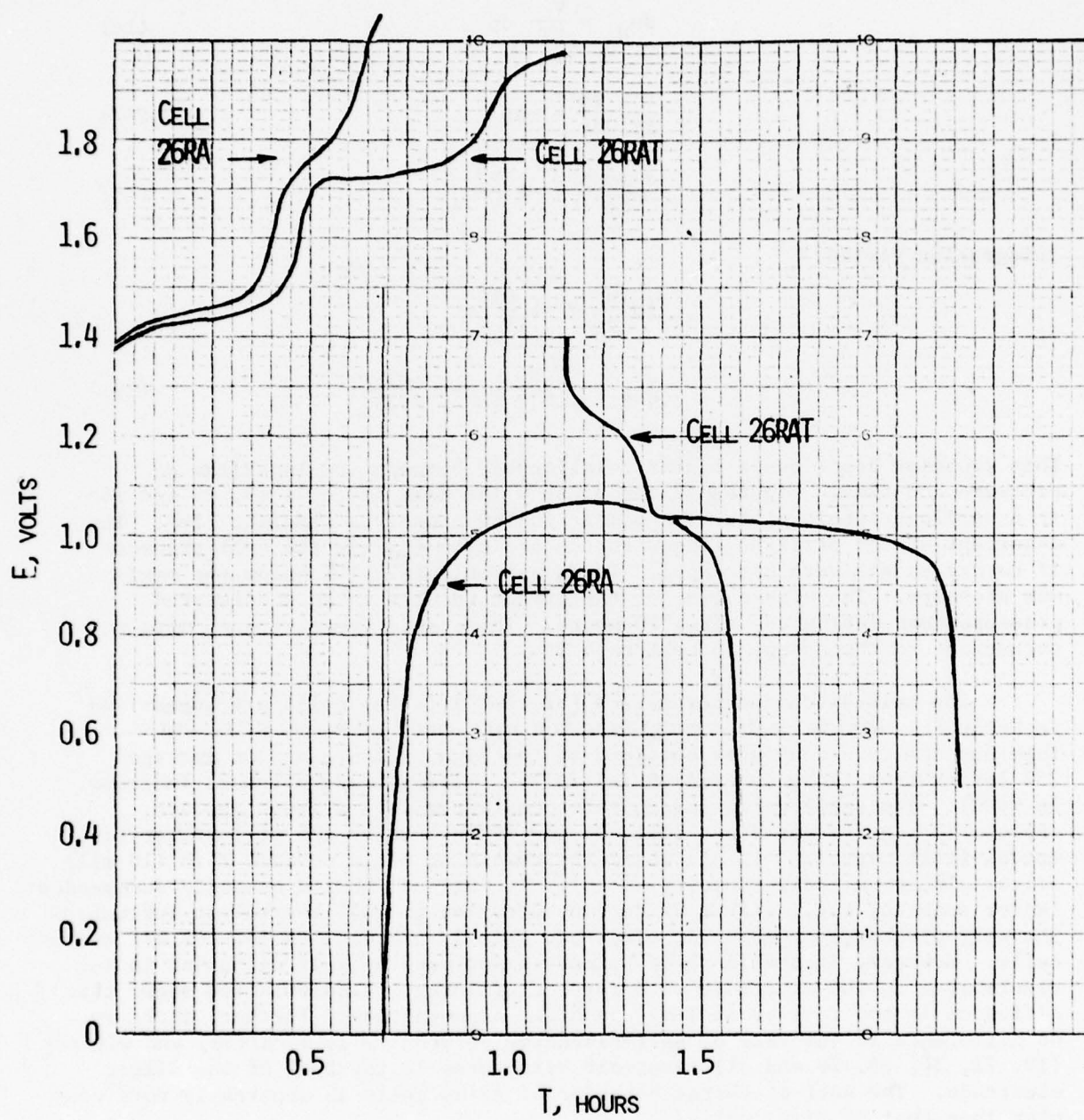


Figure 31. Typical charge-discharge curves of Cell 26RA and 26RAT.

$$dn_{H_2} = \frac{V}{RT} dp \quad (16)$$

$$\frac{V}{RT} \frac{dp}{dt} = -kp \quad (17)$$

$$\frac{d \ln p}{dt} = -k \frac{RT}{V} \quad (18)$$

Integration yields

or
$$\ln \frac{p}{p_0} = -k \frac{RT}{V} t$$

$$\log p = \log p_0 - k \frac{RT}{2.3V} t \quad (19)$$

This equation describes a linear relationship between the logarithm of pressure and time. Figures 32 and 33 show the data of cells 19, 24 and 25 in a semilogarithmic plot. The points follow closely a straight line. The intercept of the straight line with the ordinate (p_0) is the cell pressure if no oxygen gas were entrapped. It is approximately 10% below the maximum pressure. The dissipation of the oxygen results in an accelerated pressure drop during the first 10 hours. This rapid pressure drop does not correspond to the change in cell capacity.

The self-discharge parameters for the different cells are summarized in Table 27. Within each test group, the rate constants are quite uniform but the rate constants obtained at the high pressure are on average 75% larger than those determined initially. (The average pressure increase is ~40%). The small variation in rate constant within a group appears especially significant since cells 24 and 29 have thick (25 mil) silver electrodes (cell capacity ~15 Ah) while the remaining cells contain thin (10 mil) silver electrode (cell capacity ~6 Ah). It suggests that a capacity independent factor such as, e.g., silver oxide concentration in the electrolyte influences the self-discharge. Geometric electrode area is a common factor for all tested cells. However, it should be of primary importance only if diffusion in the electrolyte in the electrode were rate determining. A calculation shows that diffusion is too fast by at least an order of magnitude. Further, there is no difference in the rate of self-discharge between cells with (29) and without (19, 21, 24, 25, 28 and 31) reservoir structures in the back of the silver electrode. The self discharge behavior of Ag/H₂ cells is apparently more complex than that of Ni/H₂ cells.

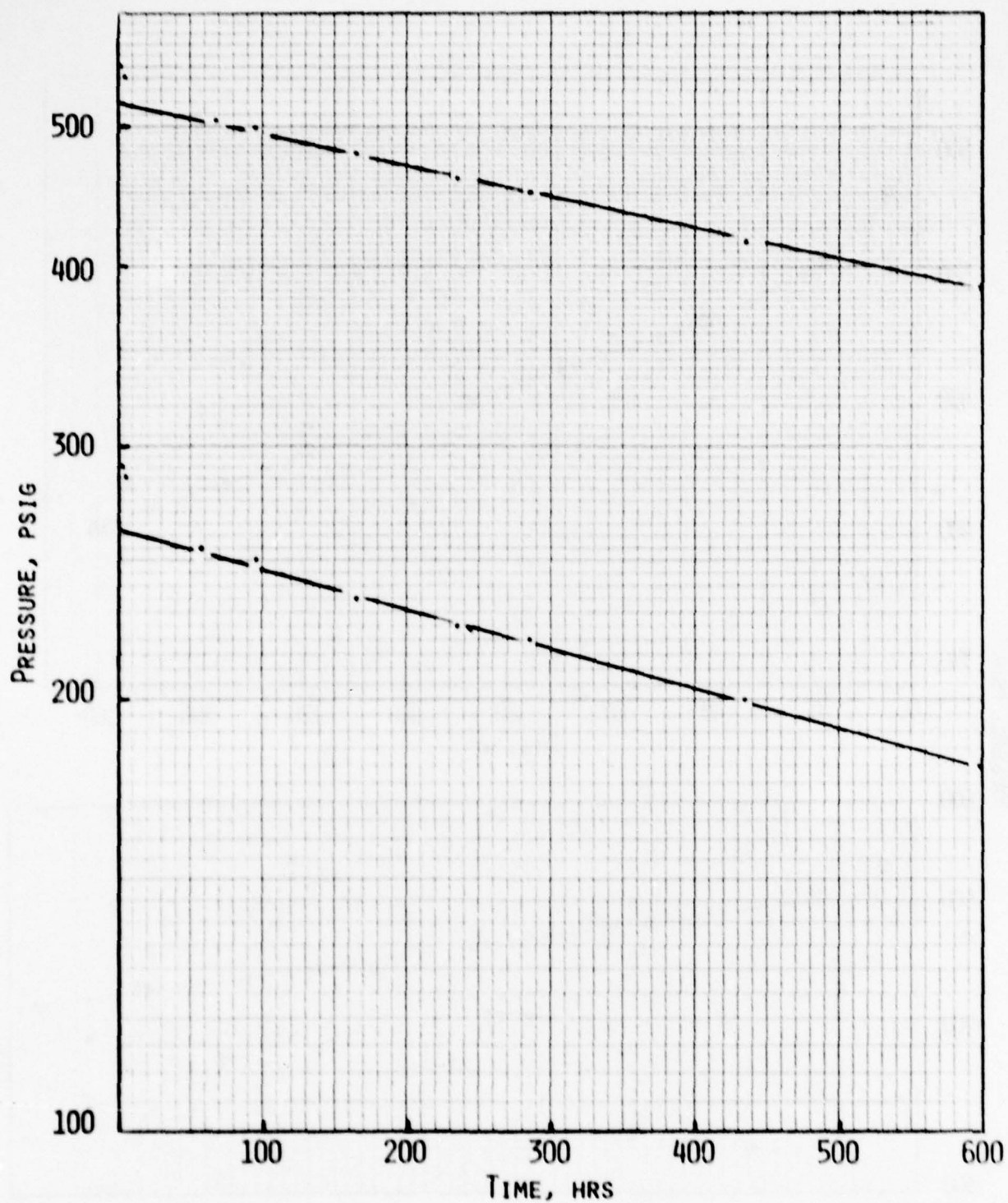


Figure 32. Logarithmic plot of Ag/H₂ cell pressure vs. time during self-discharge, 23°C. Upper Cell No. 24, lower Cell No. 19.

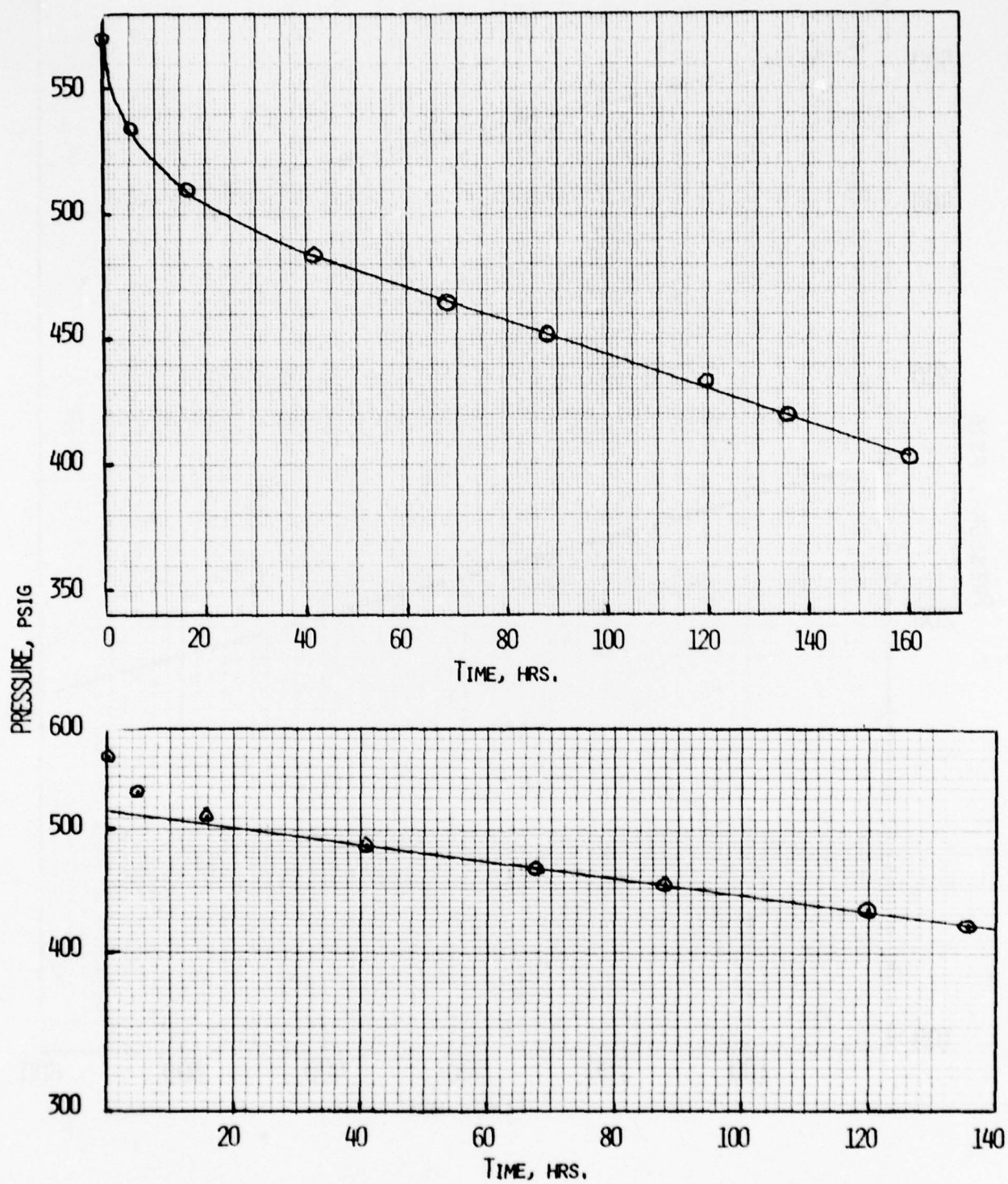


Figure 33. Pressure change with time during self discharge test of Cell No. 25 subsequent to extended cycle testing (lower-semi log plot of data).

TABLE 27
SELF-DISCHARGE PARAMETERS FOR Ag/H₂ CELLS AT 23°C

Cell No.	P _{max} (psi)	P _o (psi)	Slope		-k × 10 ⁵ (moles atm ⁻¹ hr ⁻¹)	Pre-charge (psi)
			$\frac{-kRT}{2.3V} \times 10^4$ (hr ⁻¹)	$\Delta P/Ahr$ (atm/Ahr)		
19	290	267	2.9	1.8	0.58	105
21	271	227	3.2	1.6	0.85	111
24	549	525	2.3	2.0	0.50	102
28	270	255	2.9	1.8	0.65	100
29	405	328	4.1	2.2	0.84	135
31	320	267	3.4	1.9	0.68	95
19	705	691	5.1	1.8	1.20	590
21	704	692	4.0	1.6	1.05	593
24	958	950	4.2	2.0	0.92	589
28	692	686	8.6	1.8	2.02	587
29	775	749	5.0	2.2	0.99	600
31	703	689	4.5	1.9	0.99	590
25	570	518	6.5	1.8	1.55	100

Cells No. 19, 21, 28 and 31 - thin Ag electrodes.
Cells No. 24, 25 and 29 - thick Ag electrodes.

4.3.5 Discussion

Testing of rolled Ag/H₂ cells revealed the full severity of the electrolyte management problem. Some cell configurations (e.g., thick Ag plate with P2291 membranes) showed normal behavior during the initial part of charge. After passage of a certain amount of charge the voltage started and continued to rise beyond 2.5V. Current reversal (discharge) at this time results in severe polarization.

Analysis of the data as shown, for example, in Table 28, in this context reveals certain trends. Maintaining electrolyte balance in thick electrode cells (high current density) is more difficult than in thin plate cells. Electrolyte management with RAI 2291 appears to be most difficult. More electrolyte on the silver side helps cell performance (prevents drying of the Ag side; compare, e.g., Cell 20 and 29 both with 2 layers of P2193 but with low and high electrolyte level respectively). If the increased electrolyte capacity is supplied at the hydrogen side as is the case in the thin plate Cells 28 or 31 no such improvement follows. The NASA separator shows the best performance.

The potential dip on cell discharge is caused by high resistive polarization of the dry Ag side absorber layers. Upon continued discharge electrolyte migrates towards the silver side and the voltage recovers.

It is quite apparent that electrolyte management and specifically drying out of the silver side absorber layer is the critical failure mode. This is despite the fact that water is produced at the silver electrode on charge. The hydrogen side actually expells electrolyte during charge. It was especially surprising to find such dramatic manifestation of this effect at the low rates used for cell formation (\sim C/60).

These findings can be understood after close examination of the transport processes taking place in Ag/H₂ cells, specifically those occurring in the membrane layers. A simulation run of our electrolyte management computer program with parameters from our membrane transport measurements showed that electromigration transports water from the silver side to the hydrogen side and this transport leads to drying of the silver side and flooding of the hydrogen side despite the production of water at the silver electrode and consumption of water at the hydrogen electrode. Relatively rapid diffusion results in negligible concentration gradients. Thus only electrolyte flow from the hydrogen side to the silver side could compensate for the water transport by transference. In an open stack the hydrostatic forces can only result from capillary action between "dry" components on one side and "wet" components on the other side of the membrane. We conducted measurements which show the presence of this effect, however, the rates of electrolyte flow are, except for the NASA separator, very small.

TABLE 28

CHARGE CAPACITY - VOLTAGE BEHAVIOR DURING THE
FIRST AND SECOND FORMATION CHARGE CYCLE

Cell No.	Barrier Type	Layers	Capacity (Ahr)			
			First Charge		Second Charge	
			to 1.7 V	to 2.0 V	to 1.7 V	to 2.5 V
17	NASA	2	7.98 (1.73V)	7.70 (2.3V)	6.65 (1.74V)	-
19	PAI 2193	2	3.22	-	7.02 (1.77V)	-
21	PAI 2291	3	1.04 (1.84V)	-	6.78 (1.75V)	-
23	Visking	3	5.18 (1.86V)	-	6.41 (1.74V)	-
28	PAI 2193	2	2.80 (1.80V)	-	6.97 (1.82V)	-
30	NASA	2	7.90 (1.73V)	-	7.63 (1.72V)	-
31	PAI 2291	3	1.40	6.24	7.02 (1.92V)	-
32	Visking	3	2.88	8.23 (2.08V)	7.05 (1.75V)	-
18	NASA	2	18.50 (1.73V)	-	17.05 (1.77V)	-
20	PAI 2193	2	11.14	13.39 (2.41V)	10.46	14.65
22	PAI 2291	3	8.55	9.25	6.79	8.33
24	Visking	3	7.85	10.65	17.85 (1.75V)	-
25	NASA	1	19.21 (1.73V)	-	15.72 (1.75V)	-
26	PAI 2291	1	5.82	6.45	8.86	9.99
27	Visking	1	8.97	17.13 (2.24V)	17.58 (1.76V)	-
29	PAI 2193	2	10.23 (1.88V)	-	17.12 (1.80V)	-

() Denotes maximum voltage reached.

This electrolyte management problem is naturally not specific to rolled stacks. The reason for its more immediate effect is the vertical arrangement which allows easy draining of excess electrolyte from the hydrogen side of the stack into the pressure vessel. In stacked arrangements the electrolyte has to cascade from the top of the stack down resulting in rewetting of lower lying components. The flow of electrolyte around the membrane edges is probably responsible for, in some cases, very rapid Ag bridging. The relatively large initial decrease in capacity of the stacked cells is probably also a reflection of electrolyte loss from parts of the cell stack.

Solutions to this problem require careful quantitative balancing of the individual transport steps in the barrier membranes. The following parameters can be used for trade-off: (1) type of membrane, (2) number of membrane layers (electromigration is independent of number of layers while diffusion and flow are affected proportionally), (3) current density (electrode thickness), (4) reservoir sizes at the Ag and H₂ electrode sides (number of absorber layers), (5) type of absorber component (pore size and pore size differences on both sides of the membrane will influence the hydrostatic driving force for flow).

5. Laboratory Ag/H₂ Cells

5.1 General Remarks

The boiler plate cell tests showed that the Ag/H₂ systems is considerably more complex than had initially been expected. To more thoroughly characterize the system and to be able to design practical cells a large number of carefully controlled experiments are needed. Small laboratory cells are much more suitable for this task than full size boiler plate cells. Among the specific problems which will be addressed in the laboratory cell experiments are: (1) electrolyte movement during charge and discharge, (2) electrolyte loss from the cell stack, (3) electrolyte capacity and pore structure of the absorber layers, (4) cell stack configuration. Components and stack arrangements which have proved successful in laboratory cells will later be tested in full size boiler plate cells.

5.2 Experimental

For closer characterization of electrolyte movement and to determine viable solutions to this problem, we set up small laboratory cells. An arrangement schematically shown in Fig. 34 is set up in a reaction kettle in a hydrogen atmosphere (1 atm). The components dimensions were as follows: Electrode size: 1.5 × 2 in. = 19.35 cm², barrier membranes: 1.75 × 2.25 in. = 25.4 cm². Ag electrode 25 mil thick with approximately 1.5 Ah capacity. The component package was held under constant compression by two compression springs. Most experiments were carried out at nominally C/2 rate. Charging was terminated

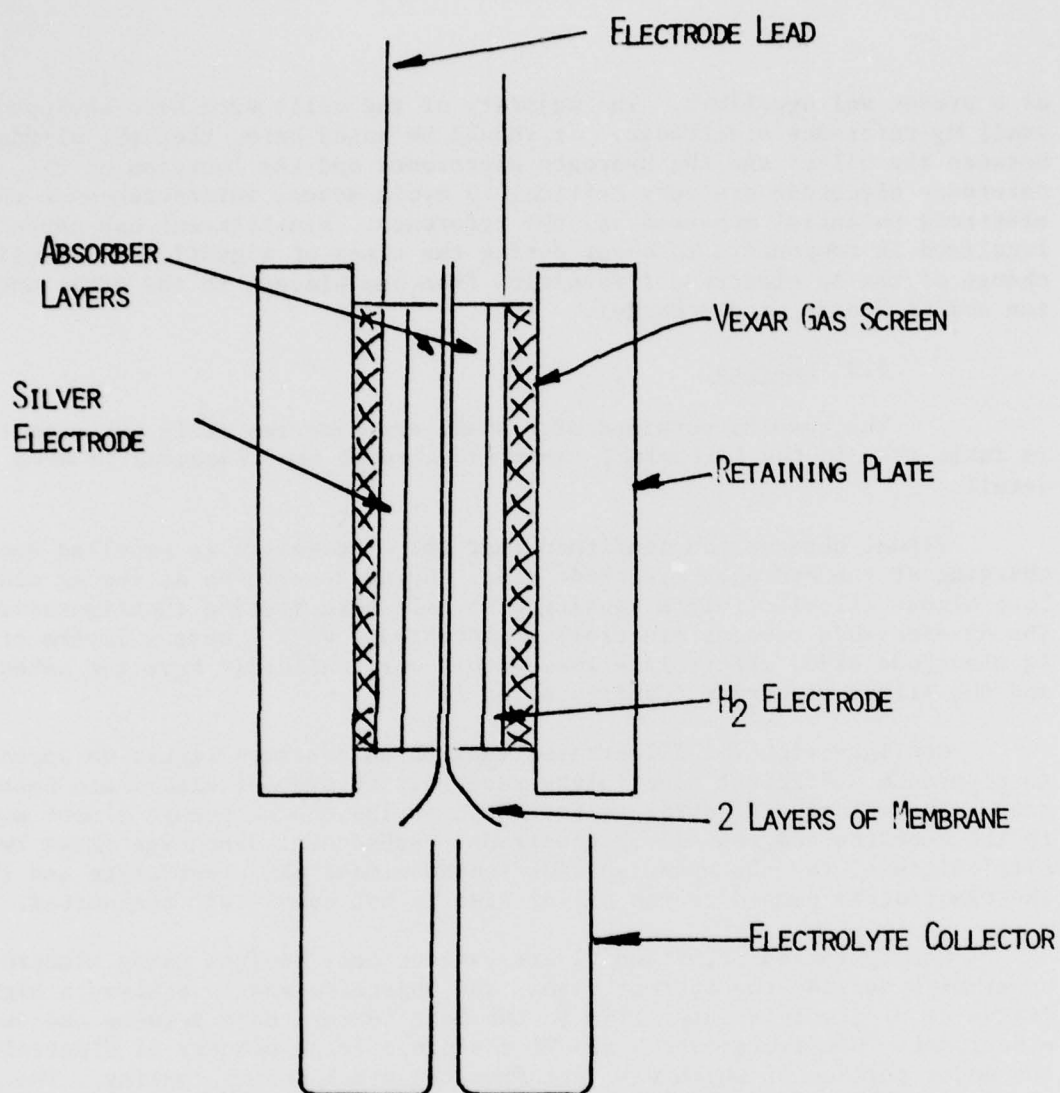


Figure 34. Schematic of small experimental Ag/H₂ cell.

at a preset voltage limit. The majority of the cells were also equipped with small H_2 reference electrodes. It should be noted here, that the alignment between the silver and the hydrogen electrodes and the location of the reference electrode are very critical to avoid severe interference in the electrode potential measured vs. the reference. Misalignment can cause very localized iR components to occur during the times of significant potential change of the Ag electrode (transition from one plateau to the other and at the end of charge or discharge).

5.3 Results

The results obtained with small experimental cells are summarized in Table 29. In the following, important aspects are discussed in more detail.

Visual observation confirmed that the electrolyte is expelled during charging at the hydrogen electrode side. Nylon reservoirs at the Ag side lose almost all electrolyte causing high cell polarization (Configuration I). The Ag electrode remains electrolyte saturated. With asbestos layers at the Ag electrode side, electrolyte loss occurs more uniformly from the asbestos and the silver electrode (Configuration II).

Configuration III illustrates that three asbestos layers do appear to provide a sufficient electrolyte reservoir to prevent high ohmic polarization. The relative electrolyte reduction during charge occurs almost equally in the asbestos and the silver electrode. Subsequent discharge shows two difficulties: (a) the hydrogen side loses almost all electrolyte and (b) the electrolyte pumped to the silver side is not completely reabsorbed.

Configuration IV, V and VI are various cell designs using electrolyte reservoirs outside the current path. The objective was to achieve a high degree of electrolyte saturation in the main current path between the two electrodes. Configurations V and VI contained large amounts of electrolyte, the major portion of which was lost from the stack during cycling. The discharge capacity is limited by "drying" of the H_2 side. The following observations are considered significant. The inefficiency of the silver electrode charging leads to approximately 10 to 15% (more charge input) despite voltage cutoff. Electrolyte is expelled from the silver side rather than wicked back into the nylon reservoirs. A pella window to provide a direct connection between membrane and reservoir (Configuration VI) reduces but does not appear to eliminate this difficulty. At the hydrogen side too, a pella reservoir will not refill through an asbestos separator. The objective of cells in Configurations VII to X was to circumvent the difficulty of refilling a large pore reservoir through a fine pore matrix by the use of a "window" arrangement where the reservoir directly touches the membrane, surrounding the electrode in a frame-like manner. This was partially successful, however,

TABLE 29

SUMMARY OF SMALL TEST CELL RESULTS

Stack and Components	Dry Wt. (g)	KOH in Component			KOH Collected		Comments
		Vac. Impreg. (g)	After Charge (g)	Saturation %	Ag Side (g)	H ₂ Side (g)	
I1 Vexar H ₂ El. 2 P2505 2 P2291 1 P2505 Ag El. Vexar	0.360	0.037					Repeat KOH abs. 0.259 2.083 0.186 0.909 0.797
	2.735	0.237					
	0.212	1.995					
	0.177	0.210					
	0.102	0.983					
	6.00	0.811					
	0.322	0.065					
I2 Vexar H ₂ El. 2 P2505 2 P2291 1 P2505 Ag El. Vexar	0.312		-				Charge to 2 V 0.6 Ah
	2.792		0.123				
	0.264		1.475	80			
	0.171		0.108				
	0.100		0.072	7			
	6.086		0.895	110			
	0.337		-		0.074	0.549	
I3 Vexar H ₂ El. 2 P2505 2 P2291 1 P2505 Ag El. Vexar	0.382		0.043				Charge to 2 V 0.75 Ah
	2.800		0.100				
	0.210		1.597	84			
	0.181		0.110				
	0.100		0.070	7			
	6.058		0.872	106			
	0.325		0.012		0.007	0.832	

TABLE 29
(CONTINUED)

Stack and Components	Dry Wt. (g)	KOH in Component			KOH Collected		Comments
		Vac. Impreg. (g)	After Charge (g)	Saturation %	Ag Side (g)	H ₂ Side (g)	
II1 Vexar	0.300	0.031					
H ₂ El.	2.769	0.202					
2 P2505	0.203	1.720					
2 P2291	0.179	0.132					
2 Asbest	0.750	1.433					
Ag El.	5.849	0.840					
Vexar	0.348	0.018					
II2 Vexar	0.308	0.021					
H ₂ El.	2.772	0.189					
2 P2505	0.201	1.823					
2 P2291	0.183	0.130					
2 Asbest	0.757	1.968					
Ag El.	5.830	0.839					
Vexar	0.308	0.016					
II3 Vexar	0.321		0.038				Charge to 1.7 V
H ₂ El.	2.800		0.116	80			0.9 Ah
2 P2505	0.208		1.512				
2 P2291	0.174		0.112	46			
2 Asbest	0.745		0.789	68			
Ag El.	5.964		0.563				
Vexar	0.321		0.007		0.042	0.911	

TABLE 29
(CONTINUED)

Stack and Components	Dry Weight (g)	KOH in Component		% Saturation	KOH Collected		Comments
		Vacuum Impregnation (g)	After Cycling		Ag Side (g)	H ₂ Side (g)	
III ₂ Vexar	0.347	0.021	0.040				Disassembled after charge, 1.05 Ah.
H ₂ Electrode	2.798	0.091	0.092				
2 Pellon 2505	0.234	1.559	1.383	89			
2 RAI 2291	0.208	0.109	0.097				
3 Asbestos	1.137	1.716	0.746	43			
Ag Electrode	5.756	0.809	0.428	53			
Vexar	0.291	0.018	0.008		0.004	1.953	
III ₃ Vexar	0.306		0.028				Cycled 3 times, disassembled in discharge state. 1st cycle charge 1.125 Ah, discharge 1.06 Ah.
H ₂ Electrode	2.736		0.108				
2 Pellon 2505	0.231		0.239	15			
2 RAI 2291	0.183		0.115				
3 Asbestos	1.148		1.429	83			
Ag Electrode	5.951		0.723	89			
Vexar	0.295		0.013		0.465		

TABLE 29
(CONTINUED)

Stack and Components	Dry Weight (g)	KOH in Component		KOH Collected		Comments
		After Cycling (discharged) (g)	% Saturation	Ag Side (g)	H ₂ Side (g)	
IV ₁ 96	Vexar	0.325				
	H ₂ Electrode	2.759				
	2 Pellion 2505	0.211				
	2 RAI 2291	0.192	15			
	3 Asbestos	1.157	>100			
	Ag Electrode	6.030	76			
	2 Pellion 2505	0.247	69			
	Vexar	0.305		(total 1.856)		Single charge-discharge H ₂ side dried
	Vexar	0.326				
	H ₂ Electrode	2.809				
IV ₂	2 Pellion 2505	0.205	40			10 cycles, 1.8 V cutoff
	2 RAI 2291	0.188				
	3 Asbestos	1.129	>100			
	Ag Electrode	5.742	91			
	2 Pellion 2505	0.195	65			
	Vexar	0.312		1.500	0.914	Accidental overdischarge caused large electrolyte loss at Ag side.

TABLE 29
(CONTINUED)

Stack and Component	Dry Weight (g)	KOH in Component		KOH Collected		Comments
		After Cycling (discharged) (g)	% Saturation	Ag Side (g)	H ₂ Side (g)	
V						
Pellon 2505	0.114	0.023	3			Wicked asbestos on H ₂ side - 34 cycles, 1.8 V cutoff.
Asbestos	-	-				
Pellon 2505	0.114	0.024	3			
Vexar	0.336	0.008				
H ₂ Electrode	2.811	0.079				
Asbestos	0.814	0.751	62			
2 RAI 2291	0.182	0.331				
Asbestos	0.377	0.308	51			
Ag Electrode	5.880	0.742	92			
3 Pellon 2505	0.342	0.071	9	2.339	4.808	
						Capacity Ah Cycle Charge Discharge 1 1.32 1.04 2 1.16 1.01 3 1.10 0.91 10 0.60 0.49
VI						
Pellon 2505	0.588	0.007	2			Wicked asbestos on H ₂ side - window on Ag side. Ten cycles, 1.8 V cutoff (half size Ag electrode)
Asbestos	-	-	-			
Pellon 2505	0.057	0.009	2			
Vexar	0.166	0.003				
H ₂ Electrode	0.975	0.025				
Asbestos	0.426	0.359				
2 RAI 2291	0.190	0.163				
Asbestos	0.189	0.276	92			
Ag Electrode	3.246	0.472	>100			
Pellon Window	0.049	0.120	31			
Pellon 2505	0.111	0.332	44	2.700	1.469	
						Capacity Ah Cycle Charge Discharge 1 0.64 0.55 2 0.62 0.54 3 0.57 0.46 10 0.27 0.18

TABLE 29

Stack and Components	KOH in Component		KOH Collected		Comments
	Dry Weight (g)	After Cycling (discharged) (g)	Saturation (%)	H ₂ Side (g)	
VII Vexar	0.337	0.017			Pellon windows around asbestos on each side
H ₂ electrode	2.817	0.071			
Pellon window	0.050	0.118	31		
Asbestos	0.196	0.179	60		
2 RAI 2291	0.178	0.076			
Pellon window	0.051	0.256	67		
Asbestos	0.189	0.281	94		
Ag electrode	3.679	0.409	101		
Pellon 2505	0.119	0.489	64	0.316	
					Capacity Ah Cycle Charge Discharge 1 0.58 0.54 10 0.30 0.28 40 0.15 0.15 80 0.12 0.12 93 0.11 0.11
VIII Vexar	0.353	0.014			Pellon windows.
Vexar	0.167	0.009			
H ₂ electrode	0.975	0.024			
3 Pellon windows	0.181	0.092	8		
Asbestos	0.189	0.149	50		
2 RAI 2193	0.562	0.735			
Pellon window	0.054	0.038			
Asbestos	0.192	0.272	64		
Ag electrode	3.195	0.477	118		
Pellon 2505	0.121	0.082	11	0.008	
					Capacity Ahr Cycle Charge Discharge 2 0.71 0.72 10 0.55 0.41 21 0.12 0.11

TABLE 29
(CONTINUED)

Stack and Components	Dry Weight (g)	KOH in Component	KOH Collected				Comments	
			After Cycling (discharged) (g)	(%)	Cycle	Ag Side (cm ³)* H ₂ Side		
IX Vexar	0.315	0.016			1	c	0.2 c	*Cumulative electrolyte readings c = after end of charge, d = after end of discharge of indicated cycle. Capacity Ah Cycle Charge Discharge 1 0.625 0.610 5 0.687 0.649 10 0.607 0.550 17 0.238 0.187
Vexar	0.169	0.007			2	0.1 d	0.5 d	
H ₂ electrode	1.134	0.045			6	0.1 c	0.5 c	
3 Pellon windows	0.164	0.102	9		6	0.7 d	1.4 d	
Asbestos	0.188	0.196	65		7	0.8 d	1.6 d	
RAI 2193	0.533	0.666			9	0.9 c	1.8 c	
2 Pellon windows	0.108	0.574	76		17	1.2 d	2.5 d	
Asbestos	0.191	0.312	64					
Ag electrode	3.360	0.433	107					
2 Pellon 2505	0.223	1.250	82					
X Vexar	0.341	0.014			1	0 c	0.5 c	(1) 3 Asbestos weighed together. Cell reimpregnated after 17th charge. Capacity Ah Cycle Charge Discharge 2 0.63 0.45 5 0.41 0.33 10 0.28 0.24 16 0.25 0.22 18 0.54 0.63 20 0.51 0.53 27 0.39 0.36
H ₂ electrode	1.697	0.077			11	0 d	0.8 d	
Asbestos	0.382	0.184	31			0 c	2.2 c	
2 RAI 2291	0.212	0.226			18	0 c	0.3 c	
Asbestos (1)	0.973	1.573	105		19	0 d	0.7 d	
Asbestos window	-	-			26	0 d	1.0 d	
Ag electrode	3.254	0.403	100			0 d	1.5 d	
Asbestos	-	-						
Vexar	0.334	0.013						

TABLE 29
(CONTINUED)

Stack and Components	Dry Weight (g)	KOH in Components		KOH Collected		Comments
		After Cycling (discharged) (g)	Saturation (%)	Ag Side (g)	H ₂ Side (g)	
XI Vexar H ₂ electrode 2 Asbestos* Ag electrode Vexar	0.296					No argentistatic barrier. Capacity Ah Cycle Charge Discharge 1 1.285 1.28 5 1.21 1.20 10 1.21 1.20 20 1.265 1.26 30 1.26 1.25 40 1.275 1.265
	1.591					
	1.294					
	6.245					
	0.339					

*Asbestos size 2 x 2-1/2".

TABLE 29
(CONTINUED)

Stack and Components	Dry Weight (g)	KOH in Component		KOH Collected		Comments
		After Cycling (dischg) (g)	Sat. (%)	Ag Side (cc)	H ₂ Side (cc)	
XI Vexar H ₂ electrode 2-Asbestos Ag electrode Vexar	0.296	-	-			No argentistatic membrane.
	1.591	0.062				Capacity, Ah
	1.294	3.728	109			Mid-discharge, Volts
	6.245	1.101	137			1st Plateau 2nd Plateau
	0.339	-	-			Cycle Charge Dischg.
				6*		1 1.285 1.28 1.32 1.05
						50 1.275 1.275 1.34 1.07
						100 1.25 1.25 1.33 1.06
						111 1.23 1.23 - -
						*System oversaturated.
XII Vexar Asbestos Ag electrode Asbest. window Asbestos 2-2291 40/60 2-Asbestos H ₂ Vexar	0.337	-	-			Larger H ₂ reservoir: Ag ratio Permion 2291 40/60.
	0.951	1.893	126			Capacity, Ah
	3.171	0.462	115			Mid-discharge, Volts
						1st Plateau 2nd Plateau
						Cycle Charge Dischg.
	0.214	0.136				1 0.45 0.425 1.275 1.005
	0.760	0.543	45			10 0.341 0.308 1.37 0.94
	1.587	0.034				40 0.243 0.225 - -
	0.312	-				42 0.243 0.225 1.29 0.96

TABLE 29
(CONTINUED)

Stack and Components	Dry Weight (g)	KOH in Component		KOH Collected		Comments
		After Cycling (dischg) (g)	Sat. (%)	Ag Side (cc)	H ₂ Side (cc)	
XIII	Vexar	0.328				Permion 2291-40/20E membrane.
	Ag electrode	1.108	138			
	Asbestos	0.528	88			
	2-2291 40/20E	0.206				
	2-Asbestos	0.500	83			
	H ₂ electrode	0.130				
	Vexar	-				
				2.5	0.7	
						Capacity, Ah
						1 1.013 0.844 1.21 1.03
						5 0.507 0.450 1.28 1.01
						10 0.394 0.357 1.30 1.01
						30 0.262 0.262 1.33 1.01
						93 0.169 0.165 - -
XIV	Vexar	0.315				Permion 2291-40/20 membrane.
	Ag electrode	0.783	97			
	Asbestos	0.390	65			
	2-2291 40/20	0.411				
	2-Asbestos	0.606	51			
	H ₂ electrode	0.123				
	Vexar	-				
				1.3	0.45	
						Capacity, Ah
						1 1.13 1.31 - 1.01
						2 1.05 0.96 - 1.315
						5 0.83 0.79 - 1.31
						10 0.62 0.59 1.31 1.01
						40 0.45 0.42 1.315 0.98
						43 0.45 0.42 - -

TABLE 29
(CONTINUED)

Stack and Components	Dry Weight (g)	KOH in Component		KOH Collected		Comments
		After Cycling (dischg) (g)	Sat. (%)	Ag Side (cc)	H ₂ Side (cc)	
XV Vexar	0.318	0.014				Double Visking membrane. Capacity, Ah Cycle Charge Dischg. 1st Plateau 2nd Plateau 1 - 1.39 - 2 1.275 0.69 1.27 1.00 5 0.54 0.52 - 10 0.465 0.465 - 50 0.375 0.375 - 78 0.35 0.35 -
Asbestos	0.518	1.404	56			
Ag electrode	5.864	1.272	104			
Asbestos	0.525	1.159	83			
Visking	0.523	1.071				
2-Asbestos	0.752	0.706	59	2 ⁺	1.2	
H ₂ electrode	1.876	0.059				
Vexar	0.332	0.019				
XVI Vexar	0.326	0.015				Single Visking membrane with one electrolyte collector. Capacity, Ah Cycle Charge Dischg. 1st Plateau 2nd Plateau 1 1.20 1.01 1.30 1.00 2 1.07 0.73 1.29 0.92 5 0.675 0.65 - 10 0.61 0.59 - 11 0.585 0.585 1.29 0.88
Asbestos	0.519	1.720	69			
Ag electrode	5.926	0.933	77			
Asbestos	0.530	1.447	103			
Visking	0.264	0.511				
2-Asbestos	0.749	0.681	57	2 ⁺		
H ₂ electrode	1.693	0.081	57			
Vexar	1.310	0.056				

TABLE 29
(CONTINUED)

Stack and Components	Dry Weight (g)	KOH in Component		KOH Collected		Comments
		After Cycling (dischg) (g)	Sat. (%)	Ag Side (cc)	H ₂ Side (cc)	
XVII Vexar Asbestos Ag electrode 2-NASA ++ Asbestos H ₂ electrode Vexar	0.336	0.018	-			Two NASA separators - shiny side in towards each other. Capacity, Ah Mid-discharge, Volts Cycle Charge Dischg. 1st Plateau 2nd Plateau 1 0.975 0.94 1.24 0.96 5 1.23 1.16 1.27 0.97 10 1.20 1.18 - - 40 1.08 1.08 - - 48 1.03 1.02 1.26 0.93
	0.517	1.818	73			
	5.926	0.874	109			
	3.930	1.943	121			
	0.388	0.606	101			
	1.693	0.114	-			
	0.310	0.016	-	1.6	2 ⁺	
XVIII Vexar Asbestos Ag electrode Asbestos 2 Celgard 3400 2-Asbestos H ₂ electrode Vexar	0.302	0.018	64			Celgard 3400 microporous polypropylene (38% porous). Capacity, Ah Mid-discharge, Volts Cycle Charge Dischg. 1st Plateau 2nd Plateau 1 1.26 1.27 1.29 1.02 10 1.20 1.20 1.33 1.05 21 1.14 1.13 1.33 1.06
	0.518	1.600	102			
	6.148	0.817	87			
	0.515	1.066	-			
	0.100	0.063	73			
	0.754	0.875				
	2.723	0.104		2 ⁺	0.2	
	0.309	0.019				

TABLE 29
(CONTINUED)

Stack and Components	KOH in Component		KOH Collected		Comments
	Dry Weight (g)	After Cycling (disch) (g)	Sat. (%)	Ag Side (cc)	H ₂ Side (cc)
XIX ⁽¹⁾ Vexar H ₂ Asbestos +NASA Ag Asbestos	0.324	-			
	1.883	0.036			
	0.375	0.354	57		
	1.998	0.643	64		
	6.504	0.778	97		
	0.513	0.343	44		
				1.7	7th cycle
XIX ⁽²⁾ Vexar H ₂ Asbestos +NASA Ag Asbestos	0.325	0.016			
	1.879	0.069			
	0.393	0.535	86		
	1.981	0.934	93		
	5.923	0.865	108		
				1.2 cc after 3rd cycle	
				>2 cc after 6th cycle.	
	0.509	0.970	123		
Cell overcharged.					
Capacity, Ah					
Cycle Charge Dischg.					
1 1.24 1.24 1.26 1.00					
2 1.41 1.37 1.27 1.01					
5 1.33 1.31 - -					
10 1.22 1.24 - -					
20 1.01 1.00 1.28 1.00					
30 0.84 0.84 - -					
39 0.68 0.64 1.26 0.98					
Mid-discharge, Volts					
1st Plateau 2nd Plateau					
Capacity, Ah					
Cycle Charge Dischg.					
1 1.32 1.24 1.24 0.98					
5 1.13 1.13 - -					
10 0.99 0.99 1.27 1.00					
30 0.86 0.84 1.28 0.98					
59 0.81 0.79 1.27 0.98					
Mid-discharge, Volts					
1st Plateau 2nd Plateau					

TABLE 29
(CONTINUED)

Stack and Components	KOH in Component		KOH Collected		Comments	
	Dry Weight (g)	After Cycling (dischg) (g)	Sat. (%)	Ag Side (cc)		H ₂ Side (cc)
XX Vexar Asbestos Ag Electrode Asbestos 2-Celgard 3401 2 Asbestos H ₂ Electrode Vexar	0.339	0.602				
	0.375	0.798				
	6.523	0.939	117			
	0.375	0.483	78			
	0.099	0.053				
	0.762	0.875	71	>2cc	>2 cc	
	2.488	0.063				
XXI Vexar H ₂ +NASA Ag Vexar	0.324	0.061				
	1.690	0.075				
	1.991	0.898	90			
	6.140	0.821	102	>2cc		
	0.334	0.005				
XXII Vexar H ₂ +NASA +NASA Ag Vexar	0.324	0.021				
	2.725	0.182				
	4.010	1.290	65			
	6.691	0.670	83	0.1cc	>2cc	
	0.306	0.034				
E limits increased.						
	Capacity, Ah					
	Cycle	Charge Dischg.				
	Mid-discharge, Volts					
	1st Plateau	2nd Plateau				
	1	0.98 0.98	1.22	0.96		
	5	0.99 0.97	1.24	0.96		
	10	0.98 0.97	1.26	0.95		
	20	0.96 0.96	1.25	0.95		
	40	0.79 0.77	1.18	0.90		
	45	0.47 0.23	-	-		
	Capacity, Ah					
	Cycle	Charge Dischg.				
	Mid-discharge, Volts					
	1st Plateau	2nd Plateau				
	1	- 0.99	1.10	0.94		
	5	0.88 0.83	1.24	0.94		
	10	0.66 0.60	1.20	0.92		
	20	0.47 0.45	1.20	0.88		
	29	0.43 0.41	1.18	0.89		

TABLE 29
(CONTINUED)

Stack and Components	Dry Weight (g)	KOH in Component		KOH Collected		Comments	Capacity, Ah		Mid-discharge, Volts		
		After Cycling (dischg) (g)	Sat. (%)	Ag Side (cc)	H ₂ Side (cc)		Cycle	Charge	Dischg.	1st Plateau	2nd Plateau
XXIII Vexar H ₂ + NASA Asbestos Ag Vexar	0.308 2.253 1.722 0.375 6.511 0.297	0.020 0.199 0.847 0.538 0.892 0.013	97 87 110	1.3cc			1 2 5 10 30 49	1.30 1.22 1.00 0.98 0.90 0.79	1.16 1.12 0.94 0.95 0.81 0.83	1.25 1.25 1.22 1.22 1.20 1.25	1.00 1.00 0.96 0.98 0.98 0.99
XXIV Vexar H ₂ Electrode + NASA Ag Electrode Asbestos Vexar	0.293 2.104 1.789 6.745 0.381 0.293	0.017 0.101 1.005 0.905 1.110 0.005	115 113 45	>2cc			1 5 10 30 50	1.20 1.42 1.44 1.31 1.27	1.20 1.43 1.43 1.31 1.28	1.27 1.27 1.28 1.30 1.31	1.03 1.03 1.04 1.04 1.04
XXV Vexar H ₂ Asbestos + NASA Ag Vexar	0.313 1.691 0.383 1.783 6.628 0.303	0.016 0.068 0.460 0.800 0.780 0.014	74 91 97	0.9cc 5th cycle 1.2cc 12th cycle >2cc 20th cycle			1 2 10 30 50	1.28 1.32 1.18 1.10 0.95	1.13 1.31 1.17 1.11 0.99	1.30 1.30 1.28 1.27 1.27	1.01 1.00 0.98 0.96 0.92

TABLE 29
(CONTINUED)

Stack and Components	Dry Weight (g)	KOH in Component		KOH Collected		Comments
		After Cycling (dischg) (g)	Sat. (%)	Ag Side (cc)	H ₂ Side (cc)	
XXI-2 Vexar H ₂ electrode *+NASA Ag electrode Vexar	0.325 1.750 1.789 6.534 0.334	0.010 0.046 0.803 0.542 0.009	92 68			NASA treated side to Ag. Capacity, Ah <u>Cycle</u> <u>Charge</u> <u>Dischg.</u> <u>1st Plateau</u> <u>2nd Plateau</u> 1 1.05 1.31 1.28 1.02 2 1.25 1.26 1.26 1.02 10 1.07 1.07 1.27 1.02 20 0.96 0.96 1.24 1.00 40 0.90 0.94 1.25 1.00 80 0.91 0.92 1.25 0.99 100 0.92 0.92 1.26 0.99 140 0.75 0.81 1.26 1.00 200 0.79 0.85 1.32 1.05 250 0.73 0.71 1.24 0.98 253 0.53 0.51 1.22 0.94
XXIII-2 Vexar H ₂ electrode +NASA Asbestos Ag electrode Vexar	0.437 1.661 1.748 0.389 6.168 0.350	0.020 0.077 0.837 0.582 0.994 0.017	96 94 124			Capacity, Ah <u>Cycle</u> <u>Charge</u> <u>Dischg.</u> <u>1st Plateau</u> <u>2nd Plateau</u> 1 1.17 1.09 1.24 0.97 2 1.05 1.03 1.24 0.97 10 1.20 1.18 1.25 1.01 30 1.07 1.05 1.24 1.00 47 1.07 1.08 1.26 1.01

*Arrow denotes direction towards which the barrier portion of the NASA membrane faces.

TABLE 29
(CONTINUED)

Stack and Components	KOH in Component		KOH Collected		Comments
	Dry Weight (g)	After Cycling (dischg) (g)	Sat. (%)	Ag Side (cc) H ₂ Side (cc)	
XXV-2 Vexar H ₂ electrode Asbestos +NASA Ag electrode Vexar	0.410 1.665 0.372 1.773 6.312 0.316	0.026 0.087 0.590 0.942 1.000 0.012	95 108 124		Cell was re-impregnated two times (both after 7 cycles.) Capacity, Ah Cycle Charge Dischg. 1st Plateau 2nd Plateau 1 1.13 1.30 1.20 0.98 2 1.24 1.22 1.21 0.98 10 0.81 0.75 1.24 0.90 20 0.26 0.25 1.20 0.86
XXVI Vexar H ₂ electrode Asbestos +NASA Ag electrode Vexar	0.309 2.725 0.374 1.760 6.500 0.304	0.020 0.091 0.456 0.765 0.664 0.013	74 87 83	1.3 cc's 5th discharge. Full > 2 cc's prior to 12th cycle.	NASA treated side to Ag. Capacity, Ah Cycle Charge Dischg. 1st Plateau 2nd Plateau 1 1.20 1.24 1.28 1.02 2 1.40 1.37 1.28 1.02 10 1.39 1.37 1.30 1.02 18 1.16 1.14 1.27 0.99 20 0.62 0.60 - 0.98
XXVII Vexar H ₂ electrode +NASA +NASA Ag electrode Vexar	- 1.576 1.740 1.739 6.551 0.293	- 0.121 0.915 0.901 1.080 0.024	105 103 134		NASA both treated sides to Ag. Capacity, Ah Cycle Charge Dischg. 1st Plateau 2nd Plateau 1 0.99 1.26 1.21 0.97 2 1.13 1.06 1.22 0.97 5 1.00 0.94 1.24 0.95 10 0.66 0.60 1.22 0.90

TABLE 29
(CONTINUED)

Stack and Components	KOH in Component		KOH Collected		Comments	
	Dry Weight (g)	After Cycling (dischg) (g)	Sat. (%)	Ag Side (cc)		H ₂ Side (cc)
XXVIII-A Vexar H ₂ electrode Asbestos +NASA Pellon Ag electrode Vexar	0.380 1.583 0.394 1.774 0.226 6.567 0.330	0.079 0.069 0.629 0.967 1.562 1.118 0.013	102 111 91 139			Pellon has wick to 40% KOH. Capacity, Ah <u>Cycle</u> <u>Charge</u> <u>Dischg.</u> <u>1st Plateau</u> <u>2nd Plateau</u> 1 1.31 1.26 1.19 0.93 10 1.18 1.18 1.25 0.98 20 1.09 1.05 1.26 0.98 40 0.96 0.96 1.26 0.96 58 0.99 0.94 1.24 0.98
XXVIII-B Vexar H ₂ electrode Asbestos +NASA Ag electrode Pellon Vexar	0.417 2.067 0.386 1.763 6.617 0.208 0.326	0.017 0.094 0.604 0.922 1.188 1.439 0.010	97 105 148 84			Pellon has wick to 40% KOH. Capacity, Ah <u>Cycle</u> <u>Charge</u> <u>Dischg.</u> <u>1st Plateau</u> <u>2nd Plateau</u> 1 1.31 1.19 1.22 0.95 2 1.22 1.10 1.22 0.96 9 1.06 1.07 1.21 0.94
XXIX Vexar H ₂ electrode 2 Pellon 2505 +NASA 1 Pellon 2505 Ag electrode Vexar	0.318 1.975 0.240 1.735 0.107 6.564 0.343	0.031 0.112 0.994 0.806 0.513 0.862 0.006	65 107	1.0 cc after 5th cycle. >2.0 after 10 cycles.		Rolled Cell No. 25 analog. Capacity, Ah <u>Cycle</u> <u>Charge</u> <u>Dischg.</u> <u>1st Plateau</u> <u>2nd Plateau</u> 1 1.35 1.37 1.26 1.01 5 1.24 1.28 1.30 1.02 10 1.18 1.24 1.31 1.04 30 1.17 1.18 1.32 1.04 50 1.09 1.11 1.32 1.04 59 1.11 1.11 1.32 1.05

110

TABLE 29
(CONTINUED)

Stack and Components	Dry Weight (g)	KOH in Component		KOH Collected		Comments
		After Cycling (dischg) (g)	Sat. (%)	Ag Side (cc)	H ₂ Side (cc)	
XXX						
Vexar	0.425	0.022				*Cell was accidentally overdischarged for many hours.
H ₂ electrode	2.687	0.097				
2 KI	0.249	0.600	*74			
+NASA	1.776	1.010	115			
Ag electrode	6.502	1.074	134			
Vexar	0.311	0.054				

TABLE 29
(CONTINUED)

Stack and Components		KOH in Component		Comments
		Dry Weight (g)	After Cycling (dischg) (g)	
XXX-2	Vexar	0.327	0.008	Repeat of Configuration XXX.
	H ₂ Electrode	1.629	0.057	
	2-XT	0.272	0.720	Capacity, AH
	**NASA	1.746	0.996	
	Ag Electrode	6.173	1.008	Mid-discharge, Volts
	Vexar	0.302	0.007	
				Cycle Charge Dischg.
				1st Plateau 2nd Plateau
				1 1.01 1.03 1.27 1.00
				10 1.13 1.12 1.30 1.03
XXXI	Vexar	0.400	0.027	Repeat of Configuration XXX.
	H ₂ Electrode	2.974	0.080	
	2-PP 1242-1	0.315	0.028	Capacity, AH
	*NASA	1.747	1.275	
	Ag Electrode	6.594	1.023	Mid-discharge, Volts
	Vexar	0.343	0.010	
				Cycle Charge Dischg.
				1st Plateau 2nd Plateau
				1 0.58 0.62 1.21 0.89
				8 0.74 0.68 1.23 0.90
XXXI	Vexar	0.400	0.027	Repeat of Configuration XXX.
	H ₂ Electrode	2.974	0.080	
	2-PP 1242-1	0.315	0.028	Capacity, AH
	*NASA	1.747	1.275	
	Ag Electrode	6.594	1.023	Mid-discharge, Volts
	Vexar	0.343	0.010	
				Cycle Charge Dischg.
				1st Plateau 2nd Plateau
				1 0.58 0.62 1.21 0.89
				8 0.74 0.68 1.23 0.90

*Arrow denotes direction towards which the barrier portion of membrane faces.

TABLE 29
(CONTINUED)

Stack and Component	KOH in Component			Comments
	Dry Weight (g)	After Cycling (dischg) (g)	Sat. (%)	
XXXII Vexar H ₂ Electrode 2-Composite A +NASA Ag Electrode Vexar	0.411 1.550 0.335 1.781 6.555 0.375	0.012 0.102 0.746 1.192 1.064 0.008	92 136 132	EIC reservoir. Capacity, AH Cycle Charge Dischg. 1st Plateau 2nd Plateau 1 0.99 1.01 1.22 0.96 10 0.94 0.92 1.23 0.95 20 0.60 0.59 1.19 0.88 Reimpregnated 1 0.76 1.12 1.20 0.95 9 0.92 0.93 1.28 1.00 20 0.77 0.74 1.23 0.94 30 0.56 0.53 1.24 0.93
XXXIII Vexar H ₂ Electrode 2-Composite B +NASA Ag Electrode Vexar	0.396 2.105 0.443 1.735 6.352 0.307	0.010 0.105 1.231 0.840 0.998 0.005	72 104 125	EIC reservoir. Capacity, AH Cycle Charge Dischg. 1st Plateau 2nd Plateau 1 1.42 1.33 1.28 1.04 10 1.22 1.21 1.25 1.02 30 0.87 0.85 1.28 1.00 50 0.64 0.62 1.30 0.99 58 0.54 0.54 1.28 0.98

TABLE 29
(CONTINUED)

Stack and Component	KOH in Component			Comments
	Dry Weight (g)	After Cycling (dischg) (g)	Sat. (%)	
XXXIV				Stack wicked to reservoir of 40% KOH.
Vexar	0.457	0.012		
H ₂ Electrode	1.983	0.037		
3-Asbestos	1.413	1.595	72	
Visking	0.262	0.535	-	
Pellon (wick)	0.258	1.577	-	
Ag Electrode	6.150	0.987	123	
Vexar	0.473	0.017		
				Capacity, AH
				Mid-discharge, Volts
				Cycle Charge Dischg. 1st Plateau 2nd Plateau
				1 0.90 1.10 1.18 0.95
				10 1.20 1.20 1.24 0.96
				60 1.03 1.01 1.27 1.00
				100 0.90 0.91 1.25 0.97
				140 0.94 0.95 1.25 0.97
				180 0.91 0.90 1.27 0.99
				196 0.92 0.89 1.25 0.96
XXXV				Nylon reservoir - cell began rapid cycling.
Vexar	0.429	0.031		
H ₂ Electrode	1.878	0.081		
3-Kendall				
149-000	0.436	0.443	32	
+NASA	2.006	1.507	151	
Ag Electrode	6.482	1.022	127	
Vexar	0.454	0.020		
				Capacity, AH
				Mid-discharge, Volts
				Cycle Charge Dischg. 1st Plateau 2nd Plateau
				4 1.20 0.92 1.12 0.84

TABLE 29

Stack and Components	Dry Weight (g)	KOH in Component		Comments
		After Cycling (dischg) (g)	Sat. (%)	
XXXVI Vexar H ₂ Electrode 4-KT +NASA Ag Electrode Vexar	0.465 1.697 0.607 2.008 6.512 0.394	0.019 0.079 0.977 0.803 0.106 0.229	50 80 13	Overcharged after rapid cycling. Capacity, AH Cycle Charge Dischg. 1st Plateau 2nd Plateau 2 1.09 1.07 1.19 0.92 10 1.16 1.14 1.24 0.97 20 1.09 1.07 1.23 0.95 28 0.47 0.45 1.10 0.84
XXXVII Vexar H ₂ Electrode 1-KT +NASA Ag Electrode Vexar	0.407 1.555 0.154 2.013 6.473 0.422	0.012 - 0.488 1.037 0.814 0.015	100 104 101	Capacity, AH Cycle Charge Dischg. 1st Plateau 2nd Plateau 1 1.18 1.05 1.20 0.93 2 1.14 1.09 1.20 0.92 7 0.90 0.83 1.12 0.85 Cell disassembled - "old" H ₂ electrode put in - reim- pregnated. 2 1.17 1.16 1.29 1.05 10 1.23 1.22 1.29 1.02 20 0.92 0.90 1.22 0.91 36 0.77 0.71 1.20 0.86 Cutoff limits increased prior to cycle 36. 1 1.02 1.10 1.26 0.99 10 1.00 1.00 1.27 0.99 20 0.96 0.90 1.26 0.95 30 0.85 0.83 1.24 0.91 39 0.56 0.56 1.20 0.86
XXXVII A	-	-	-	
XXXVII B Vexar H ₂ Electrode 1-KT +NASA Ag Electrode Vexar	- 1.555 0.154 2.046 6.167	- 0.095 0.448 0.944 0.982	- 92 94 122	

TABLE 29
(CONTINUED)

Stack and Component	KOH in Component			Comments
	Dry Weight (g)	After Cycling (dischg) (g)	Sat. (%)	
XXXVIII Vexar *H ₂ Electrode Asbestos †NASA Ag Electrode Vexar	0.433 1.843 0.467 1.983 6.250 0.420	0.030 0.071 1.041 1.129 1.055 0.016	 140 113 141	*Coretex Teflon membrane on H ₂ electrode (Type S10515) with 20% TFE. H ₂ electrode could not sustain discharge.
XXXIX Vexar H ₂ Electrode 2-Composite C †NASA Ag Electrode Vexar	0.431 1.872 0.370 1.996 6.222 0.484	0.009 0.078 1.088 0.915 0.865 0.012	 61 92 108	EIC reservoir. Capacity, AH Cycle Charge Dischg. 1st Plateau 2nd Plateau 2 1.14 1.09 1.28 1.03 10 1.00 0.98 1.30 1.02 21 0.90 0.87 1.30 1.01 31 0.92 0.91 1.35 1.08 35 0.60 0.60 1.16 0.83
XL Vexar H ₂ Electrode 2-Composite B-1 †NASA Ag Electrode Vexar	0.400 1.984 0.650 1.980 6.220 0.412	0.013 0.159 1.767 1.125 0.776 0.008	 103 113 97	Withstands overdischarge - EIC reservoir. Capacity, AH Cycle Charge Dischg. 1st Plateau 2nd Plateau 1 1.11 0.94 1.19 0.91 9 0.88 1.05 1.21 0.96 14 1.03 1.01 1.23 0.96 40 0.92 0.93 1.24 0.98 80 0.55 0.56 1.16 0.87

TABLE 29
(CONTINUED)

Stack and Component	KOH in Component			Comments
	Dry Weight (g)	After Cycling (dischg) (g)	Sat. (%)	
XLI Vexar H ₂ Electrode Asbestos NASA Ag Electrode Ag Electrode Vexar	0.400	0.012		Capacity, AH
	1.703	0.117		
	0.459	0.701	94	1st Plateau
	2.016	0.973	97	2nd Plateau
	6.062	0.793		
	6.273	0.848		
	0.394	0.008	102	
				1 1.10 1.01 1.32 1.05
				10 1.59 1.55 1.33 1.06
				20 1.51 1.46 1.26 0.98
XLII Vexar H ₂ Electrode Asbestos NASA Ag Electrode Vexar	0.426	0.021		Mid-discharge, Volts
	1.811	0.097		
	0.467	0.940	126	
	2.029	1.226	123	
	6.221	1.003	125	
	0.453	0.013		Capacity, AH
				Mid-discharge, Volts
				1 0.77
				1st Plateau
				2nd Plateau
XLIII Vexar H ₂ Electrode Asbestos NASA Ag Electrode Vexar	0.456	0.020		20% TFE/Pt H ₂ electrode with normal Goretex S10415 membrane.
	0.692	0.053		
	0.476	0.682	92	Capacity, AH
	2.044	0.947	95	Mid-discharge, Volts
	6.173	0.759	94	
	0.398	0.010		
				1 1.26 1.11 1.23 0.95
				10 1.24 1.28 1.24 0.98
				20 1.24 1.24 1.25 0.99
				40 1.32 1.33 1.28 1.00
				70 1.18 1.18 1.26 0.99
				109 1.17 1.18 1.26 1.00

TABLE 29
(CONTINUED)

Stack and Component	KOH in Component		Comments
	Dry Weight (g)	After Cycling (dischg) (g) Sat. (%)	
XLV Vexar H ₂ Electrode +NASA 1-KT Ag Electrode Vexar	0.435	0.011	30% TFE bonded H ₂ electrode. <u>Capacity, AH</u> <u>Cycle Charge Dischg.</u> <u>1st Plateau</u> <u>2nd Plateau</u> 1 1.15 1.09 1.27 1.00 2 1.33 1.29 1.26 1.00 10 1.22 0.83 1.21 0.88 15 0.90 0.79 1.21 0.88 20 0.81 0.75 1.20 0.86 30 0.64 0.41 1.16 0.84 36 0.44 0.25 - -
	1.562	0.094	
	1.994	117	
	0.122		
	6.197	131	
	0.442		
XLVI Vexar H ₂ Electrode +NASA 1-KT Ag Electrode Vexar	0.454	0.022	20% TFE bonded H ₂ electrode. <u>Capacity, AH</u> <u>Cycle Charge Dischg.</u> <u>1st Plateau</u> <u>2nd Plateau</u> 1 1.02 0.94 1.24 0.97 3 1.22 1.13 1.19 0.93 7 0.96 0.79 1.14 0.84 11 0.38 0.26 1.04 - (C/4) 14 1.20 1.14 1.20 1.00 (C/1.3) 16 0.88 0.44 0.96 -
	1.570	87	
	1.932	75	
	0.118	125	
	6.201		
	0.452		

TABLE 29
(CONTINUED)

Stack and Components	KOH in Component		Comments
	Dry Weight (g)	After Cycling (dischg) (g) Sat. (%)	
XXXVI-A Vexar H ₂ Electrode 4-KT +NASA Ag Electrode Vexar	0.457 1.704 0.604 1.969 6.298 0.441	0.018 0.072 1.384 1.030 0.579 0.011	71 103 72
Repeat of XXXVI.			
Capacity, AH			
Mid-discharge, Volts			
Cycle Charge Dischg. 1st Plateau 2nd Plateau			
1	1.21	1.18	1.27 1.01
20	1.20	1.20	1.28 1.01
80	1.05	1.05	1.29 1.01
100	0.94	0.91	1.28 0.99
140	0.91	0.91	1.28 0.99
203	0.87	0.88	1.26 0.99
XLVII Vexar H ₂ Electrode +NASA Wick (Pellon/KT) +NASA Ag Electrode Vexar	0.464 1.708 1.967 0.283 1.954 6.309 1.470	0.029 - 1.017 1.422 1.086 0.957 0.018	102 - 109 119 -
Pellon 2505 Wick impregnated w/KT cell overcharged 3X during cycling.			
Capacity, AH			
Mid-discharge, Volts			
Cycle Charge Dischg. 1st Plateau 2nd Plateau			
1	1.20	1.11	1.21 0.95
20	1.13	1.13	1.19 0.95
40	1.16	1.16	1.23 0.98
*47	1.20	1.22	1.20 0.98
48	1.18	1.16	1.24 0.98
100	0.92	0.94	1.24 0.97
116	0.94	0.92	1.26 0.98
**117	0.94	1.03	1.23 0.99
118	0.99	0.97	1.25 0.98
180	0.81	0.81	1.25 0.97
***186	0.84	0.98	1.22 0.98
187	0.90	0.90	1.25 0.98
197	0.84	0.87	1.27 0.98

*Overcharged 0.47 AH
**Overcharged 0.98 AH
***Overcharged 1.4 AH
+To normal 1.8 V cutoff.

TABLE 29
(CONTINUED)

Stack and Components	KOH in Component			Comments
	Dry Weight (g)	After Cycling (dischg) (g)	Sat. (g)	
XLVIII Vexar H ₂ Electrode 2-Zircar +NASA Ag Electrode Vexar	0.448	0.023		Zircar-polysulphone impregnated type ZYW-15. Capacity, AH Cycle Charge Dischg. 1st Plateau 2nd Plateau
	1.565	0.073	101	
	1.205	1.661	89	
	1.923	0.894	111	
	6.271	0.896		
	0.437	0.011		
				1 1.25 1.28 1.28 1.04
				2 1.40 1.43 1.28 1.05
				10 1.28 1.28 1.30 1.04
				40 1.02 1.03 1.24 0.98
				64 1.07 1.16 1.24 0.98
				80 1.01 0.97 1.25 0.94
				97 1.09 1.13 1.27 1.01

TABLE 29
(CONTINUED)

Stack and Components	KOH in Component			Comments
	Dry Weight (g)	After Cycling (dischg) (g)	Sat. (g)	
L				Zircar-polysulphone impregnated type ZYW-15.
Vexar	0.418	0.012	107	Capacity, AH
Ag Electrode	6.212	0.862	121	
†NASA	1.985	1.215	77	Mid-discharge, Volts
1-Zircar	0.610	0.632		
H ₂ Electrode	1.701	0.089		Cycle Charge Dischg.
Vexar	0.410	0.013		
				1st Plateau 2nd Plateau
				2 1.33 1.35 1.26 1.04
				10 1.18 1.22 1.27 1.01
				30 0.94 0.99 1.25 0.99
				60 1.16 1.18 1.28 1.02
				105 1.17 1.16 1.28 1.03
LI				Capacity, AH
Vexar	0.411	0.014	116	Mid-discharge, Volts
Ag Electrode	6.143	0.930	104	
†NASA	2.022	1.037	55	Cycle Charge Dischg.
1-Zircar	0.580	0.454		
H ₂ Electrode	1.572	0.052		1st Plateau 2nd Plateau
Vexar	0.384	0.015		2 1.13 1.13 1.21 1.05
				5 1.24 1.20 1.20 0.98
				10 0.45 0.45 1.10 0.84
				30 0.42 0.45 1.18 0.87

the difficulty of complete electrolyte transfer from the argentistatic membrane to the nonwoven nylon remained. Therefore Configuration X used only asbestos. Cell performance was limited by electrolyte capacity on the hydrogen side but the fact that no electrolyte appeared to be expelled on the silver side demonstrates the improved reabsorption of asbestos.

Consideration of energy density and thermal management call for minimizing the amount of electrolyte and the separator thickness. We therefore set up an extreme configuration using two asbestos layers without any membrane (Configuration XI). This cell was cycled over 100 times. It showed a stable high capacity and did not suffer from electrolyte management problems. Eventually this cell would probably fail by silver bridging. This had, however, not occurred when cycling was discontinued. The cell was disassembled and analyzed. Silver had accumulated mainly in the asbestos layer adjacent to the hydrogen electrode. Quantitative analysis for silver showed 22 mg and 0.4 mg silver in the separator and the hydrogen electrode respectively.

Configuration XVIII was similar to Configuration XI. It contained two layers of Celgard microporous polyethylene (membrane thickness 1 mil, pore size 0.02 μ , open area \sim 38%). No specific argentistatic property can be expected from such a membrane. The cell was disassembled after 21 cycles and analyzed for silver. The distribution was as follows: H₂ electrode/2 asbestos, 1 mgAg/2 Celgard, 0.8 mgAg/1 asbestos, 1.4 mgAg/Ag electrode/1 asbestos 3.3 mgAg.

Configuration XII through XVI are tests of various arrangements employing Permion 40/60, Permion 2291 40/20 and 40/20E, a "more open" lower resistance Permion membrane and Visking as argentistatic barriers. All show similar behavior characterized by a large capacity loss during the first few cycles and continued capacity decrease at slower rate. The capacity is limited by the polarization of the hydrogen electrode due to "drying" of the hydrogen electrode side. Significant electrode polarization appears to occur when the electrolyte saturation level in the asbestos falls below approximately 60%. Flooded tests on silver electrodes confirmed the state of charge and availability of capacity. For example, Configuration XIII had a capacity of 0.165 Ah during Cycle 93. Subsequent flooded testing showed that the silver electrode was almost completely charged. Flooded discharge capacities were 1.19 and 1.47 Ah in the first and second cycles respectively.

The NASA separator appears to be the only practical barrier layer and the following configurations concentrate on this membrane.

Configuration XVII employs two NASA separators. The cell loses electrolyte especially during initial cycles but it showed good capacity retention. Cell polarization is noticeably larger. The mid discharge potentials (\sim C to

C/2 rate) for the first and second plateaus respectively were 1.26 and 0.93V for two NASA separators, 1.31 and 1.01V for two Permion 40/20 versus 1.33 and 1.06V for the asbestos arrangement only. Configuration XXII is a modified version without asbestos reservoir. This cell polarized substantially on both charge and discharge and lost capacity. Such a configuration may also undergo operating difficulties associated with the interface between the two treated surfaces of the separators. Configuration XIX uses a single NASA separator and an asbestos reservoir in back of the Ag electrode. The treated side of the separator faces the Ag electrode (the H₂ electrode will not operate well with the treated side of the separator in direct contact with it). This cell has improved polarization characteristics compared to the double NASA separator system. It shows, however, also a slow decline in capacity due to electrolyte loss. In Configuration XXI, a single NASA separator system is given its most extreme test. In this case the only reservoir in the system is the separator itself; no additional asbestos is added. This cell arrangement appears to have polarization characteristics intermediate between the double separator systems and the single systems with additional reservoir(s). The amount of expelled electrolyte and at the same time the relatively high saturation of the separator suggests entrapment of excess electrolyte in the freshly impregnated cells, e.g., in the Vexar behind the Ag electrode.

In Configuration XXIII an asbestos reservoir was placed between the Ag electrode and the treated side of the NASA separator of Configuration XXI. This cell had good polarization characteristics. It showed also a slow decrease in capacity. Configuration XXV tested a reversed reservoir arrangement. Both cell polarization and capacity retention have improved. In Configuration XXIV the asbestos reservoir is placed behind the Ag electrode, out of the current path. This configuration performed surprising well. The only partially compressed asbestos behind the Ag electrode, due to the Vexar backing, appears to act as a larger reservoir structure.

Configuration XX employs a microporous polypropylene separator material (Celgard 3401). The effective pore size of this material makes this configuration essentially a barrierless cell with commensurate performance.

Configurations based on a single NASA separator have shown the most promising performance. There appears to be an acceptable compromise between considerations of electrolyte management and silver retention. Silver retention is, however, not as good as one would wish. Analysis carried out on the components of Configuration XXV showed 10 mg Ag in the separator and 0.9 mg Ag in the asbestos layer next to the NASA separator. The following configuration emphasize reservoir size and orientation of the NASA separator. Several configurations are duplicates of earlier configurations to define the observed effects more closely.

Of the configurations employing one asbestos and one NASA membrane as separator system, the best performance was achieved when the hydrogen electrode was adjacent to the asbestos side of the NASA membrane (Configurations XXIII and XXIII-2). Configurations XXV, XXV-2 and XXVI where the asbestos was in direct contact with the hydrogen electrode performed less well (more rapid capacity decline and lower discharge plateau voltages). Provision for sufficient electrolyte supply to the silver electrode side via a pellow wick (Cells XXVIII A and B) had little effect on the overall cycle behavior. The cycle performance of these cells was even exceeded by Configurations XXI and XXI-2 based solely on the use of one NASA membrane despite fairly "dry" overall operation. Replacing of the asbestos separator adjacent to the hydrogen electrode by an EIC potassium titanate separator resulted in excellent cycle behavior (Configuration XXX).

Configurations based on two NASA membranes, which would be desirable to obtain a higher degree of silver retention, did not perform well (see Configurations XXII and XXVII). The rate of back wicking through a double membrane is apparently insufficient for continued stable cell operation. Whether or not the two membrane sides face each other appears to be of little consequence (compare Configurations XXII and XXVII).

A small laboratory cell using the same configuration as the longest cycling boiler plate cell performed well.

Configuration XXX-2 confirms the attractive operation of KT based structures. This configuration (Cell XXX) was also overcharged for over an hour without ill effect. Polypropylene and a Kendall nylon (Cells XXXI and XXV respectively) performed quite poorly. The hydrogen electrode polarizes strongly on discharge due to the electrolyte starved operation. Cell capacity is, however, limited by the silver electrode.

It appears that the pore structure of polypropylene and nylon absorber layers is too open for back wicking to occur rapidly enough. We therefore thought a structure with mixed pore size distribution containing small pores for electrolyte continuity and larger pores for electrolyte storage may be desirable. Since such components are not commercially available we prepared various composites in the laboratory. Absorber layers formed from a dispersion of shredded nylon and asbestos resulted in relatively inhomogeneous structures. The asbestos fibers formed a dense surface layer even when deposition is attempted from very dilute suspensions. The shorter potassium titanate fibers, however, can be readily deposited into the relatively large pores of the non woven nylon. The following composites were tested in small laboratory cells:

Composite A: 72% Permion 1242-1, 21% Asbestos, 8% KT

Composite B: 54% KT, 38% Pellow, 5% TFE, 3% Asbestos

Composite C: 73% Pellow, 21% Asbestos, 6% KT

Of the cells using composites, performance improved with increasing content of potassium titanate. However, they did not exceed the performance of cells with the EIC KT structures.

In an effort to make the hydrogen electrodes more tolerant to operation under starved conditions, we increased their hydrophilic character by reducing the Teflon content to 20%. To retain a very hydrophobic backing at all times we attempted to use the fairly dense Goretex S10515 Teflon membrane. Such electrodes failed (Cells XXXVIII and XLII) apparently by insufficient gas access through the backing. Electrodes with 20% TFE in the catalyst mix and the usually employed backing (Goretex S10415) performed very well (see e.g., Cell XLIII).

An analysis of hydrogen electrode potentials measured vs. a reference electrode (all cells from Configuration XXIII on, contained a separate hydrogen reference electrode) showed the following: In early cycles the measured mid-charge and mid-discharge polarizations of the hydrogen electrode were about equal and had values of approximately 100 to 130 mV (at 38 mA/cm² without iR correction). Hydrogen electrode polarizations of configuration with larger hydrogen electrode side reservoirs (e.g., Cells XXXIV, XXXV, XXXVI) and also Configurations XLI and XLIII were 40 to 80 mV. During cycling polarization on discharge increased more rapidly than on charge. We analyzed also the changes in hydrogen electrode potential (not iR corrected) during the charge and discharge half cycles. They are, in a first approximation, linear with time. For freshly impregnated cells and cells with larger electrolyte reservoirs at the hydrogen electrode side the measured slopes are very small $\lesssim 20$ mV/hr (C/2 rate, ≈ 40 mA/cm²). In configuration with a more restricted electrolyte amount and in cells which have lost a significant fraction of their electrolyte during cycling, the slopes exceed 40 mV/hr. In this condition the cells are very rate sensitive and at fixed current density cycling performance degrades at a progressively accelerating rate. This suggests a fairly critical current density or rate for any given configuration and electrolyte saturation level. At higher rates the cell performance will rapidly collapse while changes below this level will have little effect on performance. This is illustrated in Figs. 35 and 36. Figure 35 shows the relatively small change in capacity and cell voltage between C/4 and C rate cycles. (Configuration XXV after reimpregnation). Figure 36 shows the large effect of changing the cycling rate on cell performance of a cell for which the critical current density is approximately C/2.

Configuration XLVII is a special interest cell showing that electrolyte stabilization via a wick will in fact lead to constant performance. Configurations XLVIII to LI examine Zircar ZYW-15, which has performed well in Ni/H₂ cells, as a possible absorber layer material. Configuration L cycled well and was discontinued after 105 cycles while Configuration LI began to fail after 5 cycles. The orientation of the NASA separator was the only difference between the two configurations. The problems of Configuration LI

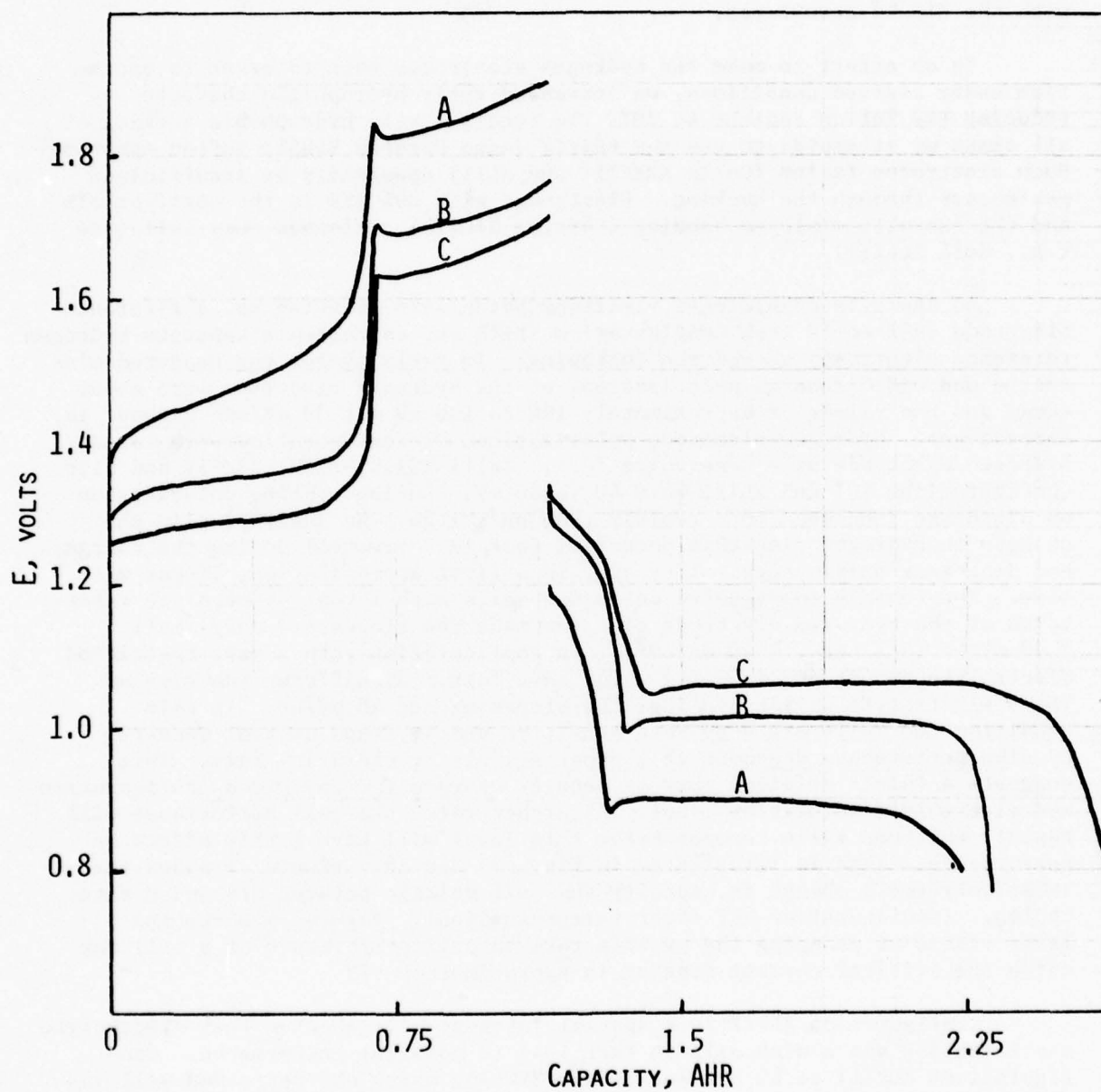


Figure 35. Cell XXV configuration showing little rate sensitivity. A = C rate, B = C/2 rate, C = C/4 rate (rates are nominal).



Figure 36. Cell XXXIX configuration showing severe rate sensitivity. A = C rate, B = C/2 rate, C = C/4 rate (rates are nominal).

result from the small H_2 side electrolyte reservoir and possibly also from the membrane-Zircar interface. Our tentative conclusion is that Zircar acts as electrolyte absorber layer without distinct performance benefits or disadvantages.

In summary, we have shown the critical importance and interdependence of membrane transport parameters, reservoir size and absorber layer properties, reservoir distribution between hydrogen and silver electrode side and charge or discharge rate. Here, the critical rate is determined not by the rate sensitivity of the electrodes (the rate sensitivity of the "wet" silver electrode is extremely small and the "wet" hydrogen electrode is only moderately rate sensitive), but by various mass transport processes in the argentistatic membrane in conjunction with the electrolyte reserve on each side of the membrane.

Of the tested argentistatic membranes only the NASA separator appears to have any practical potential in Ag/H_2 cells.

6. Advanced Boiler Plate Cells of Rolled Configuration

6.1 Test Matrix and Cell Construction

Our laboratory cell experiments and the mathematical simulation using the experimentally determined transport parameters for the various membranes showed that the NASA separator is the only membrane suitable for practical Ag/H_2 cell configurations. We established further that the number of membrane layers, the membrane orientation, the type of reservoir, the electrolyte level and the hydrophilic-hydrophobic character of the H_2 electrode are important factors. To maximize energy density, one likes to minimize the electrolyte level to the extent compatible with cell performance. The thickness of the separator-absorber layer package should remain small also for thermal reasons. Based on our experience and on the requirements for a practical Ag/H_2 battery, we have selected the cell configurations shown in the test matrix of Table 30. All cells use 25 mil thick silver electrodes. The test regime consists of three-hour cycles to 70% depth of discharge (2 hrs charge, 1 hr discharge). The charge and discharge rates are C/2.7 and C/1.4 respectively. The recharge ratio is 1.05.

The sixteen boiler plate Ag/H_2 cells were assembled using identical construction as described earlier (Section 4.1).

Cells A-1, 2, 3 and 4 are especially instrumented with pressure transducers, reference electrodes and thermocouples. The thermocouples are located in the center of the gas distribution screens next to the H_2 electrodes. Excess void space was filled with polyethylene spacers.

TABLE 30
VARIABLES AND TEST MATRIX

1. Membrane layers	M
a. No membrane	m ₀
b. 1 NASA separator	m ₁
c. 2 NASA separators	m ₂
2. Membrane orientation (direction)	D
a. Membrane film to H ₂ electrode (reservoir on H ₂ electrode side)	d ₀
b. Membrane film to Ag electrode (reservoirs on H ₂ and Ag electrode sides)	d ₁
3. Reservoir type	R
a. Asbestos	r ₀
b. Potassium titanate	r ₁
4. Electrolyte level (reservoir or absorber layer thickness)	E
a. 0 layers per cell 13, 1 layer for cell 11	e ₀
b. 1 layer	e ₁
c. 2 layers	e ₂
d. 3 layers	e ₃
5. Hydrogen electrode	H
a. 30% TFE	h ₀
b. 20% TFE	h ₁
1. Reservoir Type - Electrolyte Level - Membrane Orientation - RED Interaction	
a. M = m ₁ , D = d ₀ , H = h ₀	
b. M = m ₁ , D = d ₁ , H = h ₀	

		R	
		r ₀	r ₁
E	e ₁	①	②
	e ₂	③	④

		R	
		r ₀	r ₁
E	e ₁	⑤	⑥
	e ₂	⑦	⑧

(Cells 5 and 6 have reservoir on H₂ side, 7 and 8 have one reservoir on either side of the membrane).

TABLE 30
(CONTINUED)

II. Hydrogen Electrode - Electrolyte Level, HE Interaction.

$$M = m_1, D = d_0, R = r_0$$

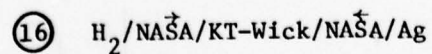
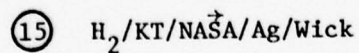
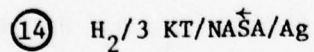
	h_0	h_1
e_1	1	(9)
e_2	3	(10)

III. Membrane - Electrolyte Level, ME Interaction.

$$D = d_1, R = r_0, H = h_0.$$

	m_0	m_1
e_0	(11)	(13)
e_2	(12)	3

IV. Special Interest Cells



6.2 Results

6.2.1 Pretest Cycling

The cells were vacuum impregnated with 40% KOH and drained after overnight stand. All cells received 100 psig. H₂ precharge followed by formation at 0.5A for 40 hrs. A typical formation cycle is shown in Fig. 37. The cells were then subjected to 3 charge-discharge cycles to determine their capacity. The six lowest capacity cells were reimpregnated after the second cycle to assure maximum electrolyte saturation. The 70% depth of discharge (DOD) for the cycle testing was based on an average capacity of 15 Ah. The collected capacity, pressure and electrolyte data are summarized in Tables 31, 32 and 33, respectively.

6.2.2 Cycle Test

Actual charge and discharge currents are based on an average capacity of 15 Ah. Typical voltage, pressure and temperature data during a test cycle are shown in Figs. 38 and 39. Table 34 summarizes the voltage data. After cycles 103 and 513 all cells were discharged to 0.5V to determine their capacity. Cell pressure and expelled electrolyte were also measured. The results are summarized in Tables 35 and 36. Table 37 lists the history of the four cells which failed during the test cycling.

We have analyzed the data for main effects and interactions based on the factorial matrices shown in Table 30 using Yates' method of evaluation. Two different responses were used for the evaluation: 1) the capacity retained after 514 cycles as a percent of the initial capacity and 2) the energy delivered by the cell after 514 cycles (capacity times mid-discharge voltage). The results are shown in Tables 38 and 39 (values for failed cells are estimates). The lack of a good estimate of experimental errors requires caution in the data analysis. As a rough guide we may assume the triple interaction (DRE) to be not significant and thus be an indication of random fluctuation.

The results suggest the following conclusions:

1. The higher levels of electrolyte were beneficial. Cells with no absorber layer or with 1 kT (6, 11, 13) failed. Cells with 2 or 3 (3, 10, 14) reservoir layers performed better than those with one absorber layer.
2. The orientation of the NASA separator has a strong influence. Orientation of the membrane film towards but not in contact with the H₂ electrode is beneficial. This orientation effect appears to be more important at higher electrolyte levels and when kT is used as absorber layer.

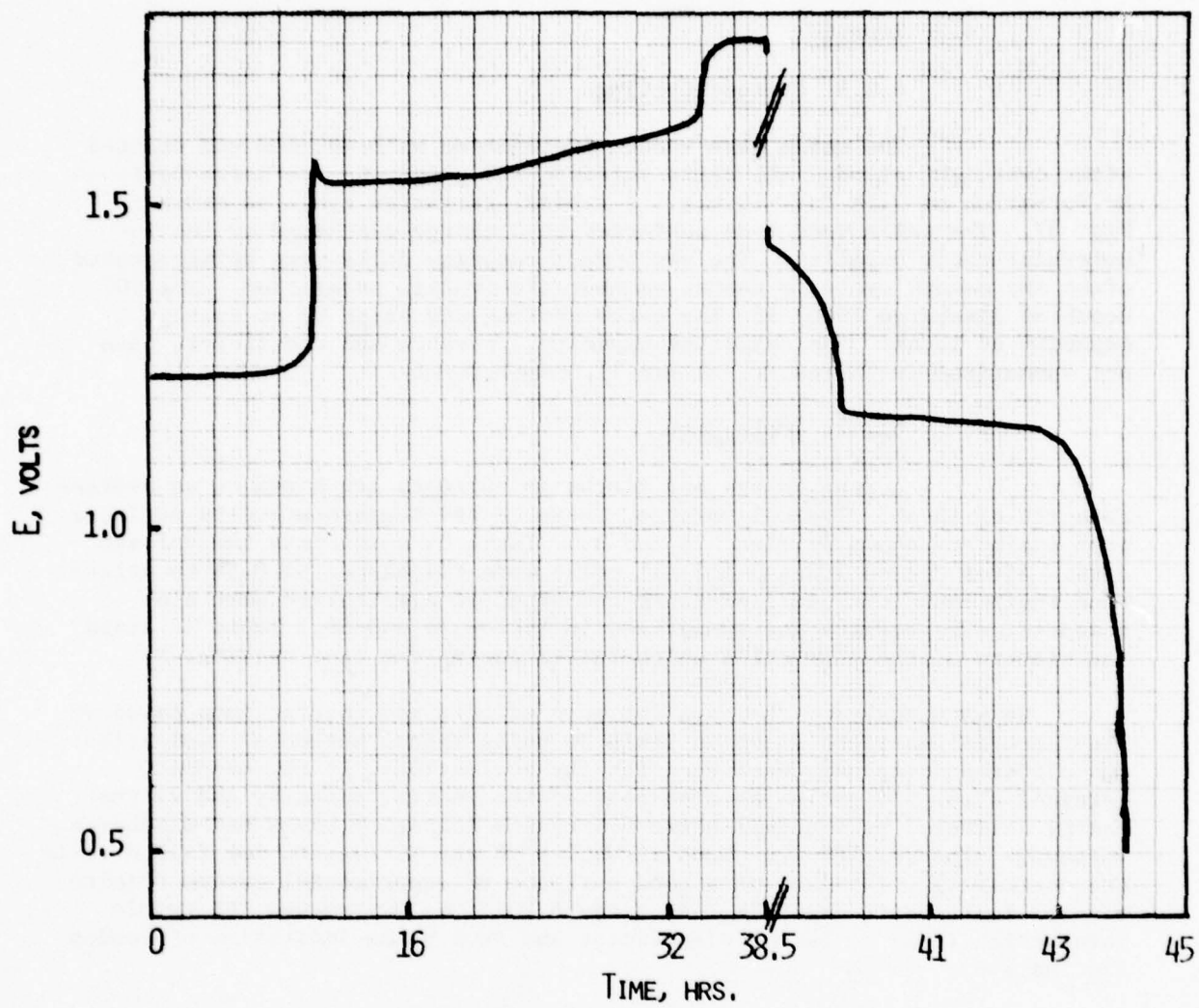


Figure 37. Cell A-1 formation cycle - charge @ 0.5 A, discharge @ 3.0 A.

TABLE 31

CAPACITY OF A-SERIES Ag/H₂ CELLS

Cell No. and Configuration	Capacity, AH						Actual DOD for Nominal 70% DOD Cycle (%)
	Formation Charge 0.5 A Dischg 3.0 A	Cycle #1	Cycle #2	Cycle #3			
		Charge 8 A Dischg 9 A	Charge 2 A Dischg 9 A	Charge 3 A Dischg 9 A			
A-1 -(1 A/NASA)+	16.8	13.7	14.6	14.6		72	
A-2 -(1 KT/NASA)+	14.9	11.1	11.8*	14.6		72	
A-3 -(2 A/NASA)+	16.4	14.6	16.0	16.0		66	
A-4 -(2 KT/NASA)+	16.1	12.6	12.3*	15.2		69	
A-5 -(1 A/NASA)+	15.4	14.2	14.8	15.0		70	
A-6 -(1 KT/NASA)+	14.5	13.1	13.6*	15.8		66	
A-7 -(1 A/NASA/1 A)+	17.2	15.9	16.2	16.2		65	
A-8 -(1 KT/NASA/1 KT)+	14.6	14.4	14.2	14.0		75	
A-9 -(1 A/NASA)+	15.1	12.6	12.9*	16.4		64	
A-10 -(2 A/NASA)+	16.0	15.9	16.5	15.8		66	
A-11 -(1 A)+	17.6	15.0	16.2	14.8		71	
A-12 -(2 A)+	18.5	16.4	14.8	16.0		66	
A-13 -(NASA)+	13.6*	11.7	12.4*	13.0		81	
A-14 -(3 KT/NASA)+	16.3	14.2	14.0*	16.2		65	
A-15 -(1 KT/NASA+/wick)	15.1	15.2	16.5	16.2		65	
A-16 -(NASA/wick/NASA)+	17.3	15.5	16.4	16.0		66	

*Reimpregnated.

TABLE 32

CELL PRESSURE OF A-SERIES Ag/H₂ CELLS

Cell No. and Configuration	Pre-Charge	End of Formation		2nd Cycle		3rd Cycle		Final Cycle Prior to Cycling	
		Charge	Dischg.	Charge	Dischg.	Charge	Dischg.	Charge	Dischg. to 70% Depth
A-1 - (1 A/NASA) ₊	100	609	135	552	157	536	142	555	243
A-2 - (1 KT/NASA) ₊	100	596	142	514	156	533	85	570	245
A-3 - (2 A/NASA) ₊	100	574	120	553	144	541	111	546	250
A-4 - (2 KT/NASA) ₊	100	623	150	505	135	575	103	633	237
A-5 - (1 A/NASA) ₊	100	635	102	595	100	585	90	605	230
A-6 - (1 KT/NASA) ₊	100	605	135	548	130	645	105	645	260
A-7 - (1 A/NASA/1 A) ₊	100	605	100	665	105	700	130	660	265
A-8 - (1 KT/NASA/1 KT) ₊	100	680	130	615	135	615	135	640	250
A-9 - (1 A/NASA) ₊	100	670	120	545	110	680	110	655	265
A-10 - (2 A/NASA) ₊	100	720	120	675	110	660	115	660	275
A-11 - (1 A) ₊	100	740	125	645	125	585	110	630	265
A-12 - (2 A) ₊	100	735	105	580	105	640	115	640	265
A-13 - (NASA) ₊	100	660	150	550	110	570	115	610	205
A-14 - (3 KT/NASA) ₊	100	700	135	565	115	675	110	665	260
A-15 - (1 KT/NASA/+wick) ₊	100	830	175	810	180	805	160	790	360
A-16 - (NASA/wick/NASA) ₊	100	700	150	655	150	650	148	645	300

TABLE 33

PRETEST ELECTROLYTE DATA FOR A-SERIES Ag/H₂ CELLS

Cell No. and Configuration	Retained after Impregnation (cm ³)	Drained after Formation (cm ³)	Gained Upon Reimpregnation (cm ³)	Drained Prior to Cycle Testing (cm ³)	Pretest Total (cm ³)
A-1 - (1 A/NA ₂) +	42	1.8	-	1.4	40
A-2 - (1 KT/NA ₂) +	33	2.4	13	13.2	30
A-3 - (2 A/NA ₂) +	32	1.7	-	1.3	29
A-4 - (2 KT/NA ₂) +	37	4.1	14	10.5	36
A-5 - (1 A/NA ₂) +	29	1.2	-	1.9	26
A-6 - (1 KT/NA ₂) +	26	1.4	7	6.9	24
A-7 - (1 A/NA ₂ /1 A) +	30	1.3	-	4.0	24
A-8 - (1 KT/NA ₂ /1 KT) +	33	4.6	-	1.5	27
A-9 - (1 A/NA ₂) +	32	3.5	4	8.0	25
A-10 - (2 A/NA ₂) +	38	3.2	-	1.4	34
A-11 - (1 A) +	31	6.5	-	1.1	23
A-12 - (2 A) +	35	1.6	-	1.5	32
A-13 - (NA ₂) +	28	3.6	10	7.8	27
A-14 - (3 KT/NA ₂) +	34	3.7	14	11.9	32
A-15 - (1 KT/NA ₂ /+/wick)	-	-	-	-	-
A-16 - (NASA/wick/NA ₂) +	-	-	-	-	-

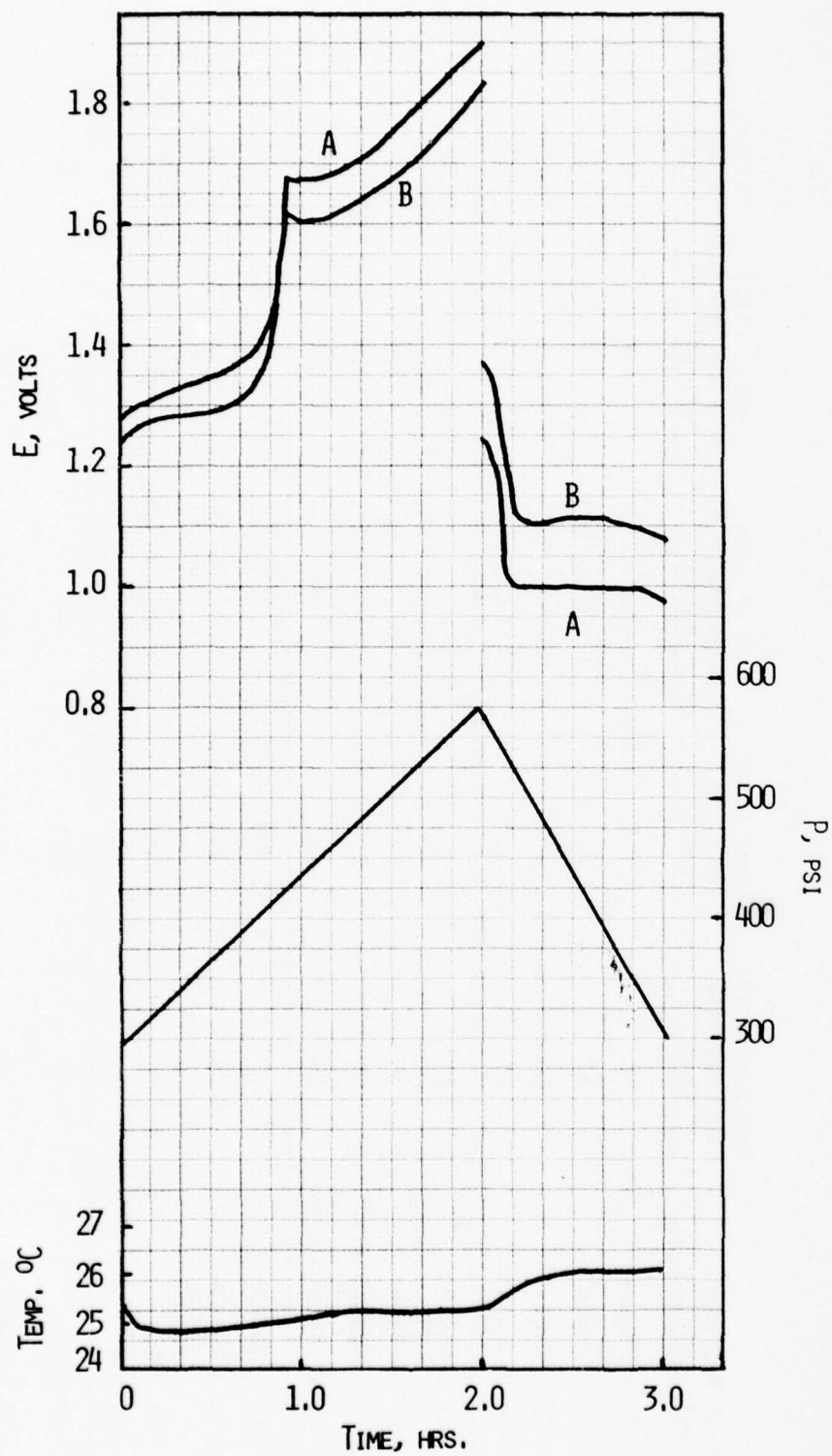


Figure 38. Typical voltage, pressure and temperature changes during a test cycle. Cell A-3, Cycle 207, A = cell voltage, B = Ag electrode vs. H₂ reference electrode.

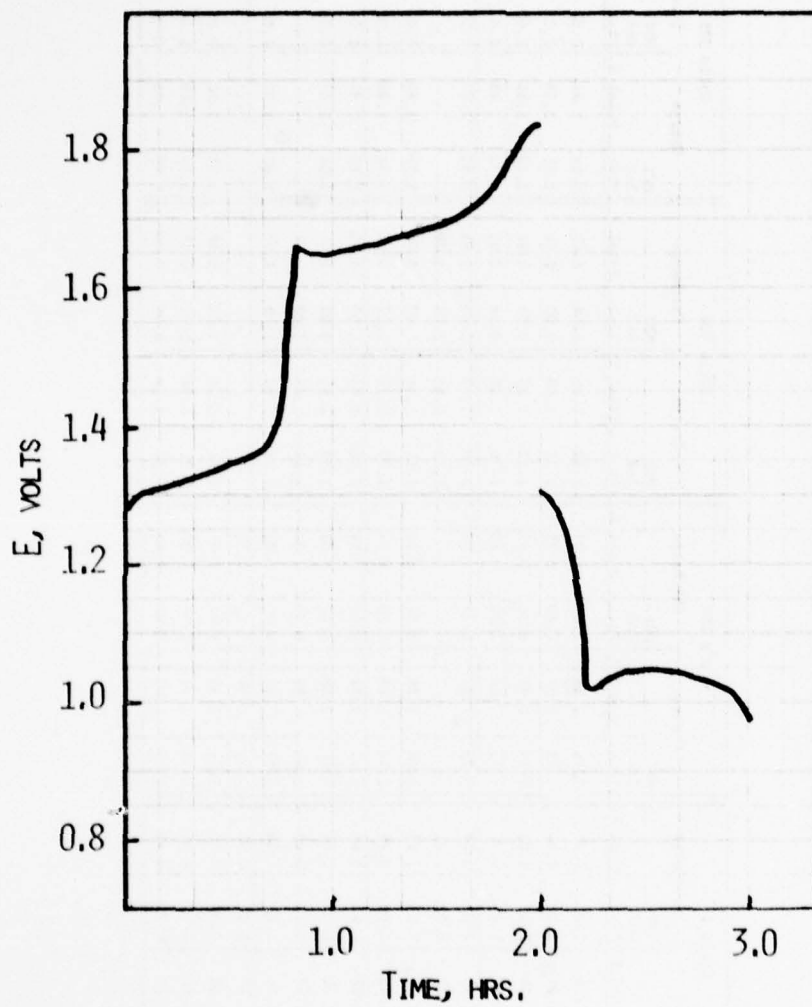


Figure 39. Typical cell voltage during Cycle 508, Cell A-7.

TABLE 34

CHARGE-DISCHARGE VOLTAGES OF Ag/H_2 CELLS

Cell No. and Configuration	Cycle 4				Cycle 100				Cycle 206				Cycle 308			
	Charge		Discharge		Charge		Discharge		Charge		Discharge		Charge		Discharge	
	MCV 2nd Plat.	Final V	MCV 2nd Plat.	Final V	MCV 2nd Plat.	Final V	MCV 2nd Plat.	Final V	MCV 2nd Plat.	Final V	MCV 2nd Plat.	Final V	MCV 2nd Plat.	Final V	MCV 2nd Plat.	Final V
A-1 -(1 A/ H_2Ag) \leftrightarrow	1.72	1.91	1.01	0.98	1.74	1.89	1.02	0.99	1.68	1.86	1.04	1.00	1.68	1.85	1.02	0.92
A-2 -(1 $\text{KT}/\text{H}_2\text{Ag}$) \leftrightarrow	1.75	1.94	1.00	0.94	1.73	1.89	1.00	0.95	1.72	1.89	1.03	0.98	1.71	1.88	1.03	0.90
A-3 -(2 A/ H_2Ag) \leftrightarrow	1.70	1.78	1.02	1.01	1.73	1.91	1.00	0.99	1.70	1.88	1.01	0.98	1.70	1.86	1.00	0.96
A-4 -(2 $\text{KT}/\text{H}_2\text{Ag}$) \leftrightarrow	1.75	1.97	1.00	0.97	1.73	1.89	1.00	0.90	1.70	1.86	0.98	0.45	1.72	1.86	1.01	0.96
A-5 -(1 A/ H_2Ag) \leftrightarrow	1.70	1.77	1.05	1.04	1.73	1.91	1.05	1.03	1.70	1.85	1.03	1.01	1.68	1.85	1.02	0.93
A-6 -(1 $\text{KT}/\text{H}_2\text{Ag}$) \leftrightarrow	1.70	1.78	1.05	1.04	-	-	-	-	1.73	1.90	1.02	1.00	-	-	-	-
A-7 -(1 A/ $\text{H}_2\text{Ag}/1 \text{ A}$) \leftrightarrow	1.70	1.75	1.03	1.03	1.64	1.69	1.04	1.00	1.65	1.76	1.03	0.98	1.70	1.85	1.04	0.96
A-8 -(1 $\text{KT}/\text{H}_2\text{Ag}/1 \text{ KT}$) \leftrightarrow	1.78	1.93	1.00	0.98	1.72	1.88	1.00	0.96	1.70	1.78	1.02	0.86	1.70	1.88	1.00	0.76
A-9 -(1 A/ H_2Ag) \leftrightarrow	1.69	1.87	1.05	1.04	1.67	1.79	1.03	0.99	1.66	1.82	1.03	0.93	1.68	1.84	1.02	0.84
A-10 -(2 A/ H_2Ag) \leftrightarrow	1.68	1.74	1.05	1.04	1.70	1.88	1.03	1.01	1.69	1.85	1.03	1.01	1.68	1.87	1.05	1.03
A-11 -(1 A) \leftrightarrow	1.64	1.72	1.10	1.09	1.65	1.89	1.10	1.07	1.66	1.91	1.08	1.04	-	-	-	-
A-12 -(2 A) \leftrightarrow	1.68	1.74	1.09	1.08	1.67	1.88	1.07	1.03	1.66	1.85	1.06	1.02	1.67	1.87	1.05	0.92
A-13 -(H_2Ag) \leftrightarrow	1.74	1.90	1.02	0.70	1.71	1.90	1.01	0.71	-	-	-	-	-	-	-	-
A-14 -(3 $\text{KT}/\text{H}_2\text{Ag}$) \leftrightarrow	1.69	1.86	1.02	1.00	1.74	1.90	1.04	1.03	1.71	1.88	1.01	0.98	1.22	1.86	1.02	0.98
A-15 -(1 $\text{KT}/\text{H}_2\text{Ag}/\text{wick}/\text{wick}$) \leftrightarrow	1.78	1.92	1.03	0.98	1.71	1.90	1.04	1.00	1.71	1.92	1.03	0.97	1.74	1.89	1.04	0.61
A-16 -($\text{H}_2\text{Ag}/\text{wick}/\text{H}_2\text{Ag}$) \leftrightarrow	1.73	1.82	0.99	0.97	1.77	1.93	1.00	0.97	1.73	1.89	0.98	0.96	1.75	1.90	0.98	0.92

TABLE 35

CAPACITIES OF ROLLED Ag/H₂ CELLS

Cell No. Configuration	Prior to Cycling	Capacity (to 0.8V) Ah Cycle 104	Cycle 514
A-1 -(1 A/NASA) ₊	14.55	13.82	11.72
A-2 -(1 KT/NASA) ₊	14.55	13.97	12.42
A-3 -(2 A/NASA) ₊	16.05	16.28	14.35
A-4 -(2 KT/NASA) ₊	15.15	11.03	(13.65)
A-5 -(1 A/NASA) ₊	15.00	14.87	12.95
A-6 -(1 KT/NASA) ₊	15.75	-	-
A-7 -(1 A/NASA/1 A) ₊	16.20	11.55	11.72
A-8 -(1 KT/NASA/1 KT) ₊	13.95	12.42	10.94
A-9 -(1 A/NASA) ₊	16.35	13.13	11.46
A-10 -(2 A/NASA) ₊	15.75	17.33	15.23
A-11 -(1 A) ₊	14.85	13.97	-
A-12 -(2 A) ₊	16.05	16.45	11.99
A-13 -(NASA) ₊	13.05	11.72	-
A-14 -(3 KT/NASA) ₊	16.20	17.33	15.84
A-15 -(1 KT/NASA/+/-wick)	16.20	14.52	10.67
A-16 -(NASA/wick/NASA) ₊	16.05	16.62	14.18

TABLE 36

PRESSURE AND ELECTROLYTE DATA DURING CYCLE
TESTING OF ROLLED Ag/H₂ CELLS

Cell No. and Configuration	Cell Pressure, psig		Electrolyte Cm ³			Drained after Rate Sensitivity Test	Final Level
	Cycle 104 P _{max} / P _{min}	Cycle 514 P _{max} / P _{min}	Pretest Level	Drained after Cycle 104	Drained after Cycle 514		
A-1 -(1 A/NA ₂ S) ₊	542 162	447 143	40	1.4	1.7	0.3	35
A-2 -(1 KT/NA ₂ S) ₊	514 99	461 104	30	2.6	1.1	0.5	26
A-3 -(2 A/NA ₂ S) ₊	593 134	529 154	29	1.1	0.9	0.6	27
A-4 -(2 KT/NA ₂ S) ₊	458 131	545 145	36	3.9	5.8	1.0	28
A-5 -(1 A/NA ₂ S) ₊	598 105	518 102	26	1.2	0.1	0.1	24
A-6 -(1 KT/NA ₂ S) ₊	-	-	24	6.9	-	2.4	14
A-7 -(1 A/NA ₂ S/1 A) ₊	470 75	480 88	24	0.3	0.9	0.1	23
A-8 -(1 KT/NA ₂ S/1 KT) ₊	595 162	560 180	27	0.8	1.8	1.6	23
A-9 -(1 A/NA ₂ S) ₊	545 112	490 110	25	3.1	1.1	1.2	20
A-10-(2 A/NA ₂ S) ₊	750 125	660 135	34	1.9	2.1	0.1	29
A-11-(1 A) ₊	610 120	-	23	1.5	-	0.7	20
A-12-(2 A) ₊	685 120	540 140	32	1.4	1.5	1.2	27
A-13-(NA ₂ S) ₊	555 155	-	27	2.5	-	1.5	19
A-14-(3 KT/NA ₂ S) ₊	705 115	660 130	32	3.1	2.4	1.4	25
A-15-(1 KT/NA ₂ S/+wick)	860 260	725 305	-	-	-	-	-
A-16-(NA ₂ S/+wick/NA ₂ S) ₊	760 230	698 260	-	-	-	-	-

TABLE 37

HISTORY OF FAILED CELLS

Cell A-6	<p>Failed on Cycle 19. Cause was a short circuit caused by a twisted lead.</p> <p>Defect was removed, cell was reconnected to the cyclor at Cycle 116 and failed during Cycle 320 by reaching the low capacity limit after 204 cycles.</p>
Cell A-13	<p>Failed during Cycle 180. Cell was reimpregnated and rejoined testing at Cycle 233. It failed again after 5 cycles.</p>
Cell A-4	<p>Failed during Cycle 206. The cell was reimpregnated and resumed cycling at Cycle 233 without further problem.</p>
Cell A-11	<p>Failed during Cycle 386.</p>

TABLE 38
 FACTORIAL EVALUATION OF CAPACITY RETENTION

Combination D R E			Cell No.	Response	Effect	
0	0	0	1	80.5	615.5	Total
1	0	0	5	86.3	-79.3	D
0	1	0	2	85.4	-41.7	R
1	1	0	6	(33)	-56.9	D, R
0	0	1	3	89.4	45.1	E
1	0	1	7	72.4	21.9	D, E
0	1	1	4	90.1	55.1	R, E
1	1	1	8	78.4	67.5	D, R, E
M E						
0	0		11	(55)	269.1	Total
1	0		13	(50)	9.7	M
0	1		12	74.7	59.1	E
1	1		3	89.4	19.7	M E
H E						
0	0		1	80.5	336.7	Total
1	0		9	70.1	-3.1	H
0	1		3	89.4	35.5	E
1	1		10	96.7	17.7	H E

TABLE 39

FACTORIAL EVALUATION OF CELL ENERGY AT CYCLE 514

Combination D R E	Cell No.	Response	Effect	
0 0 0	1	11.95	94.5	Total
1 0 0	5	13.34	-11.0	D
0 1 0	2	12.54	-9.1	R
1 1 0	6	(5.2)	-9.4	D, R
0 0 1	3	14.35	8.5	E
1 0 1	7	12.19	0.9	D, E
0 1 1	4	13.92	6.0	R, E
1 1 1	8	11.05	8.0	D, R, E
M E				
0 0	11	(8.2)	41.6	Total
1 0	13	(6.5)	0.1	M
0 1	12	12.59	12.2	E
1 1	3	14.35	3.5	M, E
H E				
0 0	1	11.95	53.7	Total
1 0	9	11.69	1.1	H
0 1	3	14.35	6.4	E
1 1	10	15.69	1.6	H, E

3. On a layer-by-layer basis kT may be slightly less advantageous than asbestos. This result can be expected on the basis of the beneficial effect of additional electrolyte. The kT separator is more compact and absorbs a smaller volume of electrolyte. Cell 14 with 3 kT layers performed very well.
4. The presence or absence of the NASA separator did not appear to make any significant difference.
5. Varying the amount of Teflon in the hydrogen electrodes between 20 and 30% has no effect on cell performance.

The performance of the two wick cells (15 and 16) was very much in line with that of the other cells. The pressure increased, however, considerably in both cells. This is probably due to silver oxide removal by migration into the electrolyte reservoir which will enhance the oxidation of additional silver. Considerable corrosion of the stainless steel pressure vessel can be expected in the area of the electrolyte pool.

After the cycle testing we have further performed several charge-discharge cycles to determine the sensitivity of the various cell configuration to changes in charge and/or discharge rate. The data is summarized in Table 40. The capacities at the 1.33 C rate were only slightly lower than at the 0.66 C rate and at the C/6 rate they were not much higher. This insensitivity to rate changes after the cycle testing is in contrast to the results obtained with new electrodes where the capacity is a fairly strong function of rate. There is no significant correlation between the rate sensitivity and the cell configuration. Apparently the active part of the silver electrode is conditioned during the repetitive cycling in such a way that the material utilization cannot be readily increased in a lower rate charge-discharge cycle.

In summary Ag/H₂ cells with a single layer of NASA separator and a 10 to 20 mil absorber layer will be able to successfully complete in excess of 500 charge-discharge cycles at 70% depth. A preferred cell would have a rolled stack consisting of 25 mil thick silver electrodes, a NASA separator with the membrane side away from the silver electrode and a 20 mil asbestos absorber layer between the separator and the hydrogen electrode. (This was the configuration of cells 3 and 10).

7. Preliminary Ag/H₂ Safety Analysis

With respect to safety aspects the Ag/H₂ cell will be very similar to the Ni/H₂ cell which is analyzed in detail under Air Force sponsorship. The cell container is a pressure vessel containing pressurized hydrogen gas. Materials such as nickel and certain Inconel alloys have been demonstrated as safe in the alkaline and hydrogen environment. Upon forceful puncture

TABLE 40

CAPACITY AND VOLTAGE DATA OF ROLLED Ag/H_2 CELLS TESTED AT VARIOUS RATES

Rate of Charge/Discharge	Cell Capacity (Ah)			Cell Discharge Voltage (V)		
	C/3	C/6	$\frac{2}{3} \text{ C}$	C/3	C/6	$\frac{4}{3} \text{ C}$
Cell No. and Configuration	C/6	C/6	$\frac{2}{3} \text{ C}$	C/6	C/6	$\frac{4}{3} \text{ C}$
A-1 -(1 A/NA $\xrightarrow{+}$ SA)+	12.35	12.63	11.97	1.15	1.15	0.91
A-2 -(1 KT/NA $\xrightarrow{+}$ SA)+	13.48	12.81	12.75	1.15	1.14	0.89
A-3 -(2 A/NA $\xrightarrow{+}$ SA)+	14.67	14.64	14.62	1.14	1.13	0.84
A-4 -(2 KT/NA $\xrightarrow{+}$ SA)+	14.27	14.55	13.68	1.13	1.12	0.86
A-5 -(1 A/NA $\xrightarrow{+}$ SA)+	14.54	14.73	14.00	1.15	1.15	0.91
A-6 -(1 KT/NA $\xrightarrow{+}$ SA)+	13.34	14.18	13.22	1.14	1.14	0.88
A-7 -(1 A/NA $\xrightarrow{+}$ SA/1 A)+	12.55	12.99	12.60	1.14	1.13	0.91
A-8 -(1 KT/NA $\xrightarrow{+}$ SA/1 KT)+	12.02	12.63	11.82	1.14	1.14	0.88
A-9 -(1 A/NA $\xrightarrow{+}$ SA)+	12.02	12.72	12.28	1.14	1.13	0.90
A-10-(2 A/NA $\xrightarrow{+}$ SA)+	14.94	15.10	15.24	1.14	1.13	0.91
A-11-(1 A)+	12.41	13.54	12.28	1.17	1.16	0.99
A-12-(2 A)+	13.87	13.82	13.37	1.14	1.14	0.95
A-13-(NA $\xrightarrow{+}$ SA)+	13.28	13.63	11.97	1.13	1.12	0.88
A-14-(3 KT/NA $\xrightarrow{+}$ SA)+	15.53	15.97	15.39	1.15	1.16	0.90
A-15-(1 KT/NA $\xrightarrow{+}$ SA/+wick)	12.08	12.72	12.28	1.15	1.14	0.88
A-16-(NA $\xrightarrow{+}$ SA/wick/NA $\xrightarrow{+}$ SA)+	15.33	15.46	14.62	1.14	1.12	0.79

hydrogen gas and potassium hydroxide can be released. The silver oxide electrode will reach more anodic potentials in its fully charged state than the nickel oxide electrode. This could, if not adequately considered, lead to anodic attack of the cell case or other internal support hardware. The results may increase cell pressure and weakening of the cell case. Proper cell design will avoid this problem. On overcharge oxygen is generated at the silver electrode which will react and thus be removed at the hydrogen electrode. Potentially dangerous H_2/O_2 mixtures can be avoided by proper cell design. Extremely high rate and sustained overcharge could lead to explosion in some cell designs). Oxygen recombination would not be compromised even if the hydrogen electrode were "poisoned" by deposition of silver since silver is a good oxygen recombination catalyst. The cell voltage is low, between 1 to 2V thus causing no specific hazard. Depending on construction, a short circuit may lead to passage of high currents. This in turn would heat up the cell and potentially render it inoperative. No specific safety problem is anticipated with this type failure. Cell pressure would fall rapidly since H_2 consumption greatly exceeds thermal gas expansion. Generation of potentially dangerous H_2/O_2 mixtures on forced overcharge can be avoided by a cathode (silver electrode) limited design (use of an adequate hydrogen precharge). Cell incineration could lead to a pressure rupture by thermal expansion of the compressed gas. Resistance to mechanical (vibration and shock) stress depends on cell design. The system has no inherent restrictions.

In summary extensive safety testing has not been performed but based on the fairly detailed understanding of the system resulting from this program and from our knowledge of the Ni/H_2 system, we considered the safety and the hazards of both systems equivalent. Case corrosion needs more attention in Ag/H_2 cells.

III. SILVER-HYDROGEN CELL DESIGN AND OPTIMIZATION

1. Electrolyte Management

In considering electrolyte management, we are primarily concerned with insuring that there is sufficient electrolyte on both sides of the separator membrane, so that neither overflow nor drying out of the reservoirs occurs. This problem is essentially one-dimensional; plate area and geometry are not involved. In order to develop an understanding of the relative importance of various separator membrane properties, a computer program was written to simulate the processes that occur when current is passed through a reservoir-membrane-reservoir package. This program proved quite useful in selecting membranes and reservoirs for practical applications.

1.1 Electrolyte Management Computer Program

The computer program simulates the effects of (1) KOH and H₂O diffusion; (2) transport of K⁺, OH⁻, and H₂O through the membrane due to current flow; (3) changes in the porosity of the Ag electrode due to chemical reaction; and (4) flow of electrolyte through the membrane due to wicking. Any number of charge-discharge cycles can be simulated. The program calculates the KOH concentration on both sides of the separator membrane, and the fill factors of the two reservoirs. In developing the program, it was not initially clear whether the Ag electrode would have the same behavior with respect to flooding and drying out as the Ag-side reservoir. For this reason, a parameter (IFILL) was provided to allow either of two assumptions to be used in the calculations: (a) the electrode and reservoir behave identically (IFILL = 0); or (b) the electrode is always full of electrolyte, in which case the fill factor applies to the reservoir alone (IFILL = 1). Later experimental observations showed that the Ag-electrode is wet even when the reservoir is dry, so the parameter IFILL should be set equal to unit.

The input structure for the electrolyte management program is summarized in Table 41. and a complete program listing is given in Appendix D. To simplify the input, default options have been provided for most of the input parameters, and these are also given in the Table. Whenever an input parameter is equal to zero -- as when a blank card is substituted for the data card -- the appropriate default value is substituted. Only the first input record must be non-zero, since NTYPE = 0 causes program exit.

1.2 Simulation of Electrolyte Transport

Sixteen runs using the standard default for records 2-5 have been carried out. A sample of the output is given in Appendix D. These runs

include all four types of separator material. The wicking rate constant has been assumed equal to zero or to 0.0002 cc per minute and IFILL = 0 or 1. Results may be summarized as follows:

1. With IFILL = 1 and WIKRAT = 0, the Ag-side reservoir dries out on the first charge cycle for all membranes except 2193 (NTYPE = 3).
2. With IFILL = 1 and WIKRAT = 0.0002, the Ag-side reservoir does not dry out. In order of decreasing fill factor after the first charge cycle, the results are Permion 2193 (NTYPE = 3), Visking (NTYPE = 2), Permion 2291 (NTYPE = 4), and NASA Separator (NTYPE = 1).
3. With IFILL = 0 and WIKRAT = 0.0002, the Ag-side reservoir does not dry out, and the order of separators with respect to fill factor after one charge cycle is as above.
4. With IFILL = 0 and WIKRAT = 0, the Ag-side reservoir dries out on the third charge cycle for all membranes except 2193.

These results indicate the importance of wicking, and it seems clear that for a flow rate constant around 0.0002 cc per minute, reservoir dryness should not occur. Later measurements showed that the wicking rate constant is in fact smaller for all membranes with the exception of the NASA separator.

In order to understand why the simulated performance of Permion 2193 is superior to that of the other membranes, eight additional runs were carried out in which the diffusion and transport numbers for this membrane were systematically varied. Results are as follows:

1. Membrane performance improves as t_{OH^-} increases (t_{K^+} decreases). Performance degrades as t_{H_2O} increases. Thus, small t_{H_2O} and t_{K^+} are desirable.
2. Increasing or decreasing both D_{KOH} and D_{H_2O} by the same factor has little effect on performance. Thus, increasing or decreasing the number of barrier membranes should have little effect.
3. Increasing D_{KOH} relative to D_{H_2O} improves performance. Increasing D_{H_2O} relative to D_{KOH} degrades performance.

These results are readily understood in qualitative terms: On charge, removal of KOH and H_2O from the Ag-side are proportional to t_{K^+} ($1 - t_{OH^-}$) and $t_{H_2O} - 0.5$ respectively. Thus, high values of t_{K^+} and t_{H_2O} favor electrolyte transport

and drying of the Ag reservoir. The relative values of the two diffusion constants is important because, as the concentration of KOH increases on the H₂ side, KOH flows from the H₂ side to the Ag side while H₂O flows from the Ag side to the H₂ side. The relative rates of flow determine the net transfer of solution, and if D_{H_2O} is much larger than D_{KOH} -- as is often the case -- the result is net flow of solution from the Ag-side to the H₂ side.

It is experimentally difficult to determine the relative values of D_{KOH} and D_{H_2O} , and indeed it is usually assumed that they are equal, which is the case in free solution where no net change in volume is possible. However, our experiments indicate that on average D_{H_2O} is several times larger than D_{KOH} , which is detrimental to membrane performance. In the case of Permion 2193, however, the diffusion constants are so small that the observed volume change is zero within the measurement error. Thus, the apparent near equality of D_{KOH} and D_{H_2O} for 2193 is probably an experimental artifact. This would explain why simulation runs for this membrane are not in accord with experimental cycling results. For membranes with larger diffusion constants (e.g., Visking), simulation results should be more accurate.

One of the most interesting results of the simulation runs is that the hydrogen side tends to fill up, rather than dry out, during charge. This is because (a) transport of K^+ and H₂O to the hydrogen side compensates for consumption of water at the hydrogen electrode and (b) diffusion of additional water into the hydrogen side tends to dilute the excess KOH. Simultaneously, the silver side tends to dry out. On discharge, the flow of electrolyte reverses, but the effect is not complete due to the excess of charge current over discharge current. This means that in the absence of wicking the hydrogen side reservoir eventually overflows or the silver side reservoir eventually dries out.

It is also noteworthy that the Ag-side and H₂-side KOH concentrations are in all cases fairly close: diffusion is adequate to prevent a steep concentration gradient. Thus, the most important membrane parameter is its wicking rate constant. Inadequate wicking, as noted above, will lead to overflow of the H₂ reservoir, or drying out of the Hg reservoir.

In summary, for adequate electrolyte management an argentistatic membrane for use in Ag/H₂ cells should have a suitable combination of the following properties: (1) a low transport number for K^+ , (2) a low transport number for H₂O, (3) a ratio of D_{H_2O}/D_{KOH} close to 1, and (4) a high back wicking rate. The four membranes investigated here are fairly similar in all properties except for the rate of back wicking. The high rate of back wicking of the NASA separator makes it the only practically usable argentistatic membrane of Ag/H₂ cells.

TABLE 41

INPUT STRUCTURE FOR THE ELECTROLYTE MANAGEMENT PROGRAM

1. NTYPE, NSEPM, IFILL, TDEGC, WIKRAT
 0 2 0 25.0 0.0
 (3I5, 2F10)

NTYPE -- Specifies membrane type (see Comment Statements)
 NSEPM -- Number of barrier membranes
 IFILL -- See above
 TDEGC -- Run temperature in degrees Celcius
 WIKRAT -- Wicking rate constant, in cc per minute per cm² of membrane.

2. CAPNAM, CAPFTR, DOD, CHGTIM, DCGTIM, RRATIO
 30. 1.1 0.8 120. 60. 1.15
 (6F10)

CAPNAM -- Nameplate capacity, amp-hours
 CAPFTR -- CAPFTR × CAPNAM = actual capacity, amp-hours
 DOD -- Depth of discharge, based on nameplate capacity
 CHGTIM -- Charge time, minutes
 DCGTIM -- Discharge time, minutes
 PRATIO -- Ratio of charge amp-hours to discharge amp-hours

3. PSBETK, PPLTHK, PPLDEN, PASADN, UTLMIN, UTLRTO
 0.001 0.0635 4.273 4.173 0.5 1.1
 (6F10)

PSBETK -- Ag substrate effective thickness
 PPLTHK -- Total Ag electrode thickness
 PPLDEN -- Mean electrode density
 PASADN -- Sinter density
 UTLMIN -- Minimum utilization of sinter Ag
 UTLRTO -- UTLRTO × UTLMIN = actual utilization

TABLE 41
(CONTINUED)

4. RINLFF, RESPOR, RH2TKI, RAGTKI, SEPTKI, ELCNDC
0.65 0.8 0.09144 0.04572 0.0254 0.4
(6F10)

RINLFF -- Initial reservoir fill factors

RESPOR -- Reservoir porosities

RH2TKI -- H₂ reservoir thickness

RAGTKI -- Ag reservoir thickness

SEPTKI -- Separator thickness (not used)

ELCNDC -- KOH concentration

*5. NSTEPS, NCYCLE, TOH, TW, DK, DW
25 3
(2I5, 4F10)

NSTEPS -- Number of integration and output steps in each charge or discharge half cycle.

NCYCLE -- Number of full charge-discharge cycles

TOH -- Hydroxide transport number

TW -- H₂O transport number

DK -- KOH diffusion constant for NSEPM layers, in cc/sec.

DW -- H₂O diffusion constant for NSEPM layers, in cc/sec.

*Note that input values of TOH, TW, DK, and DW are ignored unless NTYPE = 5. For NTYPE = 1 through 4, values appropriate to the temperature and KOH concentration are generated by the program.

2. Energy Density and Thermal Management

A computer program to aid in the design of Ag/H₂ cells of rolled stack configuration has been developed. This program optimizes the weight energy density of a cell by variation of the pressure vessel length, radius, and thickness. A particular feature of the program is that volumetric energy density can be specified by the operator; the program calculates the required H₂ pressure. The program also calculates the optimum H₂ plate (Ni) thickness and the optimal lead sizes. In addition, the program simulates the thermal performance of the cell through any number of complete charge-discharge cycles, and prints the maximum and minimum temperature at each time step. The thermal performance simulation, which requires a substantial amount of computer time, can be disabled at run time. Other features include automatic variation of the number of Ag/H₂ electrode pairs, and automatic operator-selected variation of any one of 67 different input parameters. In addition, all output may be disabled by an input switch, so that user-written plotting routines can be added without deleting the output statements.

A listing of the program, a program flowsheet, a set of guidelines for operators, a sample output listing, and a set of design diagrams are given in Appendix B. In the following section, some of the theory of the more unusual program design elements is discussed. Applications of the program are then discussed in Sections 2.2 and 2.3.

2.1 Model Development

2.1.1 Optimal Resistance of Electrode Leads

We consider a set of n electrode leads, each of length ℓ and resistance R . The material properties of the leads are the resistivity ω (in ohm-cm), the density ρ , and the thermal conductivity K (in watt-cm⁻¹.deg⁻¹). The current through each lead will be designated by i . Then, for each lead, we may write the weight W , cross-sectional area A , and energy dissipation E as

$$A = \frac{\omega \ell}{R} \quad (20)$$

$$W = A \ell \rho \quad (21)$$

$$E = i^2 R / C \quad (22)$$

where $1/C$ is the discharge time in hours.

We also designate the energy stored in the battery by SV , where S is the capacity in amp-hours and V the voltage. The net energy N that can be obtained from the battery is

$$N = SV - n i^2 R/C \quad (23)$$

The current i depends on the rate of discharge. At the one-hour rate, $ni = S$; at an arbitrary rate C (hours⁻¹), $ni = SC$. Thus, the net energy may be written as

$$N = SV - S^2 CR/n \quad (24)$$

In order to optimize the energy density, we also require an expression for the total weight of the battery, T . Approximately, T is proportional to the cell capacity, to which we add the weight of the leads. Thus

$$T = aS + nW \quad (25)$$

where a is a proportionality factor. We can now solve the lead resistance R such that

$$\frac{d(N/T)}{dR} = 0 \quad (26)$$

A little manipulation yields the quadratic equation

$$R^2 + \frac{2n\omega\ell^2\rho}{aS} R - \frac{n^2 V\omega\ell^2\rho}{aS^2 C} = 0 \quad (27)$$

In the cases we have considered, the linear term is negligible, so that

$$R \approx \frac{n\ell}{S} \sqrt{\frac{V\omega\rho}{aC}} \quad (28)$$

It is then easily shown that the heat dissipation is

$$E = S\ell \sqrt{\frac{V\omega\rho C}{a}} \quad (29)$$

and the total weight of the leads is

$$nW = S\ell \sqrt{\frac{a\omega\rho C}{V}} \quad (30)$$

Both E and nW are independent of the total number of leads.

It is useful to consider a specific example. For a 20 Ah cell designed to discharge at the 2 C rate at 1.1 volts, the net energy is

$$N = 22 - 800 R/n$$

Let us assume that the leads are 5 cm long, and are made of Ag ($\omega = 1.6 \times 10^{-6}$ ohm-cm; $\rho = 10.5$) or Ni ($\omega = 9.5 \times 10^{-6}$ ohm-cm; $\rho = 8.9$). We also assume that the battery weight (exclusive of leads) is 220 grams, i.e., $a = 11$ grams/AH. Then

$$\frac{R}{n} = 5.14 \times 10^{-4} \text{ ohms (Ni)}$$

$$= 2.29 \times 10^{-4} \text{ ohms (Ag)}$$

$$EC = .82 \text{ watts (Ni)}$$

$$= .37 \text{ watts (Ag)}$$

$$nW = 4.11 \text{ grams (Ni)}$$

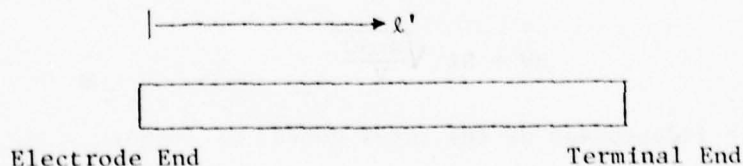
$$= 1.83 \text{ grams (Ag)}$$

The energy density is reduced from $22/220 = .100$ to $21.41/225.94 = .0948$, a reduction of about 5%.

It is of interest to consider the reduction in energy density due to off-design conditions. Suppose the resistance of the Ni leads is deliberately decreased by a factor of two to reduce the heat dissipation. Then it is easily shown that the lead weight doubles and the i^2R loss is halved. The energy density is now $21.61/230.05 = .0939$, a further reduction of about 1%. Thus, because the lead resistance was initially optimized to satisfy Eq. 27, relatively large changes in R away from the optimum value do not strongly effect the energy density.

Heating of the Leads

Let us assume that the terminals are thermally insulated, and that the only dissipation of heat takes place at the electrode to which the lead is attached. The terminal end of the lead will then have the highest temperature. For a lead length of ℓ cm, the rate of heat generation in the section of wire between some arbitrary point ℓ' and the terminal end ℓ , is



$$\frac{i^2 R}{\ell} (\ell - \ell') \quad (31)$$

The rate of heat flow across the plane at ℓ' is

$$AK \frac{dT}{d\ell'}, \quad (32)$$

where A is the cross-sectional area of the wire. Thus,

$$\frac{dT}{d\ell'} = \frac{i^2 R}{AK} \left(1 - \frac{\ell'}{\ell}\right) \quad (33)$$

Integrating over ℓ' , we obtain

$$T = T_o + \frac{i^2 R}{AK} \left(\ell' - \frac{\ell'^2}{2\ell}\right) \quad (34)$$

For $\ell' = \ell$, the temperature difference between the terminal and the electrode is

$$\Delta T = \frac{i^2 R \ell}{2AK} \quad (35)$$

Using the terminology developed earlier,

$$\Delta T = \frac{S^2 C^2 R^2}{2n^2 K \omega} \quad (36)$$

It should be noted that ΔT depends on the square of the lead resistance and is formally independent of lead length. In an optimized lead, R depends on ℓ .

The examples considered earlier provide some estimates of ΔT . For $S = 20$, $C = 2$, $\omega = 1.6 \times 10^{-6}$ ohm-cm, and $K = 4.18$ watts \cdot cm $^{-1}$ \cdot deg $^{-1}$ (Ag), $\Delta T = 6.3^\circ\text{C}$. For $\omega = 9.5 \times 10^{-6}$ ohm-cm and $K = 0.59$ watts \cdot cm $^{-1}$ deg $^{-1}$ (Ni), $\Delta T = 37.7^\circ\text{C}$. If the resistance of the Ni leads is doubled, at a penalty of 1% in the energy density, the temperature rise in the leads is reduced to 9.4°C . Thus, in a properly optimized system, it does not appear that the leads become particularly warm, and the Ag leads are especially unlikely to heat up.

2.1.2 Optimal Resistance of the H₂ Electrode

The Ni grid, which supplies the mechanical and electrical support for the H₂ electrode, may be optimized in much the same way as the leads. Consider a set on n electrodes, each of length $2Z_o$, width $2Y_o$; and thickness $2X_o$. We will assume initially that each electrode is tabbed along its entire width $2Y_o$; this assumption is later analyzed in detail. We will also assume that the current flow out of the electrode is uniform, i.e., that electrochemical reactions occur at a constant current density. With these assumptions, it is easily shown that

$$\frac{di}{dZ} = \text{constant} \quad (37)$$

and that

$$i = \frac{i_o}{2} (1 + Z/Z_o) \quad (38)$$

Along the tab ($Z = Z_o$), $i = i_o$, the current entering the electrode. At the far end of the electrode ($Z = -Z_o$), $i = 0$.

The resistance of any electrode section dZ is given by

$$dR = \frac{\omega dZ}{4X_o Y_o} \quad (39)$$

where $\omega = 9.5 \times 10^{-6}$ ohm·cm. Thus, the energy loss in the electrodes per unit time is

$$\begin{aligned} nEC &= \int_{-Z_o}^{Z_o} ni^2 dR = \frac{ni_o^2 \omega}{16X_o Y_o} \int_{-Z_o}^{Z_o} (1 + Z/Z_o)^2 dZ \\ &= \frac{ni_o^2 \omega Z_o}{6X_o Y_o} \end{aligned} \quad (40)$$

In addition, the total weight of the electrodes is

$$nW = 8 n X_o Y_o Z_o \rho \quad (41)$$

To optimize the energy density, we follow the same procedure as used for the leads, and write

$$N = SV - \frac{S^2 C \omega Z_o}{6nX_o Y_o} \quad (42)$$

The total weight of the battery is again written in the form

$$T = aS + 8nX_o Y_o Z_o \rho \quad (43)$$

Differentiation of N/T with respect to electrode thickness ($2X_o$) results in the quadratic equation

$$X_o^2 - \frac{SC \omega Z_o}{3nV Y_o} X_o - \frac{S^2 C a \omega}{48n^2 Y_o^2 V \rho} = 0 \quad (44)$$

The voltage drop across the electrode is also important to proper electrode performance. Integrating iR over the electrode surface, we obtain

$$\Delta V = \frac{i_o \omega Z_o}{4X_o Y_o} = \frac{SC \omega Z_o}{4nX_o Y_o} \quad (45)$$

Some specific examples will illustrate the magnitude involved. We again consider a system of 20 AH capacity, discharged at the 2C rate at 1.1 volts. Two sub-cases will be developed: (I) a single electrode of length $2X_o = 40$ cm and width $2Y_o = 40$ cm; and (II) a set of 10 electrodes each with $2Z_o = 10$ cm and $2Y_o = 16$ cm. In both cases the total electrode area is 1600 cm^2 , so that the current density is 25 mA/cm^2 . The results are shown in Table 42. The columns labelled with an asterisk show the effect of using double the optimum electrode thickness.

Several provisional conclusions may be drawn from this table:

1. The optimum value of the electrode thickness is very small, e.g., 0.13 mils in Case II and 0.57 mils in Case I. The lower value may be too small for manufacturability. (It should be noted that for Exmet electrodes these values are effective thicknesses, i.e., weight per unit area divided by density, not the thickness of the original sheet).
2. The voltage drops may be excessive, at least in Case I and I*. It may be necessary to specify a maximum voltage drop as well as a minimum electrode thickness.
3. The penalty in the energy density for using an electrode of double the optimum thickness is not large, e.g., 4% for Case I and 1% for Case II.
4. The penalty in the energy density due to using a small number of plates may be substantial.

2.1.3 Effect of Electrode Tabs

When an electrode is tabbed along only a small portion of its length, there is an extra penalty in the energy density due to the large i^2R losses in the area immediately surrounding the tab. It is somewhat difficult to account for these losses exactly, but a good estimate of their magnitude can be obtained by considering the optimization of the energy density in a semicircular electrode of radius r_{\max} and tab radius r_{tab} . The current flowing through such an electrode at any intermediate radius r is

TABLE 42
OPTIMUM THICKNESS FOR RECTANGULAR ELECTRODES
FULLY TABBED ALONG ONE EDGE

	Case I	Case I*	Case II	Case II*	
Electrode Thickness, $2X_0$	1.454×10^{-3}	2.908×10^{-3}	3.407×10^{-4}	6.814×10^{-4}	cm
ΔV	0.131	0.065	0.035	0.017	volts
Energy Loss per Unit Time, nEC	3.48	1.74	0.93	0.46	watts
Electrode Weight, nW	20.70	41.41	4.85	9.70	grams
Energy Density	0.0842	0.0808	0.0958	0.0948	watt-hours/ grams

$$i = i_o \left(\frac{r_{\max}^2 - r^2}{r_{\max}^2 - r_{\text{tab}}^2} \right) \quad (46)$$

and the resistance through a semi-circular shell is

$$dR = \frac{\omega dr}{2\pi X_o r} \quad (47)$$

where $2X_o$ is the electrode thickness. The energy loss per unit time is

$$nEC = \frac{S^2 C^2 \omega}{2\pi n X_o (r_{\max}^2 - r_{\text{tab}}^2)^2} \left[r_{\max}^4 \ln \left(\frac{r_{\max}}{r_{\text{tab}}} \right) - r_{\max}^2 (r_{\max}^2 - r_{\text{tab}}^2) + \frac{r_{\max}^4 - r_{\text{tab}}^4}{4} \right] \quad (48)$$

For $r_{\max}^2 \gg r_{\text{tab}}^2$, this becomes

$$nEC = \frac{S^2 C^2 \omega}{2\pi n X_o} \left[\ln \left(\frac{r_{\max}}{r_{\text{tab}}} \right) - 3/4 \right] \quad (49)$$

The weight of the electrode plus tab is

$$2\pi r_{\max}^2 X_o \rho \quad (50)$$

For given values of r_{tab} and r_{\max} , the weight is proportional to X_o and the net energy is inversely proportional to X_o . Thus, optimization with respect to thickness may be carried out as before. Table 43 gives the calculated results for the same two cases discussed previously, i.e., $S = 20$, $C = 2$, $V = 1.1$, with $n = 1$ and $n = 10$ respectively. The plate area has been maintained at 1600 cm^2 .

The table indicates that a substantial penalty in the energy density will occur if undersized tabs are used, particularly if the number of plates is small. However, it is difficult to manufacture large tabs, and it may be necessary to design plates with relatively small tabs. The question that therefore must be answered is what plate thickness to use when a rectangular plate is tabbed over only a small portion of one edge, as in the figure below.

TABLE 43

OPTIMUM THICKNESS FOR SEMI-CIRCULAR ELECTRODES

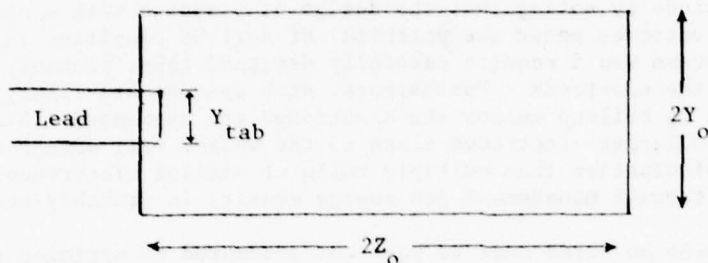
$$\frac{r_{\max}}{r_{\text{tab}}}$$

Case I: $n = 1$

	2	5	10	20	
r_{tab}	13.03	4.61	2.27	1.13	cm
$2X_o$	6.698×10^{-4}	1.373×10^{-3}	1.822×10^{-3}	2.221×10^{-3}	cm
ΔV	0.162	0.145	0.152	0.161	volts
nEC	2.28	3.44	4.23	4.92	watts
nW	12.72	20.37	26.21	31.71	grams
Energy Density	0.0896	0.0844	0.0808	0.0776	watt-hours/ gram
Energy Density for double-thick- ness electrode	0.0873	0.0811	0.0769	0.0733	watt-hours/ gram

Case II: $n = 10$

	2	5	10	20	
r_{tab}	4.12	1.46	0.72	0.36	cm
$2X_o$	2.040×10^{-4}	4.097×10^{-4}	5.3565×10^{-4}	6.441×10^{-4}	cm
ΔV	0.050	0.046	0.050	0.054	volts
nEC	0.75	1.15	1.44	1.70	watts
nW	3.87	6.08	7.70	9.19	grams
Energy Density	0.0966	0.0948	0.0935	0.0923	watt-hours/ gram
Energy Density for double-thick- ness electrode	0.0958	0.0935	0.0919	0.0905	watt-hours/ gram



To obtain an estimate of the energy loss in the tab, we may use Eq. (49) in the form

$$nE = \frac{S^2 C \omega}{2\pi n X_o} \left[\ln \left(\frac{2Y_o}{Y_{tab}} \right) - 3/4 \right] \quad (51)$$

Since this is the loss in a semi-circular electrode of radius $2Y_o$, it provides an upper bound to the tab losses for the situation illustrated above. Similarly, the losses in the remainder of the electrode can be estimated from Eq. (42) as

$$nE = \frac{S^2 C \omega Z_o}{6n X_o Y_o} \quad (52)$$

The total losses cannot exceed the sum of these two terms, so an estimate of the optimum value of X_o can be obtained by optimizing the energy density for a net energy given by

$$N = SV - \frac{S^2 C \omega}{2n X_o} \left\{ \frac{1}{\pi} \ln \left(\frac{2Y_o}{Y_{tab}} \right) - \frac{3}{4\pi} + \frac{Z_o}{3Y_o} \right\} \quad (53)$$

For Case I ($S = 20$, $C = 2$, $V = 1.1$, $Z_o = Y_o = 20$, $n = 1$), the energy loss term given by Eq. (52) is $1.267 \times 10^{-3}/X_o$. With $Y_{tab} = 2$ cm, the energy loss term given by Eq. (51) is $2.716 \times 10^{-3}/X_o$. The optimum value of $2X_o$ is 2.216×10^{-3} cm, about 50% greater than the optimum value for a fully tabbed rectangular electrode. The energy loss per unit time is no greater than 7.19 watts, about double the previous value. Finally, the energy density is at least .0732, roughly a 10% reduction from the value given previously. For Case II ($S = 20$, $C = 2$, $V = 1.1$, $Z_o = 5$, $Y_o = 8$), the penalty is less severe: with $Y_{tab} = 1$ cm, $2X_o$ increases to 7.045×10^{-4} cm, about double the previous value, while the energy loss term becomes 1.84 watts, again double the previous value. However, the energy density is now at least 0.0916 watt-hours per gram, a 4% reduction.

We may conclude by noting that the design of a system with a small number of large electrodes poses the potential of serious penalties in energy density. Such systems would require carefully designed tabs, probably along the full width of the electrode. Furthermore, such systems are likely to have problems with O_2 buildup unless the electrodes are segmented. Since, however, one or two larger electrodes close to the vessel wall appear to provide better heat dissipation than multiple rolls of smaller electrodes, a trade-off between thermal management and energy density is probably necessary.

It should also be noted that we have not attempted to optimize the resistance of the Ag grid. Since Ag is a far better conductor than Ni, and since extra conductivity is provided by the Ag sinter, the Ag grid should be as thin as manufacturing techniques will permit.

2.2 Use of the Computer Model

2.2.1 Critical Design Parameters

As noted in Appendix A, the computer model has been structured so that only the first input record need be non-blank. Use of blank cards for the other fourteen input records causes the program to substitute default values for each of the 67 design parameters. The default values are given in the program in COMMON block EIC1, and are described within the program in the COMMENT statements.

These parameters are not all of equal interest or importance. Therefore, in the following paragraphs, we discuss only the most important parameter choices, those that represent relatively critical assumptions in the cell design.

UCON1 = 0.128
UCON2 = -.286

The fraction of the Ag electrode utilized on discharge is given by the equation

$$UTL_{MIN} = UCON1 + UCON2 \times \log_{10} (-DCCRDN) \quad (54)$$

where $-DCCRDN$ is the discharge current density. In more recent studies we have found that it is more accurate to set $UCON1 = 0.205$; this choice reflects a larger Ag utilization. It should be noted that $UCON1$ and $UCON2$ are not, strictly speaking, "design" parameters, but are properties of the electrode material. For this reason they are not included in the list of 67 input parameters.

THNRTQ = 1.5 Ratio of Ni plate thickness to calculated optimum
ALDRTQ = 1.0 Ratio of Ag-lead thickness to calculated optimum
HLDRTQ = 2.0 Ratio of Ni-lead thickness to calculated optimum.

We have found that the heating due to i^2R losses in the leads and the electrodes are relatively small compared to the electrochemical effects. Therefore, in optimizing the lead and plate dimensions, the ratios of the lead and electrode thicknesses to their optimal values have been chosen close to unit.

VOLDEQ = 0.07 Volumetric energy density

The design volumetric energy density is 0.07 WH/cm^3 (70 WH/liter). We have found that the weight energy density is a maximum for roughly this value.

PPLTHQ = 0.0635 Positive plate thickness

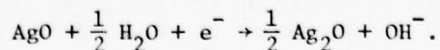
The positive plate thickness is 0.0635 cm (25 mils). We have checked the sensitivity of the weight energy density to this parameter, and found that this thickness is near optimum at the C/4 rate (vide infra).

SAFETQ = 2 Pressure vessel safety factor
 RH2RTQ = 0.3 Ratio of H₂ reservoir thickness to positive plate thickness
 RAGRTQ = 0.3 Ratio of Ag reservoir thickness to positive plate thickness
 SEPTHQ = 0.025 Barrier membrane thickness.

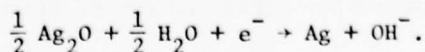
The barrier membrane thickness is 0.025 cm (10 mils). The H₂ and Ag reservoir thicknesses, defined at statement 9, are both equal to 0.014 cm (5.5 mils). Thus, the total reservoir package is 21 mils. More recent experimental work has shown that a better design is described by the parameters RH2RTQ = 0.6, RAGRTQ = 0.1, and SEPTHQ = 0.0432, for a total reservoir package of 29 mils.

TMPIDQ = 10 Percent of time in Step 1 discharge.

The discharge process occurs in three steps, with the last two steps occurring at the same voltage. In Step 1, which takes 10% of the total discharge time (6 minutes), the voltage is 1.43 and the electroneutral voltage is 1.50 (see statements immediately preceeding statement 8 in SUBROUTINE THRMAL). The electrochemical reaction is



In Step 2, which takes the next 40% of the total discharge time, the voltage drops to 1.15, but the electroneutral voltage remains at 1.50 volts and the electrochemical reaction is presumed unchanged. In Step 3, which takes the remaining 50% of the total discharge time, the voltage remains at 1.15, but the electrochemical voltage drops to 1.32, and the corresponding electrochemical reaction is



It should be noted that the difference between the cell voltage and the electroneutral voltage is largest in Step 2, and hence the temperature rise in the battery during discharge is greatest in this step. However, an even greater temperature rise can occur on overcharge, since the entire input energy is converted to heat.

DCVT1Q = 1.43 Discharge voltage, Step 1
 DCVT2Q = 1.15 Discharge voltage, Step 2
 CGVT1Q = 1.25 Charge voltage, Step 1
 CGVT2Q = 1.54 Charge voltage, Step 2

These are the voltages for the various electrochemical steps noted above. In more recent work we have inserted three statements after 9 RAGTKI.... as follows:

DCVLT1 = $1.4686 + 4.05405 \times DCCRDN$
 DCVLT2 = $1.22189 + 3.24324 \times DCCRDN$
 $V = DCVLT1 \text{ TMP1DQ}/100. + DCVLT2 \times (100.-\text{TMP1DQ})/100.$

These statements more accurately reflect the variation of discharge voltage with current density.

2.2.2 Interpretation of Program Output

In the enclosed sample output (Appendix D), results are presented in several stages. First, a reference table of all 67 main parameters is printed in the order given by COMMON block EIC1 or EIC2. Next, a reference list of operator-input parameters is given; the program always lists parameters 44 (UTLMIN, Ag utilization), although this parameter is calculated by the program, and not necessarily operator input. The plate parameters follow next. Then, for each assumption about the number of H₂-Ag electrode pairs, the program prints various information about the optimum cell design and the calculated weight energy density. Three comments are particularly worth noting:

- a) The arrangement of the electrodes varies from case to case, but the program always places an H₂ electrode on the inside of the roll. An Ag electrode is closest to the pressure vessel wall for an odd number of electrode pairs, but an H₂ electrode is closest to the wall for an even number of pairs. (This design is not necessarily optimal, and can be changed by the user).
- b) The weights and energy densities are calculated both for the given values of THNRTQ, ALDRTQ, and HLDRTQ and for unit values of these parameters. Thus, the effect on energy density of overdesigning the leads and the H₂ electrode can be seen.

- c) The weight is divided up in several ways: PV WEIGHT -- the pressure vessel weight, excluding terminals, fill tube and weld band; electrolyte weight; electrode roll (excluding electrolyte but including the support mandrel); and WTNVOL weight, which includes electrolyte, electrode roll, pressure vessel fill tube, weld band, and all support structures. The weight of the roll excludes the weight of the H₂ (Ni) plate, which is calculated separately. The sum of the weights of the leads, the H₂ plate, and the terminals is equal to the difference between the total weight and the sum of PV WEIGHT and WTNVOL WEIGHT. The last two unlabelled outputs after the volumetric energy density are the weights of the H₂ plate and the leads respectively. (The three prior unlabelled outputs are the energy dissipation, in WH, of the H₂ plate, the H₂ leads, and the Ag leads respectively).

The next print-out shows the thermal properties assumed for each of the terminals in the electrode roll. The material codes, and the values of the properties can be found in SUBROUTINE PROPTY.

For purposes of thermal simulation, the electrode roll is divided up into a number of sections. In general, we have found that one section per Ag/H₂ electrode pair is sufficient for accurate thermal simulation except during overcharge. Use of more than one section per pair requires a large number of time steps in the simulation, and hence excessive use of computer time.

A profile of the maximum (first line) and minimum (third line) temperature in the cell at equally spaced time intervals (approximately one minute) is given next. Each set of integers identifies the cell in which the maximum or minimum occurred. Finally, the maximum and minimum temperature for the entire run is given.

At the end of the run, the parameters for the "best" design are given. In the present example, only the batteries with 1 and 2 pairs of electrodes satisfy the criterion that the maximum temperature rise is below 10°C even on overcharge. The cell with 2 pairs of electrodes has the better energy density, so the parameters for this cell are printed.

Some of the results for the sample run are graphed in Figs. 40-42. Figure 40 shows the effect on the energy density of increasing the number of electrode pairs. The improvement beyond 3 or 4 layers is quite small. Figure 41 shows the calculated maximum temperature profile for the cell with 3 pairs of electrodes. The maximum temperature on discharge is 29.0°C, 4°C above the case temperature. On overcharge, however, the temperature rises to over 35°C (C/2 rate), although other simulations that we have carried out with a finer

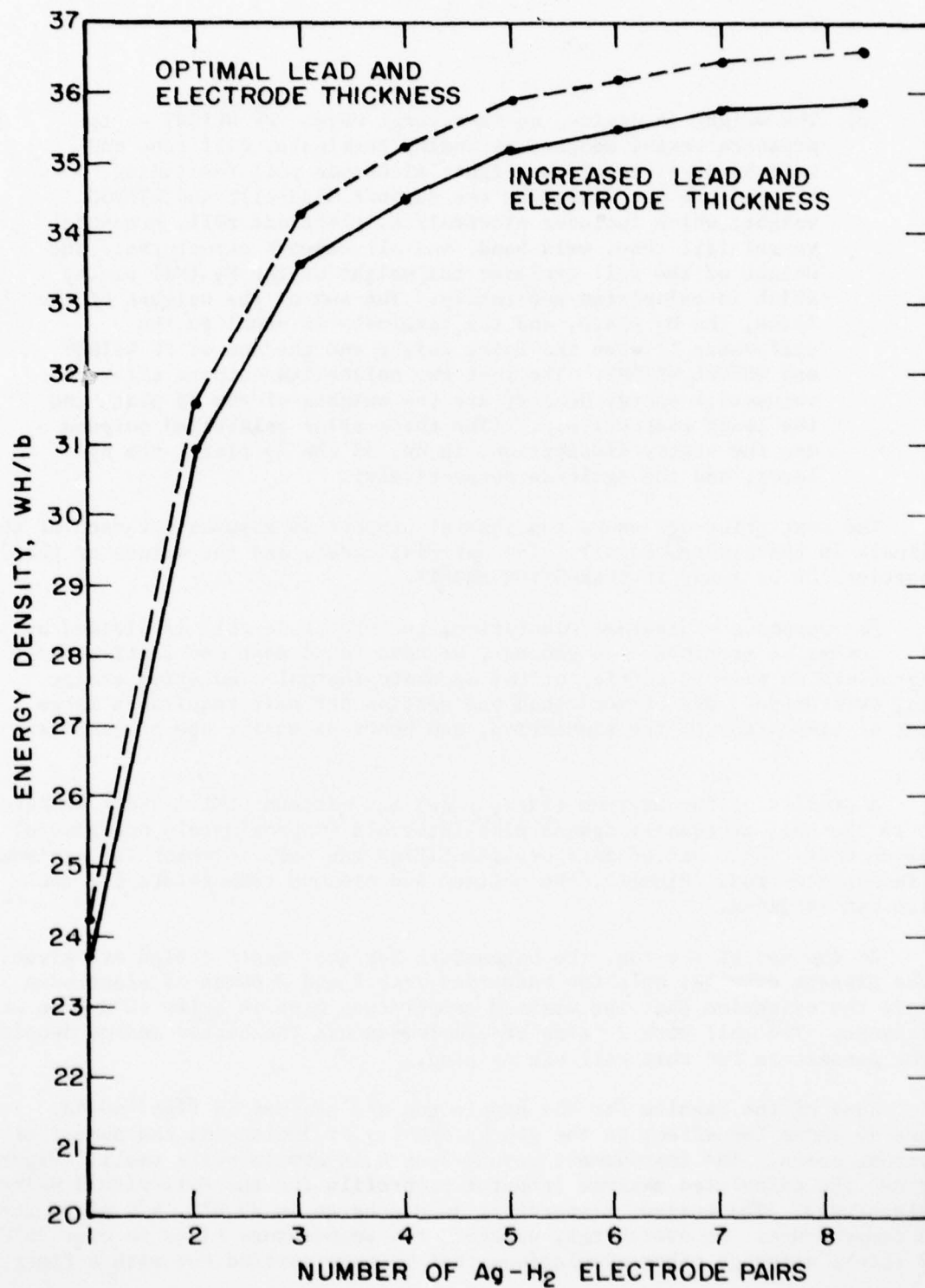


Figure 40. Effect on energy density of increasing the number of electrode pairs.

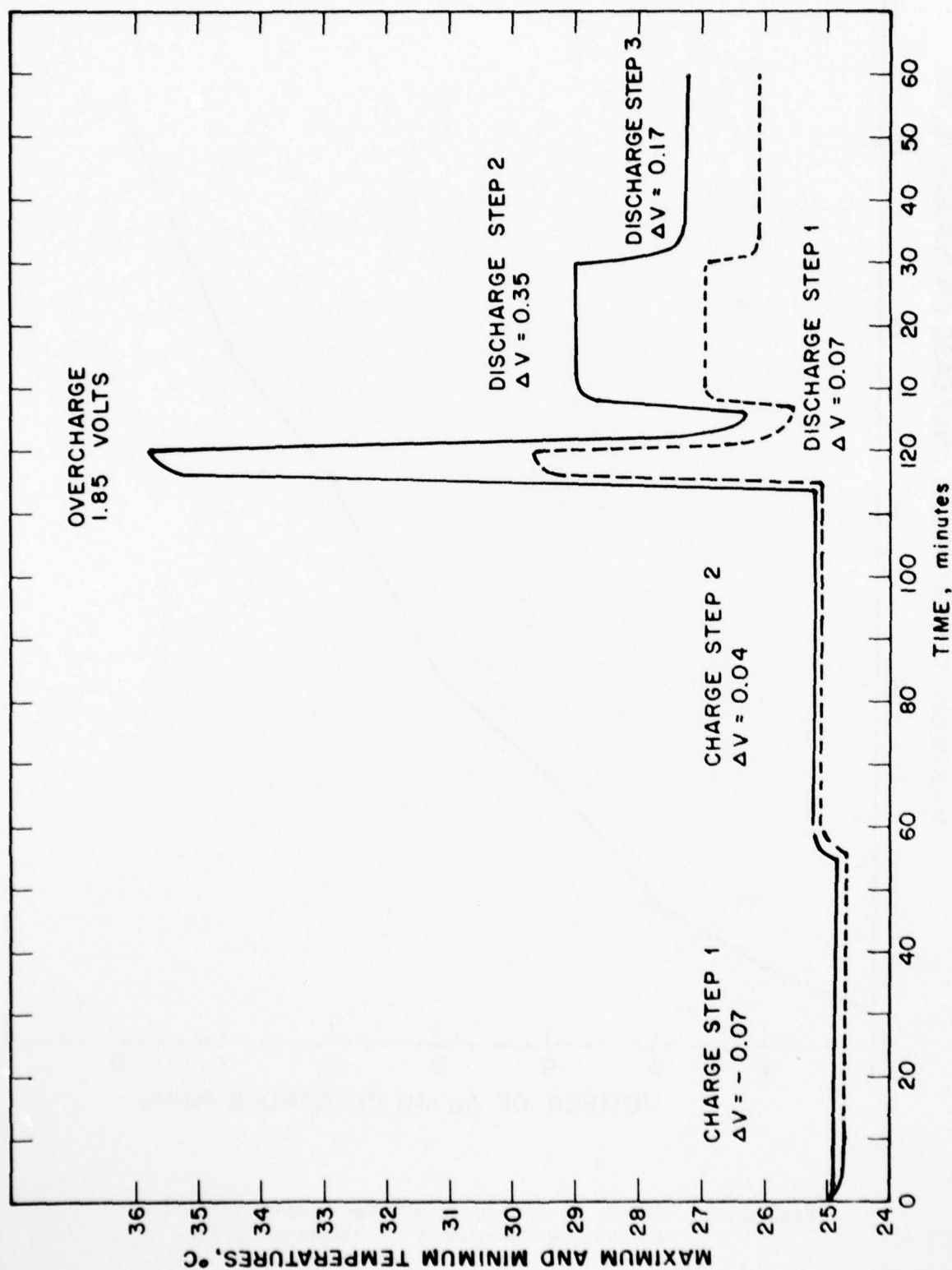


Figure 41. Temperature changes in a battery with 3 pairs of Ag/H₂ electrodes. ΔV is the difference between the cell potential and the electroneutral potential.

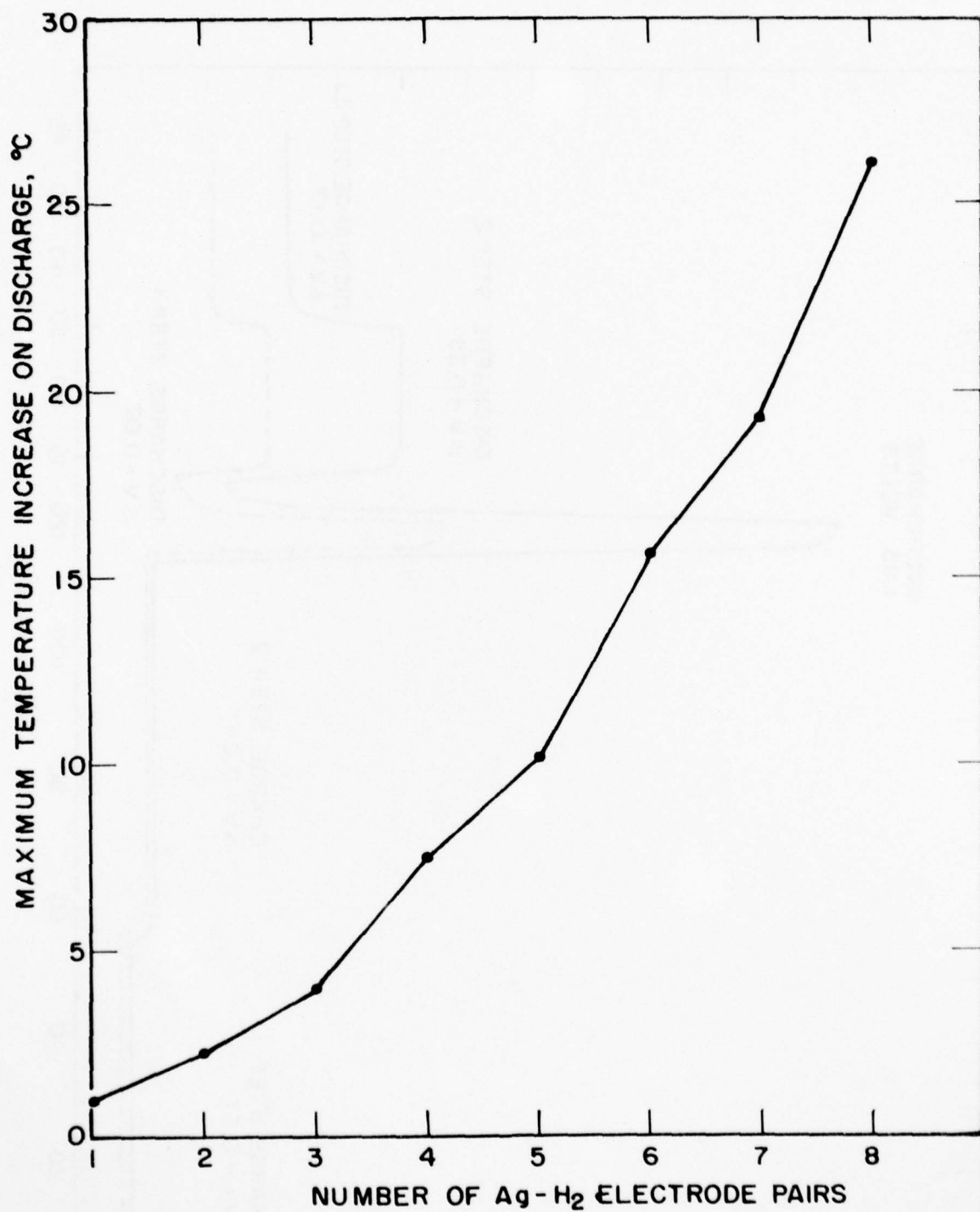


Figure 42. Effect on maximum discharge temperature of increasing the number of electrode pairs.

grid indicate that this result may be an overestimate. Figure 42 shows the maximum temperature on discharge as a function of the number of electrode pairs; because of the design variation referred to above, cells with an odd number of electrode pairs have better thermal performance than those with an even number of pairs.

It should be noted that the results plotted are for a C/rate discharge, and are calculated with $U_{CON1} = 0.128$ (see Section 2.21). Use of the more correct value, $U_{CON1} = 0.205$, and discharge at a lower rate, would result in a higher predicted energy density.

2.3 Optimized Cell Design

We have used the computer model of the rolled Ag/H₂ cells to investigate the sensitivity of an optimized design towards variation of important parameters.

The degree of silver electrode utilization has the strongest effect on energy density. This is illustrated in Fig. 43. Energy density was calculated for two different discharge rates (C/15 and C/2) and for 3 or 4 electrode layers. The calculations are based on the NASA separator layer (e.g., Asbestos).

The utilization of any particular silver electrode depends on the current density. For the Yardney silver electrodes used in this program, we found that the utilization (U) could be described as a function of the current density (i).

$$U = 0.205 - 0.286 \log i$$

The effect is a relatively strong dependence of cell energy density on discharge rate. This is shown in Fig. 44. For the relatively high discharge rate of C/1.25 specified in the accelerated AF cycle regime, an energy density of 35 Wh/lb would be expected. For lower rate applications, however, the energy density would increase dramatically. For example, at a C/8 rate 50 Wh/lb was calculated. These calculations are again based on the NASA separator and an additional absorber layer of 15 mil thickness. Figure 45 shows the same relationship of energy density vs. rate in a different plot. This figure contains, however, also the maximum temperature difference for 3 and 4 electrode layers respectively. It shows that at the C rate only. Configurations up to 3 layers are thermally acceptable. At lower rates than C/2 one could use a 4 electrode layer configuration and thus gain a small energy density advantage.

Figure 46 shows the connection between weight and volume energy density. The weight energy density goes through a shallow maximum at approximately 0.13 Wh/cm³. Practical considerations, especially those connected with cell shape and represented by the ℓ/r ratio, restrict the useful range approximately

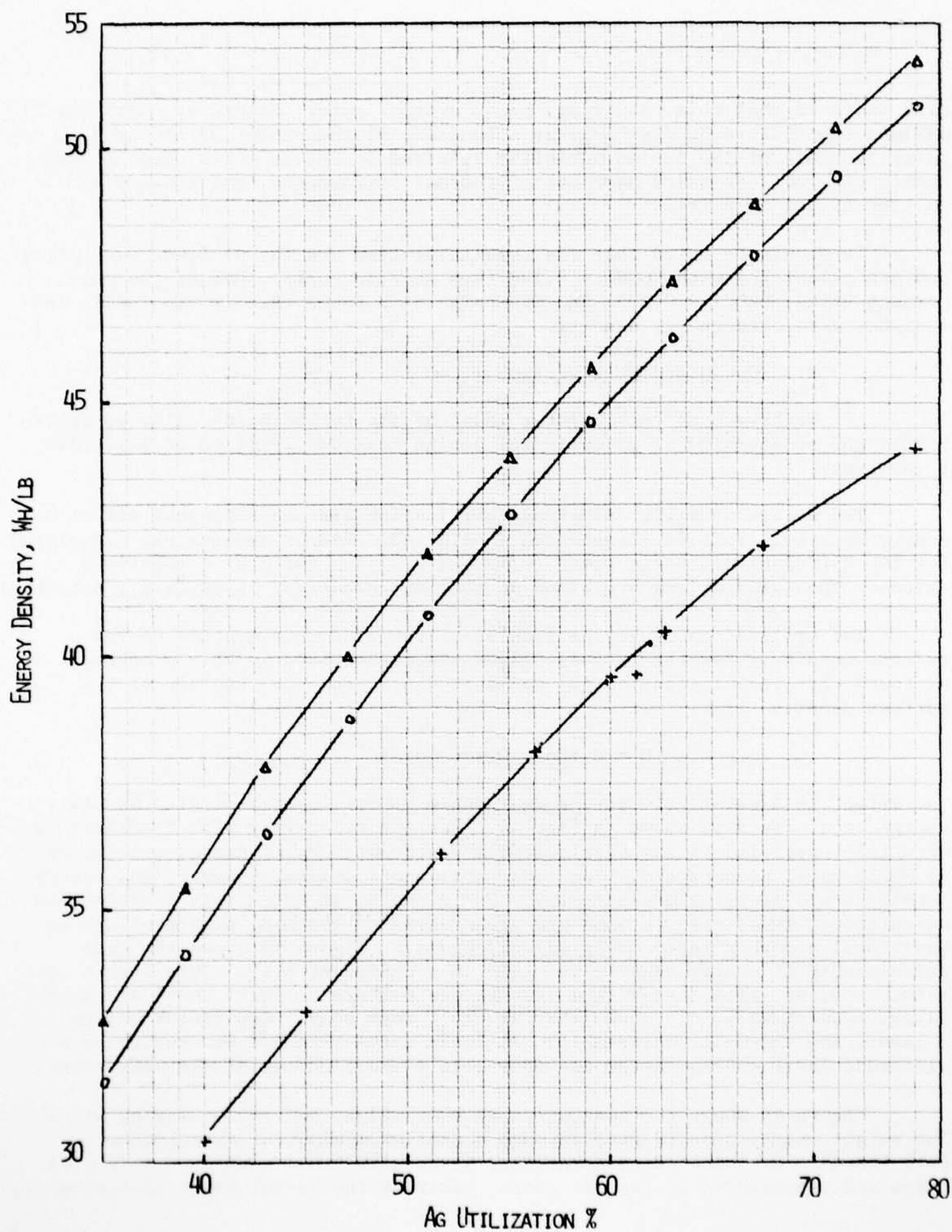


Figure 43. Energy density of a rolled 50 Ah Ag/H₂ cell as a function of Ag electrode utilization. Discharge rate C/15, ○ = 3 layers, Δ = 4 layers; x = discharge rate C/2, 3 layers.

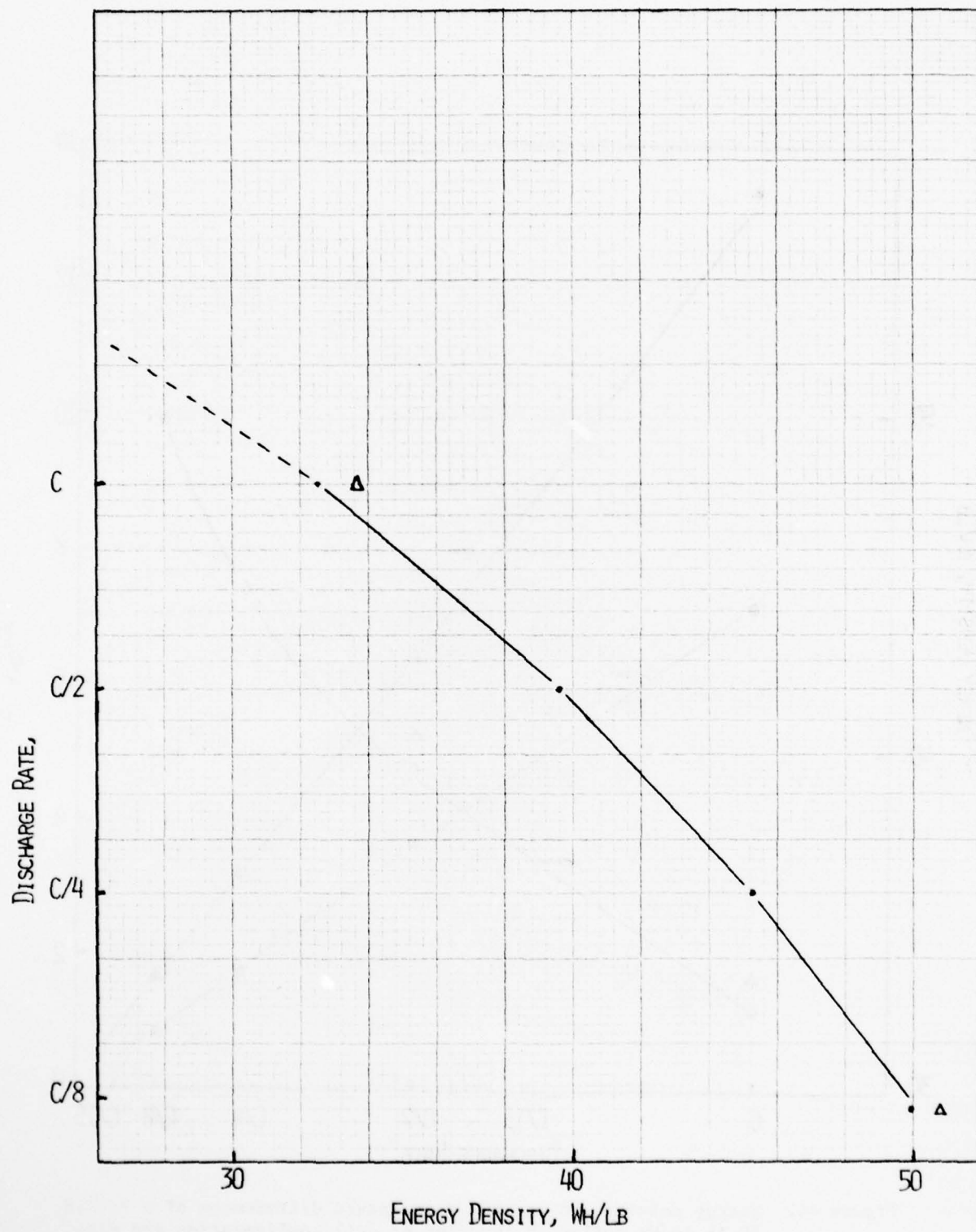


Figure 44. Energy density of a rolled 50 Ah Ag/H₂ cell as a function of discharge rate. ● 3 electrode layers, Δ 4 electrode layers.

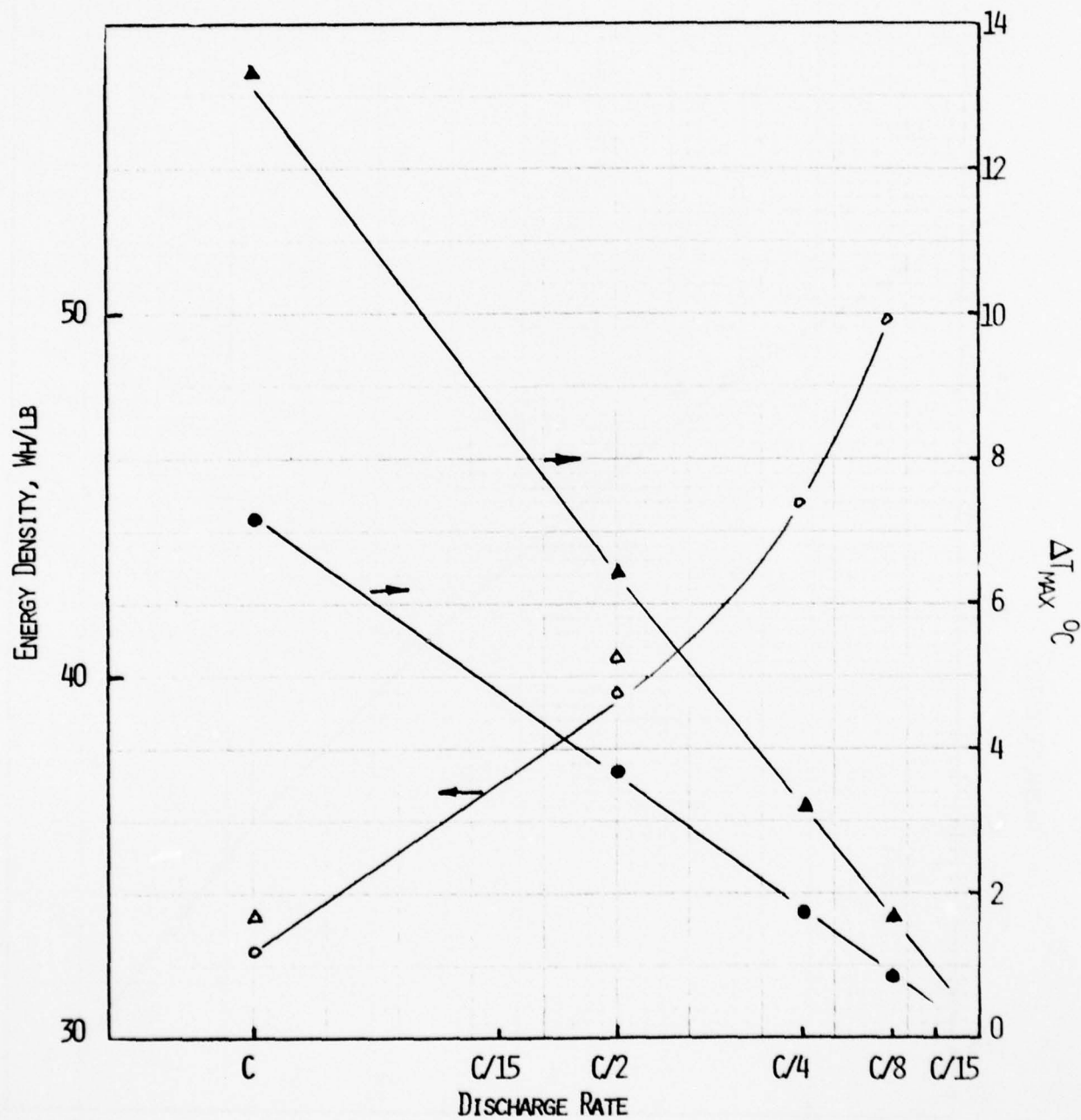


Figure 45. Energy density and maximum temperature differences of a rolled 50 Ah Ag/H₂ cell as a function of cell configuration and discharge rate. ●, ○ 3 electrode layers; Δ, ▲ 2 electrode layers.

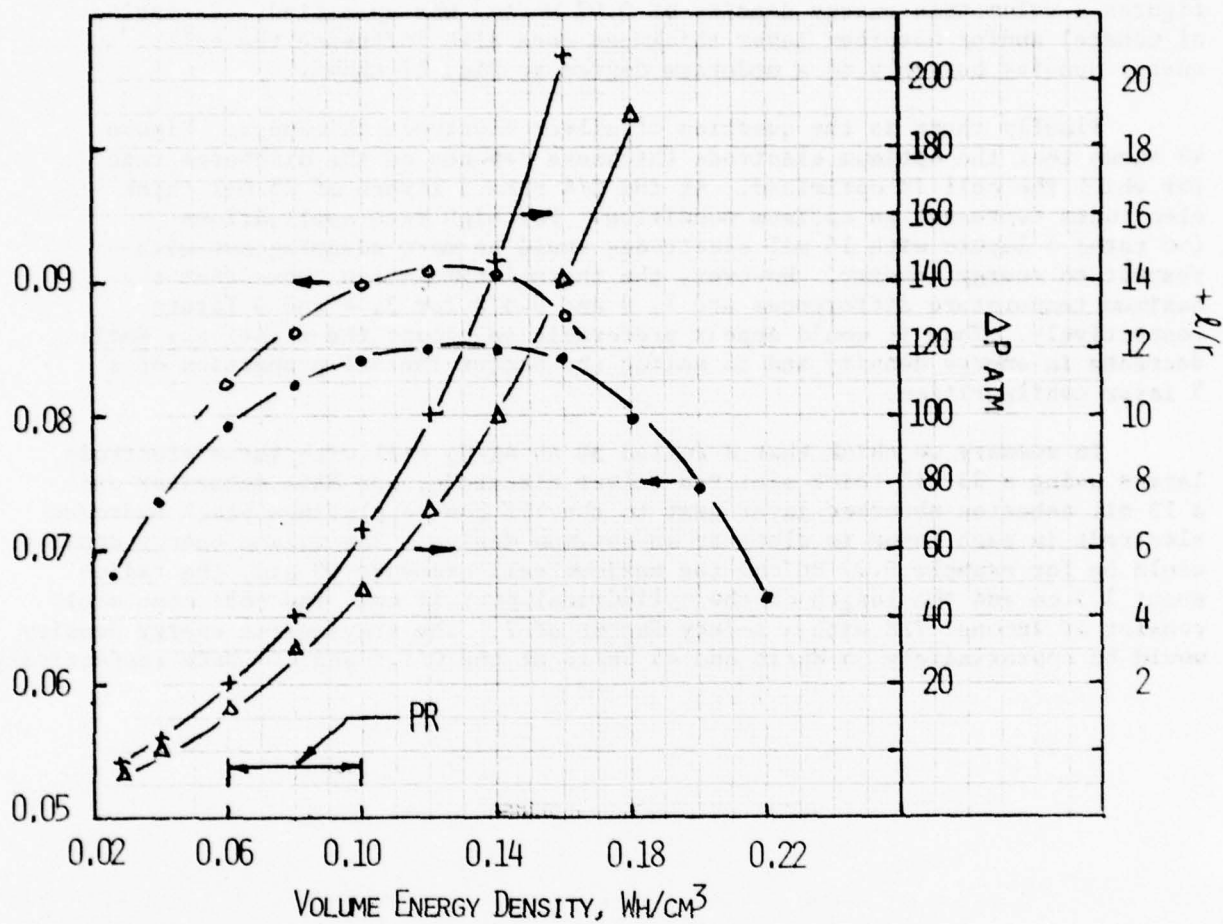


Figure 46. Change in weight energy density as a function of volume energy density of a rolled 50 Ah Ag/H₂ cell with corresponding changes in cell pressure and ratio between cell length and radius. Discharge rate C/1.5. ● = 3 electrode layers, ○ = 4 electrode layers, PR = practical range.

to between 0.06 and 0.10 Wh/cm³. For the calculations shown in the previous figures a volumetric energy density of 0.07 Wh/cm³ was specified. Variation of mandrel and/or absorber layer thickness does also influence the cell energy density but only to a moderate degree as Fig. 47 shows.

Finally there is the question of silver electrode thickness. Figure 48 shows that the optimum electrode thickness depends on the discharge rate for which the cell is optimized. At the C/4 rate 3 layers of 25 mil thick electrodes represent an optimum condition. For high rate applications (1C rate) 5 layers with 15 mil electrodes would be more advantageous with respect to energy density. However, the thermal simulation shows that the maximum temperature differences are 7, 9 and 9.3°C for 3, 4 and 5 layers respectively. Thus it would appear preferable to accept the relatively small decrease in energy density and to select the better thermal properties of a 3 layer configuration.

In summary we think that a rolled 50 Ah Ag/H₂ cell with three electrode layers using a 25 mil thick sintered silver electrode, one NASA separator and a 15 mil asbestos absorber layer next to the TFE bonded platinum black hydrogen electrode in each layer is close to an optimum design. The volume energy density would be for example 0.07 Wh/cm³ the maximum cell pressure 40 atm, the radius about 3.5 cm and the length of the cylindrical part 14 cm. The cell case would consist of Inconel 718 with a safety factor of 2. The gravimetric energy density would be approximately 35 Wh/lb and 45 Wh/lb at the C/1.5 and C/4 rate respectively.

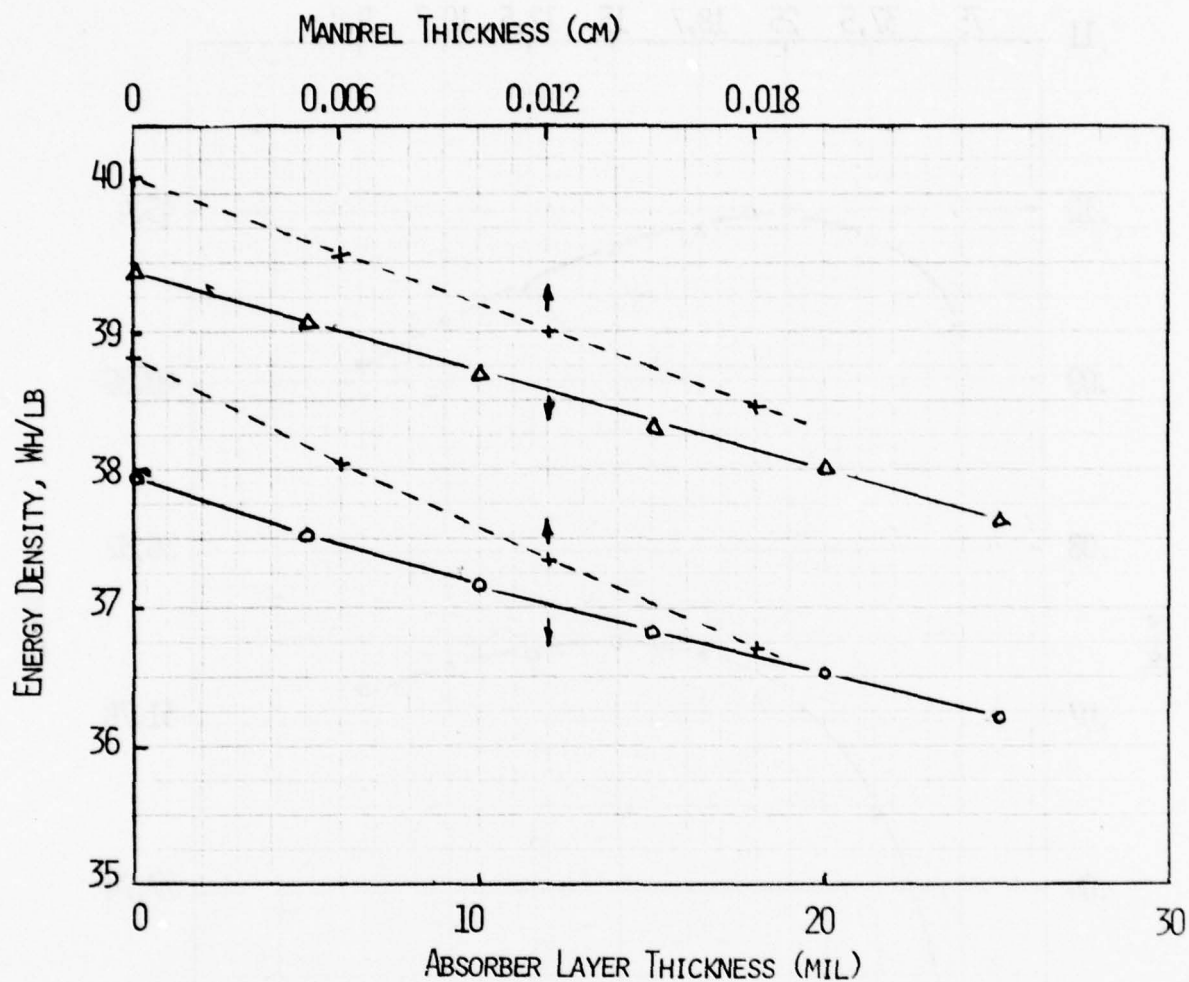


Figure 47. Change in energy density as a function of Mandrel and absorber layer thickness for a 50 Ah rolled Ag/H₂ cell. Discharge rate C/1.5, volumetric energy density 0.07 Wh/cm³. o = 3 electrode layers, Δ = 4 electrode layers.

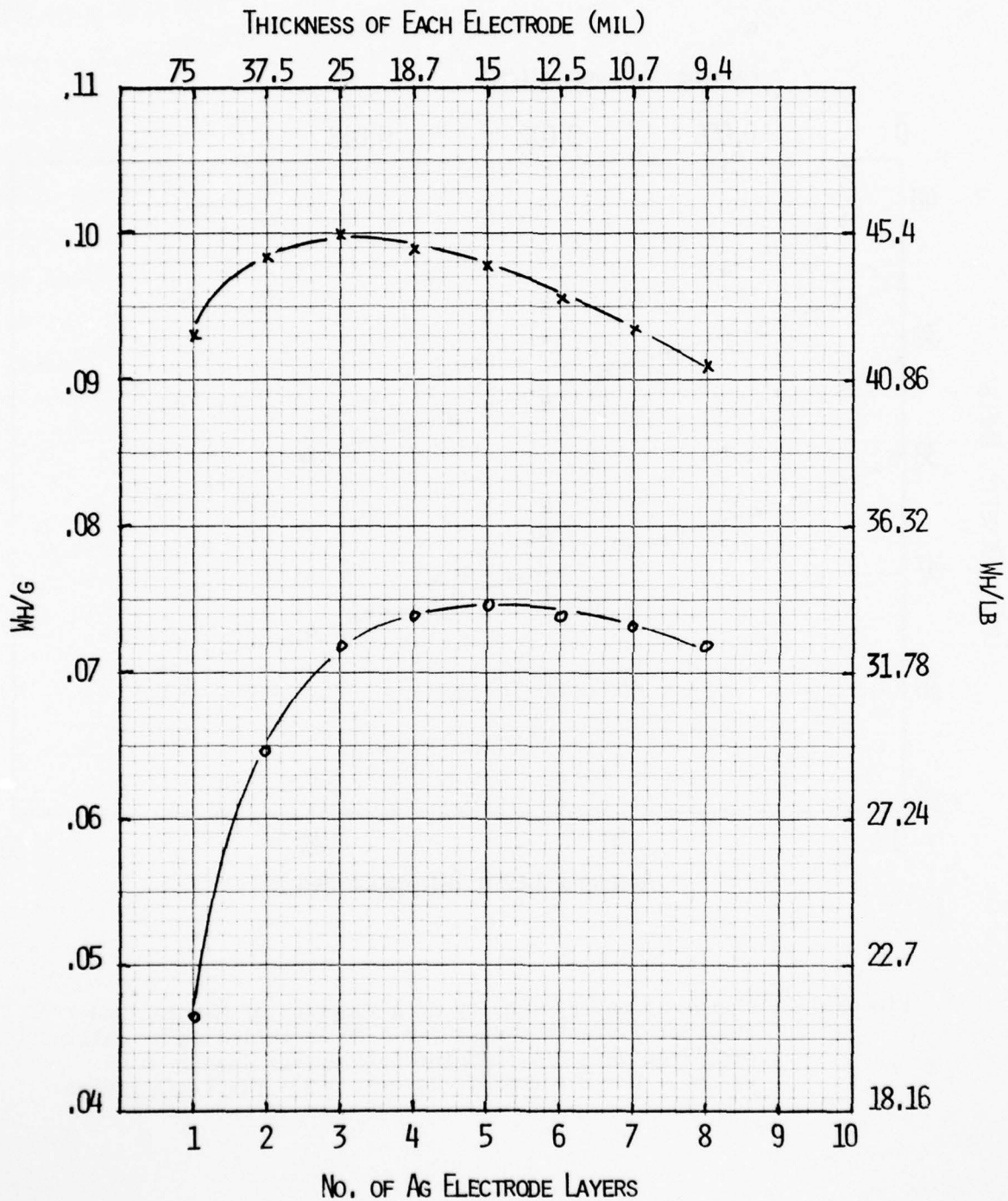


Figure 48. Energy density of a rolled 50 Ah Ag/H₂ cell with a constant amount of Ag as a function of the number of Ag electrodes. x = C/4 rate, o = C rate.

IV. SUMMARY AND CONCLUSIONS

During this program we have demonstrated the feasibility of Ag/H₂ cells with 35 to 50 Wh/lb, depending on the desired discharge rate, and with a cycle life in excess of 500 deep discharges. This demonstration and the necessary development involved extensive component level studies, performance evaluation and demonstration in several sets of laboratory cells of approximately 15 Ah and the development of a comprehensive computerized mathematical model for the design and optimization of Ag/H₂ cells of rolled stack configuration.

Electrolyte management was identified as the main problem area. The relatively high solubility of silver oxide in the electrolyte necessitates the use of argentistatic membranes similar to those employed in Ag/Zn cells. These membranes have characteristic electrolyte transport properties described by their transference, diffusion and flow parameters. We determined those parameters and showed that a suitable combination of the individual transport characteristics is required to maintain an adequate electrolyte balance during any one charge-discharge cycle and from cycle to cycle. Of the four membranes tested, Visking, P-2291, P-2193 and the NASA I O separator, only the latter was found suitable for use in practical Ag/H₂ cells. The principal property differentiating it from the other membranes was a much higher rate of electrolyte equilibration via back-wicking. Electrolyte capacity as well as the pore size and pore size distribution of the absorber layer, were also identified as important parameters. Asbestos is preferable to the relatively open structure of non-woven nylon such as P-2505.

The solubility of the silver oxide is an inherent property which will eventually lead to cell failure. Rapid formation of soft short circuits, especially by silver dendrites around the plate edges, can be avoided by appropriate cell stack design. A rolled electrode stack configuration was found especially effective. Slow diffusion of silver oxide through the membrane and subsequent reduction to Ag at the hydrogen electrode is not specifically harmful. Eventually this process will, however, lead to the formation of an electronic path between anode and cathode. No cell failures due to this process were observed during the course of this program.

A final set of 16 laboratory cells based on the NASA separator but employing different orientations, components and component arrangements according to a mathematical matrix demonstrated the feasibility and performance capability of Ag/H₂ cells. The amount of electrolyte (absorber layer thickness) and the orientation of the NASA separator were found to have the greatest influence on capacity retention.

Our mathematical modeling effort identified silver electrode utilization as the strongest energy density determining factor. Including practical configurational (radius to length ratio) and thermal restrictions a rolled design with three electrode wraps of approximately 25 mil thick silver electrodes and 15 mil thick absorber layers is close to an optimized cell.

AD-A061 426

EIC CORP NEWTON MASS
SILVER-HYDROGEN ENERGY STORAGE.(U)

F/G 10/3

AUG 78 G L HOLLECK, M J TURCHAN, F S SHUKER

F33615-76-C-2093

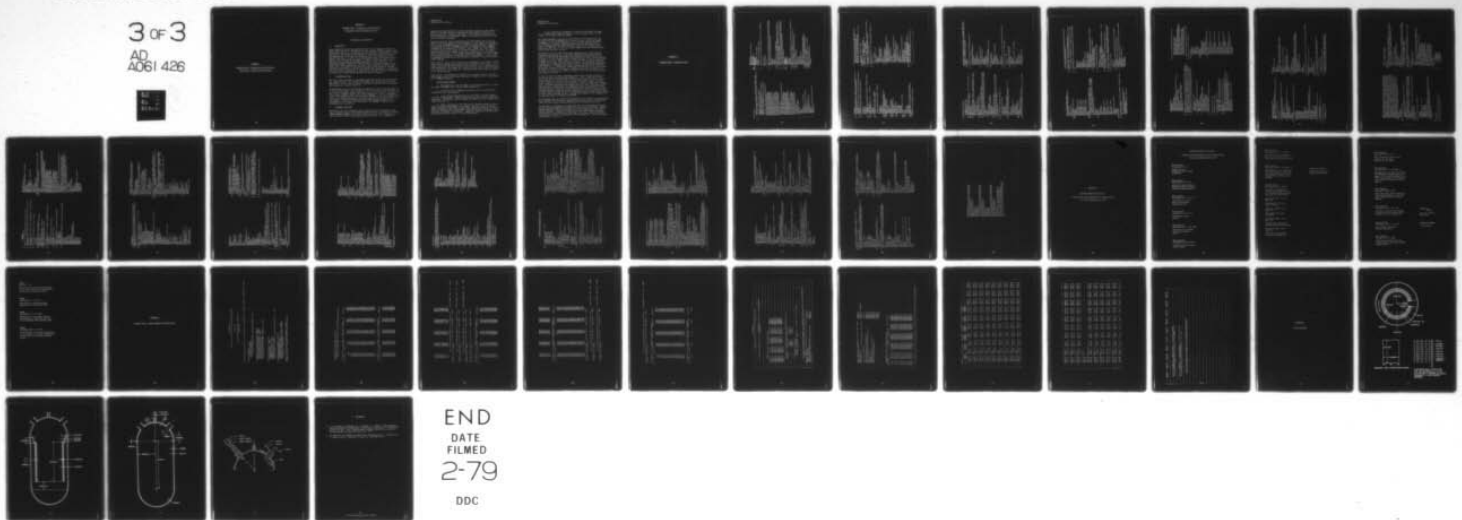
UNCLASSIFIED

AFAPL-TR-78-65

NL

3 of 3

AD
A061 426



APPENDIX A

PROGRAM EICD1: Program for the Design and Simulation of Rolled Ag/H₂ Batteries

Appendix A

PROGRAM EICD1: Program for the Design and Simulation of Rolled Ag/H₂ Batteries

Guidelines for Operators

1. Objectives

This program calculates the optimum pressure vessel length and radius for Ag/H₂ cells that can be designed by the user through parameter specification. A particular feature of the program is that volumetric energy density can be specified by the operator; the program calculates the required H₂ pressure. The program also calculates the optimum H₂ plate (Ni) thickness and the optimal lead sizes. In addition, the program simulates the thermal performance of the cell through any number of complete charge-discharge cycles, and prints the maximum and minimum temperature at each time step. The thermal performance simulation, which requires a substantial amount of computer time, can be disabled at run time. Other features include automatic variation of the number of Ag/H₂ electrode pairs, and automatic operator-selected variation of any one of 67 different input parameters. In addition, all output may be disabled by an input switch, so that user-written plotting routines can be added without deleting the output statements.

2. Preliminary Setup

The first three statements of the MAIN program specifying the standard input and output devices. Two (possibly) different input devices are provided: INP and IN. In many cases it may be convenient to specify INP as a terminal input and IN as a card or disk file.

In preliminary tests of the program one should first run the program with all 15 input records blank (zero) except for the first record, read in on INP. In this record a positive integer should be input in the first five columns (15). This integer (NOTHER) disables the thermal simulation routine. Subsequent tests of the program can be carried out with NOTHER = 0 to verify proper operation of the thermal simulation. A general description and interpretation of the output is provided in Appendix D; most features should prove self-explanatory, or, at worst, are explained in the COMMENT statements in the program and its subroutines.

3. Parameter Variation

Variation of the cell parameters may be carried out in two different ways: (A) by specification of the parameter number and range of parameter variation (INVAR, VARMIN, VARMAX) on the first input record; or (B) by reading a non-zero card for any one of the subsequent input records. It is generally

PROGRAM EICD1
Guidelines for Operators

suggested that when method (A) is used, automatic variation of the number of pairs of electrodes should be suppressed by fixing NLAYR1 = NLAYR2 on the third input record. Automatic variation of the pressure vessel radius can also be suppressed by fixing RMIN = RMAX on the third input record, but this is not generally recommended.

Input records 4-14, used in conjunction with either method (A) or (B) for parameter variation, should be self-explanatory. Each named input parameter will be found in COMMON block EIC2; a similarly named parameter, found in the corresponding location in COMMON block EIC1, is defined in the 67 COMMENT statements at the beginning of the MAIN. Thus, CAPNAM, the first parameter on the 4th input record, is the sixth named variable in EIC2. The sixth named variable is EIC1, CAPNAQ, is defined at statement C6 as the nameplate capacity, in amp-hours. In a statement preceeding, CAPNAQ = 30, thus, CAPNAM is the nameplate capacity; the default value is 30 amp-hours. A few of the more geometric parameters are best defined by reference to the four attached design diagrams.

Input record 15 can be used to specify the arrangement of electrodes, in which case a non-zero integer should be placed in column 80 of this record. A 1 in column 1 specifies that one terminal is at each end; a 0 or 2 specifies that both terminals are at the same end. Columns 2-79 are used to specify the order of the electrodes. The number of 1's (H₂ electrodes) should equal the number of 2's (Ag electrodes).

Input record 2 is fundamentally different from the other records, in that it specifically controls the thermal simulation. Parameter choice is explained in the COMMENT statements.

4. Miscellaneous Remarks

a. The program will read any number of successive data sets. A negative value of NOTHER can be used for normal program exit.

b. A non-zero value of NOREAD should only be used on machines that automatically zero unused memory.

c. In the thermal simulation routine, the number of radial segments is LSLICE = NSLICE*ILAYER + IADDIT, where ILAYER is the number of Ag/H₂ electrode pairs. The default values of NSLICE and IADDIT are 1 and 0 respectively (input record No. 2).

d) Output information on the temperatures (maximum, minimum, and cell label) is printed approximately every minute. The exact value of the time interval depends on the number of time steps (NSTEPS in record No. 2) and the charge or discharge time. With NSTEPS = 1500 and CHGTIM = 120 minutes, each time step is 120/1500 = 0.08 minutes. Temperature information in this case is provided every twelfth step; i.e., every 0.96 minutes.

PROGRAM EICD1
Guidelines for Operators

e) Cell temperature information is labelled according to the same I, J, L scheme used in input record No. 2, i.e., I varies from 1 to ITH, J from 1 to JZ, and L from 1 to LSLICE.

The thermal management subroutine is structured in such fashion that the electrode roll can be segmented in a variety of ways. ITH is the number of segments in the "theta" dimension, i.e., in the cylindrical plane; JZ is the number of segments along the cylindrical axis; and LSLICE is the number of segments in the radial direction. Most of our runs have been carried out with ITH = JZ = 1, but correct operation of the subroutine with larger values has been verified.

The subroutine first groups the KR roll components (e.g., Ag electrodes, reservoirs, separators, etc.) into LSLICE equal-thickness slabs, and calculates average thermal properties (heat capacity and conductivities) for each slab. It then simulates NCYCLE charge-discharge cycles, each consisting of NSTEPS time steps. NSTEPS must be carefully chosen to assure convergence: If NSTEPS is too small (time interval too large), the temperatures will not converge and the subroutine will produce what are clearly absurd temperatures ($>10^6$ degrees). If NSTEPS is too large, program run time will be excessive. The default value used (NSTEPS = 500) assures convergence in the present runs, but may be too small if the charge or discharge cycle time is short, or if the number of radial slices LSLICE is large, so that the slab thickness (and heat capacity) is small.

In order to keep the thermal management program from becoming unwieldy, we have incorporated two simplifying assumptions. First, conduction of heat through the gas is ignored except in the gas gaps between electrodes, and in the gap between the outermost electrode and the pressure vessel. In other words, conduction to the end caps is ignored. This is a conservative assumption: Calculated temperature differences should be larger than those measured experimentally. Nevertheless, the assumption should be reasonably accurate, since the thermal conductivity of the electrode roll should be about an order of magnitude greater than the thermal conductivity of H_2 , and the path length for heat transfer through the roll is considerably shorter than the path length for heat transfer through the gas. Secondly, we assume that the temperature of the pressure vessel is constant and uniform.

We also assume that all the heat is generated at either the H_2 or Ag electrodes; this simplifies the program but should not affect the accuracy of simulation since the total amount of heat generated will be calculated correctly.

During charge or discharge, heat generation due to electrochemical reactions will be uniform throughout the surface of a given type of electrode. However, heating caused by reaction of H_2 and O_2 will occur primarily at the ends of the H_2 electrodes. Similarly, heating due to the leads and due to voltage drops within the electrodes will also occur at the ends. Thus, temperature differences are likely to be largest at the electrode ends. This is accounted for when ITH = 1 or JZ = 1.

APPENDIX B

PROGRAM EICD1: Program Listing

[illegible]

DECLASSIFIED BY 60321 JCS/STC/SP/LJ/TML/TML
DECLV1: 660866-050750CTW04
DECLV2: 221899-3-2022-06C804
DECLV1: TWC10/100, TWC12: 100, TWC10/100.


```

RAD(K-3)=R-RAGTKI-8EPTKI-RH2TKI
RAD(K-4)=R-RAGTKI-8EPTKI-RH2TKI-MPLTHK
MATVEC(K-4)=7
K=K+4
R=R+PPLTHK-DELTAP
GO TO 204
C BELOW THIS POINT, ICNFIG(J)=1
203 R=R-DELTAP
SUM=SUM+R
MATVEC(K-1)=7
RAD(K-1)=R+DELTAP-MPLTHK
MATVEC(K-2)=6
RAD(K-2)=RAD(K-1)-RH2TKI
MATVEC(K-3)=5
RAD(K-3)=RAD(K-2)-8EPTKI
MATVEC(K-4)=4
RAD(K-4)=RAD(K-3)-RAGTKI
MATVEC(K-5)=3
RAD(K-5)=RAD(K-4)-PPLTHK
K=K+5
204 R=R-R
C RPR POINTS TO INNER EDGE OF ELECTRODE PAIR
IF((ICNFIG(J-1).EQ.1).AND.(ICNFIG(J-2).EQ.1)) R=R-GASUP1
IF((ICNFIG(J-1).EQ.1).AND.(ICNFIG(J-2).EQ.2)) R=R-GASUP2
IF((ICNFIG(J-1).EQ.2).AND.(ICNFIG(J-2).EQ.1)) R=R-GASUP2
IF((RPR-R).LE.0.0) GO TO 210
K=K+1
MATVEC(K)=2
RAD(K)=R
210 CONTINUE
K=K+1
MATVEC(K)=2
RAD(K)=R-GAPHAN
K=K+1
MATVEC(K)=8
RAD(K)=RAD(K-1)-DRLTHK
RADIN=RAD(K)
K=K+1
RAD(K)=RAD(K-1)-MVAMP
MATVEC(K)=9
K=K+1
RAD(K)=RAD(K-1)-XPRTHK
MATVEC(K)=10
K=K
IF(RAD(K).GT.0.0) GO TO 2651
ENNGT=0.0
PVVOL=100.
GO TO 375
2651 CONTINUE
C NOW CALCULATE LENGTH OF THE SILVER ELECTRODE, THE PRESSURE VESSEL
C LENGTH, AND THE VOLUME.
C
AGLNTM=PPLART*180./((SUM*PI*(360.-THETA)))
PVLNTH=AGLNTM*DELNTH+WELOGP+WRGAP
RAGSG=RADIUS*RADIUS
PVVOL=4.*PI*RAGSG*(RADIUS/3. +PVLNTH/4.)

CALL MTHVOLWEIGHT,EXGAS,ELWATE,RLWATE,PPLART,AGLNTM,RADIUS,
1PVLNTH,RADIN,AGDEN,RAD,MATVEC,KR)
C
C WE HAVE OBTAINED THE WEIGHT OF ALL COMPONENTS EXCEPT:
C PRESSURE VESSEL, TERMINALS, NEGATIVE GRID, LEADS, AND WELD BAND.C
C
C THE GAS EXCLUSION VOLUME DOES NOT YET INCLUDE TERMINALS AND LEADS,
C
C WE NOW PROCEED TO AN ITERATIVE CALCULATION OF THE MAXIMUM PRESSURE,
C ETC.
C
SUBMT=WEIGHT
PVWMT=0.0
TMWATE=0.
WTAGLO=0.0
WTH2LD=0.0
WPLATE=0.
GASCON=0.08206
TEMP=293.2
M2VOL=(PVVOL-EXGAS)/1000.
ITER=0
209 IF(ITER.EQ.2) GO TO 319
M2MOLS=H2MIN*ACTCAP/53.6
M2WATE=2.0159*M2MOLS
PHAX=M2MOLS*GASCON*TEMP/(M2VOL-0.02661*M2MOLS)-0.2+M2MOLS
1 M2MOLS/(M2VOL*M2VOL)
C VAN DER WAALS EQUATION FOR PHAX IN ATMOSPHERES
DELTAP=PHAX*SAFETY*RADIUS/SIGMA
IF(DELTAP.LT.-DELTAM) DELTA=DELTAM
C
C DELTA IS THE PRESSURE VESSEL THICKNESS
C
DELTA2=DELTA
IF(HALF*NE.0.0) DELTA2=DELTA/2.
IF(DELTA2.LT.-DELTAM) DELTA2=DELTAM
PVWATE=PI*PVDEN*((RADIUS+DELTA2)**3-RADIUS*RAGSG)/3. + DELTA*
1 PVLNTH*(2.*RADIUS+DELTA)/4.1
C HEIGHT OF PRESSURE VESSEL
WEIGHT=SUBMT+PVWATE+TMWATE+WTAGLO+M2WATE+WTH2LD+PVWMT
C THIS HEIGHT DOES NOT YET INCLUDE NEGATIVE ELECTRODE GRID, LEADS, OR
C TERMINALS, WHICH MUST BE OPTIMIZED WITH RESPECT TO ENERGY DENSITY
C
C OPTIMIZATION OF H2 PLATE
C
SCAPNAM=000
SV=5.V
C SV= DISCHARGE HATT-HOURS (STORED ENERGY THAT WILL BE DELIVERED)
C=80./DCGTIH
C C IS THE DISCHARGE RATE, E.G. C=2 IS THE 2C RATE.
A=HEIGHT/5
C A IS A PROPORTIONALITY CONSTANT BETWEEN WEIGHT AND DISCHARGE AMP-HOURS
ZZERO=AGLNTM/2.
YZERO=PPLART/(4.*ZZERO*XLAYER)
RMK=2.*YZERO
RTAB=TABRTORMX
RTAB2=RTAB*RTAB

```


1 1
 2 2
 3 3
 4 4
 5 5
 6 6
 7 7
 8 8
 9 9
 10 10
 11 11
 12 12
 13 13
 14 14
 15 15
 16 16
 17 17
 18 18
 19 19
 20 20
 21 21
 22 22
 23 23
 24 24
 25 25
 26 26
 27 27
 28 28
 29 29
 30 30
 31 31
 32 32
 33 33
 34 34
 35 35
 36 36
 37 37
 38 38
 39 39
 40 40
 41 41
 42 42
 43 43
 44 44
 45 45
 46 46
 47 47
 48 48
 49 49
 50 50
 51 51
 52 52
 53 53
 54 54
 55 55
 56 56
 57 57
 58 58
 59 59
 60 60
 61 61
 62 62
 63 63
 64 64
 65 65
 66 66
 67 67
 68 68
 69 69
 70 70
 71 71
 72 72
 73 73
 74 74
 75 75
 76 76
 77 77
 78 78
 79 79
 80 80
 81 81
 82 82
 83 83
 84 84
 85 85
 86 86
 87 87
 88 88
 89 89
 90 90
 91 91
 92 92
 93 93
 94 94
 95 95
 96 96
 97 97
 98 98
 99 99
 100 100

199

[illegible]

APPENDIX C

PROGRAM FLOWSHEET FOR EICD1:

"Calculation and Optimization of Energy Density
for Silver-Hydrogen Batteries"

PROGRAM FLOWSHEET FOR EICD1:

"Calculation and Optimization of Energy Density
for Silver-Hydrogen Batteries"

Main Program:

Statements 1 to 4

Program Set-up;

initialization of input
parameters

Main Program:

Statements 4 + 1 to 6

Input of program control
parameters and non-default
battery design parameters

Main Program:

Statements 6 + 1 to 9 + 2

Calculation of basic
battery performance
characteristics

Main Program:

Statements 9 + 3 to 11

Preliminary output
display

Main Program:

Statements 11 + 1 (to 450)

Variation of the number
of Ag-H₂ electrode
pairs

Main Program:

Statements 205 (to 375)

Variation of the pressure
vessel radius

Main Program:

Statements 205 + 1 to 2651

Calculation of the radius and
type of every identifiable
component in the electrode roll

Main Program:

Statements 2651 + 1 to 909 - 1

Calculation of the weight and
exclusion volume of selected
cell components whose size is
independent of pressure and
voltage

Subroutine WTNVOL

Weight and exclusion
volume calculations

Main Program:

Statements 909 to 9191-1

Iterative calculation of
weight and excluded volume
of components dependent upon
pressure and voltage drop

Statements 909 + 22 to
909 + 73

Optimization of the H₂
plate thickness

Statements 909 + 74 to
9090 - 4

Optimization of lead
thickness

Statements 9090 - 3 to
919 - 11

Calculation of terminal
weights and excluded volumes

Statements 919 - 10 to
9191 - 1

Iterative recalculation
of the preceeding list

Main Program:
Statements 9191 to 375

Save calculated values of all
outputs for the given
pressure vessel radius

Main Program:
Statements 375 + 1 to 398 + 4

Estimate value of radius for which
the volumetric energy density is
equal to the selected value; go to
205 to recalculate all outputs for
this value of the pressure vessel
radius

Main Program:
Statements 3990 to 399

Store and print output values for
the selected number of electrode
pairs (optimum pressure vessel
radius)

Main Program:
Statements 399 + 1 to 449

Calculate and print the thermal
properties of each identifiable
element of the electrode roll.

SUBROUTINE
PROPTY

Calculate thermal
properties

Main Program:
Statements 449 + 1 to 1111

Call thermal simulation
routine (optional)

SUBROUTINE THRMAL
(see below)

Main Program:
Statements 450 to END

Find battery design with best
energy density that meets thermal
specifications

THRMAL

ORG to 8 - 12

Temperature initialization; division
of electrode roll into 3-dimensional
partitions; preliminary setup.

THRMAL

Statements 8 - 11 to 22

Calculation of average thermal
properties of each radial slice.

THRMAL

Statements 22 + 1 to 800

Calculation of the temperature of
each element at each time interval,
for both charge and discharge steps.

THRMAL

Statements 800 + 1 to END

Determination of the time and location
of the highest and coldest temperatures
in the full set of charge-discharge
cycles.

APPENDIX D

PROGRAM EICD1: Sample Computer Program Output

EIC CORPORATION
PROGRAM FOR THE SIMULATION OF MOLDED SILVER-HYDROGEN BATTERIES

MARCH, 1977

THIS PROGRAM SIMULATES ELECTROLYTE MANAGEMENT ONLY
PROGRAM EICE2

THE NAMEPLATE CELL CAPACITY FOR THIS RUN IS 30.000 WHILE THE ACTUAL CAPACITY IS 33.000. (THE CAPACITY FACTOR RATIO IS 1.100)

OPERATIONAL PARAMETERS:

*80 DEPTH OF DISCHARGE
120.00 MINUTES CHARGE TIME
60.00 MINUTES DISCHARGE TIME
THE RATIO OF CHARGE AMP-HOURS TO DISCHARGE AMP-HOURS IS 1.1500

THE PARAMETERS FOR EACH POSITIVE PLATE ARE AS FOLLOWS:

EFFECTIVE THICKNESS OF SILVER GRID = .001000
TOTAL THICKNESS OF GRID PLUS SINTER = .063500
MEAN DENSITY OF GRID PLUS SINTER = .27300
DENSITY OF SINTER ALONE = .17337
MINIMUM UTILIZATION OF GRID SILVER = .50000
ACTUAL UTILIZATION = MULTIPLY MINIMUM BY THE FACTOR 1.10000

THE RESERVOIR PARAMETERS ARE AS FOLLOWS:

INITIAL FILL FACTOR = .65000
RESERVOIR POROSITY = .80000
H2 RESERVOIR THICKNESS = .09140
A6 RESERVOIR THICKNESS = .045720
SEPARATOR THICKNESS = .025400
INITIAL ELECTROLYTE CONCENTRATION (GRAMS KGM PER GRAM OF SOLUTION) = .00000

SEPARATOR MEMBRANE PARAMETERS ARE AS FOLLOWS:

HYDROXIDE TRANSPORT NUMBER = .703
WATER TRANSPORT NUMBER = .648
KOH EFFECTIVE DIFFUSION COEFFICIENT (CC/SEC) = .00001308
WATER EFFECTIVE DIFFUSION COEFFICIENT (CC/SEC) = .00006629
2 LAYERS OF TYPE 1 MEMBRANE MATERIAL

AG-SIDE FILL FACTORS ARE FOR ELECTRODE AND RESERVOIR COMBINED.
ASSUMED WICKING RATE IS .000000 CC PER MINUTE (FOR ZERO FILL FACTOR).

12.0	50.6	96.62	48.02	19.07
12.0	47.36	96.62	47.44	19.77
12.0	47.5	96.13	48.03	19.73
12.0	42.5	95.62	50.57	18.66
12.0	47.99	95.62	50.69	19.06
12.0	43.69	94.16	50.65	13.91
12.0	43.55	93.85	50.6	20.0
12.0	43.6	92.23	50.7	14.25
12.0	41.7	91.77	50.12	14.55
12.0	47.8	90.53	49.55	19.89
12.0	43.51	90.69	49.78	19.82
12.0	39.51	89.58	49.92	21.86

151.20	.3955	.88737	.49501	.32831
152.00	.3915	.87906	.49305	.34476
153.00	.38753	.87066	.49106	.36120
154.00	.38349	.86218	.48905	.37764
155.00	.37943	.85361	.48702	.39406
156.00	.37535	.84496	.48499	.41048
157.00	.37124	.83622	.48295	.42688
158.00	.36711	.82740	.48090	.44327
159.00	.36294	.81851	.47886	.45965
160.00	.35874	.80953	.47680	.47601
161.00	.35451	.80047	.47475	.49236
162.00	.35024	.79134	.47270	.50869
163.00	.34594	.78212	.47064	.52500

WARNING: H2-SIDE RESERVOIR OVERFLOW AT TIME 115.20 OF CYCLE 2 DURING CHARGE. MSFF(1) WAS 1.01525

WARNING: FILL FACTOR BELOW .10 ON CHRG. MSFF(1) = 1.00000, SSFF(1) = .09054
ON CYCLE 2 OF 3 Cycles.

WARNING: H2-SIDE RESERVOIR OVERFLOW AT TIME 120.00 OF CYCLE 2 DURING CHARGE. MSFF(1) WAS 1.02090

WARNING: FILL FACTOR BELOW .10 ON CHRG. MSFF(1) = 1.00000, SSFF(1) = .06732
ON CYCLE 2 OF 3 Cycles.

WARNING: H2-SIDE RESERVOIR OVERFLOW AT TIME 122.40 OF CYCLE 2 DURING DISCHARGE. MSFF(1) WAS 1.00027

WARNING: FILL FACTOR BELOW .10 ON DSCG. MSFF(1) = 1.00000, SSFF(1) = .07565
ON CYCLE 2 OF 3 Cycles.

WARNING: FILL FACTOR BELOW .10 ON DSCG. MSFF(1) = .99543, SSFF(1) = .08947
ON CYCLE 2 OF 3 Cycles.

CONCENTRATIONS AND FILL FACTORS UPON CHARGE ARE AS FOLLOWS:

CYCLE	2	OF	3	CYCLES	H2-SIDE CONC	H2-SIDE FILL	AG-SIDE CONC	AG-SIDE FILL
151.20	.3459	.78212	.47064	.52840				
152.00	.37162	.76765	.44122	.53215				
153.00	.39111	.76062	.41975	.53110				
154.00	.40583	.75899	.40397	.52486				
155.00	.41694	.76130	.39237	.51465				
156.00	.42533	.76650	.38390	.50142				
157.00	.43170	.77383	.37778	.48587				
158.00	.43656	.78272	.37347	.46854				
159.00	.44033	.79276	.37055	.44584				
160.00	.44329	.80365	.36870	.42010				
161.00	.44566	.81513	.36769	.40955				
162.00	.44762	.82705	.36734	.38837				
163.00	.44929	.83926	.36752	.36669				
164.00	.45075	.85167	.36812	.34463				
165.00	.45208	.86421	.36906	.32227				
166.00	.45333	.87682	.37029	.29965				

TIME	76.8	81.6	86.4	91.2	96.0	100.8	105.6	110.4	115.2	120.0
76.8	.4543	.88945	.37176	.2768						
81.6	.4551	.90208	.37343	.29387						
86.4	.45683	.91666	.37529	.32074						
91.2	.45809	.92719	.37730	.30754						
96.0	.45932	.93964	.37947	.30423						
100.8	.46058	.95200	.38179	.30085						
105.6	.46180	.96435	.38415	.29711						
110.4	.46303	.97670	.38650	.29336						
115.2	.46426	.98905	.38885	.28961						
120.0	.46549	.100000	.39120	.28586						

CONCENTRATIONS AND FILL FACTORS UPON DISCHARGE ARE AS FOLLOWS:

CYCLE	2 OF 3 CYCLES	H2-SIDE CONC	H2-SIDE FILL	AG-SIDE CONC	AG-SIDE FILL
-------	---------------	--------------	--------------	--------------	--------------

122.4	.46672	1.00000	.47553	.07565
124.8	.46809	.99543	.50230	.08947
127.2	.46947	.98515	.50957	.10505
129.6	.47084	.97221	.51096	.12124
132.0	.47221	.95496	.51033	.13767
134.4	.47358	.93752	.50891	.15420
136.8	.47495	.91994	.50715	.17076
139.2	.47632	.90226	.50524	.18734
141.6	.47769	.88449	.50325	.20391
144.0	.47906	.86663	.50122	.22048
146.4	.48043	.84877	.49917	.23704
148.8	.48180	.83091	.49711	.25358
151.2	.48317	.81305	.49504	.27012
153.6	.48454	.79519	.49298	.28663
156.0	.48591	.77733	.49091	.30313
158.4	.48728	.75947	.48884	.31962
160.8	.48865	.74161	.48677	.33609
163.2	.49002	.72375	.48471	.35254
165.6	.49139	.70589	.48264	.36898
168.0	.49276	.68803	.48058	.38540
170.4	.49413	.67017	.47852	.40180
172.8	.49550	.65231	.47646	.41819
175.2	.49687	.63445	.47440	.43456
177.6	.49824	.61659	.47234	.45091
180.0	.49961	.59873	.47028	.46725

WARNING: FILL FACTOR BELOW .10 ON CHRG. MSFF(1) = .98520, SSFF(1) = .09114
ON CYCLE 3 OF 3 CYCLES.

WARNING: H2-SIDE RESERVOIR OVERFLOW AT TIME 105.60 OF CYCLE 3 DURING CHARGE. MSFF(1) WAS 1.00656

WARNING: FILL FACTOR BELOW .10 ON CHRG. MSFF(1) = 1.00000, SSFF(1) = .06739
ON CYCLE 3 OF 3 CYCLES.

WARNING: H2-SIDE RESERVOIR OVERFLOW AT TIME 110.40 OF CYCLE 3 DURING CHARGE. MSFF(1) WAS 1.02117

WARNING: FILL FACTOR BELOW .10 ON CHRG. MSFF(1) = 1.00000, SSFF(1) = .04386
ON CYCLE 3 OF 3 CYCLES.

WARNING: H2-SIDE RESERVOIR OVERFLOW AT TIME 115.20 OF CYCLE 3 DURING CHARGE. MSFF(1) WAS 1.02125

WARNING: FILL FACTOR BELOW .10 ON CHRG. MSFF(1) = 1.00000, SSFF(1) = .02021
ON CYCLE 3 OF 3 CYCLES.

CONCENTRATIONS AND FILL FACTORS UPON CHARGE ARE AS FOLLOWS:

CYCLE	3 OF	3 CYCLES	H2-SIDE CONC	H2-SIDE FILL	AG-SIDE CONC	AG-SIDE FILL
TIME						
100			.34807	.80905	.47028	.46849
80			.37244	.79512	.43787	.43754
90			.39066	.78880	.41450	.47160
100			.40427	.78788	.39748	.46444
110			.41444	.79085	.38504	.45334
120			.42205	.79664	.37599	.43926
130			.42778	.80448	.36948	.42293
140			.43213	.81382	.36490	.40489
150			.43547	.82424	.36180	.38554
160			.43809	.83555	.35984	.36519
170			.44020	.84721	.35878	.34408
180			.44194	.85936	.35842	.32238
190			.44343	.87178	.35862	.30022
200			.44476	.88436	.35927	.27771
210			.44594	.89704	.36028	.25491
220			.44714	.90977	.36160	.23190
230			.44827	.92249	.36318	.20871
240			.44940	.93519	.36497	.18538
250			.45055	.94783	.36697	.16194
260			.45174	.96039	.36914	.13840
270			.45296	.97285	.37149	.11480
280			.45425	.98520	.37400	.09114
290			.45560	1.00000	.37479	.06739
300			.45693	1.00000	.37335	.04386
310			.45822	1.00000	.37222	.02023
320			.45951	.7.31052	.22402	8.54144

CONCENTRATIONS AND FILL FACTORS UPON DISCHARGE ARE AS FOLLOWS:

CYCLE	3 OF	3 CYCLES	H2-SIDE CONC	H2-SIDE FILL	AG-SIDE CONC	AG-SIDE FILL
TIME						
120			.44612	1.00000	.47553	.07565

EIC CORPORATION
PROGRAM FOR THE SIMULATION OF ROLLED SILVER-HYDROGEN BATTERIES

JUNE, 1977
THIS PROGRAM OPTIMIZES ENERGY DENSITY AND CALLS FOR SUBROUTINES TO SIMULATE THERMAL PERFORMANCE
PROGRAM EICD

REFERENCE TABLE OF ALL INPUT PARAMETERS USED

*100000 01	*150000 01	*100000 01	*200000 01	*700000 01
*500000 02	*150000 01	*100000 01	*120000 03	*400000 02
*100000 01	*100000 02	*635000 01	*650000 01	*273000 01
*110000 01	*200000 02	*100000 01	*635000 02	*350000 00
*800000 00	*600000 01	*650000 01	*116000 00	*600000 01
*890000 01	*600000 00	*100000 01	*631800 01	*800000 00
*300000 01	*160000 00	*164000 01	*650000 00	*500000 01
*000000 00	*100000 01	*600000 01	*124140 01	*100000 00
*330000 02	*139000 01	*100000 00	*541185 00	*100000 00
*119000 01	*100826 01	*125000 01	*150000 01	*100000 02
*500000 02	*200000 00	*254000 02	*200000 00	*762000 02
*508000 01	*508000 00	*100000 01	*528000 01	*294000 00
*158750 01	*158750 01	*355600 01	*932500 00	*254000 01
*476250 00	*317500 00			

REFERENCE LIST OF ALL INPUT PARAMETERS THAT DIFFER FROM THE DEFAULT VALUES

LIST NUMBER	PARAMETER VALUE	DEFAULT VALUE
39	*102414 01	*117800 01
44	*541185 00	*000000 00
46	*119000 01	*140000 01
47	*100826 01	*115000 01

PLATE PARAMETERS ARE AS FOLLOWS:
PLATE AREA 748.57 CM²
DISCHARGE AND CHARGE CURRENT DENSITIES ARE -.066794 AND .035067 AMP PER CM²
MINIMUM AG UTILIZATION IS .5411

IN THIS PART OF THE CALCULATION THE ELECTRODE PORE IS ASSUMED TO CONSIST OF 3 LAYERS, I.E. H2+O ELECTRODE PAIRS.
THE ARRANGEMENT OF ELECTRODES, FROM PRESSURE VESSEL WALL INWARD, IS (1+2, 2+3):

RESULTS OF THE OPTIMIZATION ARE AS FOLLOWS (UNITS ARE CM, GRAMS, AND MH):	
211221	
PRESSURE VESSEL RADIUS	*344192 01
PRESSURE VESSEL LENGTH	*144330 02
NUMBER OF ELECTRODE PAIRS IN THE ROLL	3.0
TOTAL WEIGHT IF H2 ELECTRODE AND LEADS HAD BEEN OPTIMIZED	*6429700 03
ACTUAL WEIGHT	*6894290 03

NET DELIVERED ENERGY IF H2 ELECTRODES AND LEADS HAD BEEN OPTIMIZED .08744/E 02
 ACTUAL NET DELIVERED ENERGY .095744/E 02
 PRESSURE VESSEL VOLUME .709034/E 03
 MAXIMUM PRESSURE .002327/E 02 (ATMOSPHERES)
 WEIGHT ENERGY DENSITY IF H2 ELECTRODES AND LEADS HAD BEEN OPTIMIZED .735913/E-01

ACTUAL WEIGHT ENERGY DENSITY .719043/E-01

VOLTAGE DROP THROUGH THE H2 PLATE IF OPTIMIZED .515303/E-01

ACTUAL VOLTAGE DROP THROUGH THE H2 PLATE .302833/E-01

OUTPUT VOLTAGE IF H2 PLATES AND LEADS HAD BEEN OPTIMIZED .057717/E 02

ACTUAL OUTPUT VOLTAGE .080236/E 02

PV WEIGHT .165613/E 03

ELECTROLYTE WEIGHT .065287/E 02

WEIGHT OF ELECTRODE COLLIER (CL. ELECTROLYTE) .223322/E 03

WEIGHT FROM SUBROUTINE WPMIS .232767/E 03

WEIGHT FROM SUBROUTINE WPMIS .099122/E-01

CALCULATED VOLUMETRIC ENERGY DENSITY .114518/E 01

WEIGHT .257051/E 02

WEIGHT .230456/E 02

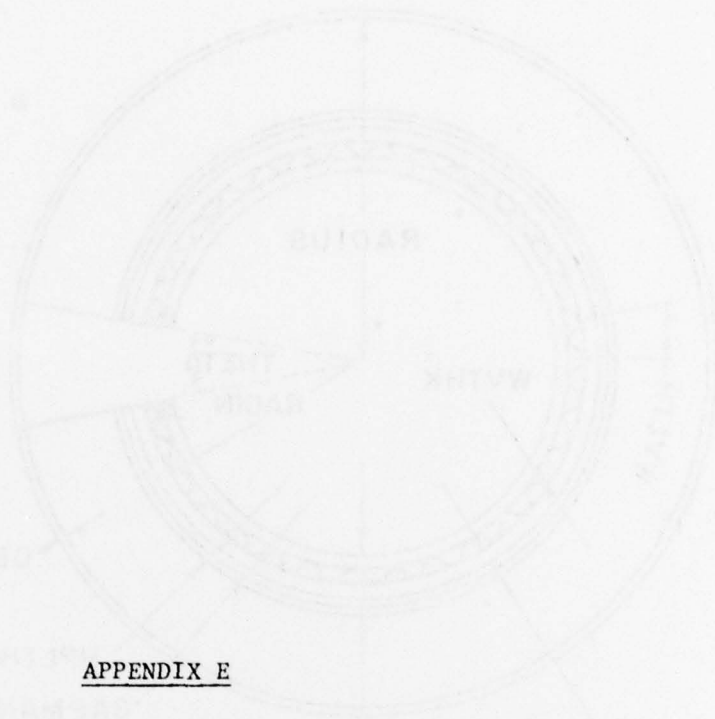
WEIGHT .347033/E 02

WEIGHT .161086/E 02

PROPERTIES OF THE BALL MATERIALS ARE AS FOLLOWS
 NUM MATERIAL, MAT. CAP. PER CC. THERMAL COND., THERMAL CONC., THICKNESS, RADIUS
 SER CODE IN PLANE PERPENDICULAR

1	1	.920000	00	.900000	01	.900000	01	.000000	01	.304192E 01
2	2	.100000	00	.266667	01	.280000	01	.100000	01	.342132E 01
3	3	.780000	00	.244477	02	.244477	02	.435000	01	.336789E 01
4	4	.600000	00	.360000	01	.360000	01	.029289	03	.332471E 01
5	5	.600000	00	.360000	01	.360000	01	.311035	01	.329299E 01
6	6	.600000	00	.360000	01	.360000	01	.317183	01	.324299E 01
7	7	.133722	00	.104156	01	.104156	01	.500000	01	.318299E 01
8	8	.100000	00	.266667	01	.280000	01	.000000	01	.313299E 01
9	9	.133722	00	.104156	01	.104156	01	.500000	01	.313299E 01
10	10	.100000	00	.266667	01	.280000	01	.000000	01	.313299E 01
11	11	.600000	00	.360000	01	.360000	01	.317183	01	.305809E 01
12	12	.600000	00	.360000	01	.360000	01	.317183	01	.305809E 01
13	13	.780000	00	.244477	02	.244477	02	.435000	01	.299046E 01
14	14	.600000	00	.360000	01	.360000	01	.317183	01	.293056E 01
15	15	.600000	00	.360000	01	.360000	01	.317183	01	.288485E 01
16	16	.600000	00	.360000	01	.360000	01	.317183	01	.285514E 01
17	17	.133722	00	.104156	01	.104156	01	.500000	01	.285514E 01
18	18	.100000	00	.266667	01	.280000	01	.000000	01	.270514E 01
19	19	.133722	00	.104156	01	.104156	01	.500000	01	.269751E 01
20	20	.100000	00	.266667	01	.280000	01	.000000	01	.269751E 01
21	21	.600000	00	.360000	01	.360000	01	.317183	01	.269751E 01
22	22	.600000	00	.360000	01	.360000	01	.317183	01	.269751E 01

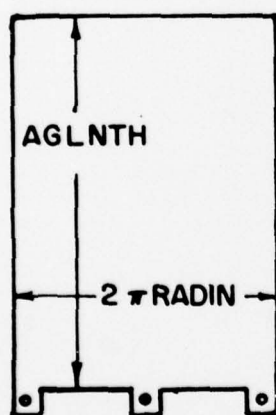
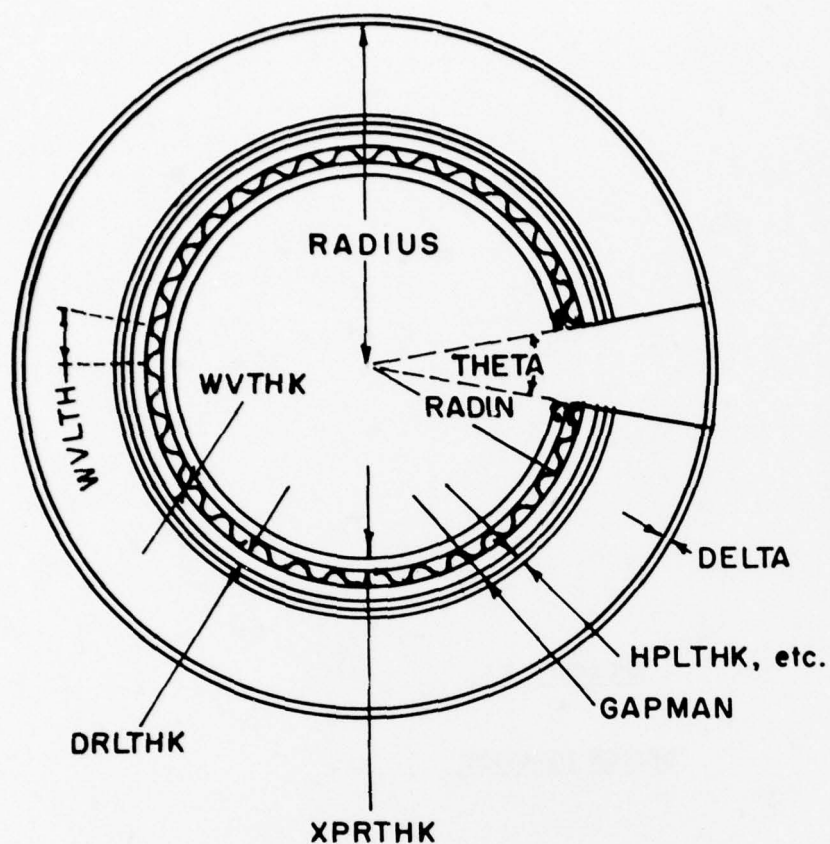
FOR PURPOSES OF CALCULATING THE TEMPERATURE PROFILE, THE BALL IS DIVIDED UP INTO SECTIONS WITH THE FOLLOWING PROPERTIES



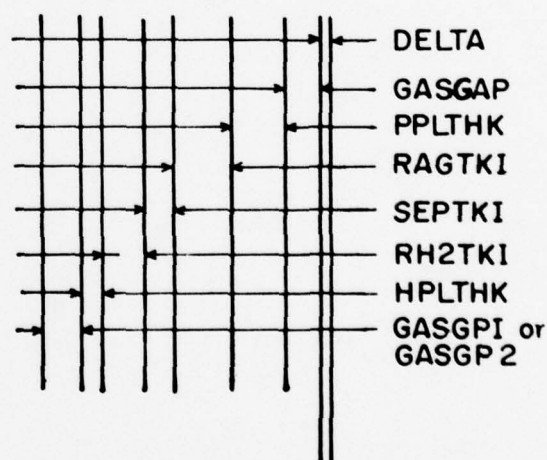
APPENDIX E

DESIGN DIAGRAMS

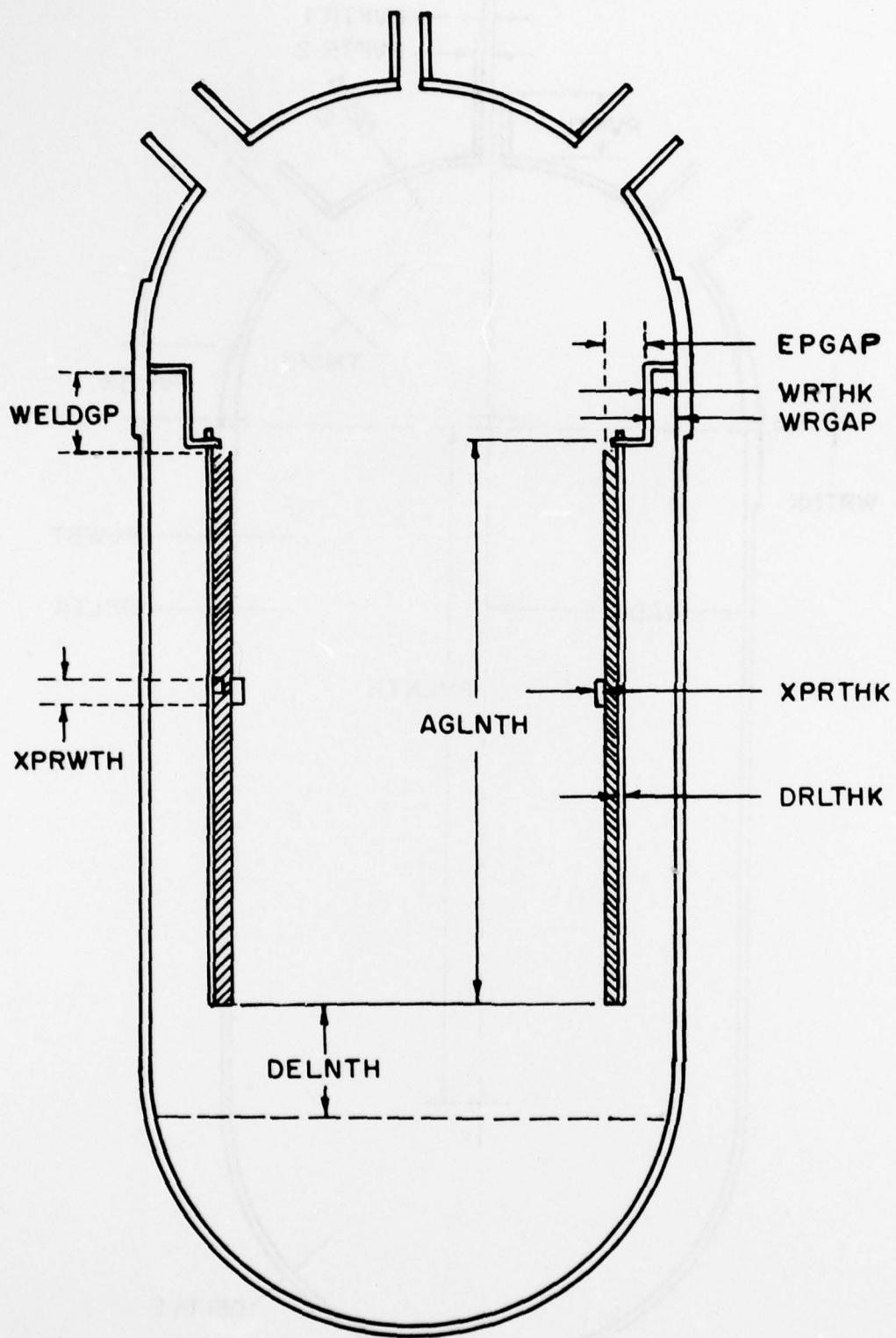


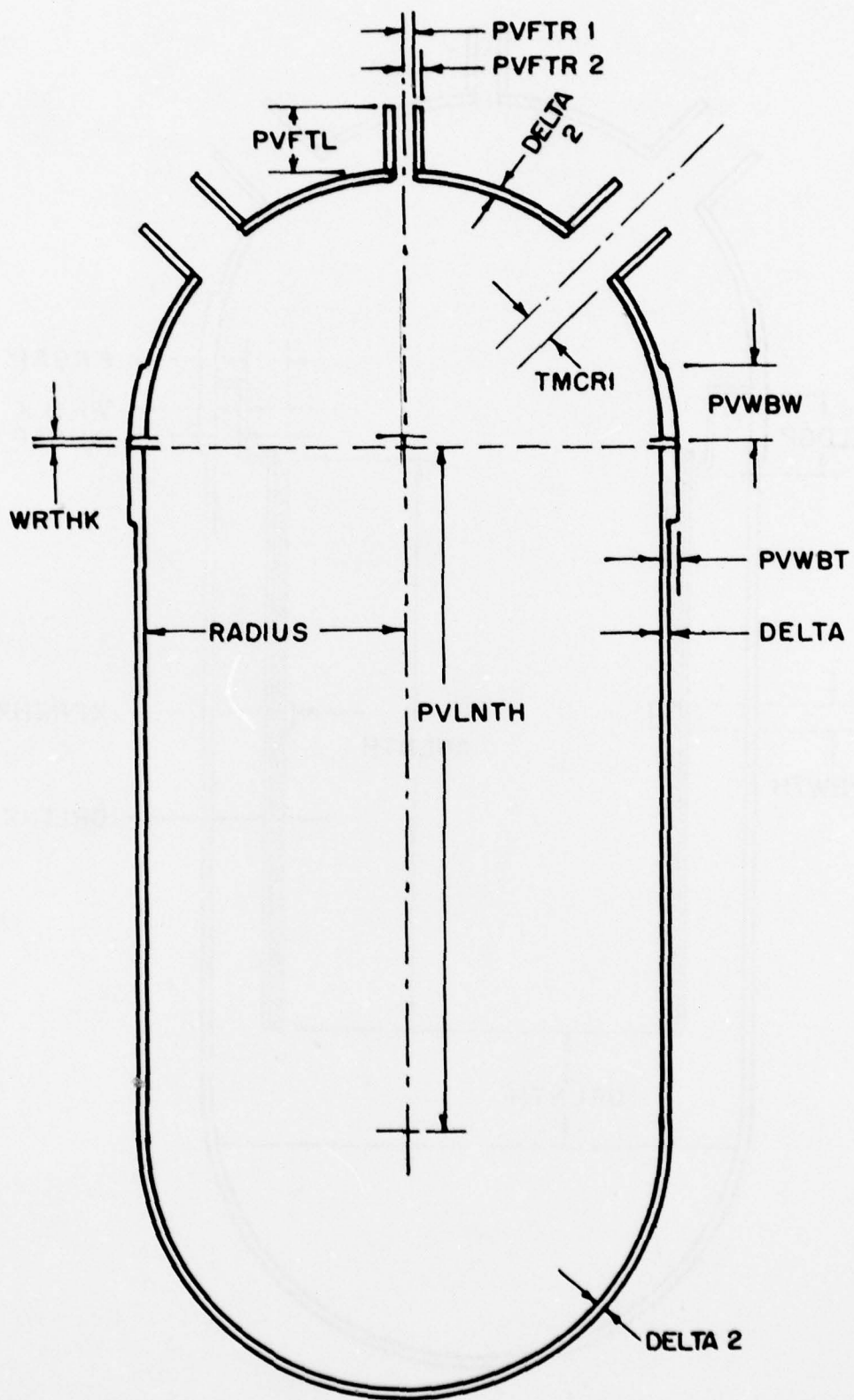


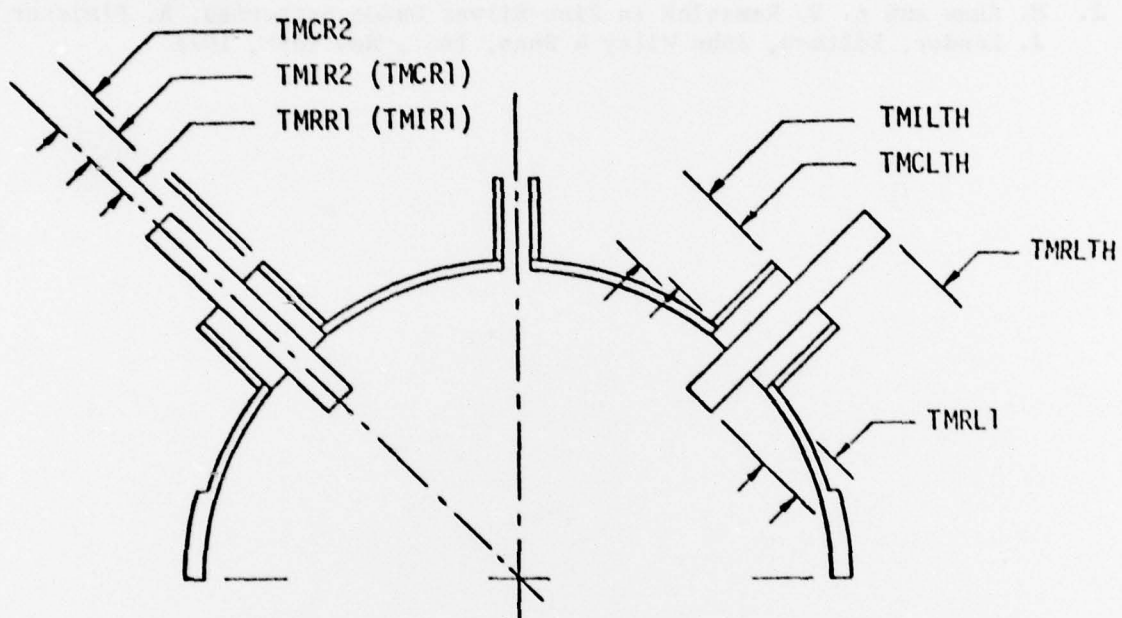
MANDREL (DRL) STRUCTURE (unrolled)



ELECTRODE ROLL STRUCTURE.
GAS GAP BETWEEN H_2 and Ag
ELECTRODES IS GASGP2; BETWEEN
ADJACENT H ELECTRODES,
GASGP₁₂.







V. REFERENCES

1. G. L. Holleck, A. Kutschker, M. J. Turchan, F. S. Shuker, "Nickel-Hydrogen Failure Mechanism Investigations", Final Report, Subcontract to Contract No. F33615-75-C-2025. Part of Final Report by Hughes Aircraft for Air Force APL AFSC Wright Patterson AFB, Ohio, Dec. 1977.
2. M. Shaw and A. H. Remanick in Zinc-Silver Oxide Batteries, A. Fleisher and J. Lander, Editors, John Wiley & Sons, Inc., New York, 1971.